Università della Calabria

Facoltà di Ingegneria

Scuola di Dottorato "Pitagora" in Scienze Ingegneristiche
I ciclo (2007-2010)

Dottorato di Ricerca in Ingegneria Chimica e dei Materiali
XXIII ciclo (2007-2010)

Dissertazione per il conseguimento del titolo di Dottore di Ricerca
in Ingegneria Chimica e dei Materiali
Settore Scientifico-Disciplinare ING-IND 27 – Chimica industriale e tecnologica

Synthesis and Characterization of Helically Coiled Carbon Nanotubes

Supervisore — *Candidata*

Ch.mo Prof. Jànos B.Nagy — Anita Csató

Il Direttore della Scuola di Dottorato

Ch.mo Prof. Sergio Rizzuti

A.A. 2010-2011

Acknowledgements

I'm surely not a poet, but I would like to write a few words for those people who helped me during these years. There are many of them, I could write a really long list of names.
First of all I would like to say thank you to Prof. János B.Nagy, who made it possible for me to start this PhD work in Calabria, supported me during the years with my work, and was always willing to help me. I'm really grateful.

I would like to acknowledge the financial, and technical support for the University of Calabria, the Doctorate School Pitagora, Prof. Sergio Rizzuti, Roberto Gaudio, the Department of Chemical and Materials Engineering, Professor Giordano Girolamo, and the Doctorate School of Chemical and Materials Engineering, and Professor Raffaele Molinari for providing the necessary financial, technical and administrative support for this research. I owe my gratitude to all the professors PhD students and researchers at UNICAL who welcomed me in Italy and give me guidance in many during this period. I'm grateful to everybody at the Laboratory of Industrial Chemistry at Unical: Anastasia, Alfredo, Corradino e Danilo, thank you for your availability and help in everyday laboratory work!

I owe my deepest gratitude to Professor Zoltán Kónya at the University of Szeged, who made transmission electron microscopy measurements possible, and gave me the possibility to work in his laboratory. Equally thanks to everybody in the Laboratory of Applied and Environmental Chemistry at the University of Szeged, for explaining the functioning of the instruments, and answering all my questions. I learnt a lot from you.

Special thanks to Andrea Szabó, (my second mum during these years☺) without her this thesis surely would not have been possible. Her help, knowledge, preciseness, altruism and friendship meant a lot to me both personally and professionally. I have to mention also Caterina Perri and Natalina Giraldi, who gave me a warm welcome in Italy and made me cheerful company during the period at the University of Calabria. Thank you for your help and I hope to see you somewhere around!

I'm really grateful to my friends, I won't list the names, but you know who you are, for your encouragement and support. Special thanks to Mario, a wonderful person who stood behind

me patiently during these years, held me when I fell and with his enthusiasm reminded me that I never have to give up!

And for closing, some words in Hungarian for my parents, so that my mother can understand something if she eventually tries to read this. És a végére néhány szó magyarul: köszönöm szépen a szüleimnek, öcsémnek akik támogattak, és rájuk támaszkodhattam (néha szó szerint értve) amikor szükségem volt rá.

Contents

Abstract

Although coiled carbon nanofibers can be synthesized on large scale, the selective synthesis of coiled carbon nanotubes is still a challenge for the scientific community.

In the present work we aimed to produce helically coiled CNTs (HCNTs) in at least 10% of the product, taking in consideration previous works. Alumina-, sepiolite and silica supported Co-; Fe-; Co-Fe and Co-Pr catalysts were prepared and tested in CNT synthesis reactions applying different conditions. Sepiolite and alumina supported catalysts showed low activity in the synthesis of HCNTs. The helices were maximum 1-2% of all the synthesized CNTs.

A more detailed study was carried out with silica supported catalysts. The catalysts were prepared with the ion-adsorption-precipitation (IAP) method. A preliminary study was carried out to observe the behavior of different silica supported catalysts. Co-; Fe-; Co-Fe and Co-Pr catalysts were prepared with different metal loadings. Special attention was dedicated to the Co-Pr catalysts that showed higher activity in the HCNT production. The 2.5%Co-2.5%Pr; 4%Co-1%Pr and the 1%Co-4%Pr catalysts were chosen for a more detailed study. The effect of the temperature, the carbon source flow and the carrier gas flow variation was tested in the synthesis of helically coiled carbon nanotubes. The most favorable reaction conditions for the HCNT synthesis in our conditions are presented in table 1.

Catalyst	**Reaction temperature (°C)**	**C_2H_2 flow (ml/min)**	**N_2 flow**	**%HCNTs**
2.5%Co-2.5%Pr	700	30	300	15
4%Co-1%Pr	650	30	300	14-15
4%Co-1%Pr	700	30	600	14-15
1%Co-4%Pr	700	30	300	15-17
1%Co-4%Pr	700	30	600	14-15

Table 1.: Most favorable reaction conditions for HCNT formation over 5%Co-Pr catalysts with different metal ratios

The synthesis products contain approximately 15% helically coiled MWCNTs. This gives the possibility to apply the synthesized HCNTs in nanocomposite materials, and exploit the

peculiar properties of these structures. However, the purification process of the samples should be optimized.

The characteristics, such as coil diameter and coil pitch, of the helices produced on 5%Co-Pr/SiO_2 catalysts were analyzed. The morphology of these helices vary from wavy coils, S-shaped tubes, to tight helices and loose telephone-cord-like nanotubes. Their coil diameter varies from 25 nm to 270 nm but the most frequent values are present in the range of 25-50 nm. The coil pitch varies from 20 nm to 300 nm. The most frequent coil pitch values ae between 20-130 nm. Occasionally, helical tubes with coil pitch higher than 300 nm were found in the samples. In most of the samples S-shaped elongated coils are prevalent, however, tight coils are typical for the synthesis using 1%Co-4%Pr and the 4%Co-1%Pr catalysts applying different nitrogen flows.

The aim of this work to obtain more than 10% of helically coiled carbon nanotubes in the synthesized product was achieved, however further study is needed to understand the formation of the helices and the role of the different reaction parameters.

I. Introduction

Carbon nanotubes have been in the center of scientific attention for the past two decades. Their extraordinary electronic, mechanical and thermal properties together with their low chemical reactivity make them promising material for numerous applications. Some of these applications are already realized and many others are in experimental phase. Multiwalled carbon nanotubes are already produced on large scale and can be bought starting from approximately 30 euros/kg. The production of singlewalled carbon nanotubes with special characteristics or determined electrical properties, and helically coiled CNTs (HCNTs) in high purity is still a challenge.

For the synthesis of CNTs several methods have been applied so far. The three most widespread methods are the arc discharge, the laser ablation and the chemical vapour deposition (CVD) method. Due to the relatively low reaction temperature, the easy control of the reaction parameters and the possibility to scale-up the process the CVD method is applied for the large-scale production of CNTs. This method is the most convenient for different applications of the produced CNTs such as their application in nanocomposite materials. When using the CVD method coil-shaped carbon nanotubes (HCNTs, helically coiled CNTs) are also present in the carbon deposit among the straight carbon nanotubes ***[1]***, while in the arc discharge and laser ablation method only straight nanotubes are formed.

The probability of the helical CNTs formation was predicted a few years before their experimental observation in a catalytically produced carbon deposit ***[2-4]***.

Due to the peculiar structure of the HCNTs they have numerous possible applications. Based on their properties and their helix-like morphology they could be used in nanocomposite materials, nanosensors and nanotransformators.

In the present work we aimed to produce helically coiled CNTs by the CCVD method in at least 10% of the product. We took as basis the so-far published results. Different support materials were tested, and the catalyst preparation and the synthesis conditions were optimized in our system aiming to augment the ratio of helical CNTs in the synthesis products, providing a basis for further study in nanocomposite materials. The morphological characteristics of the synthesized helices in the samples are described. The synthesized CNT products were characterized by thermal analysis, scanning electron microscopy (SEM), transmission electron microscopy (TEM). Selected area electron diffraction patterns (SAED) of the synthesized HCNTs with different morphology were also taken.

References:

[1]: Hernadi, K.; Thien-Nga, L.; Forro, L.: "Growth and microstructure of catalytically produced coiled carbon nanotubes" J. Phys. Chem. B 105 (2001) 12464-12468

[2]: Dunlap, B.I.: "Constraints on small graphitic helices" Phys. Rev. B 50 (1992) 8134-8137

[3]: Dunlap, B.I.: "Relating carbon tubules" Phys. Rev. B 49 (1994) 5643-5650

[4]: Amelinckx, S.; Zhang, X.B.; Bernaerts, D.; Zhang, X.F.; Ivanov, V.; B.Nagy, J.: "A formation mechanism for catalytically grown helix-shaped graphite nanotubes" Science 265 (1994) 635-639

II. Bibliography

II.1. Carbon: different structures and properties

Carbon is present in the nature in various so-called allotropic forms. A carbon atom has four valence electrons two on the 2s and two on the 2p orbitals. These can easily interact with one-another due to the negligible difference of energy between these orbitals. An s-electron of the carbon atom can pass to the p-orbital when a bond is formed, and the s and p orbitals can be hybridised in different forms. An s orbital can hybridize with 1, 2 or 3 p-orbitals forming sp^1, sp^2, sp^3 hybrid orbital, respectively. The sp^1 orbitals are formed of the hybridization of one s orbital with one p, this way the bond angle is of 180°. The sp^2 orbitals come from the hybridization of an s orbital with two p orbitals, three coplanar σ bonds are formed, where the bond angle is 120°. The fourth orbital (p_z) remains generating a π-orbital perpendicular to the plane defined by the three σ bonds. The sp^3 orbitals are created when an s orbital is hybridized with three p-orbitals and they form four σ-type bonds forming a tetrahedron, the bond angles are of 109.5°.

II.1.1. Diamond and Graphite

In the case of the diamond all the four valence electrons occupy the hybrid orbital sp^3, forming four covalent bonds connecting each carbon atom to four other atoms in a tetrahedral coordination (Figure II.1.). The electrons are strongly localized in the covalent bonds between the carbon atoms. The properties of the diamond (hardness, light colour, electronic insulation and good thermal conductance) derive from the electron structure.

Albeit in the graphite only three of the four valence electrons are bounded covalently (Figure II.1.). This way every carbon atom is connected to three others which can be found in the same plane, the bond angles are of 120°C, this way a graphene plane is formed. This graphene plane is made of hexagons in the corners of which the carbon atoms are located. The fourth electron of each atom is in a π-type orbital to form a delocalised system of electrons. The adjacent planes of the graphite are bound by van der Waals forces that causes the easy shifting of the parallel graphene layers. Hence the properties of this material are anisotropic, they vary

according to the direction in the crystalline structure. For example, the electrical conductivity is 10^4 times higher in the direction of the graphene layers then in the direction perpendicular to the layers ***[1].***

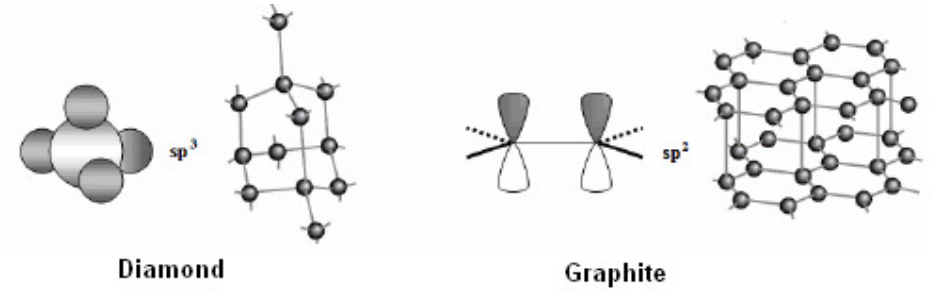

Figure II.1.: Bonds of the diamond and the graphite

II.1.2. Amorphous Carbon

The amorphous carbon is a structurally disorganized form of carbon. Microcrystalline carbon, activated carbons, carbon black and charcoal also belong here. In this structure all the three types of the bonds mentioned before (sp^1, sp^2, sp^3) can be found. Hence, it can be described as a type of hybrid between the configurations of the diamond and the graphite ***[1].*** Indeed, the structure can be considered as overlapped graphene layers with a distance of approximately 3.6 Å, connected to each other by tetrahedral carbon atoms. This way due to the different size of the crystallites and their orientation this material can exist in numerous variants with diverse mechanical or opto-electronic properties. The properties of amorphous carbon thin films are mainly determined by the ratio of sites coordinated by tetrahedral sp^3 bonds and trigonal-planar sp^2 sites and the hydrogen content (or other doping-element content, such as nitrogen, fluorine etc.).

II.1.3. Carbon Fibers

The atomic structure of a carbon fiber is similar to that of the graphite, made of graphene layers disposed according to a regular hexagonal symmetry. The difference is the interlinking between these graphene sheets; while in the case of the graphite they are parallel to one-

another creating a regular structure, carbon fibers can be turbostratic or graphitic; or they can have a hybrid structure in which turbostratic and graphitic parts are equally present, depending on the material from which it was synthesized. The turbostratic carbon fibers tend to have more elevated tensile strength while the graphitic carbon fibers have elevated Young modulus (elasticity) and thermal conductibility. The applications of this material exploit their elevated mechanical resistance, low density, the thermal isolating properties, their resistance against temperature change and chemical agents as well as their good flame retardant features. Carbon fibers are prevalently applied as fillers in composite materials above all in plastic polymers ***[2]***.

Scientific attention turned to the carbon fibers since the end of 1950-ies, the beginning of the 1960-ies when the potential of their elevated mechanical resistance was emphasized.

II.1.4. Fullerenes

Fullerenes were discovered in the '80-ies by Smalley, Kroto and Curl ***[3]***, although the existence of these peculiar carbon structures was predicted two decades before ***[4].*** This first discovered fullerene was called Buckminsterfullerene and consisted of 60 carbon atoms forming a type of socker-ball-like cage, with a diameter of approximately 1 nm. It is formed of 12 pentagons and 20 hexagons, where each pentagon is enclosed by 5 hexagons (Figure II.2.). The hybrid sp^2 orbital of the graphene is deformed in this case due to the rehybridization of π-type bonds and the curvature of the cage ***[5]***.

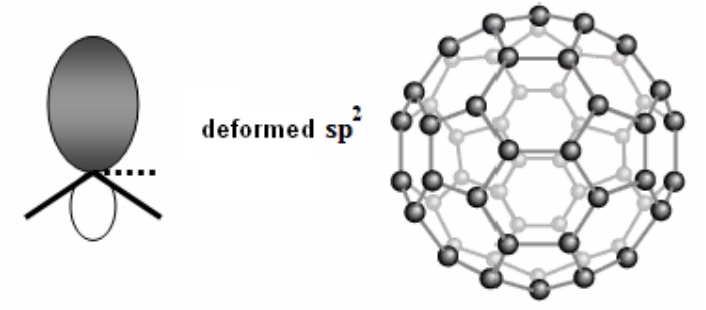

Figure II.2.: Atomic bonds of fullerenes

There are numerous other types of cages that can be built up by hexagons and pentagons. Each structure has to contain at least 12 pentagons regardless of the number of hexagons.

According to the theory of Euler this is the minimum necessary number of pentagons to close a hexagonal lattice ***[6].*** The smallest possible fullerene is the C20 that is made of 20 pentagons and not any hexagon. Other possible fullerenes are the C28, C32, C44, C50, C58, C70, C76 C84, C240, C540 etc. The most common ones are the C60 and the C70, while the others are extremely rare.

II.1.5. Carbon Nanotubes

Although the first reports of carbon nanotubes were made by Russian researchers in 1952 ***[7]*** and subsequently by Endo and co-workers in 1976 ***[8]***, only the study published by Iijima in 1991 ***[9]*** drew the scientific attention to the further study of this material. The authors described the synthesis of these hollow tubule-like graphitic structures with nanosized diameters. The research group of Iijima was working on fullerenes, which can be obtained by the arc discharge method. The multiwalled hollow fiber-like structures (Figure II.3.) were found as by-products analysing the obtained sample after a fullerene synthesis. These structures had diameters between 4-30 nm and their length was around 1 μm ***[9]***.

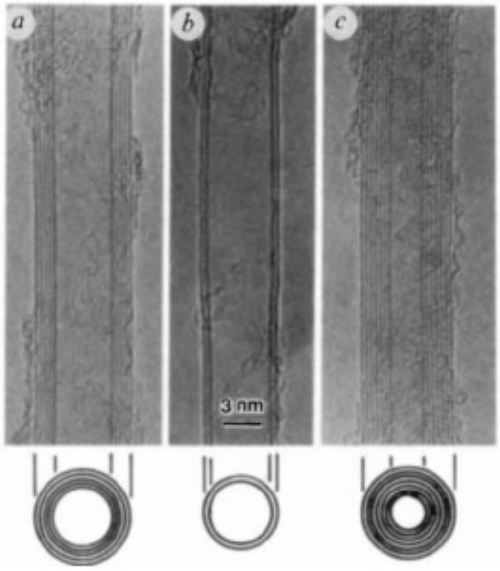

Figure II.3.: TEM pictures and corresponding cross-sections of the carbon nanotubes published by Iijima et al. ***[9]***

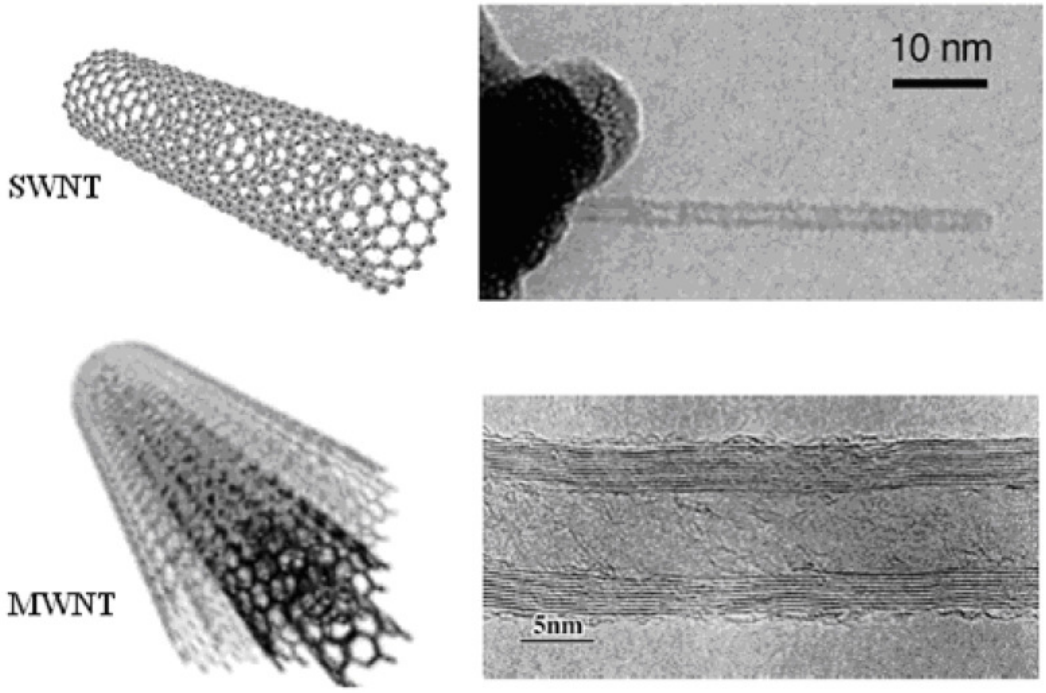

Figure II.4.: Models and TEM images of a SWCNT and a MWCNT ***[12, 13]***

While fullerenes are spherical structures made of 5 or 6 member rings, carbon nanotubes are cylinder-like structures made of six-member carbon rings that can occasionally end in a half-fullerene cap. Two years later Iijima and Ichihashi and Bethune and co-workers reported the production of single-walled carbon nanotubes ***[10, 11]***.

A single-walled carbon nanotube (SWCNT) can be described as a single graphene sheet rolled into a perfect cylinder. If the nanotube consists of not one but more concentrically rolled-up cylinders then it is a multiwalled carbon nanotube (MWCNT). Schematic representations and microscopic images of SWCNT and MWCNT are showed in Figure II.4.

Figure II.5. represents an endless graphene sheet. There are infinitely many ways to roll up this sheet. The as-obtained hollow cylinder can be described by a single vector (n, m) where n and m are integers of the vector equation $C=na_1+ma_2$ and a_1 and a_2 are the unit cell vectors of the two-dimensional lattice formed by the graphene sheet. The direction of the nanotube axis is perpendicular to this vector ***[14].***

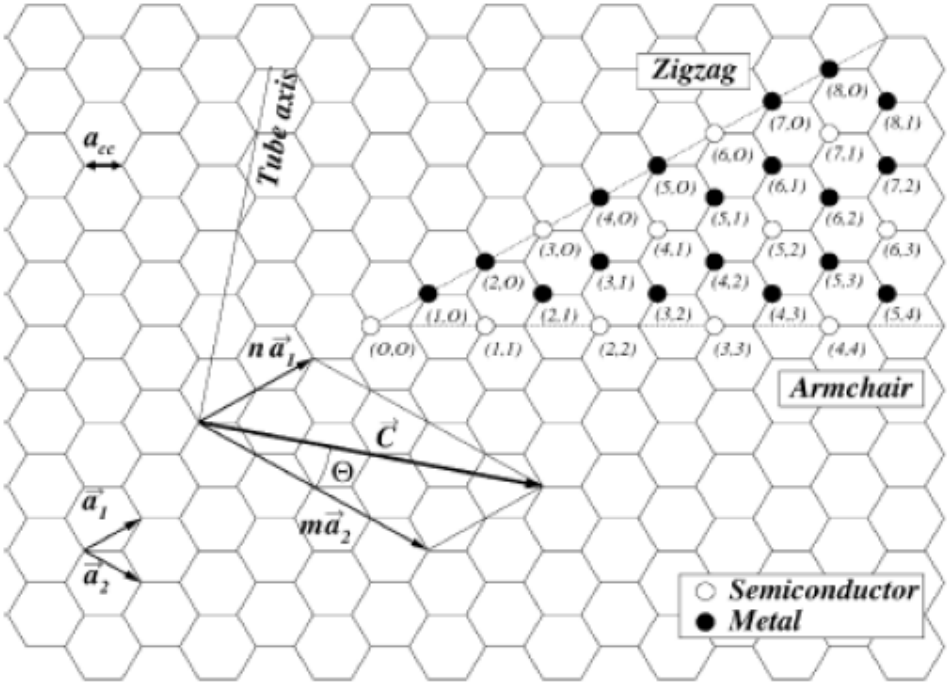

Figure II.5.: Chiral vector and chiral angle definition for a (2, 4) nanotube on graphene sheet ***[15]***

The length of the chiral vector is the circumference of the nanotube and can be given by the following equation:

$$a(n^2+m^2+nm)^{1/2}$$

where a is the length of the unit cell vector a_1 or a_2. It can be determined using the carbon-carbon bond distance (a_{CC}) according to the formula below:

$$a=\left|\overrightarrow{a_1}\right|=\left|\overrightarrow{a_2}\right|=a_{CC}\sqrt{3}$$

For the graphite a_{CC} is 0.1421 nm, for the carbon nanotubes the same value or considering the curvature of the tube a slightly higher value (a_{CC}=0.144 nm) can be used ***[16-18]***.

The chiral angle (Θ) is defined as the angle between the chiral vector and the zigzag axis.

$$\Theta = \mathrm{tg}^{-1}\left[\sqrt{3}\,\frac{m}{m+2n}\right]$$

Concerning the chirality there are three types of CNTs:

- The “armchair” type when n=m (Θ=0)
- The “zigzag” type when m=0 (Θ=30°)
- The “chiral” type when n≠m (Θ<30°)

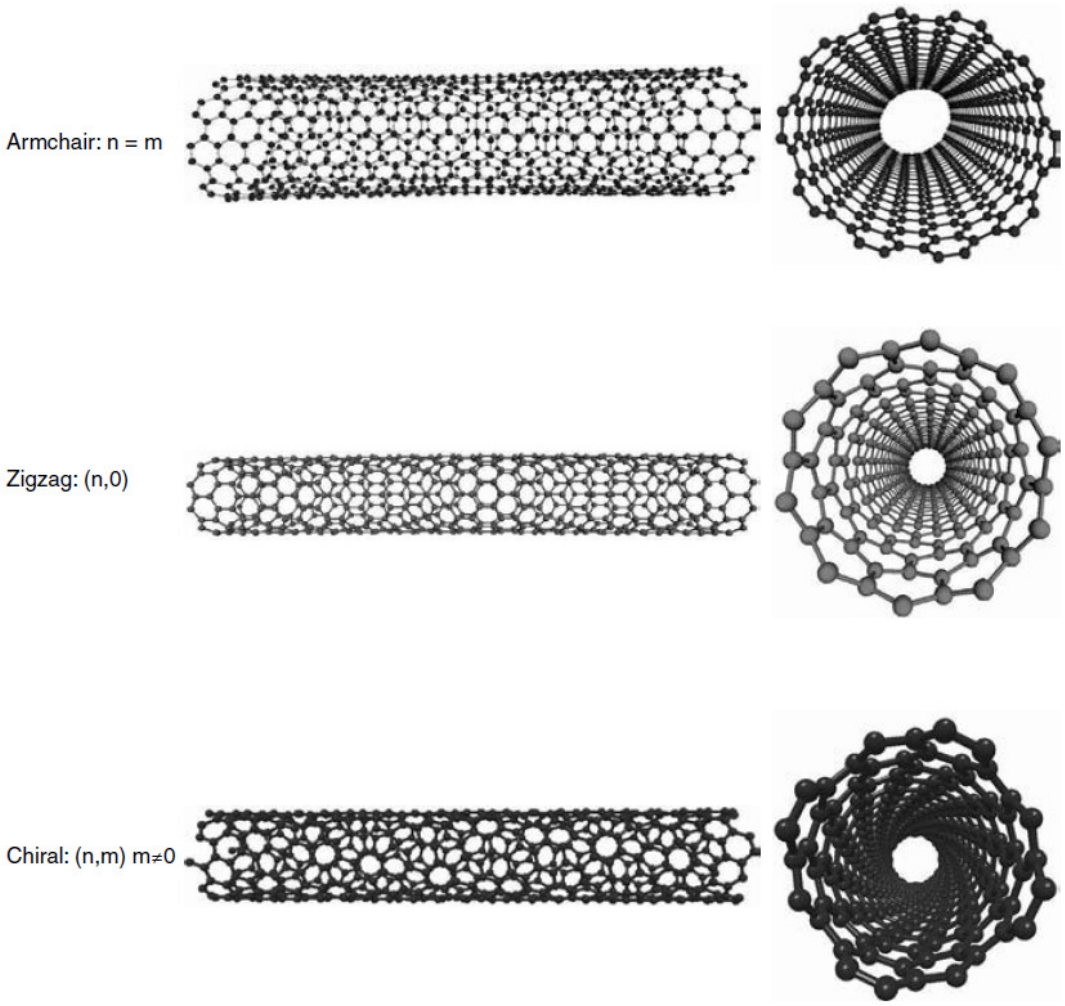

Figure II.6.: SWCNTs of different chiralities ***[2]***

Figure II.6. represents the models of SWCNTs with different chiralities. The value of (n, m) influences the mechanical and electronic properties of the nanotube.

The way how the graphene layer is rolled up -the atomic structure, without any doping- determines the electronic properties of the tube. The armchair tubes and every third zig-zag tube are metallic. Generally a SWCNT is metallic if (n-m)=3k, where k is an integer. Other singlewalled CNTs are semiconductors. For metallic tubes the density of the states at the

Fermi-level is a finite number, while for semiconductor tube it is zero. The energy of the band gap in semiconductor tubes is around 0.7 eV. The width of the band gap depends on the diameter of the tubes.

$$E_{gap}=2J_0a_{C\text{-}C}/d$$

where J_0 is the interchange energy (approximately 2.45 eV), $a_{C\text{-}C}$ is the closest C-C distance (~ 0.42 nm) and d is the tube diameter. E_{gap} decreases with the increasing diameter.
The theoretical calculations for SWCNTs are in good accordance with the experimental data. Generally the diameter of a SWCNT is between 0.6 and 2 nm while the MWCNTs can also reach diameters of a hundred nm ***[19]***.
Multiwalled carbon nanotubes can be described by three different models: they can form coaxial cylinders, coaxial polygons or rolled-up graphene sheets. The most frequently used model is the one of coaxial cylinders, however also the polygonal one is accepted mostly for nanotubes with bigger dimensions, where tri-dimensional regions can be defined ***[20].*** For the multiwalled carbon nanotubes there is only one (n, m) sequence to obtain a realistic distance between the walls. Hence MWCNTs are always conductors. The high external diameter value leads to almost negligible possibility of semiconductor properties. The interwall distance between the concentric cylinders is of 0.34 nm. This is a medium value between the distance between the layers of natural graphite (0.335 nm) and that of the turbostratic graphite ***[21]***.

II.2. Properties and Applications of Carbon Nanotubes

The extraordinary properties of carbon nanotubes are influenced by their size, crystal structure and construction. Carbon atoms are placed in a symmetric way along the axis of a carbon nanotube, like in a one-atom-thick graphene layer that is rolled-up to form a hollow cylinder.

II.2.1. Electronic structure and properties

Scanning tunnelling microscopy (STM) investigations are suitable to provide data on the structure and electron configuration, however the effect of distortions arising at the imaging cannot be neglected. Distortions occur in the measured diameter and the height values compared to the support surface, due to the existence of two tunnelling gaps in the system:

between the tip and the nanotube and between the nanotube and the surface over which it is floating. These together with the differences in the electronic structure of the CNT and that of the support may have significant effect on the tunnelling current. Nevertheless, scanning tunnelling microscopy provides useful information on the atomic structure of a carbon nanotube ***[22, 23]***.

Computational results on the atomic-resolution STM images of SWCNTs showed that in the armchair nanotubes the bonds parallel to the tube axis are not equivalent to the other bonds and the position of the lateral atoms undergoes a distortion in the STM image. Nevertheless, the atomic-resolution STM measurements are in accordance with the theoretical calculations on the electronic structure of CNTs ***[24-26]***.

According to electron diffraction analysis, in the multiwalled CNTs metallic and semiconductor shells are present in a disordered manner. Hence, their description with simple models is not at all obvious ***[27]***. Tomanek et al. demonstrated by calculations that the graphene shells forming a multiwalled CNT can rotate in one-another similar to the way C_{60} molecules do in a fullerene crystal. However, due to the diameter-length ratio of the nanotubes and the macroscopic mass, the rotation along the whole tube is unlikely. Probably, the inner tube "twists" in the outer one in a way that its deviation from the coaxial position remains inferior to 0.1 nm ***[28]***.

Zettl and co-workers managed to pull out the inner tubes of a multiwalled CNT (Figure II.7.). These inner tubes subsequently slipped into the outer shells due to the van der Waals forces. Thus the friction between the nanotube walls is negligible. Repeating the experiment several times with the same nanotube no obvious structural damage was observed in the nanotube ***[29]***.

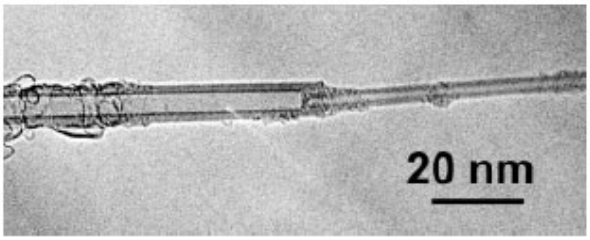

Figure II.7.: TEM image of some outer shells pulled out of a multiwalled CNT by a nanomanipulator ***[29]***

A special electron microscope probe (Figure II.8.) was constructed to measure the electronic properties of a single carbon nanotube. The electrode that contained the CNTs was gradually

immersed in the mercury electrode. The electrical conductivity could be described by a gradual curve, where the well-known quantum-conductivity equation describes the "height of the steps"

$$G_0=2e^2/h=1/(12.9\ k\Omega)$$

The G_0 conductivity doubles when a second nanotube is immersed in the mercury electrode. This phenomenon occurs just in case of defectless tubes. The conductivity was independent of the length of the tube and no heat dissipation was observed along the tube. This characterizes the ballistic conductance, typical of one single graphene layer ***[30]***.

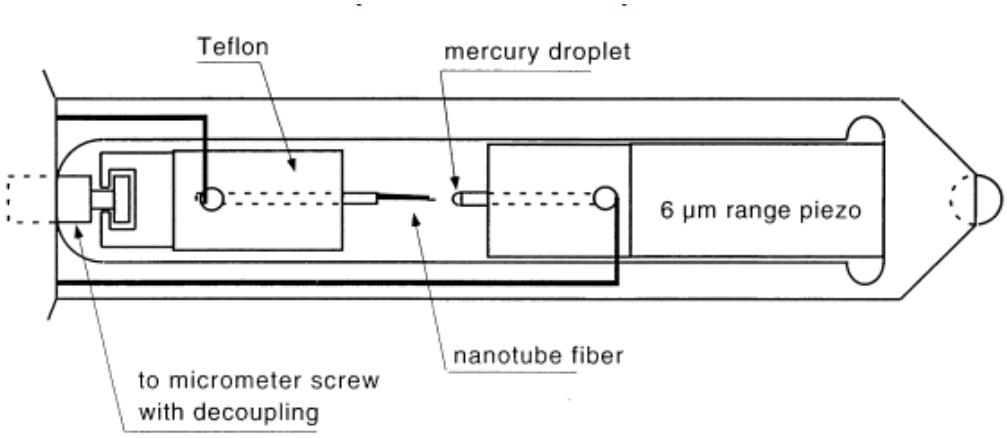

Figure II.8.: Plot of the electron microscope probe adapted for in situ measurements ***[30]***

Postma and Teepen placed a single metallic SWCNT between two gold electrodes on an electrical insulator. With the tip of an AFM (Atomic Force Microscope) probe they formed two curves on the nanotube. The structural changes imply changes in the electronic structure of the tubes, thus the curvatures act as barriers for the electrons. It depends on the applied voltage, if the electron passes between the conductors or not. This experiment rised the possibility of one-electron nanotransistors ***[31].***

Ando and Zhao determined the electrical conductivity of single nanotubes. The electrical conductivity of purified CNTs in the axis direction can vary significantly. The measured specific electrical resistance values varied between 28.1 $k\Omega\mu m^{-1}$ and 1.95 $k\Omega\mu m^{-1}$. The average resistivity was 7.2 $k\Omega\mu m^{-1}$. The average outer tube diameter is of 31.1 nm while that of the inner tube is 1 nm. The conductivity of one single multiwalled CNT was $1.85x10^3$ S/cm, using the highest value in the calculations. The 4, 6, 9, 10 μm long multiwalled CNTs burned when 4V voltage was applied ***[32].***

The peculiar electronic properties of the carbon nanotubes make them suitable for numerous applications, such as light sources, dispositives, nanotransistors and nanosensors.

II.2.2. Mechanical Properties

Most of the mechanical properties of carbon nanotubes can be explained starting from the placement of the carbon atoms in a rolled-up graphene lattice. The strong carbon-carbon bond makes the carbon nanotubes one of the strongest existing material. Their elastic modulus is in the TPa range, slightly superior to that of graphite.

The cylinder shape of the CNTs is another property that strongly influences their electronic and mechanical properties and gives rise to particular features, differing from the graphite, the most relevant of which are the breaking and the deformation characteristics. Carbon nanotubes return to their original shape also under strong bending and twisting forces, and cannot be easily broken by simple mechanical effects ***[33].***

The high specific surface area of the CNTs makes them attractive for mechanical and chemical applications. The BET surface area of multiwalled carbon nanotubes can be a few hundred m^2/g while in case of the singlewalled CNTs this value is significantly higher. The density of this peculiar material is very low. The density of the singlewalled CNTs is in the range of 0.1 g/cm^3, in the case of multiwalled CNTs it can be approximately three times higher. The density of a CNT sample can be influenced by the synthesis conditions and the level of purification ***[34]***.

The deformation of carbon nanotubes can be explained by the insertion of heptagons and pentagons in the hexagonal lattice. These so-called Stones-Wales defects differ in size and geometry from the hexagonal rings, and can be mobilized by an external force in the sp^2-lattice of the nanotube. The drifting of these defects can lead to the diminution of the nanotube diameter, thus the variation of the chirality. This phenomenon can be used for the production of nanosensors that under mechanical effects change their electronic properties.

Graphene layers have similar tensile strength to fullerenes and carbon nanotubes. These values can be applied exclusively for perfect defectless nanotubes that are difficult to obtain in practice. The elasticity of the nanotubes is described by the Young modulus, the value of which can be obtained by the following equation:

$$\Delta l/l = 1E^{-1} x Fq^{-1}$$

where l is the length of the tube, q is the cross-sectional area, F is the force applied for the elongation and E is the Young modulus.

For carbon nanotubes this value is close to the in-plane elastic modulus of a graphene layer. According to calculations and experimental data on the elastic modulus of graphite the Young modulus of defectless straight nanotubes is between 500 and 1500 GPa. When carbon nanotubes are bent under an angle of 90° they return to their original shape at the cessation of the tension. From the tension and the bending angle we can obtain information on the mechanical strength and the elasticity ***[33, 34]***.

The natural resonance frequency of a carbon nanotube depends on its diameter, length, density and elastic modulus. The elastic modulus of the CNTs with a diameter inferior to 8 nm is 1.2 TPa, this can drop to 0.2 TPa for diameters larger than 30 nm ***[30]***.

A previous theoretical study based on the properties of the graphite obtained a value of 1060 GPa for the elastic modulus of defectless carbon nanotubes. Ruoff and Lorents reported that CNTs with a 0.34 nm interwall distance and 1 nm diameter can resist 20 GPa and the natural frequency of the 1 μm long SWCNTs was around 12 MHz ***[36].***

As for the Young modulus AFM (Atomic Force Microscopy) measurements confirmed the theoretical calculations, albeit the elastic modulus of MWCNTs can be ten times lower due to the higher probability of defects in these structures. Carbon nanotubes can undergo massive elastic deformation without being broken. This can be useful for application where energy absorption or storage is needed ***[37]***. It was also found that SWCNTs are flexible and easily bent before the rupture, unlike carbon fibres ***[38]***.

Tersoff and Ruoff established that CNTs with 1 nm diameters are extremely rigid. Nanotubes thicker than 2.5 nm flatten due to van der Waals forces. The rate of the deformation increases with the tube diameter. Placing one SWCNT above another (Figure II.9.), the tubes are deformed and the cross-section becomes oval or ellipsoid-like. The end of the tubes may flatten due to the attractive forces, exacerbating the contact area that also increases with the increase of the diameter ***[35, 39, 46].***

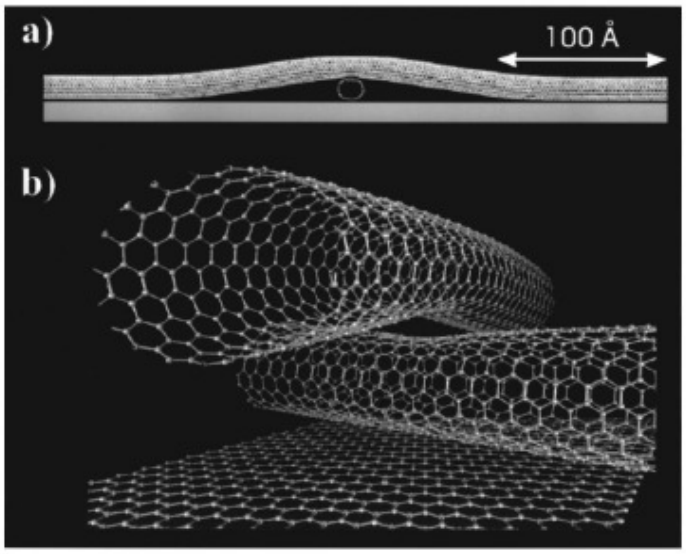

Figure II.9.: Deformation of two oblique armchair SWCNTs ***[46]***

Rochefort and co-workers modelled the radial deformation of the carbon nanotubes ***[40]***. According to their observations increasing the electrical resistance leads to the increase of the curvature angle and the formation of a hook. In case of the armchair nanotubes the bending energy grows linearly with the rotational angle until its critical point. Further rotation of the tube can result in the collapse of the structure and the formation of a flat helix. Figure II.10.(a) shows molecular models where structural changes caused by the rotation can be observed; Figure II.10.(b) illustrates the energy dependence on the separation of the tube axes, while Figure II.10.(c) presents the bonding energy versus the rotational angle ***[28]***.

The outstanding mechanical stability of carbon nanotubes spurred the researchers to examine how these extraordinary stable structures can be frittered or destroyed by external forces. Li et al. treated CNT samples with ball-milling and found that grinding in a ball mill can cause significant damage in the tubular structure. A 15 minutes treatment resulted in the formation of some carbon onions and CNTs of various length, while after a one hour intensive treatment carbon nanotubes were transformed into amorphous carbon. They also proposed a mechanism how CNTs are converted into amorphous carbon. They presume that nanotubes bend first after which a piece starts to scale off the tube similar to the way how drops are formed. Consequently this “drop” becomes completely detached and is present in the sample as a carbon onion. Under further treatment these ellipsoidal structures become more and more spherical, finally they get covered with amorphous carbon. The rest of the tube can follow the same mechanism and become completely frittered ***[41]***.

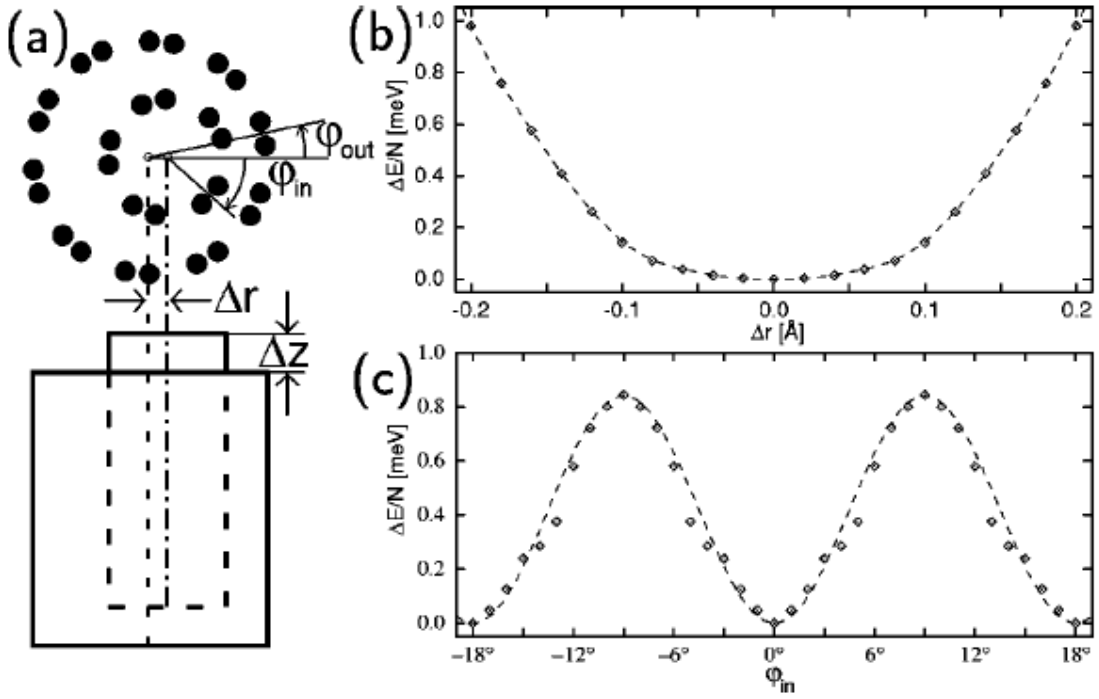

Figure II.10.: Computational molecular models: a) the occurring deformation caused by a rotational force; b) energy dependence on the separation of the tube axes Δr; c) the calculated bond energy in function of the rotational angle ***[28]***

If smaller forces (e.g. lighter balls and lower frequency) are applied nanotubes can be frittered in a way that amorphous carbon formation is not significant. If the ball-milling is carried out in an active gas atmosphere (e.g. NH_3) the reactive ends of the nanotubes can easily be functionalized ***[33-34, 42]***.

Chen et al. treated CNT samples with ball-milling using cyclodextrin as a kind of "buffer". Their hypothesis was that cyclodextrin has a dispersive rule during the treatment: CNTs get embedded into this material that hinders their amorphisation. Cyclodextrin can also act as a thermal conductor. During the fritting of the nanotubes significant heat can be formed locally where the nanotubes are broken. CNTs with diameters between 1.3-1.5 nm can also be grinded this way ***[43]***.

Zhu and co-workers treated non-purified CNT samples prepared by arc-discharge method with strong (~50 GPa) dynamic shock wave pressures. The samples contained also polycrystalline carbon. The electron microscopy investigations and X-Ray diffraction patterns of the treated samples showed that the external walls of the tubes were transformed into a curved graphitic material, while the inner walls have numerous defects and seem to be

amorphous. The X-Ray diffraction patterns of the treated sample showed reflections that are characteristic of nanocrystalline diamond ***[44]***.

Carbon nanotubes were irradiated with a high energy electron beam. The experiments were carried out in a high resolution electron microscope, where videocameras recorded how the carbon nanotubes collapsed due to the irradiation with a 800 keV electron beam ***[45]***.

Summarizing the mechanical properties of carbon nanotubes, they are extraordinarily strong, flexible materials, which difficultly undergo structural deformations. All these make them ideal nanofillers for composite materials.

II.2.3. Thermal Properties

The thermal stability and conductivity of CNTs are also fundamentally interesting and technologically important properties. Carbon structures such as fullerenes and carbon fibers are frequently used to improve thermal conductivity of different materials. As CNTs and graphite have similar physical properties, their thermal conductivity was expected to be similar as well. Ruoff and Lorents studied the mechanical and thermal properties of CNTs and based on analogies they deduced that the thermal conductivity is equal to the in-plane thermal conductivity of the graphite ***[46]***. However, the thermal conductivity of MWCNT in the radial direction is probably inferior as secondary bonds should be considered and the conduction occurs by phonons hopping the edges.

Berber et al. established a linear relation for temperatures inferior to 100 K where the thermal conductivity reaches 37000 W/mK, this decreases suddenly with the rising temperature to the value of 3000 W/mK at around 400 K ***[47]***. The thermal conductivity depends on the length of the tubes, their diameter and chirality.

The thermal behaviour, so the changes that are caused in the structure of the CNTs by thermal treatments are also of fundamental interest. Andrews et al. ***[48]*** produced high purity carbon nanotubes and examined the structural changes occurring at high temperatures. The process called graphitisation was carried out at various temperatures between 1900 and 3300 K, for 45 minutes in nitrogen atmosphere. The raw nanotubes produced from a xylol-ferrocene gas mixture at 1000 K, using Ar-H_2 flow contained iron remained from the ferrocene catalyst in carbide form. This was transformed into oxide at 1900 K. After a treatment at 2500 degrees the reflexions of the oxides cannot be observed in the X-Ray diffraction pattern (Figure II.11.). Iron could be detected only in traces by ICP-AES measurements. The nanotube

samples treated at 3300 K contained negligible amount of iron. The heat treatments ameliorated the crystalline structure of the nanotubes, most of the defects were repaired, and the interwall distance dwindled down.

The ignition temperature of the carbon nanotubes is also an important parameter. Sui et al. examined the thermal behaviour of CNTs produced by the decomposition of acetylene in an aluminium substrate. Thermal analysis showed that CNTs are more stable than fullerenes when heated in air atmosphere. The fullerenes started to burn at 700 K, carbon nanotubes produced in the alumina substrate burned at 753-758 K. Purified MWCNTs were thermally much more stable, they burn at 983 K ***[49].***

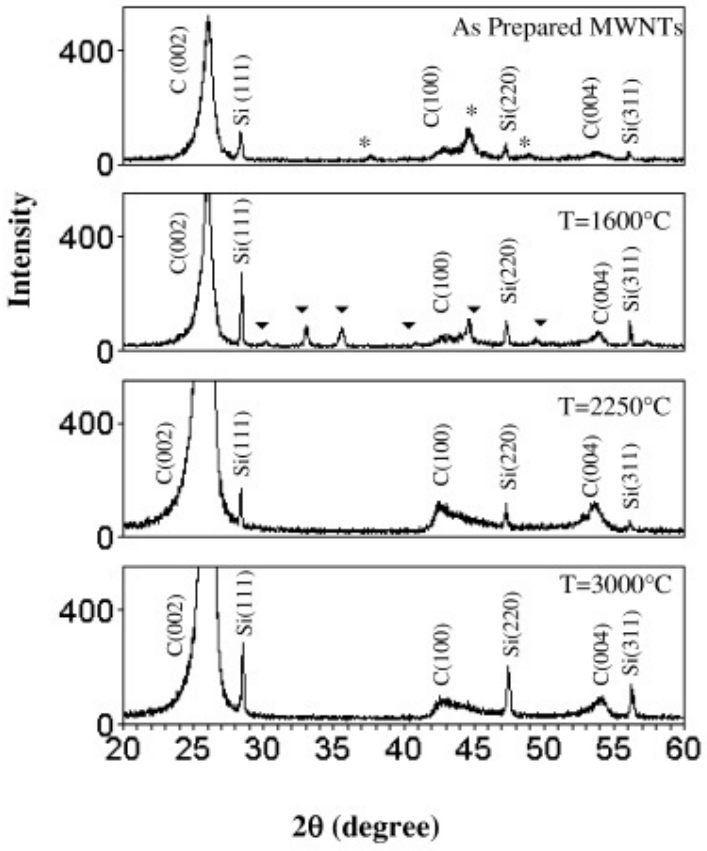

Figure II.11.: XRD patterns of MWCNTs annealed at different temperatures for 45 min.▼ indicates peaks of iron oxide, while * stands for iron carbide ***[48]***

II.2.4. Applications of Carbon Nanotubes

The low reactivity, high aspect ratio, high tensile strength, low mass density, high heat conductivity, large surface area and versatile electronic behavior of individual carbon nanotubes make them ideal candidates for numerous applications, provided that the cost of their production is sufficiently low. Today the price of CNTs depends on the quality of the CNTs and the applied synthesis process..1 g of MWCNTs are sold for as cheap as 5$ on internet ***[50]***, but depending on the quality, functionalization and type of the tube 1 g can cost also several hundreds of dollars. The number of patents referencing CNTs grows yearly in the past fifteen years ***[51]***. However the synthesis technologies evolve fast. This way the applications of CNTs is a rapidly developing field. In this short chapter general notions of the most important applications will be mentioned.

II.2.4.1. Near-field microscope probes, field emitters

The elevated mechanical strength that characterizes the carbon nanotubes makes them ideal candidates as force sensors in scanning probe microscopy. Dai and co-workers ***[52]*** first proposed the idea that was also applied using SWCNTs by Hafner et al. ***[53],*** commercial nanotube-based tips use MWCNTs for the convenience of processing. Using a SWCNT might also lead to artifacts affecting the lateral resolution when scanning rough surfaces probably caused by the low flexural modulus of the SWCNT.

Carbon nanotubes were shown to be efficient field emitters in 1995 ***[54, 55]***. This is exploited by several current applications, such as flat panel displays for television sets and computers, and other devices requiring an electron producing cathode, like X-ray sources. Compared to metallic electron emitting tips, the structural perfection of CNTs permits higher electron emission stability, higher mechanical resistance and longer lifetimes. The lower operating temperature of CNT tips saves energy ***[4]***.

II.2.4.2. Chemical- and biosensors, catalyst supports

The electrical conductance of semiconductor SWCNTs is highly sensitive to changes in the chemical composition of the surrounding atmosphere generated by the charge transfer

between the nanotubes and the gases adsorbed to its surfaces. A linear dependence was demonstrated between the concentration of the adsorbed gas and the change in electrical properties. The sensitiveness of nanotube based sensors should be three orders of magnitude higher compared to the standard solid state devices. The major challenges limiting the commercialization of CNT based sensors are the reproducibility of the devices and the ambiguous results concerning the toxicity of carbon nanotubes ***[4, 7]***.

Carbon-based materials make good supports in heterogeneous catalysis due to their high surface areas, porous structure and their stability at high temperatures (in non-oxidizing environments). The morphology and size of CNTs can be useful in catalytic applications due to their ability to disperse catalytically active metal particles. Catalytic reactions were carried out with noble metals, such as Pt, Ru, Rh, dispersed on MWCNTs or SWCNTs. The catalysts showed high activity in most of the cases ***[4, 56]***.

II.2.4.3. Gas storage, gas separation, adsorption

The use of CNTs for adsorption or separation of various gases as well as their application as adsorbents for metal and liquid materials or pollutants attracted significant scientific attention in the last decade. CNTs were found to adsorb dioxins, fluoride, lead or alcohols better than commonly used adsorbents (like activated carbon for example) ***[4]***.

Scientists tested carbon nanotubes for stocking or transporting oxygen, nitrogen, noble gases and some hydrocarbons. The obtained good results raised the possibility to use CNTs as the world's smallest gas cylinders: they combine low weight, easy transportability and good adsorption properties ***[4, 34]***.

Developing lightweight and safe systems for the storage of hydrogen is a requisite for the efficient use of H_2-air fuel cells in vehicles. Several attempts has been made by numerous research groups to reach the weight efficiency of 6.5% reversibly adsorbed hydrogen set by the U.S. Department of Energy Hydrogen Plan. The so far obtained results are contradictory. Attempts are still made by several research groups rising the question whether CNTs are the most adequate material for hydrogen storage ***[4, 34, 57]***.

II.2.4.4. Composite materials

One direction in the applications is the use of CNTs as nanofillers in composite materials. Their elevated tensile strength, low mass density, good electrical conductivity and high aspect ratio make CNTs particularly promising reinforcements in composite materials. Clue issues are the good dispersion of CNTs, the control of the CNT-matrix bonding, the alignment of the nanotubes ***[4, 34]***.

a) Polymer matrix composites

The first polymer nanocomposites using carbon nanotubes as fillers were prepared in 1994 by Ajayan et al. ***[58]***. Since then numerous publications have been dedicated to the study of CNT-polymer nanocomposites, their properties and possible applications. Generally, the modification of CNTs by polymers can be divided into two main categories involving covalent or non-covalent bonding between the CNTs and the polymer. Non-covalent bonding means the physical adsorption and/or wrapping of polymers onto the surface of the CNTs ***[4, 59]***, while in the second case strong chemical bonds are formed between the CNTs and the polymers. The grafting of CNTs can occur according to two main methodologies. The "grafting from" approach means growing polymers from CNT surfaces via in-situ polymerization. The "grafting to" approach involves the synthesis of a polymer terminated with reactive groups or a radical precursor, that is attached to the surface of the CNTs in a subsequent reaction. The mechanical, electrical, and thermal properties of the obtained CNT-polymer composites show large variation as a function of the polymer matrix, the processing method or the properties of the applied CNTs ***[34, 59]***.

b) Ceramic matrix composites

Adding CNTs in a ceramic matrix can ameliorate the elasticity, and reduce the fragility of the matrix thus creating a more resistant material that keeps the high thermal stability of the ceramic matrix. The usual processing route for these composites consists of a first step where the nanotubes are mechanically dry- or wet-mixed with the matrix (or a matrix precursor) and subsequently in a second step they are densified using hot-pressing sintering ***[4, 60]***.

c) Metal matrix composites

CNT-metal matrix composites are still rarely studied, but the interest towards this field is increasing. Al-, Cu-, Mg-, Ni-, Ni-P, Ti-, WC-Co and Zr-based bulk metallic glasses were tried as matrices. Standard powder metallurgy techniques are used generally for the preparation of these composites, leading to a dispersion that is not optimal. Other techniques such as the plasma spray forming, the nanoscale dispersion method and the rapid solidification technique have been developed. Depending on the metallic matrix the presence of the CNTs can ameliorate the tensile strength, elasticity, the attrition properties or even the corrosion resistance of the material ***[4, 61]***.

II.3. Synthesis Methods of Carbon Nanotubes

Historically, the oldest method for the carbon nanotube production is the electric arc discharge. This technique was applied in the early sixties by Bacon for the synthesis of carbon fibers called whiskers. In 1990 this technique was used by Krätschmer and Huffman, to produce fullerenes. Afterwards, the method was improved and applied for the CNT synthesis. In 1991 Iijima reported the presence of helical microtubules of graphitic carbon in fullerene samples synthesized by the electric arc discharge technique in He atmosphere. SWCNTs were also synthesized by further development of the method. Later the laser ablation method and the chemical vapour deposition (CVD) method became also widely used for the CNT production. The laser evaporation process is technically similar to the arc discharge method, while the chemical vapour deposition method differs in principle, in the reaction conditions and the quality of the product. However, the arc discharge and the different types of the CVD are the most applied techniques in the large scale production of carbon nanotubes ***[33, 34].***

II.3.1. CNT Synthesis with the Arc Discharge Method

In the early period (1991-1995) the arc discharge method was the most commonly used method for the CNT synthesis. The so-called Krätschmer-reactor is based on the electric arc discharge created between two graphene electrodes in an inert atmosphere (He, Ar) ***[62]***. This arc discharge provides the high temperature necessary for the evaporation of the carbon and the creation of the graphitic structure of the MWCNTs (T>3500°C).

Figure II.12.(a) shows the schematic representation of the arc discharge apparatus. The anode can be made of pure graphite or can contain metals. In the latter case metals are mixed with the graphite powder and introduced in a hole in the anode centre. The most commonly used metals are: Fe, Ni, Co, Mo, Y and their mixtures. For the reaction the cathode is fastened while the anode can be moved. The anode is drawn near to the cathode and when the distance between the two electrodes is small enough an arc is struck. A plasma is formed between the anode and the cathode and the flowing current can exceed the 50-150 A. The temperature of the synthesis is so high that the carbon sublimes and the anode is consumed. A constant gap is maintained between the electrodes by moving the anode. Thus the plasma can be stabilized for the required reaction time. Various products are formed in the different parts of the reactor. We can find large quantities of rubbery soot on the reactor walls; web-like structures between the cathode and the chamber walls; grey hard deposit at the end of the cathode and a spongy collaret around the cathodic deposit ***[63, 64].***

When no catalyst is used only the soot and the carbon deposit is formed. This latter one contains the MWCNTs together with graphitic carbon nanoparticles. The nanotubes synthesised this way have closed tips, their outer diameter is between 2-25 nm while their inner diameter varies from 1 to 3 nm. The length of these tubes is inferior to 1 μm.

When the anode contains also metal catalysts during the reaction the core deposit consists of MWCNTs, metal filled MWCNTs and graphitic carbon nanoparticles. The powder-like or spongy soot contains MWCNTs metal filled MWCNTs and also SWCNTs. The SWCNTs formed this way can be either single or in bundles, they have closed tips and do not contain catalyst. The diameters of most SWCNTs vary between 1.1 and 1.4 nm and can be several μm long. The collaret, if it is formed mainly consists of SWCNTs (80%). Numerous factors affect the nucleation and growth of the nanotubes during the process. The most important of these are the vapour dispersion in inert gas, the temperature, the catalyst composition, the addition of promoters and the presence of hydrogen. The quantity of the graphitic carbon nanoparticles was found to diminish by the introduction of pure hydrogen in the reactor ***[63]***.

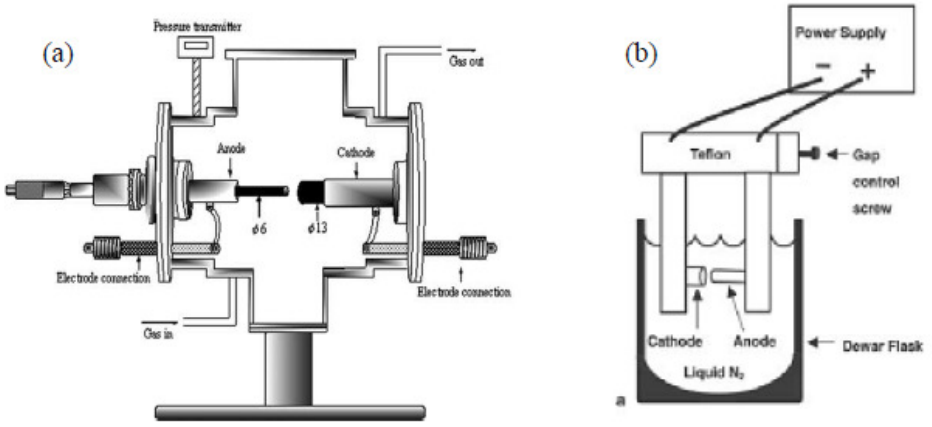

Figure II.12.: a) Scheme of the conventional arc discharge apparatus; b) experimental setup of arc discharge in liquid N_2

Journet et al. proposed the production of SWCNTs in gram quantities by the electric arc discharge technique, using Ni-Co, Co-Y and Ni-Y catalysts ***[64]***.

The catalyst and the carbon source can have significant effect on the obtained product. Wang et al. applied a polyvinyl alcohol (PVA) and PVA/Fe mixture catalyst. The synthesis product contained MWCNTs, sheet-like structures, spherical particles and beaded CNTs. The obtained product varied significantly with the PVA/Fe ratio ***[65]***. SWCNTs were also synthesized using different catalysts, for example Y/Ni and CaC_2/Ni ***[66]***, Eu/Ni, Ce/Ni or Ho/Ni catalyst ***[55].*** Ni was found to be essential for the formation of SWCNTs. A remarkable study was carried out by Marchand et al. on the formation mechanism of SWCNTs from acetylene on Ni nanoparticles. It was shown that the CNTs often rotate axially during growth following the screw-dislocation-like (SDL) model, and this rotation is driven by the insertion of dimers. Thus there must be both longitudinal and rotational sliding between the nanoparticle and the edge of the CNT in order to give space to the newly accreted carbon dimers ***[67, 68].*** DWCNTs were also synthesized using a sulphur containing catalyst or adding sulphur as pollutant to the reaction environment. However, contradictory contributions can be found in the literature on the role of the sulphur during the synthesis ***[69-71]***.

As reaction environment liquid N_2 ***[72, 73];*** deionized water and aqueous solutions for example NaCl ***[74]***; $NiSO_4$; $CoSO_4$ or $FeSO_4$ solutions ***[75-77]*** were applied**.** A schematic apparatus utilized for the synthesis of CNTs in liquid N_2 is shown in Figure II.12.(b). The quality and structure of the produced material is highly influenced by the applied pressure of the carrier/inert gas ***[78]***.

Different types of the arc discharge method were tested in the synthesis of carbonaceous nanomaterials. Imasaka et al. produced carbon nano-onions and nanotubes by intermittent arc discharge process in water environment. This technique permits a several millisecond pulse duration instead of the microsecond pulse duration of the pulsed arc method. The product was either a floating powder containing uniformly dispersed fine spherical particles or a sediment composed of MWCNTs and onion-like carbon nanoparticles ***[79]***. A plasma rotating arc discharge process was used by Lee et al. to synthesize CNTs. They noted an increase in the nanotube yield as the rotation speed of the anode increased and the collector became closer to the plasma ***[80]***.

II.3.2. CNT Synthesis by Laser Ablation Method

Carbon evaporation by laser ablation method was the first method to produce fullerenes ***[3]***. Developing this method led to a productive synthesis process applicable for the synthesis of carbon nanotubes. Figure II.13. is a schematic representation of a laser ablation apparatus. This technique favours the formation of SWCNTs, MWCNTs can also be formed employing appropriate reaction conditions. The SWCNTs produced by this method have higher purity (up to about 90%) and their structure is better graphitized than those produced by the arc process. The disadvantage of the method is the low carbon deposit. Guo et al. applied this method for the production of SWCNTs at Rice University. The principle of the method is the following: a graphite target is evaporised with a laser beam in inert atmosphere (He, Ar). The reaction takes place inside of an oven heated to high temperature (1200°C). When the graphite target is irradiated with the laser beam a carbon plasma is formed which is swept out of the high temperature zone by the inert gas flow. The product deposits onto a water-cooled copper collector positioned downstream outside the furnace ***[81, 82]***. Thess improved the method by applying a second beam, that evaporises the larger particles present in the carbon plasma leading to a more homogenous plasma thus reducing the formation of amorphous carbon ***[83]***.

Using a small graphite target containing transition metals singlewalled carbon nanotubes are formed, although the process is obstructed by the metal accumulation on the surface of the target. Yudasaka resolved this problem by using two targets, one made of pure graphite placed in front of the other containing metals. Contemporarily irradiating the two targets the formation of the SWCNTs remained constant ***[84]***.

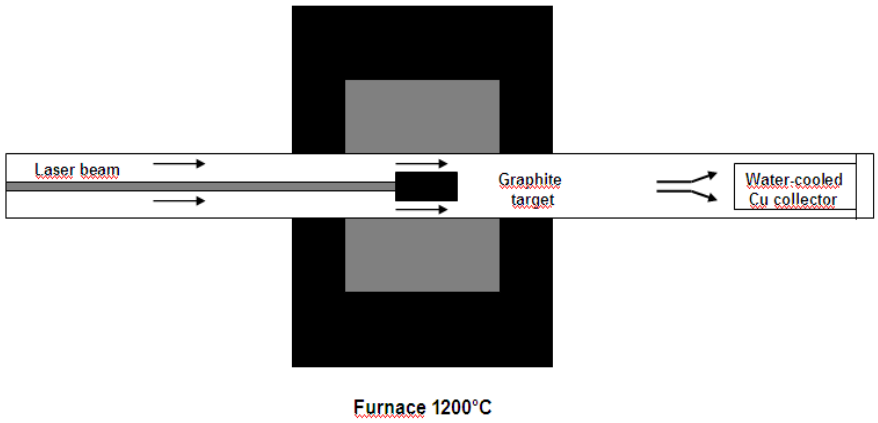

Figure II.13.: Schematic experimental setup for the laser ablation method

The quantity and the quality of the product can be controlled between certain limits by changing: (1) the type of metal catalyst or their composition; (2) the applied carrier/inert gas or its pressure; (3) the furnace temperature or (4) the laser parameters. The metal added to the target significantly influences the quantity of the formed nanotubes. Applying a Ni-Co mixture increases the yield: metal mixtures are more effective than single metal catalysts. This suggests that special properties of metal alloys formed when metal mixtures are used and this may have a crucial role in the formation of carbon nanotubes ***[34, 81-83]***.

II.3.3. Chemical Vapour Deposition (CVD) method for CNT synthesis

Carbon fibers have been produced by the catalytic decomposition of carbon-containing substances over metal surfaces for a long time. Numerous studies were published related to this topic also before the discovery of the C_{60} molecule ***[85-87]***. However, for a long time there was no evidence that this method could possibly produce carbon nanotubes as well.
Yacaman et al. ***[88]*** and Ivanov and co-workers ***[89]*** reported first on the successful synthesis of multiwalled carbon nanotubes by the CVD method. Since then several types of the CVD method has been developed applying various reaction conditions. In 1996 Dai and co-workers ***[90]*** and Fonseca et al. ***[91]*** managed to develop a version of the CVD process that led to the production of SWCNTs. Due to its simplicity, relatively low reaction temperature, and the

easy control of the reaction parameters today the catalytic chemical vapour deposition (CCVD) method is considered the most effective and economic way of producing carbon nanotubes on large-scale for industrial applications (Nanocyl).

In principle, the catalytic chemical vapour deposition is the catalytic decomposition of a hydrocarbon or carbon monoxide over a transition metal catalyst. In most of the experiments the carbon source was diluted by the addition of an inert gas (N_2, Ar, He) and the synthesis reaction was carried out at relatively low temperatures: 700-900°C. The experimental setup consisted of a reactor placed in a furnace heated to the reaction temperature of the synthesis. The catalyst was placed in a quartz-, ceramic- or metal boat that can resist the high temperature and the reductive reaction conditions. Figure II.14. shows the general scheme of the experimental setup used for the different types of CVD processes ***[92]***.

The furnace can be vertical or horizontal, the latter one is more frequently used. The vertical furnace is usually applied for the continuous CNT production. In this case the catalyst and the carbon source are injected at the top of the furnace, and the product is collected at the bottom of the chamber. Ultrafine metal catalyst particles can either be introduced into the reactor directly or formed in-situ from metallocenes. The fluidized bed reactor is a variation of the vertical furnace. Generally an upward flow of the carbon feedstock gases is used while the catalysts are placed in the centre of the reactor.

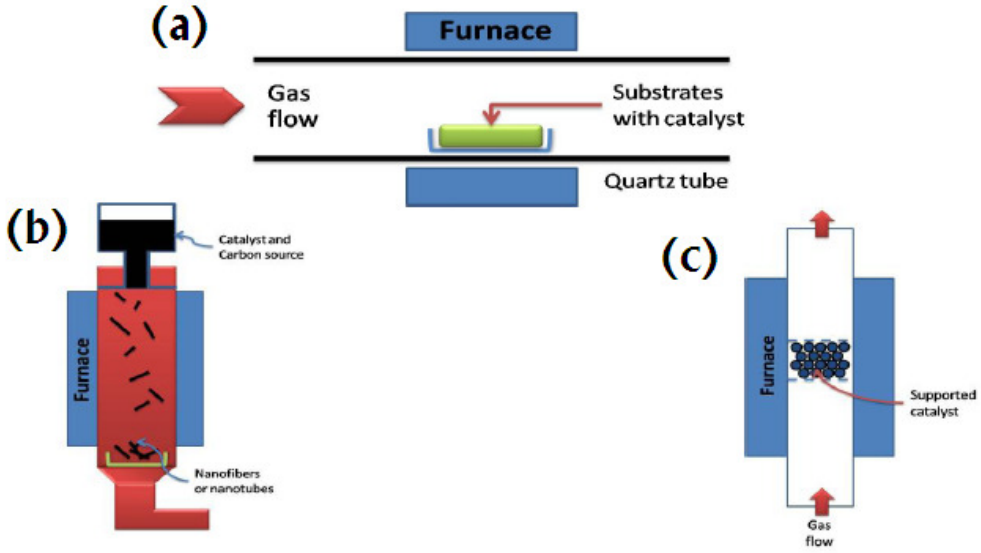

Figure II.14.: Schematic demonstration of the CVD setup: a) horizontal furnace; b) vertical furnace; c) fluidized bed reactor

CVD can produce various carbonaceous structures, such as amorphous carbon layers, filaments of amorphous carbon, graphite layers covering metal particles, carbon fibers, multiwalled carbon nanotubes and singlewalled carbon nanotubes. The CVD method allows the selective CNT growth in different forms, for example powder form ***[93, 94]*** or aligned forests ***[95, 96]*** of CNTs. The produced tubes can be found alone or in bundles, they can be straight or helically coiled with a constant coil pitch. Carbon nanotubes synthesized with this method may have amorphous carbon coating, and metal catalyst particles sometimes can be found inside the tubes (Figure II.15.) or at their tips. The possibility of growing CNTs from controlled surface sites permits applications such as field-emission displays, probe tips of scanning probe microscopes, or the construction of a specific nanotube device ***[97-99]***. The growth of planar arrays of aligned carbon nanotubes over large areas with high density on single-crystal substrates of sapphire and quartz enable their easy integration into high-performance planar devices.

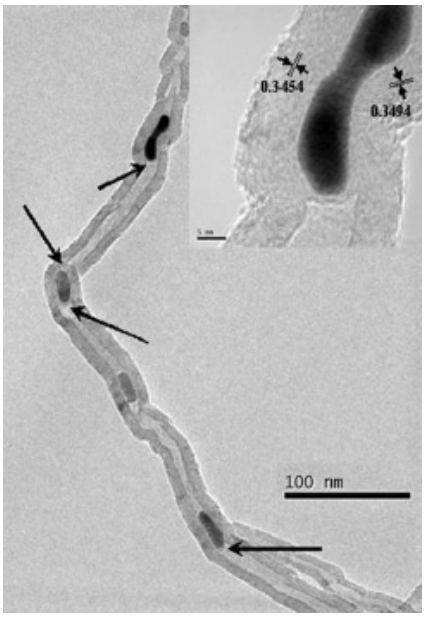

Figure II.15.: TEM micrograph of metal filled carbon nanotube obtained by the decomposition of methane on Ni/Y/Cu catalyst ***[110]***

Numerous gases and liquid-phase carbon sources have been used for the synthesis of carbon nanotubes by the CVD process. The carbon sources can be hydrocarbon gases such as methane, ethylene or acetylene, alcohols or aromatic compounds like benzene or xylene. The liquid phase carbon sources have to be vaporised before entering the reaction chamber. To avoid the oxidation of the carbon source a reductive environment has to be maintained. Thus

oxygen is generally evacuated from the reaction chamber by an inert gas flow that can remain the whole duration of the reaction. Nitrogen, helium and argon are the most frequently used gases to provide the inert atmosphere ***[123-128]***.

Recently, polymers were also applied to synthesize graphitic carbonaceous nanomaterials. Carbon nanotubes, graphite films and carbon fibers were produced by the pyrolysis of polyacrylonitrile (PAN) ***[129-131]*** and polypyrrole (PPy) ***[132-135]***. Table II.1. gives some examples of different CVD processes applying various reaction conditions, and the obtained products.

Method	Carbon source, catalyst	Product	References
Microwave plasma-enhanced	Fe/sapphire, Ni/Fe/glass, Cr/Fe/glass, stainless steel or Fe/Si substrates	Curved nanotubes with inhomogeneous diameters, aligned nanotubes	***[100]***
Hot filament enhanced CVD	With and without silica support	Vertically and perpendicularly aligned MWCNTs, SWCNTs	***[101]***
Water-assisted CVD	With buffer layer	Vertically aligned SWCNTs, DWCNTs	***[102]***
O_2-assisted plasma enhanced	$Fe/SiO_2/Si$		***[103]***
Simple CVD	Acetylene, titanate modified polygorskite	Filled CNTs, Fe_3C nanowires	***[104]***
	Toluene, without catalyst	Carbon spheres with ball-like, chain-like morphology	***[105]***
	Fe-Mo/MgO; Fe/MgO	SWCNTs, DWCNTs	***[106-109]***
	Ni/Y/Cu, methane	Metal filled CNTs, carbon onions, bamboo-shaped CNTs	***[110-111]***
Hot wire CVD	CH_4, Ni catalyst	3D double-helix microcoils	***[112]***
Hot filament enhanced CVD	$Fe\text{-}Co/SiO_2$	Perpendiculary or vertically aligned SWCNTs, MWCNTs	***[113]***
Alcohol CVD	Ferrocene-ethanol	High purity SWCNTs	***[115]***
	Cu/MgO	CNTs of multibranched morphology	***[116]***
Radio frequency enhanced CVD	Different substrates without catalyst	Carbon nanosheets, CNTs	***[117]***
DC-PECVD,	Fe/glass, CO/Ar; $CO/Ar/O_2$; $CO/Ar/H_2$	Carbon fibres; fibres bundling	***[118]***
High-power laser pulse alcohol CVD	Solid metal target	SWCNTs	***[119]***
Injection CVD	Quartz substrate, ferrocene/toluene	MWCNT films	***[120]***
Ultrasonic spray pyrolysis	Co-Mo/silicon substrate, ethanol	SWNTs d=0.8-1.2 nm	***[121]***
Alcohol CVD	Co-Mo/silicon substrate/ethanol	Individuals, grasses and forests of SWCNTs and MWCNTs	***[122]***

Table II.1.: Products obtained by different CVD methods

II.3.3.1. The catalyst in the CVD method

a) *The metal catalyst*

Numerous transition metals individually or in mixture, and rare earth promoters have been used in the CVD synthesis of MWCNTs and SWCNTs. Rare earth oxides can act as co-catalysts improving the catalytic activity and selectivity during the synthesis. The metallic catalyst can influence the growth process and morphology of the carbon nanotubes. Fe, Co, Mo and Ni are the most commonly used metal catalysts for the CNT synthesis ***[90, 123, 136]***.

b) *Catalyst Support*

Applying a support material for the better distribution of the catalyst, or the stabilization of the metal nanoparticles is important during the synthesis process. Metal oxides and carbides without any support material were tested in the catalytic decomposition of acetylene, however the results showed insufficient activity and selectivity ***[34]***. Zeolites, different forms of silica, alumina, MgO, are the most commonly applied catalyst supports. Although silica-gel and different zeolites have high pore volume, due to the pore size and the size of the nanotube diameter, only the external surface of these materials can be exploited in the CNT synthesis. During the catalyst preparation, metal catalyst particles are formed also in the inner pores, thus the decomposition of acetylene occurs also in the inner pores, however in this case no CNTs are formed. MgO supports have the advantages of easy removal by a simple hydrochloric acid treatment while the other above mentioned supports can be removed by harsh hydrofluoric acid treatment. The Fe-Mo/MgO catalyst was found to be the most effective catalyst combination for the synthesis of SWCNTs and DWCNTs ***[137-140]***. Quite pure MWCNTs can be synthesized in large quantities by the catalytic decomposition of methane on Co-Mo/MgO catalysts ***[141]***.

c) *The substrate*

Applying substrates as support material has the advantage of the controllability of the metal nanoparticle sizes, and their dispersion, hence the nanotube diameters and the morphology of the grown nanotubes. The preparation of the substrate and the catalyst is extremely important

as it determines the structure of the nanotubes. Generally, silica, alumina and glass substrates are used. When silica is used as a substrate metal-silicides are formed during the preheating. This complicates the synthesis process. Buffer-layers have been used previously to prevent the metal-silicide formation.

Metal nanoparticles: Fe; Co or Ni can be deposited on the substrate from a solution, by electron beam evaporation or by physical sputtering. As the nanotube diameter depends on the catalyst particle size, it is also highly influenced by the choice of the catalyst deposition technique. The ability to control the nanotube diameter is fundamental for the development of nanodevices. Porus silicon is an adequate support material for the growth of self-oriented nanotubes on large surfaces. Applying this substrate nanotubes are better aligned and produced with higher yield. Well-graphitized, free-standing nanotube arrays can be produced on hexagonal close-packed nano-channel alumina templates with Ni-Co catalyst. The advantage of this template method is the extraordinary controllability of the tube diameter ***[142]***.

Guo and co-workers found that the diameter of the CNTs depends on the thickness of the deposited metal film on the substrate. This way the size of the metal catalyst particles can be controlled, and this is a key parameter for the CNT growth especially for the SWCNT production. Thickness values of 2, 5 and 10 nm lead to the growth of CNTs with diameters of 5-8, 20 and 80 nm, respectively. CNTs with large diameters grow aligned while thinner nanotubes grow across the surface ***[143]***.

d) Gas phase metal catalyst

The catalyst can be introduced into the reactor also in the gas phase. This can be advantageous for the large-scale synthesis of CNTs since nanotubes are free of catalyst supports and the reaction can be operated continuously ***[142]***. In the injection CVD or pyrolysis method a metallocene-hydrocarbon solution is pumped or sprayed into the reactor. Thus there is no need for the catalyst synthesis step: the catalyst particles are formed in-situ continuously during the whole synthesis. This simplifies the CNT synthesis and gives the possibility to scale-up the method and permits continuous or semi-continuous operation.

Horváth et al. tested different metallocenes (ferrocene, cobaltocene and nickelocene) and various hydrocarbons (benzene, toluene, xylene, cyclohexane, n-pentane, n-hexane, n-heptane and n-octane) in the spray-pyrolysis method for the synthesis of CNTs. The ferrocene-nickelocene catalyst led to the highest yield, while xylene was found to be the most efficient

carbon source in the applied reaction conditions. The synthesis product consisted of mainly straight nanotubes with negligible amount of amorphous carbon ***[144]***. Aligned MWCNT films were synthesized on quartz substrate by injection CVD method. A ferrocene/toluene mixture was introduced in the reactor, and the growth of well-aligned MWCNT films (Figure II.16.) was observed at different synthesis temperatures between 590-850 °C.

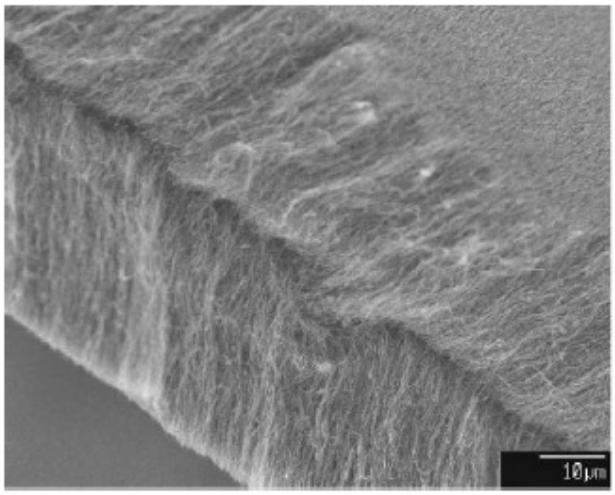

Figure II.16.: Aligned MWCNT film grown at 740 ºC on a quartz substrate by injection CVD method using a ferrocene/toluene mixture ***[120]***

Varying the synthesis conditions the following was observed: (a) longer nanotubes are formed when the injection time is longer, (b) increasing the ferrocene concentration leads to the increase of the nanotube diameter, broadening of the diameter distribution and increased formation of encapsulated nanoparticles, and (c) when higher reaction temperatures were applied unaligned CNTs with diameters around 46 nm were formed ***[120].***

II.3.3.2. Different types of CVD

To enhance the productivity and the selectivity of the CVD method different types of this synthesis process have been developed recently. Besides the commonly used thermal CVD process carbon nanotubes were produced by hot-filament CVD method (HF-CVD); plasma-enhanced CVD (PE-CVD); microwave-plasma (MP-CVD) or radiofrequency technique ***[145, 146]***. Figure II.17. shows the scheme of the apparatus used in different types of CVD methods.

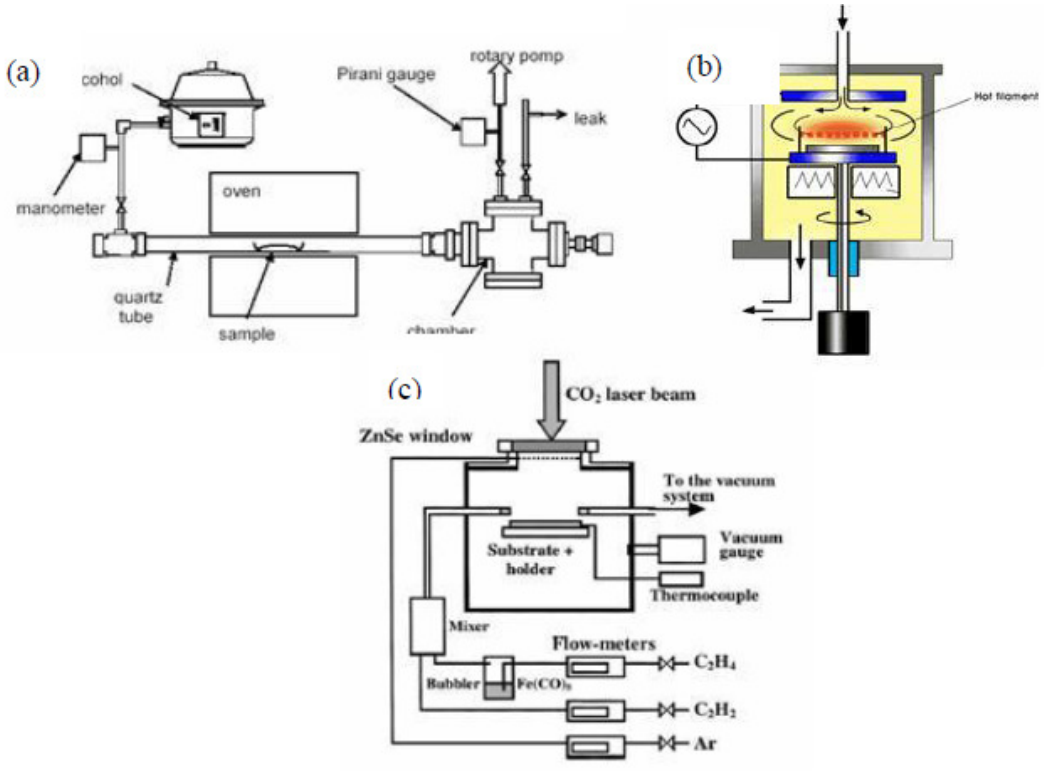

Figure II.17.: Schematic setup of different types of CVD technique: a) Alcohol-CVD; b) Plasma-enhanced CVD; c) Laser-assisted CVD

Aligned nanotubes can be grown on various substrates by thermal CVD and plasma-enhanced CVD, while CNTs with different orientations can be produced by microwave-plasma CVD. The most frequently used substrates are: Ni, Si, SiO_2, Cu/Ti/Si, stainless steel, glass.

CNTs were synthesized by the MP-CVD method applying different substrates. Applying Fe/sapphire, Ni/Fe/glass or Cr/Fe/glass curved nanotubes with inhomogeneous diameters were grown, while the aligned nanotubes were formed on stainless steel or Fe/Si substrates. Samples synthesized on Fe/Si substrate were free of amorphous carbon, hence the so-produced CNTs can be used directly without any purification ***[100]***.

Hot filament enhanced CVD technique is widely used for the deposition of diamond films from a hydrocarbon/H_2 mixture. The filament is placed near the substrate to heat the entering gases and often also the substrate itself. Metallic or carbon filaments can be used. While the first one can possibly cause contamination the latter one is more advantageous as it can promote the formation of amorphous carbon or CNTs; it does not undergo distortions due to

carbide-formation, and does not sag at the high operating temperatures. The Si support, the gas composition and pressure have significant influence on the synthesized product.

When using a catalyst film without Si-support MWCNTs were formed with diameters larger than 20 nm. The MWCNTs were perpendicularly aligned, when applying a thin catalyst film, while vertically aligned and highly dense MWCNTs were formed on thicker catalyst films. When silica support was used MWCNTs and SWCNTs were both synthesized depending on the reaction parameters. The formation of SWCNTs was achieved at relatively low temperatures applying low carbon supply ***[101]***.

Vertically aligned SWCNTs and DWCNTs were grown in high yield with water-assisted CVD ***[102]***, oxygen-assisted plasma-enhanced CVD ***[103]*** and microwave-assisted plasma enhanced CVD technique ***[147].*** Buffer layers were applied in each case. Hiramatsu et al. synthesized vertically aligned SWCNTs by MP-CVD using a mixture of Co-Ti nanoparticles deposited on a Si substrate without buffer layer ***[148]***.

The alcohol-CVD method is another widely used process. Ferrocene solution is often applied as catalyst as well as ethanol with different ratios. Also in this case the reaction parameters determine the quality and the quantity of the product. With the optimisation of the reaction conditions high purity SWCNTs can be obtained. Studies revealed that increasing the carrier gas flow rate leads to the formation of longer CNTs until a certain limit. The ferrocene/ethanol ratio is also a key parameter. Too low ferrocene concentration causes the formation of high amount of amorphous carbon, while when the concentration of ferrocene is too high, high amount of nanoparticles are formed. However, no direct effect of ferrocene concentration on tube diameters was found ***[114]***. This method was improved in a way that high-power laser pulse is used for the vaporisation of a metal target. Using Co catalyst and ethanol as carbon source the SWCNTs with diameters between 0.96-1.68 nm were synthesized. SWCNTs produced with different metal rods (Ni, Ni/Co, Fe) had very similar diameter distribution ***[131].***

Maruyama et al. studied the relationship among the nominal thickness of Co and Co-Mo catalysts, the structure of the catalyst particles, and the structure of the CNTs synthesized by alcohol-CVD method ***[122]***. The authors hypothesized that the different morphologies of CNTs: individual CNTs, random networks parallel to the substrate surface and vertically aligned forests of SWCNTs and MWCNTs can be produced by varying only the nominal thickness of the metal catalyst using the same reaction conditions. The different morphologies at the same growth time were due to the different areal density rather than the length of CNTs. Increasing the nominal thickness of the catalyst the diameter of the catalyst particles changed

while their areal density remained constant. However, it was found that longer growth time can also cause change in the morphology of the product. Optimizing the synthesis conditions for the growth of aligned SWCNT forests using Co/Mo catalyst lead to not one but a few "optimums". For example, using a 1.6/1.0 Co/Mo ratio high catalytic activity was observed at 847°C while at 947°C the activity was reduced, while when the Co/Mo ratio was 1/3 the catalyst activity was higher at this latter temperature. Similar results were obtained for the flow rate. The Mo is supposed to suppress the broadening of the diameter distribution of the SWCNT product ***[149]***.

Single-walled carbon nanotubes were synthesized by ultrasonic spray pyrolysis of ethanol applying Co-Fe/zeolite catalyst ***[150]***. The advantages of this process are the following: (1) there is no need of a vacuum pump; (2) no hydrogen is needed for the formation of SWCNTs; (3) the experimental setup is simple; (4) the synthesis temperature is relatively low. The synthesis time and the catalyst concentration significantly affected the quality and the quantity of the product.

II.3.4. Hydrothermal CNT synthesis

Different carbonaceous nanostructures and also carbon nanotubes can be produced by the hydrothermal technique. The advantages of this method are the following: (a) the starting materials are easy to obtain and are stable at ambient temperature; (b) the low temperature of the process; (c) no hydrocarbon or carrier gas is needed. MWCNTs were produced by the hydrothermal method: a mixture of polyethylene and water with a Ni catalyst was heated from 700 to 800°C under 60-100 MPa pressure. Closed and open-ended nanotubes were produced, the number of walls varied from a few walls to more than 100 graphitic carbon layers. However, a typical characteristic of CNTs formed by this method is the small wall thickness and large inner core diameter ***[151]***. The same research group produced CNTs using ethylene glycol solution in the presence of Ni catalyst. TEM analysis of the so-produced CNTs show tubes with long and large inner core and Ni inclusions at the tube tips. Typically the wall thickness of CNTs produced by the hydrothermal process is between 7-25 nm while their outer diameter varies from 50 to 150 nm ***[152]***.

CNTs in large quantities were produced using the sonochemical/hydrothermal method by Manafi et al. They obtained 2-5 μm long tubes with diameters of about 60 nm. SEM analysis

revealed the uniform diameter distribution of the catalyst nanoparticles probably due to the ultrasonic pre-treatment of the starting solution ***[153]***.

Multiwalled carbon nanocells and carbon nanotubes were grown in hydrothermal fluids from amorphous carbon at low temperatures. Carbon nanocells were formed by interconnecting multiwalls of graphitic carbon at 600°C. The bulk sample made of hollow spherical cells macroscopically appears as disordered carbon. The nanotubes observed in the sample have diameters in the range of tens of nanometers while their length is in the range of hundreds of nanometers ***[154]***. Short carbon nanotubes and nanoonions were formed from nanoporous carbon in presence of elemental cesium at 50°C ***[155]***.

II.3.5. Electrolysis

This less commonly used synthesis method for the production of CNTs was developed by Hsu et al. in 1995 ***[156]***. The principle of this method is the electroextraction of alkali (Li, K, Na) or alkaline-earth (Mg, Ca) metals from their chloride salts on a graphite cathode followed by the formation of CNTs by the interaction of the depositing metal with the cathode. The optimum temperature for the synthesis is different for each electrolyte composition. Deviation from this optimal temperature value leads to decreasing purity of the CNT sample. In the case of NaCl and LiCl electrolytes the optimum T was just above the melting point of the salts. After the electrolysis the carbonaceous product can be retrieved by dissolving the ionic salt in water and subsequently filtering the dispersion. The cathode erodes during the synthesis. The obtained product contains different carbonaceous structures such as encapsulated metal nanoparticles, carbon fibers, amorphous carbon and carbon nanotubes. The obtained nanotubes are mainly MWCNTs, however Bai et al. managed to synthesize SWCNTs with this method. They synthesized carbon nanotubes by the electrolytic conversion of graphite into CNTs in fused NaCl at 810°C using Ar as inert gas. The diameters of the formed SWCNTs are between 1.3-1.6 nm. By the addition of metals or other salts of low melting point to the electrolyte metal nanowires and filled nanotubes grow. So-produced MWCNTs have diameters of 10-20 nm, are formed of few graphene layers and their length is over 500 nm ***[157]***.

The peculiarity of this method is that it happens in the condensed phase, and uses graphite as feedstock at relatively low temperatures. The method has numerous advantages such as the simplicity of the apparatus; the possibility to control the synthesis process by the electrolysis

modes; the use of cheap raw materials; the low energy consumption of the electrolysis; the possibility to control the structure and the morphology of the product by adjusting the electrolysis conditions, and the composition of the electrolytic bath ***[158-160]***.

Novoselova et al. reported of a novel electrolytic synthesis method for the production of carbonaceous nanomaterials from ionic melts. The proposed method is based on the cathodic reduction of CO_2 to elemental carbon on metallic electrodes. Thus a new condensed carbon phase is generated on the cathode from a liquid molten salt phase. Ternary mixture of alkali metal chlorides (NaCl/KCl/CsCl) was used as electrolyte. MWCNTs were grown with an outer tube diameter of 5-250 nm and the inner tube diameter between 2-140 nm. The nanotubes were generally curved and often formed bundles. They were partially filled with electrolyte salt. The authors found that increasing the current density resulted in a decrease in the diameter of the formed tubes and an increase in the carbon yield and the CNT content of the product ***[159]***.

Matveev et al. reported on the electrolytic production of CNTs at -40 °C in liquid NH_3 from acetylene without any metal catalyst. Acetylene was prepared by the hydrolysis of calcium carbide. Gaseous acetylene was conducted through a concentrated iron chloride water solution to be purified, and subsequently through a thick layer of fresh molten potassium-hydroxide flakes to clear away the water. It was subsequently dissolved in liquid ammonia. After the electrolysis the cathode was covered with a light grey porous layer. The obtained product consisted of graphitic, turbostratic and amorphous carbon and long multiwalled CNTs with average diameters of around 15 nm. The CNTs were irregularly curled and agglomerated into bunches ***[161]***.

II.3.6. CNT Synthesis by the Solar technique

The solar technique was used only for fullerene production until 1996. Laplaze et al. reported the production of CNTs using concentrated solar light. The advantages of this method are: (a) the use of solar light for the vaporization of the target; (b) the relatively easy controllability of the synthesis parameters. Figure II.18. represents an experimental solar technique setup used in CNTs production. The incident concentrated solar energy vaporises the carbon and catalyst mixture. A parabolic mirror positioned above the chamber focussed the collected sunlight on the top of the target material. The target rod was a graphite cylinder in which holes were drilled where a mixture of graphite and catalyst powders was inserted. The pressure was

maintained by a high-flow vacuum pump. The buffer gas (Ar or He) entered around the perimeter of the quartz window and swept its interior surface preventing the condensation of carbon and catalyst vapours. The vaporization temperature was between 2627-2727 °C ***[162].***

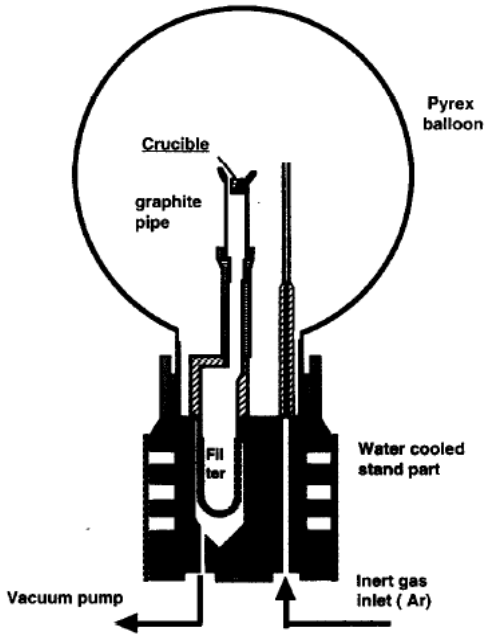

Figure II.18.: The experimental setup described by Laplaze and co-workers
The graphite crucible is filled with the mixture of powdered carbon and catalysts. Carbon nanotubes are deposited onto the graphite pipe where the temperature is highest of overall condensing zone ***[162]***

SWCNTs were produced in gram quantities by Luxembourg et al. using a 50 kW solar reactor. The experimental setup was installed at the focus of a 1 MW solar furnace. The effect of different process parameters (target length, buffer gas, sample collector location) on the sample quality was studied by the authors. The influence of the buffer gas was found to be dominant. When applying He the quality of the produced material ameliorated with the increasing target length, while when Ar was used poor quality samples were produced. The product with the highest quality was obtained using Ni-Co catalyst (2%-2%) in He atmosphere and a target length of 15 cm. The produced SWCNTs have diameters around 1.2-1.6 nm ***[163]***.

II.4. Coiled Carbon Nanotubes

The morphology of a helically coiled carbon nanotube can be described by the coil diameter and the coil pitch (the distance between adjacent corresponding points along the axis of the helix). A schematic image of a coiled carbon nanotube with its characteristics is shown in Figure II.19. According to the observations the helically coiled carbon nanotubes are multiwalled CNTs, their coil diameter can vary from 10 nm to 500 nm and the coil pitch between 1 nm and 500 nm ***[164-166]***. Experimental studies revealed that the values of both coil characteristics are mainly found in the range of 20-200 nm but sometimes there are some exceptions also. Many theoretical calculations and computational models have been engaged in the study of formation possibilities of these very peculiar structures. There are research groups who believe in joining the straight segments built up only by hexagonal lattice with knees consisting of pentagon-heptagon pairs. The other researchers suggest that the structure of helices have linear curvatures. Recently, experimental data from TEM analysis of the helical CNTs (HCNTs) seem to confirm both hypotheses ***[164-166]***. This argument will be discussed in the following paragraphs. Their interesting structure and hardly explainable growth mechanism made them an interesting field of research since their discovery.

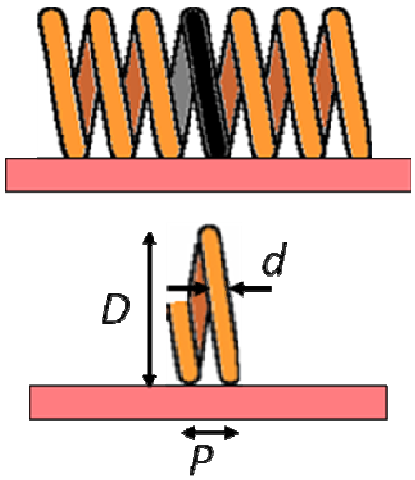

Figure II.19.: Coil diamter (D), coil pitch (P) and nanotube outer diameter (d) of a helically coiled carbon nanotube ***[167]***

II.4.1. Theoretical calculations of coiled CNTs

Coiled carbon nanofibers have been already observed in 1972 by Baker et al. ***[168]*** the possible formation of helically coiled carbon nanotubes was described by Dunlap and Ihara et al. in the early nineties ***[169-172]***. According to their hypothesis two straight nanotubes that have the same diameter can be connected by a so called "knee*"* under a defined angle. These "knee"-s are formed by inserting a five- and a seven-membered ring-pair along a diameter creating positively and negatively curved surfaces. The five-membered rings are situated at the convex side, the seven-membered rings are found at the concave site of the nanotube. The so-formed nanotube intersections form a 30° angle at the joining point ***[173]***. Later Fonseca et al. proved this angle to be of 36° with 3-dimensional modelling ***[174]***. Itoh and Ihara developed a model starting from the structure of the C_{60} fullerene where the bent or coil-shaped carbon nanotubes form irregular toruses. A torus is a particular case of a helix with a zero pitch ***[175]***. To form a torus the insertion of pentagons, and heptagons is indispensable. The toruses were taken to smaller units and reconstructed in a way that they form a certain angle with the main axis of the tube. The properties of the so-generated spirals (Figure II.20.) depended mainly of the type of the starting torus ***[172, 176]***. First toruses with different diameters were built up, and divided into five groups considering the following key parameters: the ratio of inner and outer diameter, and the height. Ordinary and elongated toruses were used to construct coil-shaped structures (Figure II.20.). As five- and seven-membered rings have distributing function, the electronic properties depend strongly on the pattern at the nanotube ends. This effect can give peculiar electronic properties to coiled structures that do not characterize straight nanotubes.

Zhang and co-workers constructed ball-stick and molecular models of small tubules and attempted to connect them at angles of 30° by introducing pairs of fivefold and sevenfold rings as previously suggested by Dunlap ***[165]***. Figure II.21. shows molecular models of single- and doublewalled carbon nanotubes with inserted pentagon-heptagon pairs.

Su et al. studied the shape formation of CNTs and put down a string equation for the possible existing shapes of the axis curve of MWCNTs. They showed that there was a threshold condition for the formation of straight multiwalled carbon nanotubes, below which straight MWCNTs are not stable and the structure undergoes shape deformation. The optimal ratio of pitch and radius was found to be 2π in good agreement with the results previously obtained by electron diffraction ***[165, 178,179]***.

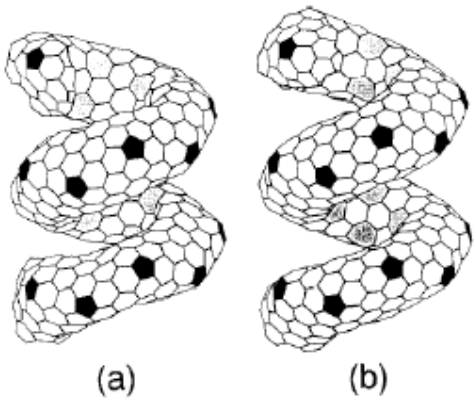

Figure II.20.: Helically Coiled C_{360} one pitch contains a torus C_{360}: a) coil length=12.9 Å and b) coil length=13.23 Å. The tilting pattern of the heptagons in the inner ridge line is changed though the pattern of the outer ridge line remains upon changing the coil length ***[177]***

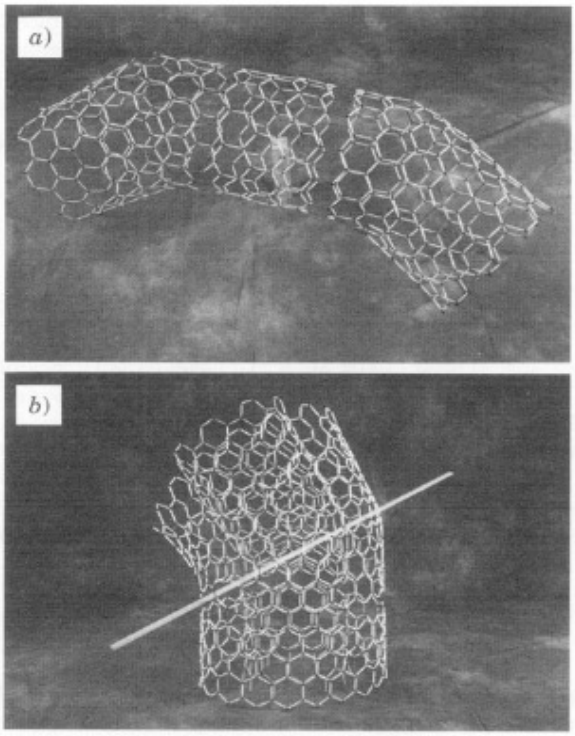

Figure II.21.: Molecular models of a) monolayer and b) double-layer polygonized tubules: a) shows two 30°connections; b) illustrates the feasibility of multiwalled tubule with fivefold and sevenfold rings aligned and a distance of 0.34 nm between the layers

Based on energetic and thermodynamic calculations, the possible existence of various forms of helically coiled and toroidal structures was described ***[180,181]***. The variety of the patterns in the inner and outer surface of these structures suggest that numerous other stable cage carbon structures may exist. Itoh and Ihara also demonstrated that the molecules in a one-dimensional chain, or a two-dimensional plane or a three-dimensional supermolecule are possible extended structures of tori. Coils might be able to transform into other forms. It would be interesting if the proposed structures and their different combinations of helix and toroidal forms could be constructed in a controlled way from the graphitic carbon cage. Structures like helical coiling around the tube, nested helical form and/or supercoils observed in biological systems could be obtained with intriguing electrical and magnetic properties.

The high resolution transmission electron microscopy (HRTEM) images and electron diffraction studies made by Ivanov et al. ***[182]*** proved the theory of Dunlap that regular and irregular helix forms are created by connecting two straight tubes with a knee.

Fonseca et al. developed and examined models of various possible knees and tubule-connections leading to curved nanotubes, tori or coils based on Dunlap's theory ***[169-171]*** of the insertion of heptagon-pentagon pairs ***[174]***. They proposed a possible explanation to the formation of both perfect tubules, tubule-connections, and bent, torus-formed or coil-like nanotubes based on the models of concentric tubules at distances close to the characteristic graphite distance with various types of knees. The perfectly graphitizable knees are described and relations are established between the tubes and the graphitic layers. The authors call the described series of knees perfectly graphitizable because the difference of diameter between the two connected segments of each knee is constant for all the series. An example is presented in Figure II.22.

According to theoretical studies carbon toroids can be generated either by introducing defects (Stones-Wales defects) as in the case of the coiled carbon nanotubes or by elastically bending a straight CNT in a way that it closes upon itself. The lower limit for the diameter in this second case was found to be 200 nm ***[178, 183,184].*** Carbon nanotube rings with an average diameter of 0.5 μm were observed with atomic force microscopy and scanning electron microscopy in carbon nanotube deposits produced by the catalytic decomposition of acetylene over a Co/NaY zeolite catalyst. The ring structures had the thickness varying from 2 to 20 nm. Some structural inhomogeneities were found on the observed rings which cast doubts about the hypothesis that carbon ring structures are perfect toroids. However, the obtained results are not sufficient to decide whether the rings are small coils or toroids ***[164]***.

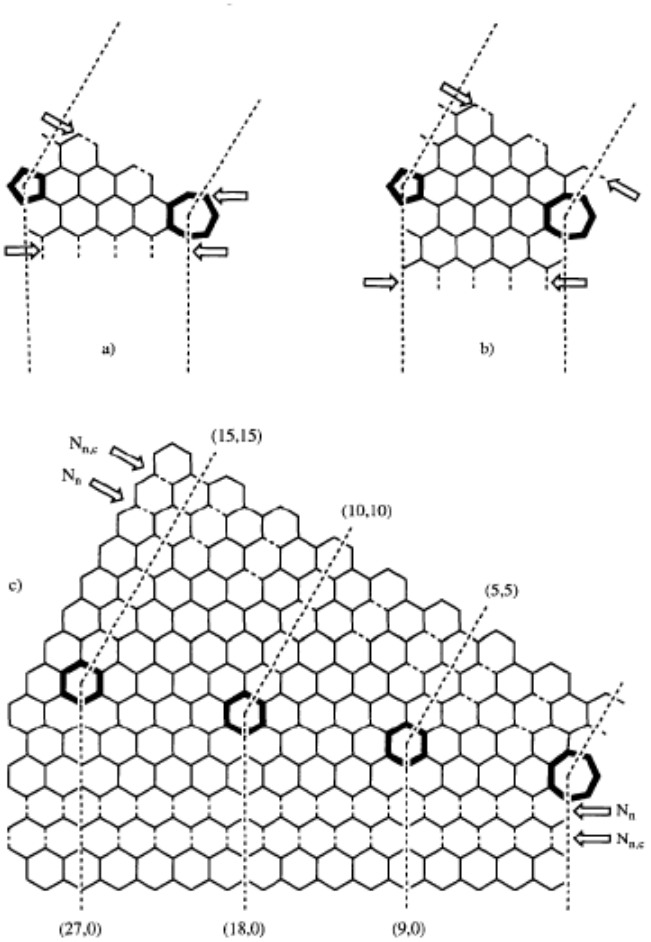

Figure II.22.: Planar presentation of (9n, 0)-(5n, 5n) knees, having a 36° bend angle generated by the insertion of fivefold and sevenfold rings. The dotted lines indicate where the knee is connected to the straight tubule: a) N_n knee where n=1; b) stretched knee n=1, c=38; c) general N_n and $N_{n,c}$ knees ***[174]***

II.4.2. Haeckelite-type nanostructures

Ernst Haeckel, in the nineteenth century pointed out the existence of peculiar structures in the nature in his book Radiolaria. Forasmuch the structures developed by Terrones and co-workers ***[185]*** from various points of views are similar to those described by Haeckel, they were given the name: *"Haeckelites"*.

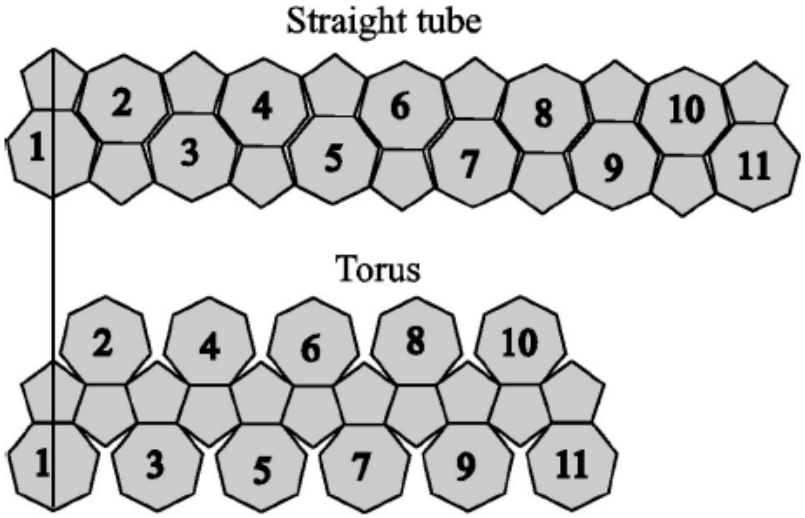

Figure II.23.: Azulenoid stripes containing both 11 units the upper one gives a straight tube, while the other a torus. The arrangement of the polygons results in different 3D structures by the proposition of László and Rassat ***[186, 187]***.

László and Rassat ***[186]*** proposed toroidal azulenoid structures where the strain energy was minimalized with appropriate distribution of fivefold and sevenfold rings on the toroidal surface. An azulenoid unit is built up from pentagon-heptagon pairs the combinations of which can form various structures. The presented structure resembles to the one that is used to generate haeckelite nanotubes, which are built of approximately equal number of pentagons, heptagons and hexagons, but form straight cylinders. Biró and co-workers ***[187]*** published a similar structure based on the azulenoid torus proposed by the above-mentioned authors ***[186]***. The planar representation of two azulenoid stripes shown in Figure II.23. are both built up from 11 azulenoid units, though the first disposition leads to the formation of a straight tube, while the second one generates a half torus. The authors underlined that structures like the torus constructed from the azulenoid stripe in Figure II.23. are unlikely to be stable in reality for the sake of the stress in the C-C bond caused by the strong curvature. They proposed the insertion of hexagons into the structure to widen the stripe (Figure II.24.).

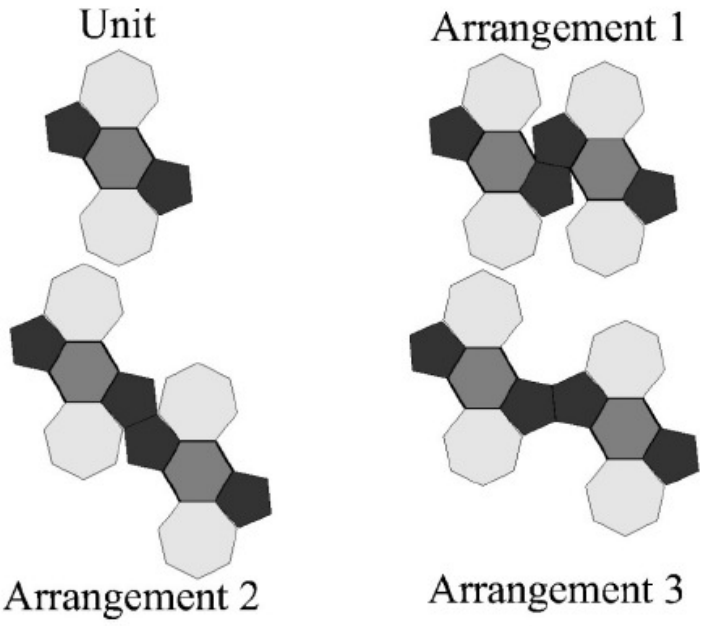

Figure II.24.: 5,7-1x6 unit generated from two azulenoid units linked by a hexagon, and three possible ways of assembling this unit in stripes ***[187]***.

Joining repeatedly units presented in Figure II.24. a stripe similar to the one presented in Figure II.25.a) can be obtained. However to further widen the stripe more hexagons (2, 3, etc.) can be introduced (Figure II.25.b)-c)). Closing these stripes following the closing rules (Table II.2.) bowl-like shapes, toroids, coils, double-helices or curled necklace-formed nanotubes were obtained, while joining several stripes leads to the formation of sheets. In the case of these structures the coiling appears naturally by rolling-up these haeckelite-like stripes. The influence of the hexagonal/non-hexagonal ring ratio on the stability of the created structures was pointed out. The conclusion was that coils built-up applying a non-hexagonal/hexagonal ring ratio higher than 1 are possible. This result is in accordance with the calculations made by Terrones et al. who claimed that haeckelite structures built with a non-hexagonal/hexagonal ring ratio higher than one can be energetically more stable than C_{60} ***[185]***.

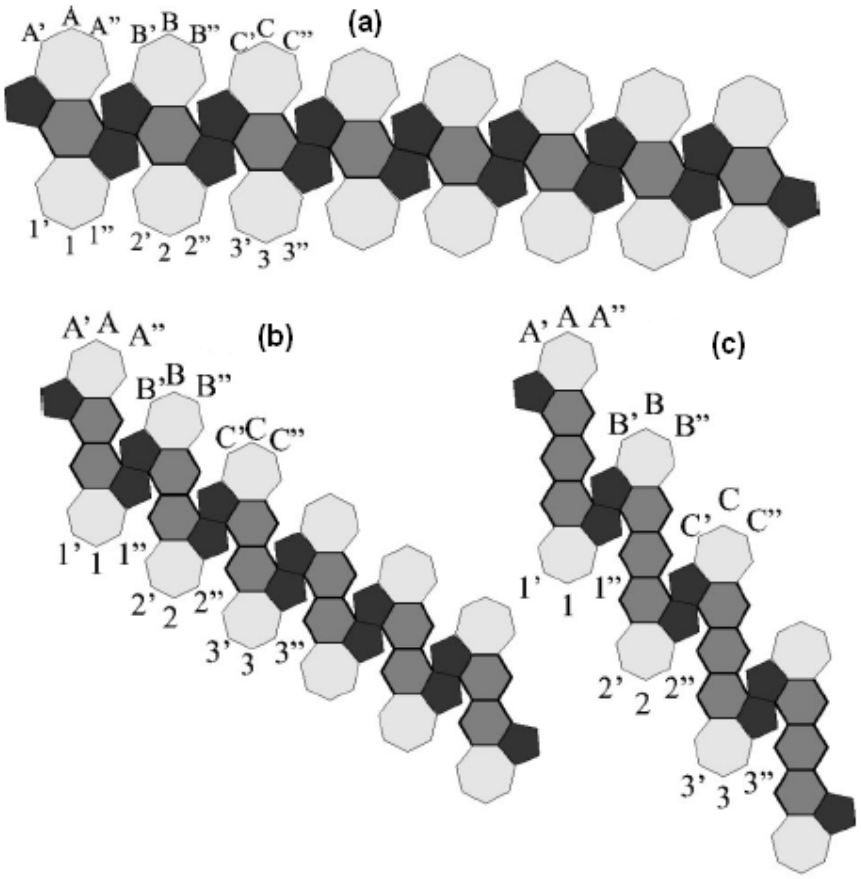

Figure II.25.: Azulene stripes: (a): 5,7-1x6; (b) 5,7-2x6 and (c) 5,7-3x6. Following the closing rules different structures are formed when rolling-up the stripe.

Stripe or sheet	Closing rule	3D structure
5,7-1x6	1' to A 1 to A' 1' to B 1 to B'' 1' to C 1 to C'	Right hand coil Curled tube Curled tube
5,7-2x6	1' to A 1 to A'' 1' to B 1 to B'' 1' to C 1 to C''	Curled tube Left hand coil Right hand coil
5,7-3x6	1' to A 1 to A'' 1' to B 1 to B'' 1' to C 1 to C''	Curled tube Curled tube Right hand coil
2x(5,7-1x6)	1'(II) to C(I) 1(II) to C1(I)	Double helix

Table II.2.: Closing rules of azulene stripes and the created 3D structures

The Haeckelite-type carbon nanotubes are generated by rolling-up a two-dimensional three-fold coordinated carbon network composed of an equal number of pentagons and heptagons and an arbitrary number of hexagons. There are three models of Haeckelite structures (Figure II.26.) that are formed from the following units:

- Rectangular unit-cell with 4 azulenes without hexagons ($R_{5,7}$)
- Hexagonal unit-cell consisting of 3 azulenes and 2 hexagons ($H_{5,6,7}$)
- Oblique unit-cell with two azulenes and two hexagons ($O_{5,6,7}$) ***[164, 185].***

A rectangular unit cell is generated by the creation of Stones-Wales-type defects on the graphene sheet transforming pyrene like rings into two pairs of pentagons and heptagons. A hexagonal unit is constructed of repetitive units of three heptagons surrounded by alternating pentagons and hexagons. An oblique unit cell consists of fivefold and sevenfold rings bound together, surrounded by hexagons.

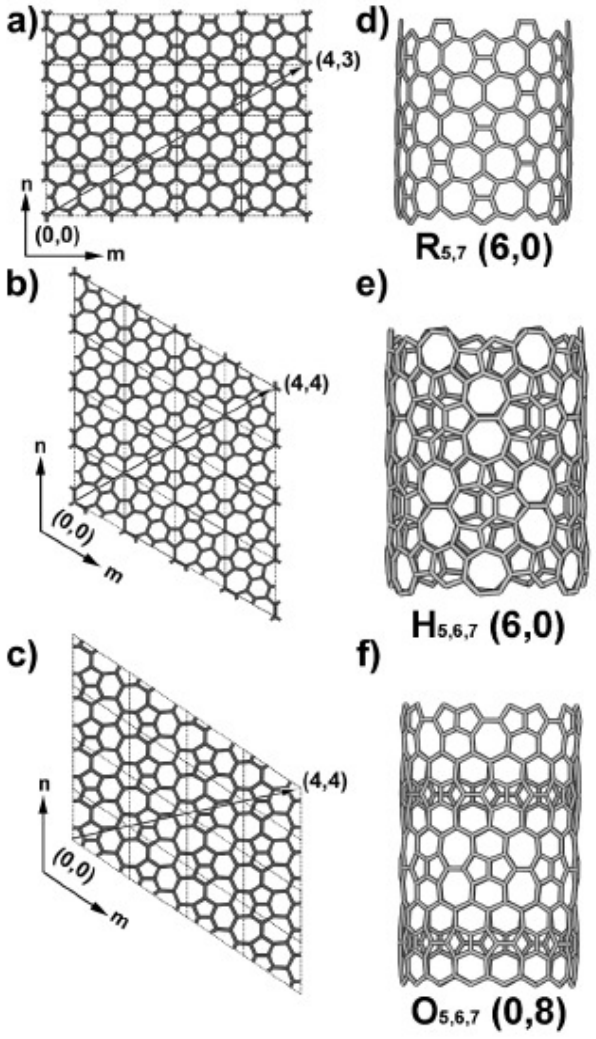

Figure II.26.: Haeckelite sheets consisting of various unit cells: a) rectangular; b) hexagonal; c) oblique ***[185]***

These models dispose of different symmetries. Energetically they are more stable than the C_{60} fullerene and less stable than the graphite. According to the experimental data the most stable structure is always the most symmetric one, thus the one where the pentagons are encircled by

heptagons and hexagons. Accordingly the isolated pentagons have crucial role in the Haeckelite structures.

Each planar structure is metallic, this means high density of states in the band gap. Their tension energy and mechanical properties are analogous to those of the graphene. Local density of states calculations revealed that the intrinsic metallic behaviour of the Haeckelite structures is independent of the orientation, the tube diameter or the chirality ***[189].***

László and Rassat proposed a structure where pentagon-heptagon pairs are joined head-to-tail inserting a certain number of hexagons in between. The process is illustrated by Figure II.27. where the insertion of three hexagons between the two azulene units shown by shaded surfaces, a1 and a2 are the primitive vectors of the lattice. Likewise the circumferential directions corresponding to the (n, 0), (n, n), (0, m) wrappings are indicated.

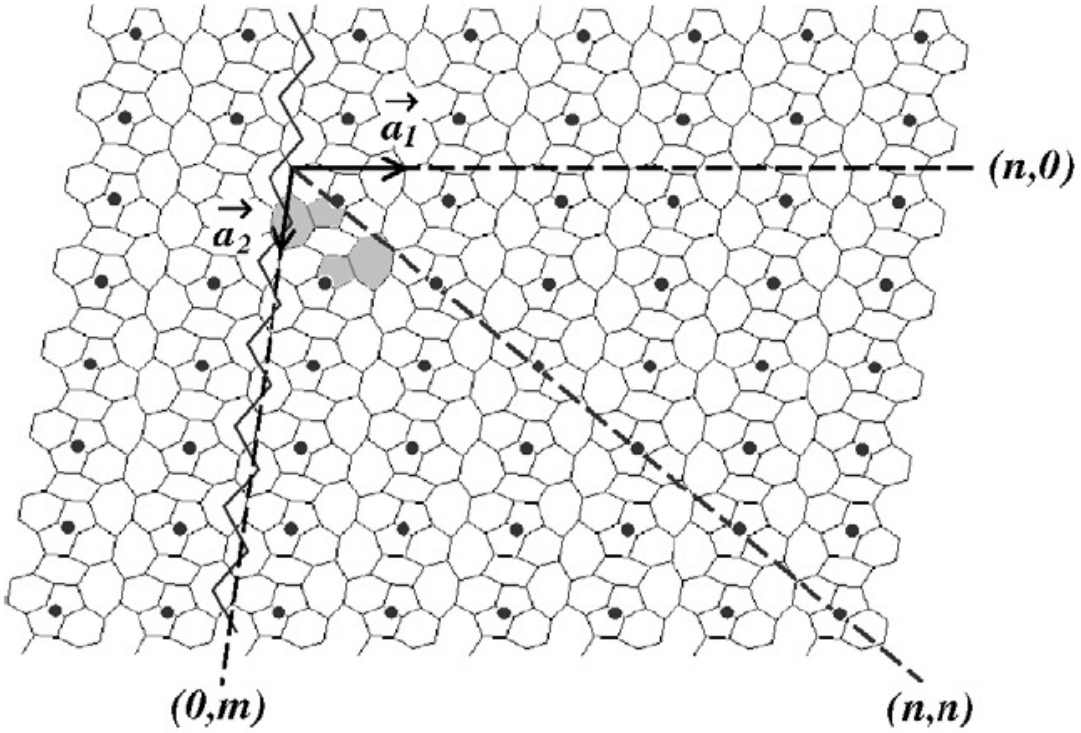

Figure II.27.: Planar periodic network containing two azulenes and three hexagons. The zig-zag line along a2 connects the centres of adjacent heptagons. The rows of heptagons are girdled by pentagon pairs whose common edges are marked with black dots. These bonds form the so-called stressors ***[188]***.

One of the presumptive reasons for the instability of this 2D structure are the pentagon-pentagon pairs. In Figure II.27. the bonds shared by two adjacent pentagons are marked with

black dots. These bonds have been called stressors ***[188-190]***. The reason is that in the tubular structures generated from the 2D pattern these bonds were placed in regions with strong local curvature and consequently high stress. Each unit cell contains one stressor. The pentagon-pentagon pairs are situated where there are convex curvatures. Another peculiar property of the Haeckelite nanotubes is the creation of heptagon-heptagon pairs. These form a kind of belt and are situated along a zig-zag line. Heptagons are situated at the concave side of the tubes. In Figure II.27. we can observe that the rows of heptagons are separated by stressor lines.

II.4.3. Haeckelite nanotubes

Lambin and co-workers modelled numerous different tubular structures created from the Haeckelite lattice. Haeckelite nanotubes can be constructed from the two-dimensional Haeckelite-pattern by rolling-up the sheet into a seamless cylinder. For energetical considerations in the applied model the nanotubes need relaxation after rolling-up the 2D lattice, which causes a strong reconstruction of the tubular structure in many cases. The nanotubes created in this way have no symmetry operations apart from screw operations ***[188 -190]***.

The simplest nanostructures are the nanotubes from the family (0, m). In this case the wrapping vector is parallel to the zig-zag chains of heptagons (Figure II.27.). There are also lines of stressors running parallel to the (0, m) direction causing protruding rings, while lines of heptagon rings lead to annular grooves in the structure. Small strain energy characterizes this family, the nanotubes have a form similar to a necklace of pearls, having the same structure there is a possibility of placing these (0, m) tubes inside one another therefore creating multiwalled necklace structures.

Just as in the case of the (0, m) family also for the (n, 0) and (n, n) Haeckelite nanotubes the stressor lines are parallel to the wrapping vector, but the zig-zag chains of heptagons are not parallel to the circumferential direction. In the planar development these chains of heptagons form an angle of 8° with the axis of the (n, 0) tubes, and a 32° angle in the (n, n) tubes. In the rolled-up structure these chains become helices. The families of (n, 0) and (0, n) tubes have numerous similarities. The (1, 0) tube for example has a spiral form and contains one stressor around its circumference. In the 2D structure the stressors form a line not parallel to the axis, which results in a helix in the rolled-up nanotube. The (1, 1) nanotube has a similar structure.

The (2, 0) and the (3, 0) nanotubes are straight nano-objects, they contain two and three stressor lines, respectively which equilibrate each-other. The (2, 2) and the (3, 3) tubes have similar morphology. In the (2, 2) structure the two stressor lines form slightly protruding features that spiral around the tube in opposite phases, separated by continuous grooves that also spiral around the tube. This is a double-screw structure similar to the one described by Biró et al. in a previous publication ***[187].***

The (n, m) nanotubes where n≠m and n, m≠0 are tubular-type structures where the number of stressor stripes in the structure is equal to nXm, however not all the stressors are "visible" when scanning along the tube axis ***[188-190]***.

Lambin et al. constructed different structures made from a Haeckelite lattice and modelled their electronic properties. Most of the observed structures behaved as semiconductors with a gap of approximately 0.6 eV, while some structures were metallic. The authors published also computed scanning tunneling microscopy (STM) images of the (3, 3) and the (0, 4) tube (Figure II.28.). However, the atomic structure cannot be described from the obtained topography due to the important perturbation of the density of states caused by the elevated number of heptagons and pentagons. The same authors computed also electron diffraction patterns of Haeckelite-nanotubes. As expected the patterns do not resemble the ones generated from graphene nanotubes ***[188]***.

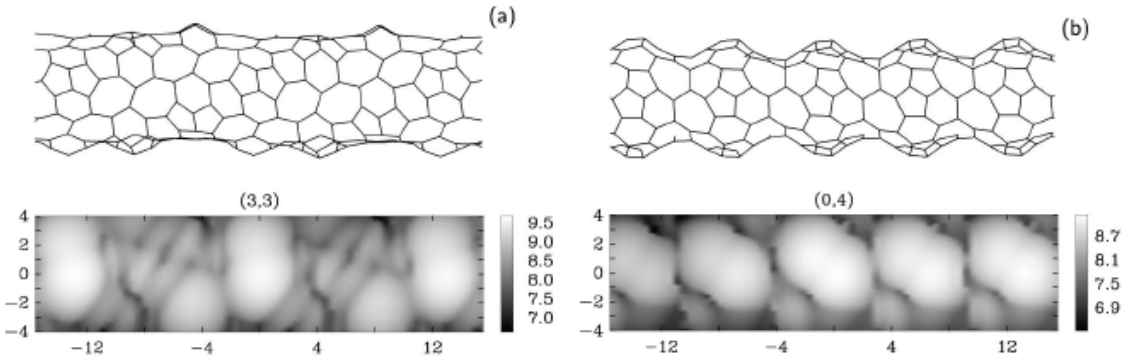

Figure II.28.: Computed STM images of two Haeckelite nanotubes: a) the (3, 3); and b) the (0, 4) one. A top view of the atomic structure can be seen above the STM image with the same scale along the axial direction.

Computational results were also compared to experimentally obtained carbon structures. The Haeckelite pattern may generate coiled, double-screw or necklace-like structures, which have been observed experimentally.

Pearl-necklace formed nanotube structures were observed in samples produced by thermal plasma process ***[191]*** and also by high-pressure carbon evaporation ***[192].*** HRTEM studies revealed the structure of the observed necklace nanostructures. They are assemblies of hollow rather spherical structures typically composed of eight concentric graphitic layers. A continuous graphitic layer consisting of approximately 10 graphitic walls surrounds the before-described spherical objects. Biró et al. claimed that these nanostructures are built from concentric ball-like elements which seem to be curved without any external constraint, and tentatively identified them with the theoretically predicted Haeckelites, though the dimensions of the observed structures are not in accordance with the computed results ***[188]***.

In previous studies of Biró et al. ***[193-195]*** single walled coiled CNTs and Y-branched nanostructures were observed and described. The CNTs were produced by decomposition of fullerenes at 450°C in the presence of Ni-nanoparticles using a HOPG (Highly Oriented Pyrolytic Graphite) substrate. The formation of carbon nanotube structures containing non-hexagonal rings may be ascribed partly to the template effect of the HOPG, partly to the low growth temperature. However, the fact that similar coiled nanotubes were found after chemical treatments can lead to the conclusion that non-hexagonal rings should not be considered as defects, but as regular building blocks of the lattice. This way coiled carbon nanotubes may be considered as structures built from the theoretically predicted haeckelite ***[193]***.

II.4.4. Growth Mechanism of coiled carbon nanotubes

When coiled carbon nanotubes were first experimentally observed Amelinckx et al. proposed a spatial-velocity hodograph to describe the formation of these regular helix structures. They considered an infinite graphene lattice, regardless of its atomic structure ***[173]***. A hodograph is a geometric space formed by the vectors representing the rate of increase of the tube along a defined circle. If these vectors are all equal and perpendicular to the plane of the circle straight nanotubes grow on the catalytic particle. Otherwise the hodograph becomes complicated. In the case of the CVD method the catalytic activity depends on the crystal-surface of the catalyst particle, hence it is anisotropic, inhomogeneous. The formation of a coiled carbon nanotubes can be explained with two hodographs. The first hodograph gives the curvature, resulting in the formation of a torus, while the second one causes the rotation of the plane of the circle leading to the creation of a coiled carbon nanotube. The second hodograph

determines the pitch diameter. As the hodograph itself may change in time, due to the time-dependence of the catalyst particle's catalytic activity, the pitch diameter might also change in time. However, the nanotube diameter remains constant being determined only by the size of the catalyst particle.

A possible growth mechanism proposed by Fonseca et al. relies on models and experimental results. They claimed that at the beginning of the catalytic decomposition of the carbon source numerous straight tubes are formed starting from the catalyst in every direction. This leads to the saturation of the catalyst. In the next step the growth of the already existing nanotubes stops due to an obstacle on the catalytic center, presumably related to the insufficient hydrocarbon supply, as it was also proposed in a previous study ***[173].*** The obstacle hinders the further straight growth of the tube thus it bends according to the geometry of the obstacle and continues growing in a new direction. Generally this occurs close to the metal particle relaxing the strain. If such a simple obstacle impedes the tube growth the nanotube will bend regularly, but no toruses are formed. This leads to the creation of tight coils. When a second obstacle comes into the way of the nanotube growth the tubule is constrained to rotate around the metal particle thus resulting in two deflections into divergent directions resulting in the formation of regular coils. The metal particle itself can act as second obstacle. The first obstacle determines the length of the segment, the second one defines the angle of twisting or the number of rotational center relocations. Figure II.29. shows the steps of tori (a)-e)) and regular helix (a)-h)) formation. Steric hindrance can arise from already formed CNTs, graphite, amorphous carbon, catalyst support even the metal particles, compelling the growing tube to bend or refract.

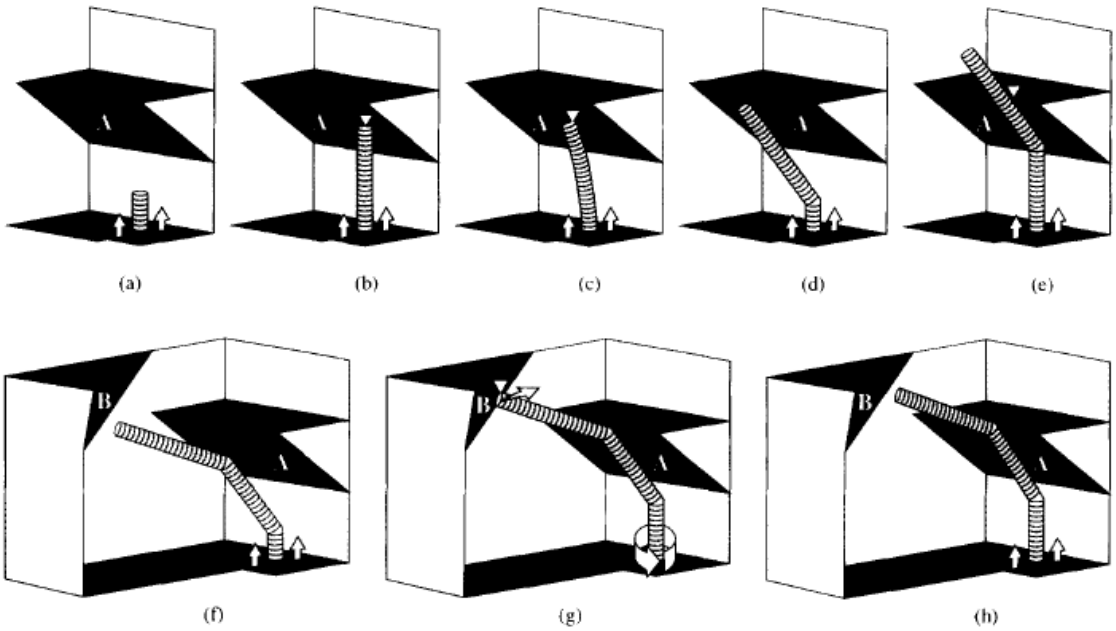

Figure II.29.: Growth mechanism of tori and regular helices proposed by Fonseca et al.: a) growing CNT on a catalyst particle; b) the growing tube encounters an obstacle; c) the tube bends due to the blockage by the obstacle; d) when the knee is formed the second growing stage starts; e) the second blockage of the tube-growth by the obstacle; f) the second knee is formed, a third growing phase starts; g) the tube reaches the second obstacle; h) regular helicity formation in the growing tubule by the second obstacle (B) ***[173]***

According to Szabó and co-workers the regular coiling of the CNTs should be in the atomic structure of the nanotubes. They examined the shape of more than 300 coiled carbon nanotubes which were synthesized in three different laboratories ***[196-198]***. They prepared a cross-correlated 3D plot of the number of coils versus the coil diameter (D) and the pitch (P) for the coiled nanotubes grown by CVD method (Figure II.30.). The authors found two so-called stability islands in this geometrical configuration space where 24.5 % of the total number of coils can be found. The first stability island (considered as a compact region) is delineated by the crossing of the region of 50-70 nm pitch and 20-60 nm diameter. The second less pronounced stability region is found between pitch 30-50 nm and the same diameters. The fact that the analyzed data comes from the analysis of 345 coiled nanotubes prepared with different catalysts in three different laboratories leads to the conclusion that the way in which carbon nanotubes are coiled has an intrinsic structural origin, and it is not defined by external factors, though some specific parameters and reaction conditions might

create peculiar growth conditions that lead to the formation of more stable coiled carbon nanotubes ***[198]***.

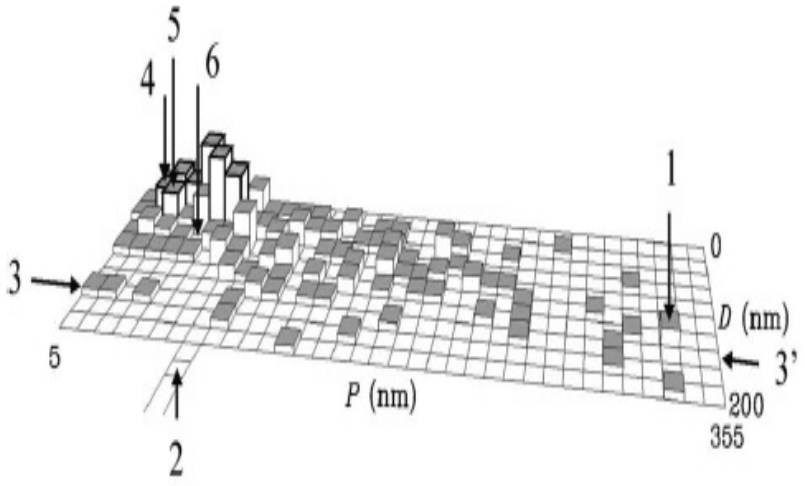

Figure II.30.: 3D representation of the distribution of coil pitch (P) and coil diameter (D). The two determined stability islands are highlighted in bold lines ***[198]***.

In the second generation models isolated pentagon-heptagon pairs are inserted in the graphene lattice, being considered not as a defect but as regular building blocks of the lattice. Researchers accepted and developed the "knees" described by Dunlap ***[169-171]***. The work of Itoh and Ihara ***[172, 177, 199]*** should be mentioned, they developed different torus prototypes, some examples are presented in Figure II.31..

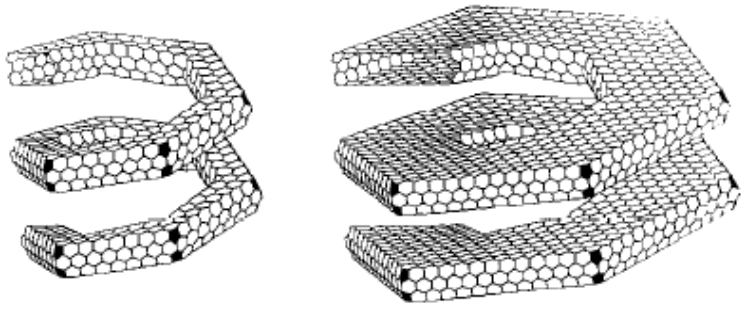

Figure II.31.: Elongated helical structures ***[177]***

The compressed toruses seen in Figure II.31. are made of straight segments. HRTEM investigations prove that a part of coiled nanotubes is formed according to this way.

Another group of the coiled nanostructures are the Haeckelite structures described more in detail in a previous paragraph. These structures are not based on the graphene structure but are formed from the haeckelite lattice where heptagons, hexagons and pentagons are regular building blocks of the structure. These models are called the third generation models. The number of hexagons built in the azulene unit can vary. The planes and ribbons created by repeating these units form cylinders following determined rules. These cylinders are naturally curved leading to various forms. The helices generated this way are continuously curved.

Figure II.32. shows HRTEM images of a coiled CNT formed by separate linear parts linked by knees and a helix with continuous curvature.

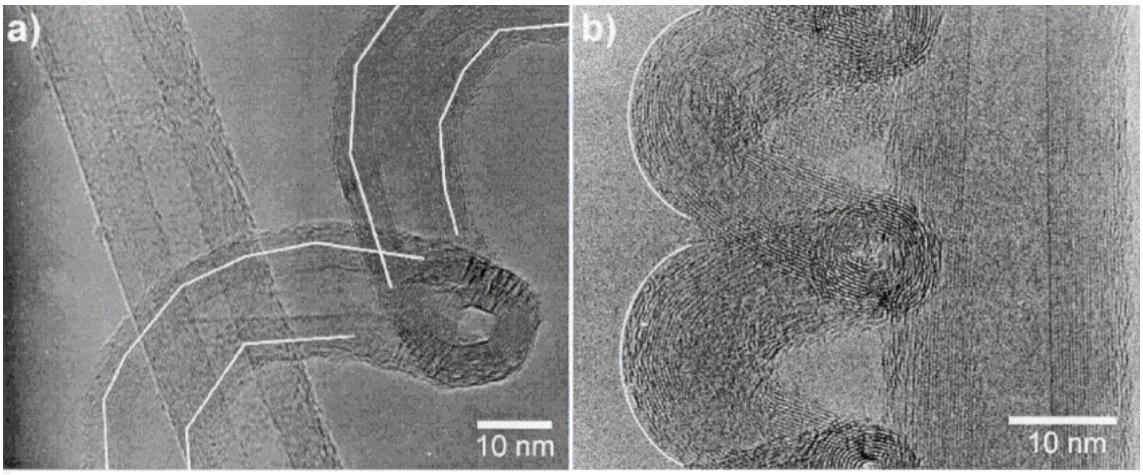

Figure II.32.: HRTEM photographs of coiled carbon nanotubes: a) separate linear parts linked by knees; b) coiled CNTs with continuous curvature ***[198]***.

II.4.5. Synthesis of Carbon Microcoils

Carbon nanocoils and microcoils have been extensively studied in the past decades. Their growth mechanism, properties, morphology and applications were well described, their CVD synthesis and characterization were substantially investigated since their early studies. However, the morphologies and structure of carbon nanocoils and coiled carbon nanotubes are rather different there are important similarities in their synthesis. The growth of helically coiled nanostructures was essentially accidental, with low yield and reproducibility until the

breakthrough of Motojima et al. ***[200-202]***. Now regularly coiled carbon microfibers can be synthesized in large scale with high reproducibility ***[175]***.

Motojima and co-workers synthesized high purity cabon microcoils. The applied synthesis method was the Ni catalyzed pyrolysis of acetylene with the addition of thiophene as impurity, with or without an external electromagnetic (EM) field, by applying or not a bias voltage to the substrate. The effect of the applied external electromagnetic field and bias voltage on the vapour growth, morphology and properties of the carbon coils was studied. The electromagnetic field applied to the reaction tube and the bias voltage applied to the substrate influences significantly the quantity and quality of the formed coils. A coil yield of 30-35 mg/cm^2 of substrate was obtained applying an external EM field and with DC or AC bias of 600-1000 V. This value was about 2 times higher than the one obtained without external electromagnetic field and bias voltage. When external EM field and bias voltage were applied regularly coiled flat coils were grown with diameters of 5.5-6.0 μm and a coil pitch of 2.5 μm. While carbon coils synthesized without applying any external EM field had circular or elliptical cross sections; their diameters are between 4.5-5.0 μm and their coil pitches are very small: 0.4-0.5 nm. The density of the carbon coils obtained applying external EM field and a bias voltage is higher. Chen and Motojima synthesized carbon microcoils with various shapes by the Ni-catalyzed pyrolysis of acetylene. By the shape of the cross section two kinds of carbon coils were produced: (1) with circular fiber cross sections (2) flat carbon coils with slender form cross section (Figure II.33.). The slender cross section of the flat coils obtained applying long reaction times was attributed to the change in the form of the catalyst particle on the effect of the electromagnetic field ***[200]***.

In Table II.3. some examples are reported of the reactions which produce different types of mirocoils and helical fibers.

Catalyst and Synthesis Conditions	Product	References
Catalyst: Ni Carbon Source: acetylene	Twisted carbon fibers	***[156]***
Catalyst: Fe-containing alloys Carbon source: acetylene T: 750-790°C	Three-dimensional spring-like carbon nanofibers	***[202]***
Catalyst: Ni Carbon Source: acetylene Pollutant: S (thiophene) External electromagnetic field (EC)	Carbon Microcoils Large scale synthesis	***[203-204]***
Catalyst: metal alloys Carbon Source: acetylene Pollutant: S (tiophene)	2D Helicoidal and Zig-zag shaped carbon nanofibers	***[205]***
$Fe_3C(+SnCl_2)$ Carbon source: acetylene	Mixed quality carbon fibers	***[206]***
Catalyst: Ni-alloy	Protein-like single helix carbon microcoils	***[207]***
Catalyst: Cu-Ni nanoparticles Carbon source: acetylene T: 241°C	Coiled carbon nanofibers	***[208]***
Catalyst: Fe-based alloy T: 700-800°C	Single-helical carbon microcoils	***[209]***
Catalyst: Ni-sulphide T: 740-760^{O}C	Thin film of quasi aligned carbon microcoils	***[210]***

Table II.3.: Examples of carbon microcoil synthesis

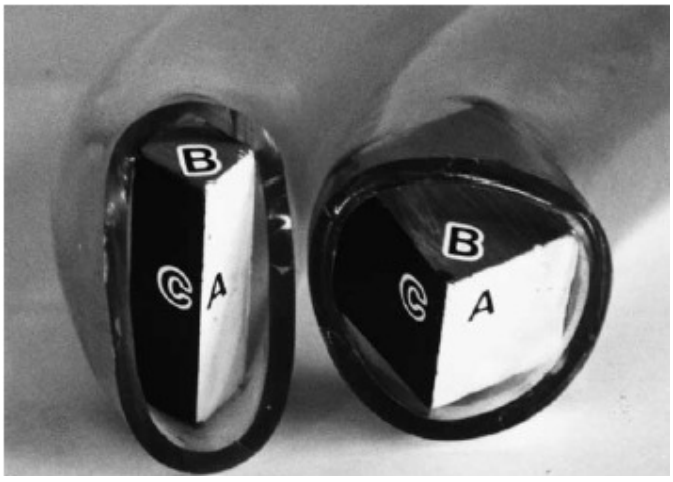

Figure II.33.: Growth model of the carbon microcoils: a) flat coils; b) circular coils ***[201]***

Hernádi et al. found that carbon deposits obtained by the decomposition of acetylene over $Fe_3C(+SnCl_2)$ can contain coiled carbon nanofibers (Figure II.34.). While pure Fe_3C is totally inactive in the acetylene decomposition, no carbon deposit was detected on its surface by electron microscopy ***[206]***.

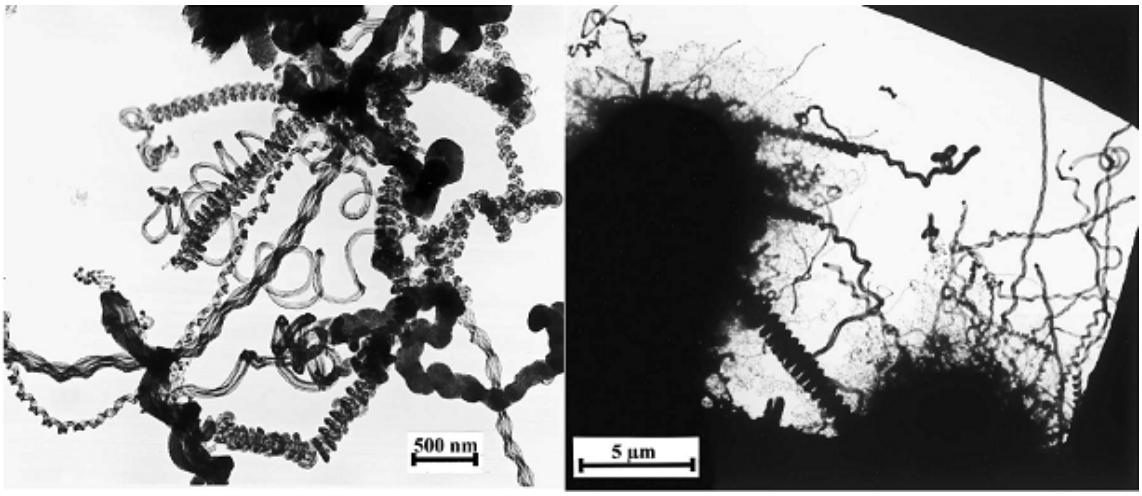

Figure II.34.: Electron microscopy images of carbon deposit over $Fe_3C(+SnCl_2)$ and over $Fe_3C(+SnO)$, respectively ***[206]***

Protein-like (or spring-like) single-helix carbon microcoils (SH-CMCs) were prepared by chemical vapour deposition using Ni-Fe catalyst at 600-700°C, while double-helix carbon microcoils (DH-CMCs) were synthesized at T=700-800°C using Ni powder as catalyst. The single-helix microcoils were embedded into polysilicone matrix to form artificial skin-biometric tactile sensor. Their electrical parameters were also studied and the results compared with double-helix carbon nanotubes. The SH-CMC sensor elements were found to be more stable and sensitive than the DH-CMC sensor elements ***[207]***.

Chen and Motojima investigated the influence of the CVD conditions on the CMC growth. Samples were synthesized with different gas flow rates of N_2, Ar or H_2O and reaction times. The H_2 flow rate significantly affected the ratio of the circular CNCs in the sample. The authors proposed that this might be due to the reduction of oxygen contained on the surface of the catalyst grain. A lower hydrogen flow rate may result in a high oxygen content giving the thin layer more of a ceramics property, and lower viscosity due to the Ni-C-O-S of a quasi-liquid-like or liquid-crystal-like phase and thus it is more difficultly deformed by the external EM field or bias voltage. The addition of H_2O did not affect the ratio of the circular CMCs in

the sample, however the elasticity of the carbon microcoils was improved by the addition of H_2O to the reaction atmosphere ***[201, 211, 212]***.

Regularly coiled carbon nanofibers with a symmetric growth mode were produced by the catalytic decomposition of acetylene at 241°C. Cu-Ni alloy nanoparticles, produced by the hydrogen arc plasma method were used as catalyst. Only two helically coiled carbon nanofibers were grown symmetrically on a single Cu-Ni alloy catalyst particle. The two helical fibers had identical cycle number, coil diameter, coil length and fiber diameter but had opposite helical senses ***[208]***.

Three dimensional spring-like carbon nanocoils were produced by the catalytic pyrolysis of acetylene at 750-790°C using an Fe-based catalyst. The spring-like coils were grown uniformly on the substrate. There were almost no other carbon species, the deposit was pure spring-like carbon nanocoils, the coil yield versus acetylene conversion was about 20%. The coil diameter ranged from 0.5 to 3 μm. The coil pitch was nearly the same with the coil diameter in size. Spring-like nanostructures with laces were frequently observed (see Figure II.35.) ***[202]***.

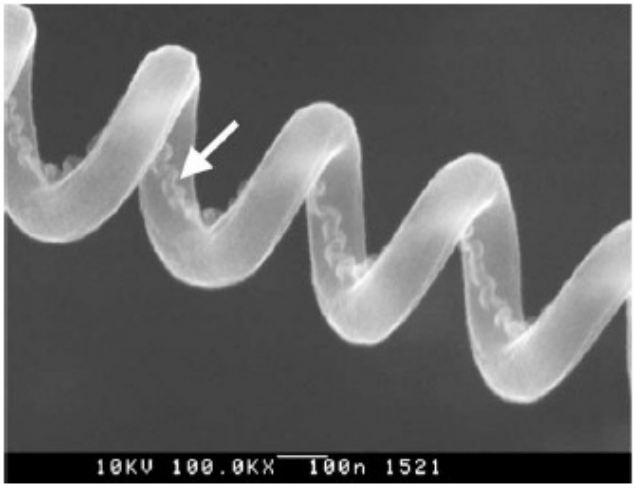

Figure II.35.: Spring-like carbon nanocoil with laces. The arrow indicates the laces ***[202]***.

The catalyst particles were present at the growth tips and the tip morphology suggested that the coiled fibers grew by mono-directional growth mode. The spring-like coils were assumed to be composed of two fused nanocoils. The authors attributed a key-role to the control of the metal catalysts in the formation of the nanocoils, and claimed that by changing the composition and the solid state conditions of the catalysts different morphologies and sizes of

the spring-like nanocoils could be obtained. The properties of the spring-like coils were compared to those of the double-helix microcoils (see Figure II.36.).

Comparison of the morphology of spring-like nano-coils and double-helix carbon micro-coils

Items	Spring-like carbon nano-coils	Double-helix carbon micro-coils
Coiling-chirality	A right-hand or left-hand coiled fiber within a piece of coil	Two right-hand or left-hand coiled fiber within a piece of coil
Main morphology	Spring-like form	Solenoid-like form
Coil sizes		
Coil length	Several hundred μm to 1 mm in 60 min	Several mm in 60 min
Inner coil diameter	Several hundred nm to 2 μm	Several hundred nm to several dozen μm
Outer coil diameter	Several hundred nm to 2 μm	Several μm
Coil pitch	The same with coil diameter	0 to several μm

Comparison of the growth tip spring-like nano-coils and double-helix carbon micro-coils

Items	Spring-like nano-coils	Double-helix carbon micro-coils
Spiral dimension	Three dimensions	Three dimensions
Tip growth or base growth	Tip growth	Tip growth
Driving force of coiling	Anisotropy of the catalytic activity	Anisotropy of the catalytic activity
Catalyst grain rotation way	Rotating around the fiber axis which is on the symmetric face of the deposition faces	Rotating around the fiber axis which is on the symmetric face of the deposition faces

Comparison of the microstructure of spring-like coils and double-helix carbon micro-coils

Items	Spring-like coils	Double-helix carbon micro-coils
Fiber numbers/growth directional	One/one direction	Two/bi-directions
Relationship between a coil and fibers which form the coils	Two fiber grows out of two crystal faces of the catalyst grain, then combine together to become a fiber	Two fibers which grow out of the crystal faces of the catalyst grain grow symmetrically, and coil at same coiling-chirality and same step
How many parts a fiber consists of	Two	Usually three
Presence of hollow in a fiber axis	Yes	No
Crystallinity	Amorphous, but slightly crystallized	Almost amorphous

Figure II.36.: Comparison of some characteristics of spring-like nanocoils with double-helix microcoils ***[202]***

Yang et al. ***[202]*** synthesized carbon nanocoils with a twisting form with a coil diameter of 300-400 nm using Fe-based alloy catalyst. A sputtered Fe-alloyed film catalyst was used in the decomposition of acetylene at 700-800°C in large scale with high contents in the deposits and good reproducibility. The coil yield versus acetylene feedstock was about 60% while the content in the deposits was 100%. The catalyst particle observed on the growth tip was identified as Fe_5C_2 or Fe_7C_3 single crystal in which some of the Fe atoms were substituted with Cr atoms. The authors hypothesis that carbon nanoparticles may be the carbon supply source for the growth of macroscopic nanocoils: the catalyst face supplies microscopic carbon nanoparticles by helical deposition patterns on the catalyst surface so the macroscopic patterns of carbon nanocoils are formed. That is to say that carbon nanocoils are composed of

helical carbon structures that originate from the helical carbon nanoparticle present on the growth tip.

II.4.6. Synthesis of Coiled CNTs

As it was discussed before the three most commonly used methods for the synthesis of straight nanotubes is the electric arc discharge, the laser evaporation and the chemical vapour deposition method. Samples derived from arc discharge and laser evaporation methods contain only straight nanotubes due to the growth temperature of these methods. Carbon deposits obtained with the CVD method can contain also coiled carbon nanotubes. In the arc discharge and laser evaporation process the high temperature (>2000%C) needed for the vaporization of the solid graphite leads to a higher mobility of the carbon atoms, thus the perfect hexagonal lattice can be created to form straight carbon nanotubes. The relatively low growth temperature of the CVD process instead results in lower mobility of the carbon atoms. This way it favours the formation of non-hexagonal rings and results in a poor crystalline graphitic lattice. From the microscopic point of view the curvatures of CNTs: bending, branching, plane buckling, coils etc, are due to the introduction of pentagon-heptagon pairs in the hexagonal graphene network. A regularly orientated formation of fivefold and sevenfold rings along the nanotube would produce a coiled CNT ***[175]***.

Coiled carbon nanotubes were fist observed experimentally by a Belgian research group in 1994. They found regularly coiled multiwalled carbon nanotubes with inner-outer diameter of 15-20 nm in a sample synthesized by the catalytic decomposition of acetylene over silica-supported Co catalyst at 700°C. The reaction was carried out at atmospheric pressure. The authors suggested that the coiled tubes consisted of regularly polygonized helices where the bending of the tube was related to the insertion of pentagon-heptagon pair carbon rings in the hexagonal network ***[77, 213]***. Figure II.37. shows TEM and HRTEM images of one of the first observed coiled nanotubes.

Hernádi et al. found that the Co supported silica catalyst prepared from Co-acetate solution of pH=9 was efficient in producing CNTs with good yield. Electron microscopy observations (Figure II.38.) revealed higher ratio of coiled nanotubes in these samples. Using catalysts at pH=8 or pH=9 every catalyst particle was covered with regular carbon nanotubes after the CVD reaction, while the deposit grown on the catalysts prepared at pH<7 was more

heterogeneous: fewer catalyst particles were covered by well-turbostratic tubes and the relative amount of irregular tubes and fibers significantly increased ***[214]***.

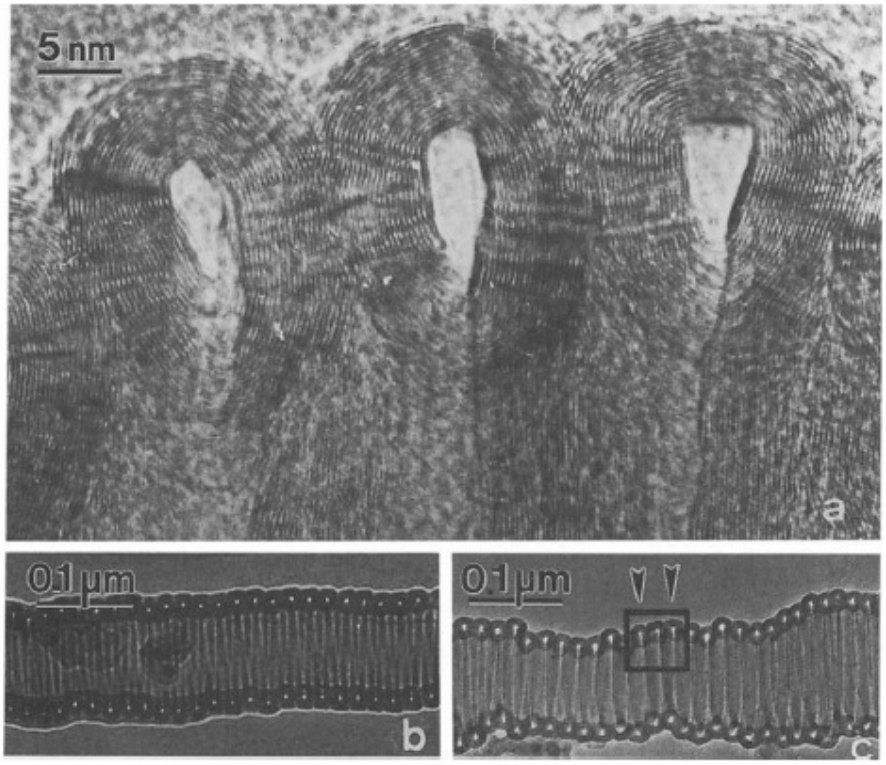

Figure II.37.: a) HRTEM image of a tightly wound helicoidal carbon nanotube; b)-c) lower resolution images of tightly coiled helices ***[214]***.

Bai et al. developed a method for the synthesis of coiled nanostructures with controlled diameter on alumina substrate. The obtained structures depended on the substrate preparation procedure and on the electrochemical deposition conditions. The diameters of the produced coils ranged from a few nanometers to a few micrometers depending mainly on the metal catalyst size. The most favourable conditions for the production of coiled nanostructures was DC electrochemical deposition with iron sulphate solution. The authors retained also possible to scale-up the process ***[215]***.

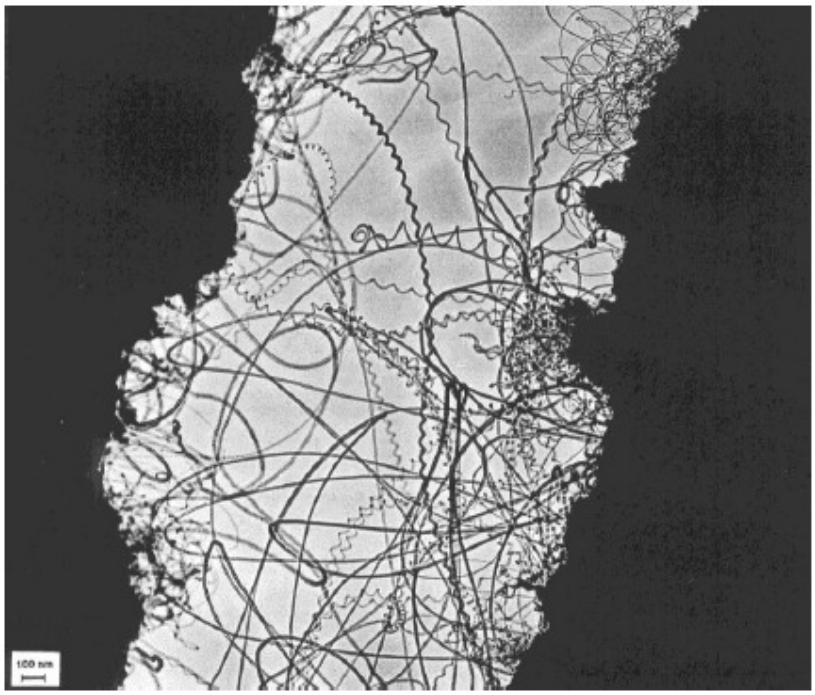

Figure II.38.: TEM image of a CNT sample produced in the Co/silica (pH=9) catalyzed decomposition of acetylene at 700°C ***[214]***.

Helically coiled multiwalled carbon nanotubes (HCNTs) were produced by co-pyrolysis of $Fe(CO)_5$ as floating catalyst precursor and pyridine or toluene as carbon source between 1050-1150°C under low flow of hydrogen. At lower temperature values the synthesis product contained only carbon-coated iron nanoparticles. The coiled CNTs had diameters between 30-80 nm. Metal nanoparticles were found in various shapes on the tips of the coiled CNTs, which led to the presumption that tube growth might follow the tip-growth model. The worm, taper or droplet-curved shape of the nanoparticles at the ends of the HCNTs suggests that the catalyst might be in a molten state during the CNT growth ***[216]***.

Biró et al. reported on the formation of carbon nanotube knees and Y-branches on a graphene substrate held at room temperature by the decomposition of fullerene at 450°C in the presence of 200 nm Ni-particles. The authors hypothesize that the formation of carbon nanostructures containing non-hexagonal rings is partly due to the templating effect of the HOPG substrate, partly due to the growth at room temperature which can augment the possibility of the insertion of non-hexagonal rings ***[193, 195]***.

Hernádi et al. tested various iron catalysts, in the decomposition of different hydrocarbons between 650-800°C. The formation of coiled nanotubes was observed using a Fe/silica

catalyst prepared by the Ion Adsorption Precipitation (IAP) method when starting from a pH=9 metal solution. Figure II.39. shows TEM image of produced coiled nanotubes ***[217]***.

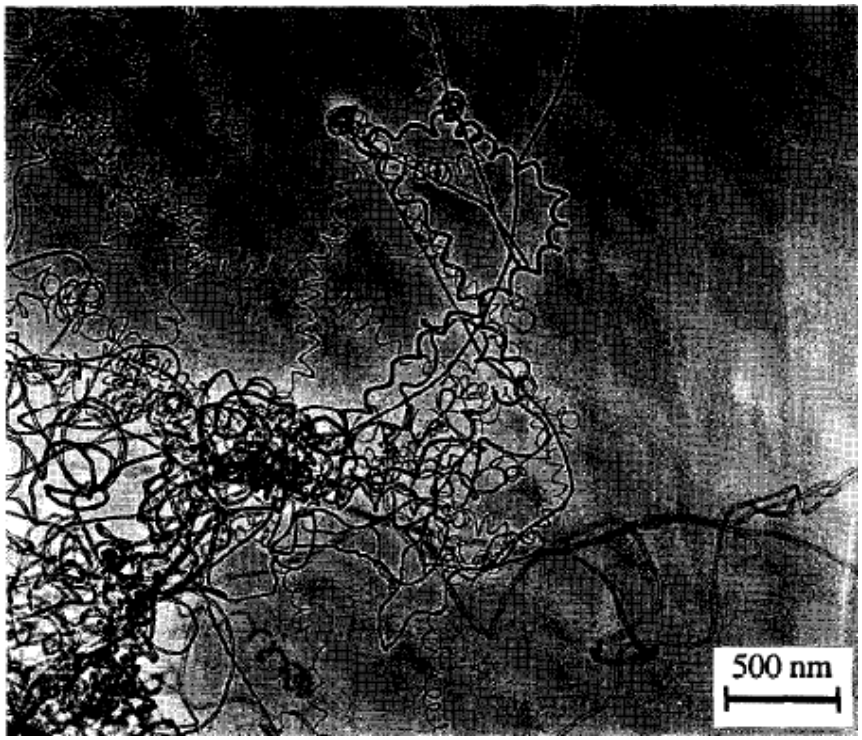

Figure II.39.: TEM image of the carbon deposit obtained by the decomposition of acetylene over Fe/silica catalyst prepared by the ion-adsorption-precipitation method using pH=9 initial solution ***[217]***.

Szabó et al. tested different support materials and different metal combinations in the synthesis of carbon nanotubes. Table II.4. shows their results on Fe, Co, Fe/Co, Co/Pr and Fe/Pr catalysts supported on Al_2O_3, $CaCO_3$, NaCl, NaY and SiO_2 supports ***[167]***.

On alumina support only the Co/Fe catalyst was active in the production of coiled CNT. The coils had diameters between 150-200 nm. Embedded metal nanoparticles were found in the graphene layers. Irregular coiled CNTs were found on the Co/Fe catalyst supported by $CaCO_3$ and on the Co/Fe catalyst supported by NaY. The Fe/NaY and Co/NaY catalysts produced somewhat more regular coils. The silica supported catalysts were found to be the most active in the formation of coiled CNTs, hence silica supported catalysts were prepared by two different synthesis methods: the ion adsorption precipitation method (IAP) and the sol-gel method (SG) and different metal loadings. Comparing the results they found that the 5%

Co/SiO_2 catalyst prepared by the sol-gel method and the 12.5% Co-2.5% Pr/SiO_2 catalyst prepared by the IAP method were the most effective catalysts for the HCNT production. However, also in these cases the ratio of HCNT in the product is around 15% ***[167]***.

Support	Al_2O_3		$CaCO_3$			NaCl	
Metal catalyst	Fe	Co-Fe	Fe	Co-Fe	Co	Co	Co-Fe
Wt% metal(s)	5.0	3.5-1.5	5.0	3.5-1.5	5.0	5.0	3.5-1.5
Coiled NTs	-	+	-	+	-	+	
Straight NTs	++++	++++	+++	++++	+++	+	++
C deposit (wt%)	70	70	20	20	20	10	15

Support	NaY-FAU			SiO_2			
Metal catalyst	Fe	Co-Fe	Co	Fe	Co-Fe	Co-Pr	Fe-Pr
Wt% metal(s)	5.0	2.5-2.5	5.0	5.0	2.5-2.5	2.5-2.5	2.5-2.5
Coiled NTs	+	+	+	-	+	++	-
Straight NTs	++	++++	++	+	++++	+++	-
C deposit (wt%)	30	80	20	10	40	30	10

Table II.4.: Quality of the NTs produced on various catalysts according to TEM observations (++++: very much, +++: much, ++: small,+: very small) ***[167]***

Lu et al. produced coiled carbon nanotubes by CVD under reduced pressure at lower gas flow rates. They used traditional silica supported Co-nanoparticles as catalyst. The selected area electron diffraction patterns suggested that the examined helix was polygonized, which was confirmed by HRTEM measurements. The authors proposed a growth mechanism, in which a carbon core is formed on a catalytic particle and the subsequent growth of the carbon helices is controlled by the kinetics ***[218]***.

Spiral nanofibers containing Pd metal clusters were grown by $Pd_2(dba)_3$ (Tris dibenzylideneacetonedipalladium) supported by $AlPO_4$-5 catalyzed decomposition of acetylene at 700°C. The authors emphasized the sensibility of the coiled CNT formation to the reaction temperature. The spiral structures have been observed only within a narrow temperature range of 700°C for the applied conditions. The sample synthesized at 650°C contained no spiral nanotubes, while only a few helices were present in the deposit of a

reaction carried out at 750°C. TEM observations and XRD analysis showed the presence of Pd-metal clusters in the nanotubes ***[219]***.

Helical carbon nanotubes were synthesized by manganese-nodule catalyzed pyrolysis of acetylene. The acetylene flow was started 0-20 minutes delayed after the placement of the mineral catalyst. A triple helical nanostructure was first described in the so-produced deposit ***[220]***.

Lu and Lau synthesized coiled carbon nanotubes by the decomposition of acetylene under reduced pressure at relatively low gas flow rates. Coils with different pitches and coil diameters were observed by TEM, while HRTEM measurements indicate a graphitic lattice and polygonization characteristics of the coiled CNTs. Figure II.40. shows a TEM image of the longest nanocoil with regular pitch found in the sample. The authors found that the addition of a low percentage of SWCNTs coils enhance the heat absorbability of the composites, this great potential in the development of heat shielding polymer based composites is attributed to the incorporation of the coiled CNTs in the matrix ***[221]***.

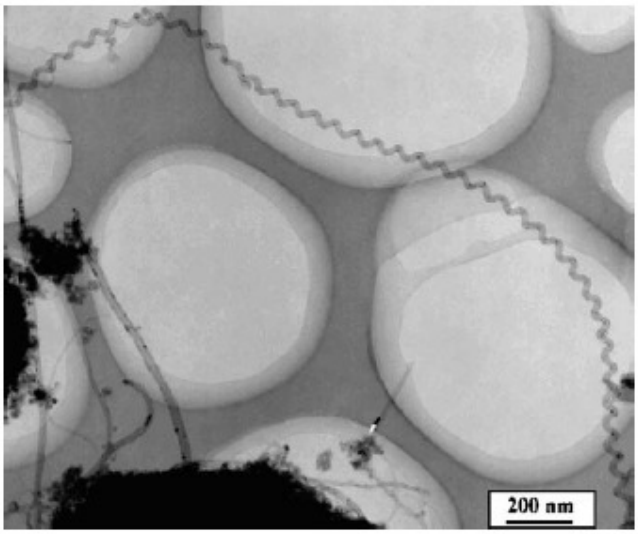

Figure II.40.: The longest HCNT (5.5 μm) with regular pitch found by Lu et al. in the deposits synthesized by the catalytic decomposition of acetylene on finely divided Co nanoparticles supported on silica gel ***[221]***

Wen and Shen reported the synthesis of carbon nanofibers/nanotubes by the Ni-catalyzed pyrolysis of acetylene. A small amount of co-catalyst: PCl_3 was added to the acetylene but its role is not thoroughly understood ***[222]***.

Wang and co-workers synthesized highly compressed coiled carbon nanotubes by spray pyrolysis of an ethanol solution containing cupric acetate as catalyst precursor at 850°C. The coiled CNTs possessed uniform shape with a sharp radius of curvature and a small coil pitch. The nanotubes had inner diameters between 10-20 nm while their external diameter ranged from 30 to 50 nm. The Cu is supposed to have a key role in the growth of the coiled CNTs. The copper containing catalyst particles may be in a molten or semi-molten state during the reaction ***[223]***.

Xie et al. synthesized regularly coiled carbon nanotubes by hot filament CVD and microwave CVD techniques at 700°C. The applied catalysts were the following: Fe supported on $MgCO_3$, Fe supported on silica and Ni supported on zeolite. The catalysts were sprayed on the graphite plate (for the thermal filament CVD) or onto the silica substrate (for the microwave CVD) and subsequently loaded into the reactors ***[224]***.

Well graphitized hollow nanotubes were grown on Co nanoparticles dispersed on porous silica. The deposits contained straight filaments and regularly coiled carbon nanotubes. The coiled tubules had small diameter and no amorphous carbon coating. The samples were analysed by transmission electron microscopy and the selected area electron diffraction (SAED) pattern of a graphite helix was also taken. According to the obtained results the coiled tubules consisted of regularly polygonized, coaxial graphene tubules whose angular bends were aligned ***[165]***.

Hernádi et al. synthesized CNTs on Co supported silica gel. They prepared a series of catalysts at different pH values: 7.5; 8; 8.5 and 9. The catalysts were tested in the decomposition of acetylene at 720°C. The characterization of the samples revealed that the spirals had generally tubular structures, fairly well graphitized with an inner core. HRTEM images reveal the structure and graphitization of the walls (Figure II.41.). Irregular structure was often observed on HRTEM micrographs instead of the polygonized structure presumed before. Thin tubes with a pitch in order of the diameter or very large coils were generally less well graphitized. Coils with various diameters, pitches and coil diameters were obtained. An example of a typical helical nanotube found in the sample is shown in Figure II.42. ***[196]***.

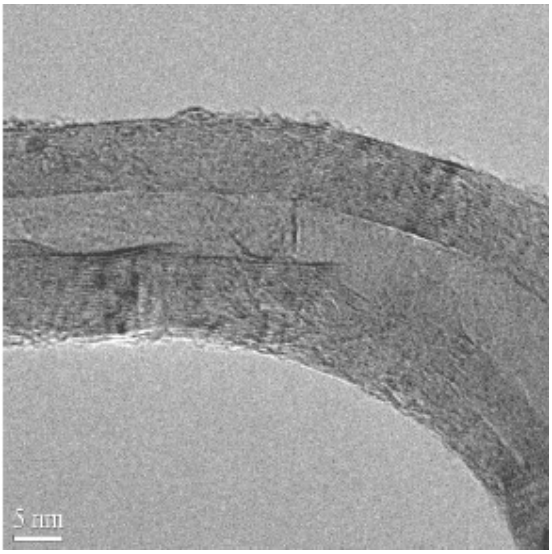

Figure II.41.: HRTEM image of a coiled carbon nanotube wall structure. On the upper part the stretching of the planes permits the regular curvature. Irregular structure in the inner part of the spiral: buckling planes and interrupted layers close to the core ***[196]***.

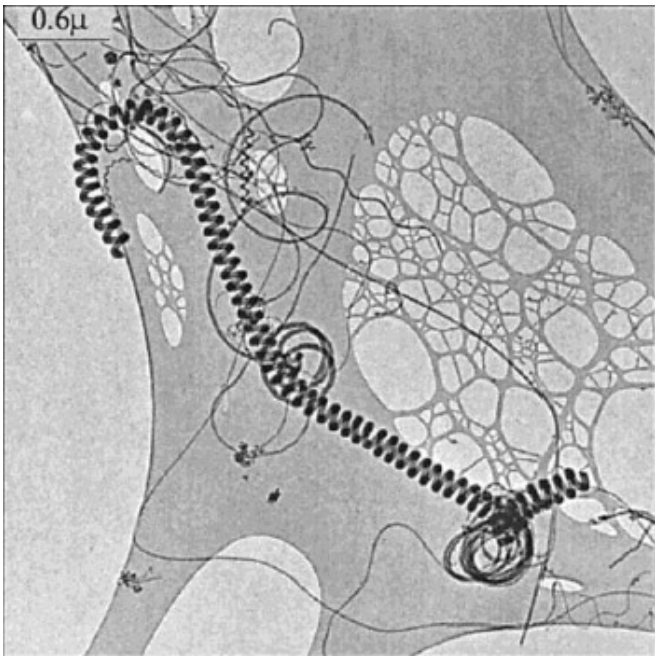

Figure II.42.: A long, nanometer size telephone-cord-like CNT with a coil pitch of 50 nm obtained by Hernádi et al. ***[196]***.

The role of the asymmetric catalyst particles on the coiled CNT formation was studied by Fejes et al. ***[225]***. Asymmetric Co and Fe particles were prepared by milling or by

crystallization from oversaturated solutions. The as prepared catalysts were applied in the decomposition of acetylene at 720°C. Samples treated in ammonia atmosphere led to the enhanced formation of coiled carbon nanotubes.

In Table II.5. we reported some example of the synthesis that produce different types of helically coiled carbon nanotubes.

Catalyst and Synthesis Conditions	Product	References
Catalyst: Co/Fe/Pr supported by $SiO_2/Al_2O_3/CaCO_3$ Carbon source: acetylene T: 700°C	HCNTs	***[166]***
Carbon Source: acetylene	Helically coiled CNTs	***[173]***
Co/SiO_2 Carbon source: acetylene T: 700°C	Coiled MWCNTs (d:15-20nm)	***[178]***
Metal/Al_2O_3 (electrochemical deposition) Carbon source: acetylene T: 650°C	Helically coiled CNTs	***[215]***
Catalyst: $Fe(CO)_5$ floating catalyst Carbon source: pyridine or toluene T: 1050-1150°C	HCNTs (d:30-80nm)	***[216]***
Catalyst: Fe/silica Carbon source: acetylene, ethylene, propylene	Irregularly coiled CNTs	***[217]***
Catalyst: manganese Carbon source: acetylene T: 750°C	HCNTs	***[221]***
Catalyst: Ni (PCl_3: co-catalyst) Carbon source: acetylene	CNCs/HCNTs	***[222]***
Catalyst: Cu-acetate (in solution) Carbon source: EtOH (spray pyrolysis)	Coiled CNTs (d:50-30nm)	***[223]***
Catalyst: Fe/$MgCO_3$; Fe/SiO_2; Ni/zeolite Thermal filament CVD /Microwave CVD T: 700°C	HCNTs	***[224]***
Catalyst: Fe/In-Sn-O	CNT rolls	***[226]***
Catalyst: Co, Fe, Co-Fe/Al_2O_3 or SiO_2 Carbon Source: acetylene	Helically coiled CNTs	***[227]***
Catalyst: Fe Carbon source: ethanol	Helical CNTs	***[228]***

Table II.5.: Examples of coiled CNT synthesis

II.4.8. Reaction Conditions for Coiled CNT synthesis

Nevertheless, according to theoretical studies the coiling of coiled carbon nanotubes has an intrinsic, structural origin some parameters and reaction conditions favour the formation of coiled carbon nanotubes instead of straight ones ***[166, 198]***.

A key-parameter might be the pressure and the gas supply ***[197]***. Experimental results show that applying higher temperature and gas pressure during the nanotube synthesis leads to the increase of the proportion of the coiled carbon nanotubes in the product. At higher temperatures the gas supply is limited, higher gas pressure causes the increase of the acetylene proportion on the active metal surface. Hence, more graphene layers are formed consecutively which leads to the formation of thicker multiwalled carbon nanotubes with higher wall number. According to the literature ***[166, 178]*** thicker tubes favour the formation of helices. Thus the acetylene flow rate can control the formation mechanism of the coils. If the reaction is carried out at atmospheric pressure, an important proportion of acetylene is transformed into amorphous carbon. The carbon deposits on the surface of the support, and the nanotubes. The relation between the gas supply and consumption plays an important role in the nanotube growth. The acetylene pressure tampers with the number of activated catalyst particles. Lower pressure leads to fewer activated catalyst particles, hence slower gas consumption. If the gas supply is higher than the gas consumption, further increase of the gas flow rate augments undecomposed acetylene molecules. Oppositely, the increase of the gas pressure leads to the increase of the active catalytic sites, hence the increase of the gas consumption. When the gas consumption is faster than the supply, the gas supply becomes the limiting parameter for the nanotube growth. In this case higher gas flow rate leads to an increase in the quantity of the formed carbon nanotubes.

The majority of the synthesis reactions that produced helically coiled nanotubes in significant proportions used nitrogen as carrier gas. Nitrogen is an inert gas, however, it is not completely sure that it remains inert during the reaction conditions of some synthesis reactions. Nitrogen can possibly influence the coiling mechanism or even favour the formation of pentagons in the lattice ***[229]***. Kovacs and co-workers ***[230]*** found that the presence of transition metals such as Ni during the CNx deposition facilitates the generation of fullerene-like closed walls. This finding is similar to the theory based on the formation of a special haeckelite layer on the metal surface ***[166]***. Coiled nanostructures were also formed where nitrogen was not applied as carrier gas in the reaction, however, the structures obtained in these reactions are generally

not tubular regardless of rare exceptions. This suggests that impurities such as nitrogen and sulphur can influence the coil formation, since otherwise the created coils have amorphous or non-tubular structure.

Choosing the right catalyst is also a key parameter. As supported catalysts were used in the present work, in the following paragraph we are going to consider this group of catalysts. Commonly supported catalysts can be prepared by impregnation, ion-adsorption-precipitation (IAP) or sol-gel method. According to Piedigrosso and Kónya ***[231]*** the impregnated catalysts showed low activity in the formation of coiled nanostructures. The applied pH during the catalyst preparation may be a crucial point to obtain regularly curved tubes ***[196, 232]***. At pH=7 the catalyst shows low activity, only few carbon nanotubes are formed. At pH=8 the carbon deposit increases and better graphitized tubes grow on the catalyst, while rising the pH to 9 the proportion of the coiled nanotubes rises in the synthesis product.

The Co^{2+} ions can be precipitated by the addition of an ammonia solution. The precipitate can easily be deposited on the surface of the silica gel. At higher pH values Co^{2+}-amino complexes are also formed that influence the quality of the catalyst and the synthesis product. The precipitated particles are generally colloidal and asymmetric. These particles are easily adsorbed on the surface of the silica gel. The pH of the cobalt solution influences the shape and the size of the formed cobalt particles. The bigger $Co(OH)_2$ aggregates formed at higher pH values are more likely to form asymmetric groups on the surface of the support material. Taking in consideration an early study this can explain why higher pH values favour the formation of coiled nanotubes and why the formed tubes have larger diameters. The decrease of the carbon deposit with the increasing pH can be due to the increased solubility of cobalt salts caused by the formation of amino-complexes or the diminution of active sites because of the formation of bigger catalytic particles ***[173, 196]***. The catalytic activity of a symmetric catalyst particle is homogeneous along any circumference of the particle hence straight nanotubes are formed during the decomposition of acetylene. When the catalyst particle is asymmetric coiled nanotubes start to grow. A possible reason can be the local inhomogeneity in the acetylene decomposition. The coil pitch is influenced by the minimum and maximum of the catalytic activity along the particle circumference. If the difference between the minimal and maximal catalytic activity along the catalyst particle, is high more elongated coils with higher pitch and diameter values are formed. When this difference is not important smaller and tighter coils grow. The symmetry of the catalyst particle thus the inhomogeneity or homogeneity of the particles catalyst activity have significant influence on the shape of the generated nanotubes.

Fonseca et al. carried out synthesis reactions with different catalysts and carbon sources. They found that the silica supported cobalt catalyst was the most effective for the production of helically coiled carbon nanotubes ***[233]***. Szabó claimed that applying praseodymium as co-catalyst favours the formation of coiled nanostructures, and its role can be similar to that of nitrogen or sulphur impurities in the system ***[166]***.

II.4.9. Properties and possible applications of coiled carbon nanotubes

Based on theoretical studies regularly coiled helical carbon nanotubes have outstanding mechanical, electrical and magnetic properties attributed to their extraordinary coiled morphology combined with the properties of carbon nanotubes ***[175, 234].*** According to the theoretical investigations coiled carbon nanotubes can show also semi-metallic behaviour due to the high density of the states at the Fermi level. The sharp peak at the Fermi levels may also result in superconductive properties ***[235, 236]***.

Some studies aimed to determine the mechanical properties of coiled carbon nanotubes especially the Young's modulus (E), the shear modulus (G) and Poisson ratio (υ). Theoretically applying the equation: $E=2(1+\upsilon)G$, two known parameters give the third one. Measuring uniaxial tension/compression or bending is a well-known characterization method for carbon nanotubes ***[237]***. The simplest way to characterize carbon nanocoils is uniaxial stretching. With a nanomanipulator a carbon nanocoil was extended to a maximum elongation of 33%, the relation between the elongation (δ) and tension load (P) along the coil axis was monitored. Chen et al. fixed an individual coiled carbon nanotube between two AFM cantilevers. Tension was loaded to a maximum relative elongation of 42%. The results showed the elastic spring behaviour of the nanocoil, the K spring constant was found to be 0.12 N/m in the low-strain regime (Figure II.43.) ***[238, 239]***.

The mechanics of coiled CNTs in uniaxial tension over a long stretching distance were further studied. The estimations given for double coils could be compared to the experimental data published by Chen and Ruoff and good accordance was found. They also revealed that the shear modulus of the tube can also be determined by the uniaxial tensile test. However, the authors found complicated to precisely determine the Poisson ratio. For multicoils there is no possibility of comparison due to the lack of experimental data in the literature.

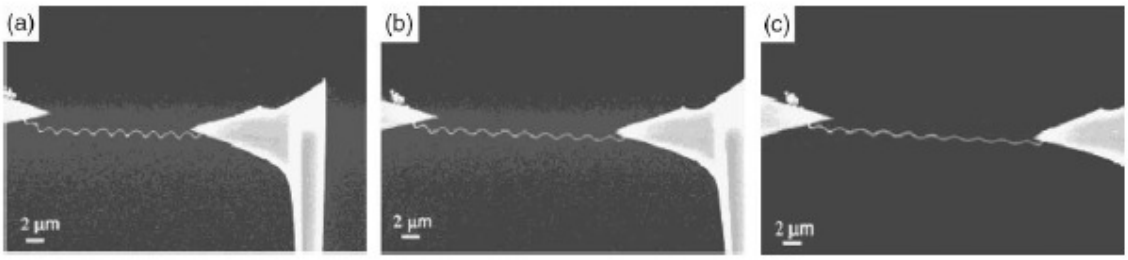

Figure II.43: a) Relaxed coil before loading; b) at 20% of relative elongation; c) at 33% of relative elongation ***[238]***

Coiled multiwalled carbon nanotubes with different parameters have not shown any significant difference from straight multiwalled carbon nanotubes in their Raman spectra and X-Ray diffraction pattern ***[175]***. Yang and co-workers observed the Raman spectra of carbon coils prepared with different conditions and catalysts. The results suggested that the structures of all the examined carbon coils are nanocrystalline phases in amorphous networks regardless of the synthesis conditions or the applied catalyst ***[240]***.

Based on theoretical studies and characterizations ***[178]*** the excellent mechanical, electrical and magnetic properties of regularly coiled carbon nanotubes can be of great interest for various applications such as nanoelectric devices, nanocomposites or nanoelectromechanical systems (NEMS). Due to their properties they seem to be promising materials for electromagnetic wave absorbents, tunable micro-devices, bioactivators, Li-battery electrodes and hydrogene containers ***[241-243]***. Lakeman and co-workers used coiled carbon fibers for the fabrication of semiconducting infrared detection elements ***[244]***. Pan et al. published about their possible application in flat field emission displays ***[245]***. Motojima and co-workers studied the electromagnetic wave absorption properties of carbon microcoils ***[246]***. Carbon nanocoils are outstanding candidates for promising future innovations for nanodevices, specific sensors ***[247],*** chiral catalysts etc ***[248]***.

The helix-shaped windings of a suspended coiled carbon nanotube show characteristic mechanical resonances that are determined by the elastic modulus, mass, shape and dimensions ***[249, 250]***. The suspended windings were resonantly excited in situ at the fundamental frequency by an ultrasonic transducer connected to the substrate. Volodin and Buntinx reported the possible use of coiled carbon nanotubes with attached electrodes as self-sensing mechanical resonators ***[250]***. When placing the tip of an atomic force microscope (AFM) above the winding the cantilever is not able to follow its fast oscillations. The

generation of an oscillation-amplitude dependent signal occurs caused by the nonlinear force-to–distance dependence ***[251]***. Being adsorbed on a silicon substrate coiled multiwalled carbon nanotubes retained a three-dimensional structure with sections of freely suspended windings. Some of these coiled CNTs had small diameters and pitches (only a few tens of nanometers). The resonance frequency of these small mechanical structures was in the microwave GHz region. Self-sensing coiled carbon nanotube sensors are applicable for measuring masses and small forces in the femtogram range.

Carbon nanocoils could be also applicable for helicoidal mass transport along them by a thermal gradient ***[252]***, or according to other investigations by an electric field ***[253]***.

The addition of coiled carbon nanotubes, instead of straight CNTs, to a polymer matrix could give the nanocomposites outstanding properties as the Young modulus of 0.7 TPa was determined by Volodin and co-workers ***[251]***. Due to the helical structure fracture toughness and mechanical strength the composites could be significantly improved also without direct chemical bonding between the nanotubes and the matrix. Coiled carbon nanotubes as nanofillers might provide a way to investigate the interfacial bonding behaviour and the fracture mechanism of the nanocomposites ***[175]***. Lau et al. compared the mechanical properties of SWCNT-epoxy nanocomposites and the HCNT-epoxy nanocomposites and discussed the different reinforcing ability and the fracture mechanism. The authors showed by Vicker's fracture measurements that the coiled CNTs were approximately three times superior to SWCNTs in hardening the matrix. The nanocoil-epoxy nanocomposites showed higher fractural strength than the SWCNT-epoxy nanocomposites. Examining the fracture surface led to the conclusion that the SWCNT-epoxy nanocomposites were broken in a ductile manner, showing poor adhesion between the nanotubes and the epoxy matrix, while the nanocoil-epoxy composites were fractured in a brittle manner showing good mechanical bonding between the coils and the epoxy matrix ***[254]***.

II.5. Characterization methods of carbon nanotubes

Morphological and structural characterization methods are indispensable to understand the mechanical and electronic properties of the carbon nanotubes. The most frequently applied techniques for the characterization of the CNTs are summarized in the following table:

Analytical method		Information	References
Transmission Electron Microscopy (TEM)		Formation, morphology and structure, presence of metal nanoparticles	***[256]***
High Resolution Electron Microscopy (HRTEM)		Diameter, open/close tube's ends, for MWCNTs the number of walls	***[256]***
Electron Diffraction (ED)		Crystal structure and graphitization	***[256]***
Scanning Electron Microscopy (SEM)		Morphology of CNTs, purity of the samples	***[256]***
Energy-Dispersive X-Ray Spectroscopy (EDS)		Chemical composition, carbon purity of the CNTs	***[256]***
Scanning Tunneling Microscopy (STM)		3D imaging and information on electronic states, geometry of CNTs	***[261]***
Atomic Force Microscopy (AFM)		3D imaging, geometry of CNTs	***[262]***
Raman Spectroscopy		Vibrational properties; detailed 1D physics and chemistry; graphitization and disorganization form G-and D-bands; SWCNTs and DWCNTs tube diameters from Radial Breathing Modes (RBMs), changes in the electronic structure, information about the role of reaction parameters and materials used for the CNT production	***[34, 263, 264]***
X-Ray Photoelectron Spectroscopy (XPS)		Chemical composition	
X-Ray Diffraction (XRD)		Interwall distance of the MWCNTs; distance between the tubes in bundles, structural defects, sample purity	***[34, 260]***
^{13}C NMR Spectrocopy		Information of built-in functional groups (the bonding of carbon atoms to other species)	***[34]***
BET (Brunauer, Emmett, Teller) specific surface area measurements		Specific surface area, porosity (pore volume and diameter), adsorption properties	***[256]***
Infrared spectroscopy (IR), Fourier transformation infrared spectroscopy (FT-IR)		Characterize absorbed material on CNTs (e.g. NO_2, NH_3, H_2, N_2 etc.), evaluate all the modifications of the CNTs structure and the nature of the compounds added to the CNT surface by functionalization, give information about impurities remaining from synthesis	***[34, 256, 257]***
Thermal Analysis	Thermogravimetric Analysis (TG)	Ignition temperature of the carbonaceous material in the CNT sample (purity, graphitization, presence or absence of amorphous carbon), thermal stability, purity, the amount of metal particles, the presence of defects	***[256, 257]***
	Differential Thermal Analysis (DTA)		***[256, 257]***
	Differential Scanning Calorimetry (DSC)		***[256, 257]***

Table II.6.: Analytical techniques for CNTs characterization

According to the information we need to obtain one can choose the most adapted characterization method. In this chapter we describe more in detail the analytical methods applied in the current work.

II.5.1. Transmission Electron Microscopy

Electron microscopy is indispensable for the nanotechnology of today. Due to its high resolution it can provide essential information on the structure and morphology of nanosized materials ***[34, 256]***.

The first transmission electron microscope was developed by Ernst Ruska in 1933 who received the Nobel prize in 1986 for his invention. The limited resolution of a visible light microscope is connected to the wavelength of the visible light. Electron microscopes were evolved to obtain higher resolution. The smallest distance that can be resolved using an electron beam is:

$$\delta=(0.61\lambda)/\mu\sin\beta$$

λ is the wavelength of the radiation, $\mu\sin\beta$ is the numerical aperture. According to Brooglie's law the wavelength of the electron is related to their energy, E and ignoring relativistic effects:

$$\lambda = \frac{1.22}{E^{\frac{1}{2}}}$$

For example if E=100 keV then $\lambda\approx4$ pm. This resolution cannot be reached due to the imperfections of the electron lenses. As an electron beam is used the electron microscope has to contain a device that displays electron intensity as light intensity. The nature of the radiation used has to be considered also. Applying an ionizing radiation might damage the sample especially some polymers, certain minerals and ceramics. On the other side the secondary signals can be used in Analytical Electron Microscopy (AEM) ***[255]***.

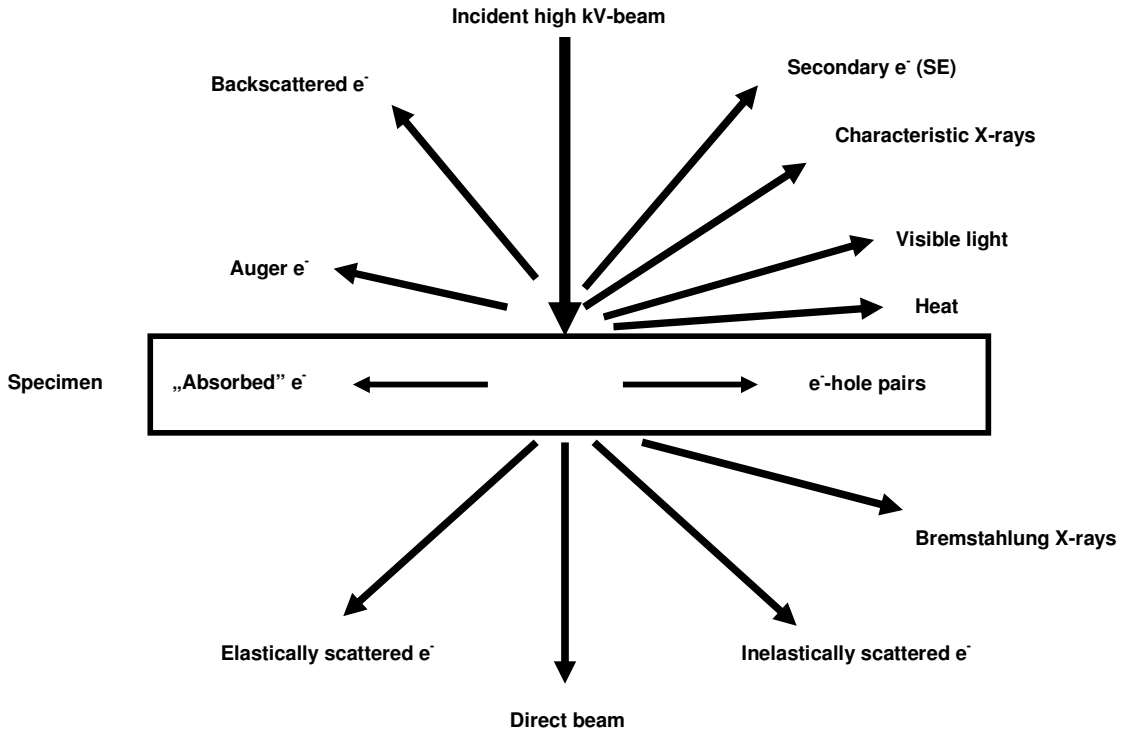

Figure II.44.: Generated signals when an electron beam interacts with the probe

Figure II.44. shows the generated signals when an electron beam interacts with the specimen. The transmitted elastically scattered electrons are used for the image formation and electron diffraction, while inelastic scattering is used for analytical purposes. There are three generations of the evolution of transmission electron microscopes and the theory of imaging: the conventional transmission mode based on the wavelength contrast; high resolution transmission electron microscopy based on phase contrast and the newest method is the negative spherical aberration imaging (NCSI) that uses magnetic lenses with changeable spherical aberration. The first two generations are commonly used in nanomaterials analysis.

The simplest way to describe the operation of a transmission electron microscope is the analogy with a visible light microscope. Instead of the light source an electron source is applied. The most common electron sources nowdays are LaB_6 crystals or field emission cathodes. Instead of the glass lenses electromagnetic lenses are applied by creating inhomogeneous rotationally symmetric magnetic fields. One of the main advantages of electron microscopy is that it can provide information both on the morphology and location

by imaging and on the crystal structure by electron diffraction. The objective lens has double function: on one hand it focuses the electrons coming from different points of the specimen in the image plane, while on the other hand it collects the electrons scattered by the same angle. Electrons can only travel in vacuum without being scattered or absorbed, thus a pump system consisting of different levels (rotational-, oil-diffusion-, turbomolecular- and ion-getter pumps) creates the different vacuums in the microscope. In the past tungstein filaments were used as electron source, while in the new generation microscopes LaB_6 and field emission cathodes are built in. Nowdays microscopes with an accelerating voltage of 200-300 kV are the most frequently used. Applying 300 kV as accelerating voltage permits electrons to travel with a speed of around $2.3*10^{10}$ cm/s. The function of the electron lenses in the electron microscopes is the same as the optical lenses in the visible light microscopes. The condenser-lenses generate parallel electron beams. The rule of the objective lens is imaging while the intermediate lenses make the magnification. The projective lenses project the image onto the screen. The performance of the microscope is determined by the defects of the objective lens. High resolution transmission electron microscopy (HRTEM) can give detailed description on the structure of CNTs: diameters and the number of walls constructing the tubes can be precisely given. Due to the high obtained resolution one can see if the carbon nanotubes have open or closed tips; whether they are fragmented or not or even if they have amorphous carbon filling inside ***[34, 256]***. However, this information can many times be obtained even with conventional electron microscopy, with slightly less accuracy and sometimes in an indirect way. For example, the number of wall constructing a multiwalled carbon nanotube can be deduced of the inner and outer diameter of the tube.

II.5.2. Scanning Electron Microscopy (SEM)

Imaging in Scanning Electron Microscopy occurs by scanning, that is to say a focused electron beam scans the surface of the specimen and the whole image is obtained pixel-by pixel and line-by line. As electrons interact with the specimen (Figure II.44.) they produce different signals. They can be scattered and cause the emission of secondary electrons ***[4, 255]***. This way an electron steps from a higher energy outer shell to fill the created hole in the lower energy inner shell and the energy is dissipated in form of characteristic X-rays or the energy is carried away by electrons (Auger electrons). For thin samples some electrons are transmitted and can be detected at the other side of the sample: this is called Scanning

Transmission Electron Microscopy (STEM). According to the needed information and the built in detectors of our instrument we can choose the radiation which we want to detect. Every signal generated by the interaction of the material and the electron beam can be used for imaging. The secondary electron detection gives information about the surface of the sample. The backscattered electrons and characteristic X-rays give information about the chemical composition of the specimen to some hundreds of nanometers depth. The energy of the emitted X-rays is characteristic of the energy between the two shells and the atomic structure of the element from which they are emitted. The operational mode where they are detected is called EDS or Energy-dispersive X-ray Spectroscopy. Also for scanning electron microscopy the resolution is limited by the wavelength attributed to the electron beam (thus its energy).

Exploiting the detection of different radiations with scanning electron microscopy we can gain information on the surface morphology of carbon nanotubes. If the EDS mode or backscattering is applied the chemical composition of the nanotube sample, hence their purity, the presence or absence of the catalyst or the support, or some functional groups can be conjected ***[4, 255]***.

II.5.3. Thermal Analysis

Dr. Bryan Higgins was the first to use a balance to register the modification of a sample after a thermal treatment in 1780. However, the first thermobalance was developed in 1912 by Urbain, operating with a precision of 0.1 mg. Thermal analysis means the examination of the weight changes of a material undergoing a chosen temperature program ***[257]***.

II.5.3.1. Thermogravimetric analysis (TGA)

During the thermogravimetric analysis the mass of a sample exposed to a determined temperature program is measured. It gives information about the temperatures where certain chemical or physicochemical reactions, such as evaporation, desorption etc. take place. The principle of the apparatus is quite simple: it consists of a furnace, a precision balance and a pan loaded with the sample. The atmosphere of the specimen probe can be controlled. Different atmospheres can be applied in order to study the behaviour of the sample. Certain

physical phenomena such as evaporation or fusion can be characterized in an inert atmosphere.

In the case of the carbon nanotubes the determination of the ignition temperature of the different carbonaceous structures present in the sample or the quantity of inorganic materials is possible in oxygen or air atmosphere ***[256, 257]***.

II.5.3.2. Differential Thermal Analysis (DTA) and Differential Scanning Calorimetry (DSC)

The DTA analysis measuring the temperature difference between the sample and a reference material exposed to the same temperature program.

$$\Delta T = T_{sample} - T_{reference}$$

Generally, the reference material is chosen to not suffer any change in the temperature range of the program. Thus if $\Delta T > 0$ the reaction is exothermic and if $\Delta T < 0$ the reaction is endothermic. The DTA apparatus is similar to the TG apparatus, but the sample holder pan is doubled and furnished of a double thermocouple to measure the temperature difference between the sample and the reference. The similarity between the TG and DTA instruments permits the coupling of these two apparatuses. This way the TG and DTA curves of a sample are simultaneously recorded which facilitates the identification of the changes in the materials.

The DSC instrument has a link between the sample and the reference. This link permits the measurement of the thermal flux between the reference and the analysed sample. Like the DTA also the DSC can be realised simultaneously with the TGA in the same instrument. This is called simultaneous thermal analysis (STA). With the DSC the enthalpies of reactions and transitions can be calculated ***[257]***.

II.5.3.3. Thermal Analysis for carbon nanotubes

This technique is often employed not just to investigate the thermal stability of the material but also to provide information concerning the purity, the amount of metal particles and the

presence of defects. The analysis can be performed either in nitrogen gas flow or in air flow, although, while TGA measurements in nitrogen gas give few information because of the negligible weight loss of the material due to its high stability in such an inert environment, TGA technique in oxidative atmosphere can play a threefold role:

- The metal and catalyst content of CNTs can be estimated by evaluating the residual weight % at the end of the thermal-oxidative curve
- The start temperature of the oxidative process can be correlated with the presence of lattice defect, either of the pristine material or after any treatment (i.e. the less the defects, the higher the temperature)
- The shape of the weight derivative (wt %/°C) curve throughout the analysis can give some information about the presence of carbon by-products, such as amorphous carbon, in the pristine material. Indeed carbonaceous particles are presumably burned out first due to the selective etching at faster oxidative etching rate than CNTs. On the other hand, the shape of the curve can also be used to evaluate the modification of the CNTs structure after functionalization treatment. ***[34, 256]***

II.5.4. X-Ray Diffraction

X-rays were discovered by Wilhelm Conrad Röntgen in 1885 who received the Nobel-prize in 1901 for the discovery. Max von Laue discovered the diffraction of X-rays by crystals receiving the Nobel-prize in 1914. However the mechanism of X-ray diffraction by crystals was explained by Sir William Henry and William Lawrence Bragg. The phenomenon was called Bragg's law. Bragg's law explains the X-Ray diffraction patterns (Figure II.45.) and obtains information on the molecular or atomic structure of the crystals.

The X-ray diffraction is based on the interference of monochromatic X-rays and a crystalline sample. Usually the X-rays applied for the X-ray powder diffraction are generated by a metal anode, most frequently copper but molybdenum and cobalt are also commonly used. The anode is bombarded with electrons emitted by a high temperature tungsten filament. Electrons are ejected from the K-shell of the copper followed by an electron drop from an outer shell to the K-shell follow and the emission of X-ray radiation (Figure II.46.).

The emitted X-rays are filtered to produce monochromatic radiation and subsequently directed on the sample. The interaction of these incident rays with the sample produces constructive interference when the conditions satisfy Bragg's law: $2d\sin\theta=n\lambda$, where d is the interlayer distance of the crystal, θ is the angle formed by the incident beam with the crystal planes, λ is the wavelength of the radiation and n is an integer ***[257]***.

These diffracted rays are detected. The sample is scanned trough a range of 2θ angles to obtain all possible diffraction directions of the lattice.

As carbon nanotubes are made of one or more graphene sheets rolled-up to form a cylinder their diffraction pattern is presumably similar to that of the graphite. In this manner we will find a reflexion corresponding to the d_{100} diffraction line of the graphite. This will occur around an angle of a $2\theta=44.5°$. The graphitic distance d_{002} is normally not present for the singlewalled carbon nanotubes. For multiwalled CNTs the presence of the interlayer distance can vary between 0.3700 to 0.3541 nm corresponding to a 2θ angle of 24°-25°. For the normal graphite the interlayer distance is of 0.3370 nm corresponding to a diffraction line at $2\theta=26.5°$. If there are nanotubes in bundles present in the sample the distance between the tubes in the bundle will also be present in the sample around the same angle value. Amorphous carbon shows a broadened, large diffraction peak without a precise line. This is caused by the disordered structure of this type of carbonaceous material. The presence of metallic cobalt in the sample can be observed at $2\theta=42.8$ corresponding to the d_{111} distance ***[257-259]***.

The structural changes in the carbon nanotubes can be detected by X-Ray diffraction. Structural deformations of multiwalled carbon nanotubes occurring at high pressure values were studied by Ming and co-workers. The as-produced nanotubes show sharp reflexions even after a treatment at 5.5 GPa. While the diffraction pattern of a CNT sample treated at 950°C showed reflexions with decreased intensity. After a treatment at 1200°C the X-Ray diffraction patterns show characteristics of amorphous carbon. These observations were in good agreement with the SEM measurements ***[260]***.

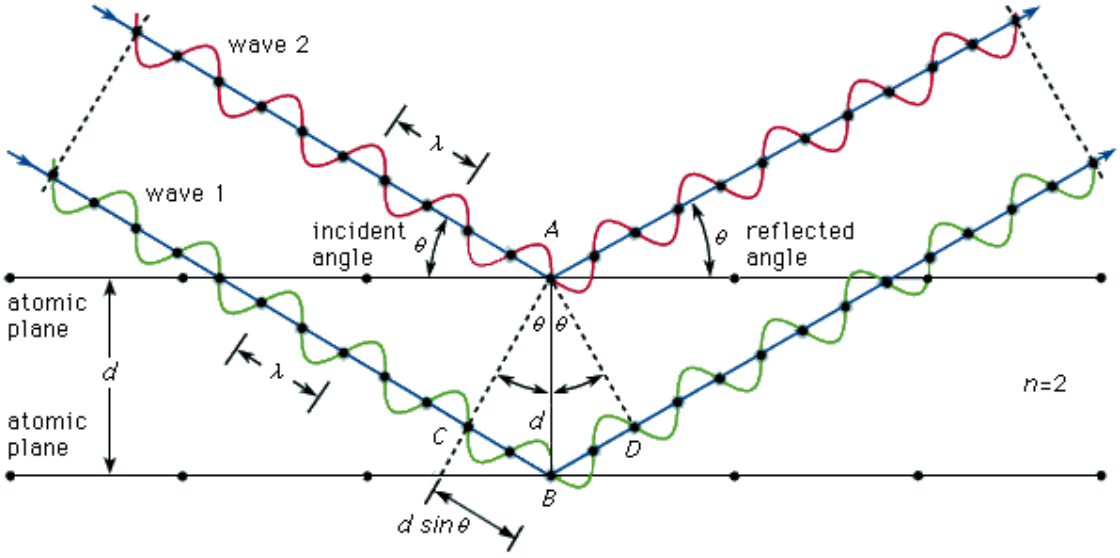

Figure II.45.: Bragg's law: the schema of X-ray diffraction ***[34, 257, 258]***

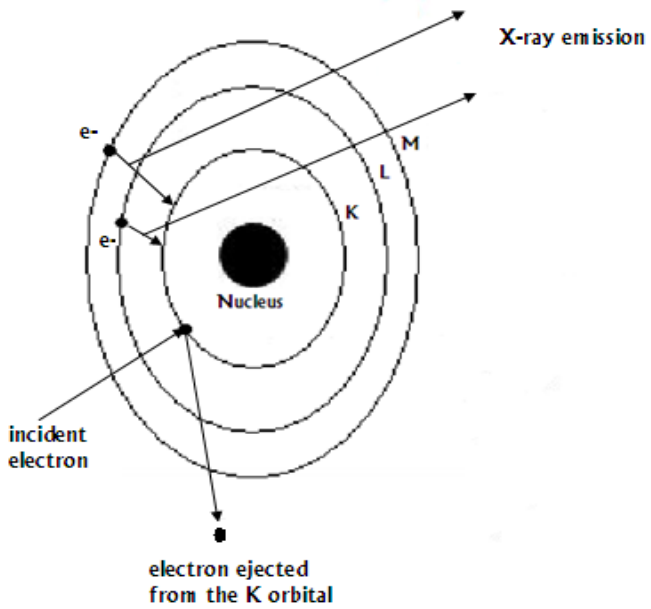

Figure II.46.: Schema of X-ray emission ***[257]***

References

[1]: Eley, D.D.; Pines, H.; Weisz, P.B.: "Advances in catalysis and related subjects", Academic Press New York, 16 (1966) pp.180-188 and 289

[2]: O'Conell, M.J.: "Carbon nanotubes: properties and applications" Taylor&Francis LLC US (2006) pp. 313

[3]: Kroto, H.W.; Heath, J.R.; O'Brien, S.C.; Curl, R. F. and Smalley, R.E.: "C60: Buckminsterfullerene" Nature 318 (1985) 162-163

[4]: Bushran, B.: "Springer Handbook of Nanotechnology" *Eds.:* Bushran, B. Nanoprobe Laboratory for Bio- and Nanotechnology and Biomimetics (NLB2) Ohio State University Columbus, USA (2004) pp. 1919

[5]: Hirsch, A.: "The Chemistry of fullerenes" Wiley-VCH Verlag GmbH, Weinheim, Germany (2002) pp 423

[6]: Ebbesen, T.W.: "Carbon Nanotubes" Phys. Today 49, (1996) 26-32

[7]: Raduskhevich, L.V.; Lukyanovich, V.M.: "O stukture ugleroda, obrazojucegosja pri termiceskom razlozenii okisi ugleroda na zeleznom kontakte" Russ. J. Phys. Chem. (Zurn Fisic Chim) 26 (1952) 88-95

[8]: Oberlin, A.; Endo, M.; Koyama, T.: "Filamentous growth of carbon through benzene decomposition" J. Chryst. Growth 32 (1976) 335-349

[9]: Iijima, S.: "Helical microtubules of graphitic carbon" Nature 354 (1991) 56-58

[10]: Bethune, D.S.; Kiang, C.H.; de Vries, M.S.; Gorman, G.; Savoy, R.; Vazquez, J.; Beyers, R.: "Cobalt catalysed growth of carbon nanotubes with single-atomic-layer walls" Nature 363 (1993) 605-607

[11]: Iijima, S.; Ichihashi, T.: "Single-shell carbon nanotubes of 1 nm diameter" Nature 363 (1993) 603-605

[12]: Krishna, A.; Dujardin, E.; Ebbesen, T.W.; Yianilos, P.N.; Treacy, M.M.J.: "Young's modulus of single-walled carbon nanotubes" Phys. Rev. B 58 (1998) 14013-14019

[13]: Thostensona, E.T.; Ren, Z.; Chou,T.W.: "Advances in the science and technology of carbon nanotubes and their composites: a review" Comp. Sci. Technol. 61 (2001) 1899-1912

[14]: Saito R.; Dresselhaus M. S.: "Physical Properties of Carbon Nanotubes" Imperial College Press. London (2003) pp. 259

[15]: Belin, T.; Epron, F.: "Characterization methods of carbon nanotubes: a review" Mat. Sci. Eng. B 119 (2005) 105-118

[16]: Jorio, A.; Saito, R.; Hafner, J.; Lieber, C.; Hunter, M.; McClure, T.; Dresselhaus, G.; Dresselhaus, M.: "Structural (n, m) determination of isolated single-wall carbon nanotubes by resonant Raman Scattering" Phys. Rev. Lett. 86 (2001) 1118-1121

[17]: Murakami, Y.; Miyauchi, Y.; Chiashi, S.; Maruyama, S.: "Direct synthesis of high-quality single-walled carbon nanotubes on silicon and quartz substrates" Chem. Phys. Lett. 377 (2003) 49-54

[18]: Saito, R.; Dresselhaus, G.; Dresselhaus, M.: "Trigonal wraping effect of carbon nanotubes" Phys. Rev. B 61 (2000) 2981-2990

[19]: Dresselhaus, M.S.; Dresselhaus, G.; Eklund P.C.: "Science of fullerenes and carbon nanotubes: Their properties and applications" Academic Press, San Diego (1996) pp 965

[20]: Ajayan, P.; Ebbesen, T.: "Nanometre-size tubes of carbon" Rep. Prog. Phys. 60 (1997) 1025-1062

[21]: Amelinckx, S.; Lucas, A.; Lambin, Ph.: "Electron diffraction and microscopy of carbon nanotubes" Rep. Prog. Phys. 62 (1999) 1471-1524

[22]: Márk, G.I.; Biró, L.P.; Gyulai, J.: "Simulation of STM images of three-dimensional surfaces and comparison with experimental data: Carbon nanotubes" Phys. Rev. B 58 (1998) 1245-1248

[23]: Biró, L.P.; Gyulai, J., Lambin Ph.; B.Nagy, J.; Lazarescu, S.; Márk, G.; Fonseca, A.; Surján, P.R.; Szekeres, Zs.; Thiry, P.; Lucas, A.A.: "Scanning tunnelling microscopy (STM) imaging of carbon nanotubes" Carbon 36 (1998) 689-696

[24]: Wilder, J.W.G.; Venema, L.C.; Rinzler, A.G.; Smalley, R.E.; Dekker, C.: "Electronic structure of atomically resolved carbon nanotubes" Nature 391 (1998) 59-62

[25]: Odom, T.W.; Huang, J.L.; Kim, Ph.; Lieber, Ch.M.: "Atomic structure and electronic properties of single-walled carbon nanotubes" Nature 391 (1998) 62-64

[26]: Mintmire, J.W.; Dunlap, B.I.; White, C.T.: "Are fullerene tubules metallic?" Phys. Rev. Lett. 68 (1992) 631-634

[27]: Zhang, X.B.; Zhang, X.F.; Amelinckx, S.; Van Tendeloo, G.; Van Landuyt, J.: "The reciprocal space of carbon tubes: a detailed interpretation of the electron diffraction effect" Ultramicroscopy 54 (1994) 237-249

[28]: Kwon, Y.K.; Tomanek, D.: "Electronic and structural properties of carbon nanotubes" Phys. Rev. B 58 (1998) R16001-16004

[29]: Cumings, J.; Zettl, A.: "Low-Friction Nanoscale Linear Bearing Realized from Multiwall Carbon Nanotubes" Science 289 (2000) 602-604

[30]: Wang, Z.L.; Poncharal, P.; de Heer, W.A.: "Measuring physical and mechanical properties of individual carbon nanotubes by in situ TEM" J. Phys. Chem. Solids 61 (2000) 1025-1030

[31]: Postma, H.W.Ch.; Teepen, T.; Yao, Z.; Grifoni, M.; Dekker, C.: "Carbon Nanotube Single-Electron Transistors at Room Temperature" Science 293 (2001) 76-79

[32]: Ando, Y.; Zhao, X.; Shimoyama, H.; Sakai, G.; Kaneto, K.: "Physical properties of multiwalled carbon nanotubes" Int. J. Inorg. Mat. 1 (1999) 77-82

[33]: Niesz, K.: "Kémia szén nanocsövekkel" PhD thesis University of Szeged (2003) pp 79

[34]: Kónya, Z.; Biró, L.P.; Hernádi, K.; B.Nagy, J.; Kiricsi, I.: "Szén nanocsövek előállítása, tulajdonságai és alkalmazási lehetőségei" A kémia legújabb eredményei 2001, Akadémiai Kiadó Budapest (2002) 121-300

[35]: Hertel, T.; Walkup, R.E.; Avouris, P.: "Deformation of carbon nanotubes by surface van der Waals forces" Phys. Rev. B 58 (1998) 13870-13873

[36]: Ruoff, R.S.; Lorents, D.C.: "Mechanical and thermal properties of carbon nanotubes" Carbon 33 (1995) 925-930

[37]: Wong, E.W.; Sheehan, P.E.; Lieber, Ch.M.: "Nanobeam Mechanics: Elasticity, Strength, and Toughness of Nanorods and Nanotubes" Science 277 (1997) 1971-1975

[38]: Vigolo, B.; Penicaud, A.; Coulon, C.; Sauder, C.; Pailler, R.; Journet, C.; Bernier, P.; Poulin, Ph.: "Macroscopic Fibers and Ribbons of Oriented Carbon Nanotubes" Science 290 (2000) 1331-1334

[39]: Tersoff, J.; Ruoff, R.S.: "Structural Properties of a Carbon-Nanotube Crystal" Phys. Rev. Lett. 73 (1994) 676-679

[40]: Rochefort, A.; Avouris, P.; Lesage, F.; Salahub, D.R.: "Electrical and mechanical properties of distorted carbon nanotubes" Phys. Rev. B 60 (1999) 3824-13830

[41]: Li, Y.B.; Wei, B.Q.; Liang, L.; Yu, Q.; Wu. D.H.: "Transformation of carbon nanotubes to nanoparticles by ball milling process" Carbon 37 (1999) 493-497

[42]: Pierard, N.; Fonseca, A.; Kónya, Z.; Willems, I.; Van Tendeloo, G.; B.Nagy, J.: "Production of short carbon nanotubes with open tips by ball milling" Chem. Phys. Lett. 335 (2001) 1-8

[43]: Chen, J.; Dyer, M.J.; Yu, M.F.: "Cyclodextrin-Mediated Soft Cutting of Single-Walled Carbon Nanotubes" J. Am. Chem. Soc. 123 (2001) 6201-6202

[44]: Zhu, Y.Q.; Sekine, T.; Kobayashi, T.; Takazawa, E.; Terrones, M.; Terrones, H.: "Collapsing carbon nanotubes and diamond formation under shock waves" Chem. Phys. Lett. 287 (1998) 689-693

[45]: Chopra, N.G.; Ross, F.M.; Zettl, A.: "Collapsing carbon nanotubes with an electron beam" Chem. Phys. Lett. 256 (1996) 241-245

[46]: Ruoff, R.S.; Lorents D.C.: „Mechanical and thermal properties of carbon nanotubes" Carbon 33 (1995) 925-930

[47]: Berber, S.; Kwon, Y.K.; Tomànek, D.: „Unusually High Thermal Conductivity of Carbon Nanotubes" Phys. Rev. Lett. 84 (2000) 4613-4616

[48]: Andrews, R.; Jacques, D.; Qian, D.; Dickey, E.C.: "Purification and structural annealing of multiwalled carbon nanotubes at graphitization temperatures" Carbon 39 (2001) 1681-1687

[49]: Sui, Y.C.; Acosta, D.R.; Gonzales-León, J.A.; Bermúdez, A.; Feuchtwanger, J.; Cui, B.Z.; Flores, J.O.; Saniger, J.M.: "Structure, thermal stability and deformation of multi branched carbon nanotubes synthesized by CVD in AAO template" J. Phys. Chem. 105 (2001) 1523–1527

[50]: www.cheaptubes.com

[51]: Fam, D.W.H.; Palaniappan, Al; Tok, A.I.Y.; Liedberg, B.; Moochhala, S.M.: "A review on technological aspects influencing commercialization of carbon nanotube sensors" Sensor. Actuator B 157 (2011) 1-7

[52]: Dai, H.J.; Hafner, J.H.; Rinzler, A.G.; Colbert, D.T.; Smalley, R.E.: "Nanotube nanoprobes in scanning probe microscopy" Nature 384 (1996) 147-150

[53]: Hafner, J.H.; Cheung, C.L.; Wooley, A.T.; Lieber, C.M.: "Structural and functional imaging with carbon nanotube AFM probes" Progr. Biophys. Mol. Biol. 77 (2001) 52-55

[54]: de Heer, W.A.; Châtelain, A.; Ugarte, D.: "A carbon nanotube field emission electron source" Science 270 (1995) 1179-1180

[55]: Rinzler, A.G.; Hafner, J.H.; Nikolaev, P.; Lou, L.; Kim, S.G.; Tomanek, D.; Colbert, D.; Smalley, R.E.: "Unraveling nanotubes: Field emission from an atomic wire" Science 269 (1995) 1550-1553

[56]: Wu, B.; Kuang, Y.; Zhang, X.; Chen, J.: "Noble metal nanoparticles/carbon nanotubes nanohybrids: Synthesis and applications" Nano Today 6 (2011) 75-90

[57]: Dillon, A.C.; Gilbert, K.E.H.; Parilla, P.A.; Allemann, J.L.; Hornyak, G.L.; Jones, K.M.; Heben, M.J.: "Hydrogen storage in carbon single-walled nanotubes" Proceedings of the 2002 US.DOE Hydrogen Program Review (NREL/CP-610-32405)

[58]: Ajayan, P.M.; Stephan, O.; Colhex, C.; Trauth, D.: "Aligned carbon nanotube arrays formed by cutting a polymer resin-nanotube composite" Science 265 (1994) 1212-1214

[59]: Spitalsky, Z.; Tasis, D.; Papagelis, K.; Galiotis, C.: "Carbon nanotube-polymer composites: Chemistry, processing, mechanical and electrical properties" Prog. Polym. Sci. 35 (2010) 357-401

[60]: Samal, S.S.; Bal, S.: "Carbon nanotube reinforced ceramic matrix composites- A review" J. Min. Min. Char. Eng. 7 (2008) 355-370

[61]: Bakshi, S.R.; Lahiri, D.; Agarwal, A.: "Carbon nanotube reinforced metal matrix composites-A review" Int. Mat. Rev. 55 (2010) 41-64

[62]: Krätschmer, W.; Lamb, L.D.; Fostiropoulos, K.; Huffman, D.R.: "Solid C_{60}: a new form of carbon" Nature 347 (1990) 354-358

[63]: Fonseca, A.; B.Nagy, J.: "Carbon nanotubes formation in the arc-discharge process" In "Carbon Filaments and Nanotubes: Common Origins, Differing Applications?" Eds. by Biró, L.P.; Bernardo, C.A.; Tibbetts G.G.; Lambin, Ph.; Kluwer Academic Publishers; Dordrecht (2001) pp. 372; 75-78

[64]: Journet, J.; Maser, W.K.; Bernier, P.; Loiseau, A.; de la Chapelle, M.L.; Lefrant, S.; Deniard, P.; Lee, R.; Fisher, J.E.: "Large-scale production of single-walled carbon nanotubes by the electric-arc discharge technique" Nature 388 (1997) 756-758

[65]: Wang, Y.-H.; Chiu, S.-Ch.; Lin, K.-M.; Li, Y.-Y.: "Formation of carbon nanotubes from polyvinyl alcohol using arc-discharge method" Carbon 42 (2004) 2535-2541

[66]: Shi, Z.; Lian, Y.; Liao, F.H.; Zhou, X.; Gu, Z.; Zhang, Y.; Iijima, S.; Li, H.; Yue, K.T.; Zhang, S.-L.: "Large-scale synthesis of single-wall carbon nanotubes by arc-discharge method" J. Phys. Chem. Solids 61 (2000) 1031-1036

[67]: Yao, M.; Liu, B.; Zou, Y.; Wang, L.; Li, D.; Cui, T.; Zou, G.; Sundquist, B.: "Synthesis of singlewalled carbon nanotubes and long nanotube ribbons with Ho/Ni catalyst by arc-discharge" Carbon 43 (2005) 2894-2901

[68]: Marchand, M.; Journet, C.; Guillot, D.; Benoit, J.M.; Yakobson, B.I.; Purcell, S.T.: "Growing a Carbon Nanotube Atom by Atom: "And Yet It Does Turn" Nano Lett. 9 (2009) 2961-2966

[69]: Hutchinson, J.L.; Kiselev, N.A.; Krinchnaya, E.P.; Krestinin, A.V.; Loutfy, R.O.; Morawsky, A.P.; Muraydan, V.E.; Obraztsova, E.D.; Sloan, J.; Terekhov, S.V.; Zakharov, D.N.: "Double-walled carbon nanotubes fabricated by a hydrogen arc discharge method" Carbon 39 (2001) 761-770

[70]: Saito, Y.; Nakahira, T.; Uemura, S.: "Growth conditions of double-walled carbon nanotubes in arc-discharge" J. Phys. Chem. B 107 (2003) 931-934

[71]: Huang, H.; Kajiura, H.; Tsutsui, S.; Murakami, Y.; Ata, M.: "High-quality double-walled carbon nanotubes super bundles grown in a hydrogen-free atmosphere" J. Phys. Chem. B 107 (2003) 8794-8798

[72]: Ishigami, M.; Cumings, J.; Zettl, A.; Chen, S.: "A simple method for the continuous production of carbon nanotubes" Chem. Phys. Lett. 319 (2000) 457-459

[73]: Sano, N.; Nakano, J.; Kanki, T.: "Synthesis of single-walled carbon nanotubes with nanohorns by arc in liquid nitrogen" Carbon 42 (2004) 686-688

[74]: Wang, S.-D.; Chang, M.-H.; Lan, K.M.-D.; Wu, Ch.-Ch.; Cheng, J.-J.; Chang, H.-K.: "Synthesis of carbon nanotubes by arc discharge in NaCl solution" Carbon 43 (2005) 1778-1814

[75]: Hsin, Y.L.; Hwang, K.C.; Chen, F.R.; Kai, J.J.: "Production and in-situ metal filling of carbon nanotubes in water" Adv. Mat. 13 (2001) 830-833

[76]: Lange, H.; Sioda, M.; Huczko, A.; Zhu, Y.Q.; Kroto, H.W.; Walton, D.R.M.: "Nanocarbon production by arc discharge in water" Carbon 41 (2003) 1617-1623

[77]: Zhu, H.W.; Li, X.S.; Jiang, B.; Xu, C.L.; Zhu, Y.F.; Wu, D.H.; Chen, X.H.: "Formation of carbon nanotubes in water by electric arc discharge technique" Chem. Phys. Lett. 366 (2002) 664-669

[78]: Szabó, A.; Perri, C.; Csató, A.; Giordano, G.; Vuono, D.; B.Nagy, J.: "Synthesis Methods of Carbon Nanotubes and Related Materials" Materials 3 (2010) 3092-3140

[79]: Imasaka, K.; Kanatak, Y.; Oshiro, Y.; Suchiro, J.; Hara, M.: "Production of carbon nanoonions and nanotubes using an intermittent arc discharge in water" Thin Solid Films 506-507 (2006) 250-254

[80]: Lee, S.J.; Baik, H.K.; Yoo, J.; Han, J.H.: "Large-scale synthesis of carbon nanotubes by plasma rotating arc technique" Diam. Rel. Mat. 11 (2002) 914-917

[81]: Guo, T.; Nikolaev, P.; Rinzler, A.G.; Tomanek, D.; Colbert, D.T.; Smalley, R.E.: "Self-Assembly of Tubular Fullerenes" J. Phys. Chem. 99 (1995) 10694-10697

[82]: Guo, T.; Nikolaev, P.; Thess, A.; Colbert, D.T.; Smalley, R.E.: "Catalytic growth of single-walled manotubes by laser vaporization" Chem. Phys. Lett. 243 (1995) 49-54

[83]: Thess, A.; Lee, R.; Nikolaev, P.; Dai, H.; Petit, P.; Robert, J.; Xu, Ch.; Lee, Y.H.; Kim, S.G.; Rinzler, A.G.; Colbert, D.T.; Scuseria, G.E.; Tomanek, D.; Fischer, J.E.; Smalley, R.E.: "Crystalline Ropes of Metallic Carbon Nanotubes" Science 273 (1996) 483-487

[84]: Yudasaka, M.; Komatsu, T.; Ichihashi, T.; Iijima, S.: "Single-wall carbon nanotube formation by laser ablation using double-targets of carbon and metal" Chem. Phys. Lett. 278 (1997) 102-106

[85]: Walker Jr., P.L.; Rakaszawski, J.F.; Imperial, G.R.: "Carbon Formation from Carbon Monoxide-Hydrogen Mixtures over Iron Catalysts. I. Properties of Carbon Formed" J. Phys. Chem. 63 (1969) 133-140

[86]: Ruston, W.R.; Warzee, M.; Hennaut, J.; Waty, J.: "The solid reaction products of the catalytic decomposition of carbon monoxide on iron at 550°C" Carbon 7 (1969) 47-50

[87]: Robertson, S.D.: "Carbon formation from methane pyrolysis over some transition metal surfaces—I. Nature and properties of the carbons formed" Carbon 8 (1970) 365-368

[88]: Yacaman, M.J.; Yoshida, M.M.; Rendon, L.; Santiesteban, J.G.: "Catalytic growth of carbon microtubules with fullerene structure" Appl. Phys. Lett. 62 (1993) 202-204

[89]: Ivanov, V.; B.Nagy, J.; Lambin, Ph.; Lucas, A.A.; Zhang, X.B.; Zhang, X.F.; Bernaerts, D.; Van Tendeloo, G.; Amelinckx, S.; Van Landuyt, J.: "The study of carbon nanotubules produced by catalytic method" Chem. Phys. Lett. 223 (1994) 329-335

[90]: Dai, H.J.; Rinzler, A.G.; Nikolaev, P.; Thess, A.; Colbert, D.T.; Smalley, R.E.: "Single-wall nanotubes produced by metal-catalyzed disproportionation of carbon monoxide" Chem. Phys. Lett. 260 (1996) 471-475

[91]: Fonseca, A.; Hernadi, K.; Piedigrosso, P.; Biro, L.P.; Lazarescu, S.D.; Lambin, Ph.; Thiry, P.A.; Bernaerts, D.; B.Nagy, J.: "Fullerenes Volume IV: Recent advances in physics and chemistry of fullerenes and related materials" (Editor: Kadish, K.M.; Ruoff, R.S.) Electrochem. Soc. Inc., Proc. Vol. 97-14 (1997) 884

[92]: Teo, K.B.K.; Singh, Ch.; Chhowalla, M.; Milne, W.I.: "Catalytic synthesis of carbon nanotubes and nanofibers" In Encyclopedia of Nanoscience and Nanotechnology; Nalwa, H.S., Ed.; American Scientific Publisher: Valencia, CA, USA, 2003; Vol. 1, 665–668

[93]: Flahaut, E.; Govindaraj, A.; Peigney, A.; Laurent, C.; Rousset, A.; Rao, C.N.R.: „Synthesis of single-walled carbon nanotubes using binary (Fe, Co, Ni) alloy nanoparticles prepared in situ by the reduction of oxide solid solutions" Chem. Phys. Lett. 300 (1999) 236–242

[94]: Couteau, E.; Hernadi, K.; Seo, J.W.; Thien-Nga, L.; Miko, Cs.; Gaal, R.; Forro, L.: „CVD synthesis of high-purity multiwalled carbon nanotubes using $CaCO_3$ catalyst support for large-scale production" Chem. Phys. Lett. 378 (2003) 9–17

[95]: Ren, Z.F.; Huang, Z.P.; Xu, J.W.; Wang, J.H.; Bush, P.; Siegal, M.P.; Provencio, P.N.: "Synthesis of large arrays of well-aligned carbon nanotubes on glass" Science 282 (1998) 1105–1107

[96]: Fan, S.S.; Chapline, M.G.; Franklin, N.R.; Tombler, T.W.; Cassell, A.M.; Dai, H.J.: „Self-oriented regular arrays of carbon nanotubes and their field emission properties" Science 283 (1999) 512–514

[97]: Ren, Z.F.; Huang, Z.P.; Wang, D.Z.; Wen, J.G.; Xu, J.W.; Wang, J.H.; Calvet, L.E.; Chen, J.; Klemic, J.F.; Reed, M.A.: „Growth of a single freestanding multiwall carbon nanotube on each nanonickel dot" Appl. Phys. Lett. 75 (1999) 1086–1088

[98]: Bonard, J.M.; Kind, H.; Stockli, T.; Nilsson, L.A.: "Field emission from carbon nanotubes: The first five years" Solid State Electronics 45 (2001) 893–914

[99]: Choi, W.B.; Chung, D.S.; Kang, J.H.; Kim, H.Y.; Jin, Y.W.; Han, I.T.; Lee, Y.H.; Jung, J.E.; Lee, N.S.; Park, G.S.; Kim, J.M.: „Fully sealed, high-brightness carbon-nanotube field-emission display" Appl. Phys. Lett. 75 (1999) 3129–3131

[100]: Liu, G.Y.; Zhong, D.Y.; Xia, S.H.; Cheng, S.F.; Ding, Y.G.; Lu, Y.J.; Shao, Y.J.; Li, H.Y.; Hangfu, L.J.; Wang, E.G.: „CNTs grown on the surface of various materials by large volume MP-CVD for VME applications" Appl. Surf. Sci. 215 (2003) 209–213

[101]: Chaisitsak, S.; Yamada, A.; Konagi, M.: „Hot filament enhanced CVD synthesis of carbon nanotubes by using a carbon filament" Diam. Rel. Mat. 13 (2004) 438–444

[102]: Hata, K.; Futaba, D.H.; Nizuno, K.; Namai, T.; Yumura, M.; Iijima, S.: „Water-assisted highly efficient synthesis of impurity-free single-walled carbon nanotubes" Science 306 (2004) 1362–1364

[103]: Zhang, G.; Mann, D.; Zhang, L.; Javey, A.; Li, Y.; Yenilmez, E.; Wang, Q.; McVittie, J.P.; Nishi, Y.; Gibbons, J.; Dai, H.: „Ultra-high-yield growth of vertical single-walled carbon nanotubes: Hidden roles of hydrogen and oxygen" Proc. Natl. Ac. Sci., USA 102 (2005) 16141–16145

[104]: Cheng, J.; Zhang, X.; Liu, F.; Tu, J.; Ye, Y.; Ji, Y.; Chen, Ch.: „Synthesis of carbon nanotubes filled with Fe_3C nanowires by CVD with titanate modified polygarskite as catalyst" Carbon 41 (2003) 1965-1970

[105]: Qian, H.-S.; Han, F.-M.; Zhang, B.; Guo, Y.-Ch.; Yue, J.; Peng, B.-X.: „Non-catalytic CVD preparation of carbon spheres with specific size" Carbon 42 (2004) 761-766

[106]: Ago, H.; Uehara, N.; Yoshihara, N.; Tsuji, M.; Yumura, M.; Tomonaga, N.; Setoguchi, T.: „Gas analysis of the CVD process for high yield growth of carbon nanotubes over metal-supported catalysts" Carbon 44 (2006) 2912–2918

[107]: Qingwen, L.; Hao, Y.; Yan, C.; Jin, Z.; Zhongfan, L.: „A scalable CVD synthesis of high-purity single-walled carbon nanotubes with porous MgO as support material" J. Mat. Chem. 12 (2002) 1179–1183

[108]: Liu, B.C.; Lyu, S.C.; Jung, S.I.; Kang, H.K.; Yang, C.W.; Park, J.W.; Park, C.Y.; Lee, C.J.: „Single-walled carbon nanotubes produced by catalytic chemical vapor deposition of acetylene over Fe–Mo/MgO catalyst" Chem. Phys. Lett. 383 (2004) 104–108

[109]: Ago, H.; Imamura, S.; Okazaki, T.; Saito, T.; Yumura, M.; Tsuji, M.: „CVD growth of single-walled carbon nanotubes with a narrow diameter distribution over Fe/MgO catalyst and their fluorescence spectroscopy" J. Phys. Chem. B 109 (2005) 10035–10041

[110]: Kang, J.L.; Li, J.J.; Du, X.W.; Shi, C.S.; Zhao, N.Q.; Cui, L.; Nash, P.: „Synthesis and growth mechanism of metal filled carbon nanostructures by CVD using Ni/Y catalyst supported on copper" J. Alloy. Comp. 456 (2008) 290–296

[111]: Kang, J.; Li, J.; Du, X.; Shi, Ch.; Zhao, N.; Nash, Ph.: „Synthesis of carbon nanotubes and carbon onions by CVD using a Ni/Y catalyst supported on copper" Mat. Sci. Eng. A 475 (2008) 136–140

[112]: Chen, X.; Hasegawa, M.; Yang, S.; Nitta, Y.; Katsuno, T.; Motojima, S.: "Preparation of carbon microcoils by catalytic methane hot-wire CVD process" Thin Solid Films 516 (2008) 714-717

[113]: Chaisitsak, S.; Yamada, A.; Konagai, M.: „Hot filament enhanced CVD synthesis of carbon nanotubes by using carbon filament" Diam. Rel. Mat. 13 (2004) 438-444

[114]: Chaisitsak, S.; Nukeaw, J.; Tuantramont, A.: „Parametric study of atmospheric-pressure single-walled carbon nanotubes growth by ferrocene-ethanol mist CVD" Diam. Rel. Mat. 16 (2007) 1958–1966

[115]: Borowiak-Palen, E.; Rümmeli, M.H.: „Activated Cu catalysts for alcohol CVD synthesized non-magnetic bamboo-like carbon nanotubes and branched bamboo-like carbon nanotubes" Superlat. Microstruct. 46 (2009) 374–378

[116]: Gan, B.; Ahn, J.; Zhang, Q.; Rusli; Yoon, S.F.; Yu, J.; Huang, Q.-F.; Chew, K.; Ligatchev, V.A.; Zhang, X.-B.; Li, W.-Z.: „Y-junction carbon nanotubes grown by in situ evaporated copper catalyst" Chem. Phys. Lett. 333 (2001) 23–28

[117]: Zhu, M.; Wang, J.; Outlaw, R.A.; Hou, K.; Manos, D.M.; Holloway, B.C.: „Synthesis of carbon nanosheets and carbon nanotubes by radio frequency plasma enhanced chemical vapor deposition" Diam. Rel. Mat. 16 (2007) 196–201

[118]: Mori, S.; Suzuki, M.: „Effect of oxygen and hydrogen addition on the low-temperature synthesis of carbon nanofibers using a low-temperature CO/Ar DC plasma" Diam. Rel. Mat. 17 (2008) 999–1002

[119]: Nishide, D.; Kataura, H.; Suzuki, S.; Okubo, S.; Achiba, Y.: „Growth of single-wall carbon nanotubes from ethanol vapor on cobalt particles produced by pulsed laser vaporization" Chem. Phys. Lett. 392 (2004) 309–313

[120]: Singh, Ch.; Shaffer, M.; Kinloch, I.; Windle, A.: „Production of aligned carbon nanotubes by the CVD injection method" Physica B 323 (2002) 339–340

[121]: Khatri, I.; Soga, T.; Jimbo, T.; Adhikari, S.; Aryal, H.R.; Umeno, M.: „Synthesis of single walled carbon nanotubes by ultrasonic spray pyrolysis method" Diam. Rel. Mat. 18 (2009) 319-323

[122]: Kakehi, K.; Noda, S.; Maruyama, S.; Yamaguchi, Y.: „Individuals, grasses, and forests of single- and multi-walled carbon nanotubes grown by supported Co catalysts of different nominal thicknesses" Appl. Surf. Sci. 254 (2008) 6710–6714

[123]: Sinnott, S.B.; Andrews, R.: „Carbon Nanotubes: Synthesis, properties and applications" Crit. Rev. Sol. State Mat. Sci. 26 (2001) 145–249

[124]: Dai, H.J.; Rinzler, A.G.; Nikolaev, P.; Thess, A.; Colbert, D.T.; Smalley, R.E.: „Single-wall nanotubes produced by metal-catalyzed disproportionation of carbon monoxide" Chem. Phys. Lett. 260 (1996) 471–475

[125]: Hernadi, K.; Fonseca, A.; B.Nagy, J.; Siska, A.; Kiricsi, I.: „Production of nanotubes by the catalytic decomposition of different carbon-containing compounds" Appl. Cat. A: General 199 (2000) 245–255

[126]: Nikolaev, P.; Bronikowski, M.J.; Bradley, R.K.; Rohmund, F.; Colbert, D.T.; Smith, K.A.; Smalley, R.E.: „Gas-phase catalytic growth of single-walled carbon nanotubes from carbon monoxide" Chem. Phys. Lett. 313 (1999) 91–97

[127]: Maruyama, S.; Kojima, R.; Miyauchi, R.; Chiashi, S.; Kohno, M.: „Low-temperature synthesis of high-purity single-walled carbon nanotubes from alcohol" Chem. Phys. Lett. 360 (2002) 229–234

[128]: Öncel, C.; Yürüm, Y.: „Carbon nanotube synthesis via the catalytic CVD method: A review on the effect of reaction parameters" Fullerens Nanotubes and Carbon Nanostructures 14 (2006) 17–37

[129]: McCann, J.T.; Lim, B.; Ostermann, R.; Rycenga, M.; Marquez, M.; Xia, Y.: „Carbon nanotubes by electrospinning with a polyelectrolyte and vapor deposition polymerization" Nano Lett. 7 (2007) 2470–2474

[130]: Laskoski, M.; Keller, T.M.; Qadri, S.B.: „Direct conversion of highly aromatic phthalonitrile thermosetting resins into carbon nanotube containing solids" Polymer 48 (2007) 7484–7489

[131]: Yang, L.C.; Shi, Y.; Gao, Q.S.; Wang, B.; Wu, Y.P.; Tang, Y.: „The production of carbon nanospheres by the pyrolysis of polyacrylonitrile" Carbon 46 (2008) 1816–1818

[132]: Shang, S.; Yang, X.; Tao, X.: „Easy synthesis of carbon nanotubes with polypyrrole nanotubes as the carbon precursor" Polymer 50 (2009) 2815–2818

[133]: Yang, C.M.; Weidemthaler, C.; Spliethoff, B.; Mayanna, M.; Schuth, F.: „Facile template synthesis of ordered mesoporous carbon with polypyrrole as carbon precursor" Chem. Mat. 17 (2005) 355–358

[134]: Jang, J.; Yoon, H.: „Fabrication of magnetic carbon nanotubes using a metal-impregnated polymer precursor" Adv. Mat. 15 (2003) 2088–2091

[135]: Dong, H.; Jones, W.E.: „Preparation of submicron polypyrrole/poly(methyl methacrylate) coaxial fibers and conversion to polypyrrole tubes and carbon tubes" Langmuir 22 (2006) 11384–11387

[136]: Dupuis, A.-C.: „The catalyst in the CCVD of carbon nanotubes-a review" Mat. Sci. 50 (2005) 929-961

[137]: Ago, H.; Uehara, N.; Yoshihara, N.; Tsuji, M.; Yumura, M.; Tomonaga, N.; Setoguchi, T.: "Gas analysis of the CVD process for high yield growth of carbon nanotubes over metal-supported catalysts" Carbon 44 (2006) 2912-2918

[138]: Qingwen, L.; Hao, Y.; Yan, C.; Jin, Z.; Zhongfan, L.: "A scalable CVD synthesis of single-walled carbon nanotubes with porous MgO as support material" J. Mat. Chem. 12 (2002) 1179-1183

[139]: Liu, B.C.; Lyu, S.C.; Jung, S.I.; Kang, H.K.; Yang, C.W.; Park, J.W.; Park, C.Y.; Lee, C.J.: "Single-walled carbon nanotubes produced by catalytic chemical vapour deposition of acetylene over Fe-Mo/MgO catalyst" Chem. Phys. Lett. 383 (2004) 104-108

[140]: Ago, H.; Imamura, S.; Okazaki, T.; Saito, T.; Yumura, M.; Tsuji, M.: "CVD growth of single-walled carbon nanotubes with a narrow diameter distribution over Fe/MgO catalyst and their fluorescence spectroscopy" J. Phys. Chem. B 109 (2005) 10035-10041

[141]: Valles, C.; Perez-Mendoza, M.; Maser, W.K.; Martinez, M.T.; Alvarez, L.; Sauvajol, J.L.; Benito, A.M.; Valles, C.: "Effects of partial and total methane flows on the yield and structural characteristics of MWCNTs produced by CVD" Carbon 47 (2009) 998-1004

[142]: Mamalis, A.G.; Vogtlander, L.O.G.; Markopoulos, A.: "Nanotechnology and nanostructured materials: trends in carbon nanotubes" Prec. Eng. 28 (2004) 16-30

[143]: Jayatissa, A.H.; Guo, K.: "Synthesis of carbon nanotubes at low temperature by filament assisted atmospheric CVD and their field emission characteristics" Vacuum 83 (2009)853-856

[144]: Horváth, Z.E.; Kertesz, K.; Petho, L.; Koos, A.; Tapaszto, L.; Vertesy, Z.; Osvath, Z.; Darabont, Al.; Nemes-Incze, P.; Sarkozi, Zs.; Bíró, L.P.: "Inexpensive, up-scalable nanotube growth methods" Curr. Appl. Phys. 6 (2006) 135-140

[145]: Qui, J.L.; Wang, X.; Tian, H.W.; Peng, Y.S.; Liu, C.; Zheng, W.T.: "Synthesis of carbon nanomaterials by radio frequency plasma enhanced chemical vapour deposition" J. Alloy. Comp. 486 (2009) 265-272

[146]: Kato T.; Jeong, G.-H.; Hirata, T.; Hatakeyama, R.: „Structure control of carbon nanotubes using radio-frequency plasma enhanced chemical vapor deposition" Thin Solid Films 457 (2004) 2-6

[147]: Hiramatsu, M.; Nagao, H.; Taniguchi, M.; Amano, H.; Ando, Y.; Hori, M.: "High-rate growth of films of dense, aligned double-walled carbon nanotubes using microwave plasma-enhanced chemical vapour deposition" Jpn. J. Appl. Phys. 44 (2005) 693-695

[148]: Hiramatsu, M.; Deguchi, T.; Nagao, H.; Hori, M.: "Area-selective growth of aligned single-walled carbon nanotube films using microwave plasma-enhanced CVD" Diam. Rel. Mat. 16 (2007) 1126-1130

[149]: Sugime, H.; Noda, S.; Maruyama, S.; Yamaguchia, Y.: "Multiple "optimum" conditions for Co-Mo catalyzed growth of vertically aligned single-walled carbon nanotube forests" Carbon 47 (2009) 234-241

[150]: Khatri, I.; Kishi, N.; Zhang, J.; Soga, T.; Jimbo, T.; Adhikari, S.; Aryal, H.R.; Umeno, M.: "Synthesis and characterization of carbon nanotubes via ultrasonic spray pyrolysis method on zeolite" Thin Solid Films 518 (2010) 6756-6760

[151]: Gogotsi, Y.; Libera, J.A.; Yoshimura, M.: "Hydrothermal synthesis of multiwall carbon nanotubes" J. Mat. Res. 15 (2000) 2591-2594

[152]: Gogotsi, Y.; Naguib, N.; Libera, J.: "In situ chemical experiments in carbon nanotubes" Chem. Phys. Lett. 365 (2002) 354-360

[153]: Manafi, S.; Nadali, H.; Irani, H.R.: "Low temperature synthesis of multi-walled carbon nanotubes via sonochemical/hydrothermal method" Mat. Lett. 62 (2008) 4175-4176

[154]: Calderon Moreno, J.M.; Swamy, S.S.; Fujino, T.; Yoshimura, M.: "Carbon nanocells and nanotubes grown in hydrothermal fluids" Chem. Phys. Lett. 392 (2000) 317-322

[155]: Stevens, M.G.; Subramoney, S.; Foley, H.C.: "Spontaneous formation of carbon nanotubes and polyhedra from cesium and amorphous carbon" Chem. Phys. Lett. 292 (1998) 352-356

[156]: Hsu, W.K; Hare, J.P.; Terrones, M.; Kroto, H.W.; Walton, D.R.M; Harris, P.J.H.: "Condensed-phase nanotubes" Nature 377 (1995) 687

[157]: Bai, J.B.; Hamon, A.-L.;Marraud, A.; Jouffrey, B.; Zymla, V.: "Synthesis of SWCNTs and MWCNTs by a molten salt (NaCl) method" Chem. Phys. Lett. 365 (2002) 184-188

[158]: Grobert, N.: "Carbon nanotubes-becoming clean" Mat. Today 10 (2007) 28-35

[159]: Novoselova, I.A.; Oliinyk, N.F.; Volkov, S.V.; Konchits, A.A.; Yanchuk, I.B.; Yefanov, V.S.; Kolesnik, S.P.; Karpets, M.V.: "Electrolytic synthesis of carbon nanotubes from carbon dioxide in molten salts and their characterization" Physica E: Low-dimensional Systems and Nanostructures 40 (2008) 2231-2237

[160]: Zeng, Q.; Li, Z.; Zhou, Y.: "Synthesis and application of carbon nanotubes" J. Nat. Gas. Chem. 15 (2006) 235-246

[161]: Matveev, A.T.; Golberg, D.; Novikov, V.P.; Klimkovich, L.L.; Bando, Y.: "Synthesis of carbon nanotubes below room temperature" Carbon 39 (2001) 155-158

[162]: Laplaze, D.; Bernier, P.; Maser, W.K.; Flamant, G.; Guillard, T.; Loiseau, A.: "Carbon nanotubes: The solar approach" Carbon 36 (1998) 685-688

[163]: Luxemburg, D.; Flamant, G.; Laplaze, D.: "Solar synthesis of single-walled carbon nanotubes at medium scale" Carbon 43 (2005) 2302-2310

[164]: Ahlskog, M.; Seynaeve, E.; Vullers, R.J.M.; Van Haesendonck, C.; Fonseca, A.; Hernádi, K.; B.Nagy, J.: "Ring formations from catalytically synthesized carbon nanotubes" Chem. Phys. Lett. 300 (1999) 202-206

[165]: Zhang, X.B.; Zhang, X. F.; Bernaerts, D.; Van Tendeloo, G.; Amelinckx, S.; Van Landuyt, J.; Ivanov, V.; B.Nagy, J.; Lambin, Ph.; Lucas, A.A.: "The texture of catalytically grown coil-shaped carbon nanotubules" Europhys. Lett. 27 (1994) 141-146

[166]: Szabó, A.: "Spirális szén nanocsövek katalitikus előállítása és jellemzése" PhD thesis, Szegedi Tudományegyetem Alkalmazott és Környezeti Kémiai Tanszék (2005) pp. 87

[167]: Szabo, A.; Fonseca, A.; Biro, L.P.; Konya, Z.; Kiricsi, I.; Volodin, A.; Van Hasendonck, C.; B.Nagy, J.: "Synthesis, characterization and use of coiled carbon nanotubes" Nanopages 1 (2006) 263-293

[168]: Baker, R.T.K.; Barber, M.A.; Harris, P.S.; Feates, F.S.; Waite R.J.: "Nucleation and growth of carbon deposits from the nickel catalyzed decomposition of acetylene" J. Cat. 26 (1) (1972) 51-62

[169]: Dunlap, B.I.: "Connecting carbon tubules" Phys. Rev. B 46 (3) (1992) 1933-1936

[170]: Dunlap, B.I.: "Relating carbon tubules" Phys. Rev. B 49 (8) (1994) 5643–5651

[171]: Dunlap, B.I.: "Constraints on small graphitic helices" Phys. Rev. B 50 (11) (1994) 8134-8137

[172]: Ihara, S.; Itoh, S.: "Helically coiled cage forms of graphitic carbon" Phys. Rev. B 48 (8) (1993) 5643-5647

[173]: Amelinckx S.; Zhang X.B.; Bernaerts D.; Zhang X.F.; Ivanov V.; B.Nagy J.: "A Formation Mechanism of Catalytically Grown Helix-Shaped Graphite Nanotubes" Science 265 (1994) 635-639

[174]: Fonseca A.; Hernádi K.; B.Nagy, J.; Lambin, Ph.; Lucas, A.A.: "Model Structure of Perfectly Graphitizable Coiled Carbon Nanotubes" Carbon 33 (1995) 1759-1775

[175]: Lau, K.-T.; Lu, M.; Hui, D.: "Coiled carbon nanotubes: Synthesis and their potential applications in advanced composite structures" Composites: Part B Engineering 37 (2006) 437-448

[176]: Ihara, S.; Itoh, S.; Kitakami, J.: "Toroidal forms of graphitic carbon**"** Phys. Rev. B 47 (1993) 12908-12911

[177]: Ihara, S.; Itoh, S.: "Helically Coiled and Toroidal Cage Forms of Graphitic Carbon" Carbon 33 (7) (1995) 931-939

[178]: Fejes, D.; Hernádi, K.: "A review of the properties and CVD synthesis of coiled carbon nanotubes" Materials 3 (2010) 2618-2642

[179]: Zhong-can, O.Y.; Su, Z.B.; Wang, C.L.: "Coil formation in multishell carbon nanotubes: competition between curvature elasticity and interlayer adhesion" Phys. Rev. Lett. 78 (1997) 4055-4058

[180]: Galpern, E.G.; Stankevich, I.V.; Chistyakov, A.L.; Chernozatonskii, L.A.: „Torelenes (t)-c(n) as a new class of carbon clusters - electronic-structure of (t)-c200, (t)-c210, (t)-c276, and (t)-c408" Fullerene Sci. Technol. 2 (1994) 1-11

[181]: Itoh, S.; Ihara, S.: „Isomers of the toroidal forms of graphite carbon" Phys. Rev. B 849 (1994) 13970-13974

[182]: Ivanov, V.; B.Nagy, J.; Lambin, Ph.; Lucas, A.A.; Zhang, X.B.; Zhang, X.F.; Bernaerts, D.; Van Tendeloo, G.; Amelinckx, S.; Van Landuyt, J.: „The study of carbon nanotubules produced by catalytic method" Chem. Phys. Lett. 223 (1994) 329-335

[183]: Meunier, V.; Lambin, Ph.; Lucas, A.A.: "Atomic and electronic structures of large and small carbon tori" Phys. Rev. B 57 (1998) 14886-14890

[184]: Charlier, J.-C.: "Defects in carbon nanotubes" Acc. Chem. Res. 35 (2002) 1063-1069

[185]: Terrones H.; Terrones M.; Hernández, E.; Grobert, N.; Charlier, J.-C.; Ajayan, P.M.: "New metallic allotropes of planar and tubular carbon" Phys. Rev. Lett. 84 (2000) 1716-1719

[186]: László, I.; Rassat, A.: "Toroidal and spherical fullerene-like molecules with only pentagonal and heptagonal faces" Int. J. Quantum Chem. 84 (2001) 136-139

[187]: Bíró, L.P.; Márk, G.I.; Koós, A.A.; B.Nagy, J.; Lambin, Ph.: "Coiled carbon nanotube structures with supraunitary nonhexagonal to hexagonal ring ratio" Phys. Rev. B 66 (2002) 165405(-1-6)

[188]: Lambin, Ph.; Bíró, L.P.: "Structural Properties of Haeckelite Nanotubes" New J. Phys. 5 (2003) 141.1-141. 14

[189]: Bíró, L.P.; Márk, G.I.; Horváth, Z.E.; Kertész, K.; Gyulai, J.; B.Nagy, J.; Lambin, Ph.: "Carbon nanoarchitectures containing non-hexagonal rings: "necklaces of pearls" Carbon 42 (2004) 2561-2566

[190]: Lambin, Ph.; Márk, G.I.; Bíró, L.P.: "Structural and electronic properties of coiled and curled carbon nanotubes having a large number of pentagon-heptagon pairs" Phys. Rev. B 67 (2003) 205413-1-9

[191]: Zha, F.-X.; Roth, S.; Carroll, D.L.: „Periodic, pearl chain-like nanostructure observed by scanning tunneling microscopy" Carbon 44 (2006) 1695-1698

[192]: Blank, V.D.; Gorlova, I.G.; Hutchinson, J.L.; Kiselev, N.A.; Ormont, A.B.; Polyakov, E.V.; Sloan, J.; Zakharov, D.N.; Zybtsev, S.G.: "The structure of nanotubes fabricated by carbon evaporation at high gas pressure" Carbon 38 (2000) 1217-1240

[193]: Bíró, L.P.; Echlich, R.; Osváth, Z.; Koós, A.; Horváth, Z.E.; Gyulai, J.; B.Nagy, J.: "Room temperature growth of single-wall coiled carbon nanotubes and Y-branches" Mat. Sci. Eng. C 18 (2002) 3-7

[194]: Bíró, L.P.; Lasarescu, S.D.; Thiry, P.A.; Fonseca, A.; B.Nagy, J.; Lucas, A.A.; Lambin, Ph.: "Scanning tunnelling microscopy observation of tightly wound single-wall coiled carbon nanotubes" Europhys Lett. 50 (2000) 494-500

[195]: Bíró, L.P.; Echlich, R.; Osváth, Z.; Koós, A.; Horváth, Z.E.; Gyulai, J.; B.Nagy, J.: "From straight nanotubes to Y-branched coiled carbon nanotubes" Diam. Rel. Mat. 11 (2002) 1081-1085

[196]: Hernadi, K.; Thien-Nga, L.; Forro, L.: „Growth and microstructure of catalytically produced coiled carbon nanotubes" J. Phys. Chem. B 105 (2001) 12464-12468

[197]: Lu, M.; Liu, W.-M.; Guo, X.-Y.; Li, H.L.: "Coiled carbon nanotubes growth via reduced-pressure catalytic chemical vapor deposition" Carbon 42 (2004) 805-811

[198]: Szabó, A.; Fonseca, A.; B.Nagy, J.; Lambin, P.H.; Biró, L.P.: „Structural origin of coiling in coiled carbon nanotubes" Carbon 43 (2005) 1628-1633

[199]: Itoh, S.; Ihara, S.: „Toroidal forms of graphitic carbon. II. Elongated tori" Phys. Rev. B 48 (1993) 8323-8328

[200]: In-Hwang, W.; Chen, X.; Kuzuya, T.; Kawabe, K.; Motojima, S.: „Effect of external electromagnetic field and bias voltage on the vapor growth, morphology and properties of carbon micro coils" Carbon 38 (2000 565-571

[201]: Chen, X.; Yang, S.; Motojima, S.: „Morphology and growth models of circular and flat carbon coils obtained by the catalytic pyrolysis of acetylene" Mat. Lett. 57 (2002) 48-54

[202]: Yang, S.; Chen, X.; Motojima, S.; Ichihara, M.: „Morphology and microstructure of spring-like carbon micro-coils/nano-coils prepared by catalytic pyrolysis of acetylene using Fe-containing alloy catalysts" Carbon 43 (2005) 827-834

[203]: Motojima, S.; Kawaguchi, M.; Nozaki, K.; Iwanaga, H.: "Preparation of coiled carbon fibers by catalytic pyrolysis of acetylene, and its morphology and extension characteristics" Carbon 29 (3) (1991) 379-385

[204]: Chen, X.; Saito, T.; Kusonoki, M.; Motojima, S.: "Three dimensional vapour growth mechanism of carbon microcoils" J. Mat. Res. 14 (11) (1999) 4329-4336

[205]: Yang, S.; Chen, X.; Motojima, S.: "Preparation and Morphologies of Elastic Carbon Microcoils/nanocoils by Various Catalysts" Transact. Mat. Res. Soc. Jap. 29 (2004) 485-488

[206]: Hernádi, K.; Fonseca, A.; B.Nagy, J.; Fudala, Á.; Bernaerts, D.; Kiricsi, I.: „Catalytic production of carbon nanofibers over iron carbide doped with Sn^{2+}" Appl. Cat. A 228 (2002) 103-113

[207]: Yang, S.; Chen, X.; Motojima, S.: „Tactile sensing properties of protein-like single-helix carbon microcoils" Carbon 44 (2006) 3352-3355

[208]: Yu, L.Y.; Quin, Y.; Cui, Z.L.: "Synthesis of coiled carbon nanofibers by Cu-Ni alloy nanoparticles catalyzed decomposition of acetylene at the low temperature of 241°C" Mat. Lett. 59 (2005) 459-462

[209]: Yang, S.; Chen, X.; Kusonoki, M.; Yamamoto, K.; Iwanaga, H.; Motojima, S.: "Microstructure and microscopic deposition mechanism of twist-shaped carbon nanocoils based on the observation of helical nanoparticles on the growth tips" Carbon 43 (2005) 916-922

[210]: Mukhopadhyay, K.; Ram, K.; Rao, K.U.B.: „Thin film of carbon micro-spring forest" Mat. Lett. 61 (2007) 2004-2006

[211]: Chen, X.; Yang, S.; Kato, Y.; Motojima, S.: „Influence of CVD conditions on the growth of carbon microcoils with circular cross-sections" Mat. Lett. 61 (2007) 2900-2903

[212]: Motojima, S.; Chen, X.: Encyclopedia of Nanoscience and. Nanotechnology (editor: Nalwa, H. S) 6 (2004), pp. 775-794.

[213]: Bernaerts, D.; Zhang, X.B.; Zhang, X.F.; Van Tendeloo, G.; Amelinckx, S.; Van Landuyt, J.; Ivanov, V.; B.Nagy, J.: "Electron-microscopy study of coiled carbon tubules" Phil. Mag. A 71 (1995) 605–630

[214]: Hernadi, K.; Fonseca, A.; Piedigrosso, P.; Delvaux, M.; B.Nagy, J.; Bernaerts, D.; Riga, J.: „Carbon nanotube production over Co/silica catalysts" Cat. Lett. 48 (1997) 229-238

[215]: Bai, J.B.: „Growth of nanotube/nanofibre coils by CVD on an alumina substrate" Mat. Lett. 57 (2003) 2629-2633

[216]: Hou, H.Q.; Jun, Z.; Weller, F.; Greiner, A.: „Large-scale synthesis and characterization of helically coiled carbon nanotubes by use of $Fe(CO)_5$ as floating catalyst precursor" Chem. Mat. 15 (2003) 3170-3175

[217]: Hernadi, K.; Fonseca, A.; B.Nagy, J.; Bernaerts, D.; Lucas, A.A.: „Fe-catalyzed carbon nanotube formation" Carbon 34 (1996) 1249-1257

[218]: Lu, M.; Li, H.L.; Lau, K.T.: „Formation and growth mechanism of dissimilar coiled carbon nanotubes by reduced-pressure catalytic chemical vapor deposition" J. Phys. Chem. B 108 (2004) 6186-6192

[219]: Liu, C.J.; Wu, T.W.; Hsu, L.S.; Su, C.J.; Wang, C.C.; Shieu, F.S.: „Transport properties of spiral carbon nanofiber mats containing Pd metal clusters using $Pd_2(dba)_3$ as catalyst" Carbon 42 (2004) 2635-2640

[220]: Cheng, J.; Zhang, X.; Tu, J.; Tao, X.; Ye, Y.; Liu, F.: „Catalytic chemical vapor deposition synthesis of helical carbon nanotubes and triple helices carbon nanostructure" Mat. Chem. Phys. 95 (2006) 12-15

[221]: Lu, M.; Lau, K.T.; Xu, J.C.; Li, H.L.: "Coiled carbon nanotubes growth and DSC study in epoxy-based composites" Coll. Surf. A 257-258 (2005) 339-343

[222]: Wen, X.K.; Shen, Z.M.: "Synthesis of regular coiled carbon nanotubes by Ni-catalyzed pyrolysis of acetylene and growth mechanism analysis" Carbon 39 (2001) 2369-2374

[223]: Wang, N.J.; Su, L.F.; Wu, Z.P.: "Growth of highly compressed and regular coiled carbon nanotubes by spray-pyrolysis method" Cryst. Growth Design 8 (2008) 1741-1747

[224]: Xie, J.N.; Mukhopadyay, K.; Yadev, J.; Varadan, V.K.: "Catalytic chemical vapour deposition synthesis and electron microscopy observation of coiled carbon nanotubes" Smart Mat. Struct. 12 (2003) 744-748

[225]: Fejes, D.; Nemeth, Z.; Hernadi, K.: „CVD synthesis of spiral carbon nanotubes over asymmetric catalytic particles" React. Kin. Cat. Lett. 96 (2009) 397-404

[226]: Zhang M.; Nakayama Y.; Pan L.: "Synthesis of Carbon Tubule Nanocoils in High Yield Using Iron-Coated Indium Tin Oxide as Catalyst" Jpn. J. Appl. Phys. 39 (2000) 1242-1244

[227]: Nagaraju N.; Fonseca A.; Kónya Z.; B.Nagy J.: "Alumina and silica supported metal catalysts for the production of Carbon Nanotubes" J. Mol. Cat. A: Chemical 181 (2002) 57-62

[228]: Yong, Z.; Fang, L.; Zhi-hua, Z.: „Synthesis of heterostructured helical carbon nanotubes by iron-catalyzed ethanol decomposition" Micron 42 (2011) 547-552

[229]: Zhong, Z.; Liu, B.; Sun, L.; Ding, J.; Lin, J.; Tan, K.L.: "Dispersing and coating transition metals Co, Fe and Ni on carbon materials" Chem. Phys. Lett. 362 (2002) 135- 143

[230]: Kovács, Gy.J.: "CNx-Ni nanokompozit vékonyrétegek szerkezete és tulajdonságai" PhD thesis Eötvös Lóránd Tudományegyetem, Műszaki Fizikai és Anyagtudományi Kuatóintézet (2007) pp. 134

[231]: Piedigrosso, P.; Kónya, Z.; Colomer, J.-F.; Fonseca, A.; Van Tendeloo, G.; B.Nagy, J.: "Production of differently shaped multi-wall carbon nanotubes using various cobalt supported catalysts" Phys. Chem. Chem. Phys. 2 (2000) 163-170

[232]: Thien-Nga, L.; Hernádi, K.; Forró, L.: "Catalytic growth of carbon nanorods on a high-T_c substrate" Adv. Mat. 13 (2001) 148-150

[233]: Fonseca, A.; Hernádi, K.; B.Nagy, J.; Bernaerts, D.; Lucas, A.A.: "Optimization of catalytic production and purification of buckytubes" J. Mol. Cat. A: Chemical 107 (1996) 159-168

[234]: Lau, K.-T.; Hui, D.: "The revolutionary creation of new advances materials-carbon nanotube composites" Composites Part B 33 (2002) 263-277

[235]: Agaki, K.; Tamura, R.; Tsukada, M.; Itoh, S.; Ihara, S.: "Electronic structure of helically coiled carbon nanotubes: Relation between the phason lines and energy band features" Phys. Rev. B 53 (1996) 2114-2120

[236]: Agaki, K.; Tamura, R.; Tsukuda, M.: "Electronic structure of helically coiled cage of graphitic carbon" Phys. Rev. Lett. 74 (1995) 2307-2310

[237]: Waters, J.F.; Riester, L.; Jouzi, M.; Guduru, P.R.; Xu, J.M.: "Buckling instabilities in multiwalled carbon nanotubes under uniaxial tension" Appl. Phys. Lett. 85 (2004) 1787-1789

[238]: Chen, X.; Zhang, S.; Dikin, D.A.; Ding, W.; Ruoff, R.S; Pan, L.; Nakayama, Y.: "Mechanics of a carbon nanocoil" Nano Lett. 3 (2003) 1299-1304

[239]: Fonseca, A.; Galvano, D.S.: "Mechanical properties of nanosprings" Phys. Rev. Lett. 92 (2004) 1-4

[240]: Yang, S.; Chen, X.; Katsuno, T.; Motojima, S.: "Controllable synthesis of carbon microcoils/nanocoils by catalysts supported on ceramics using catalyzed chemical vapour deposition process" Mat. Res. Bull. 42 (2007) 465-473

[241]: Chen, X.; Motojima, S.: "The growth patterns and morphologies of carbon micro-coils produced by chemical vapour deposition" Carbon 37 (1999) 1817-1823

[242]: Wang, Z.L.; Yin, J.S.: "Graphitic Hollow Calabashes" Chem. Phys. Lett. 289 (1998)189-192

[243]: Liu, J.; Zhang, X.; Zhang, Y.; Chen, X.; Zhu, J.: "Nano-sized double helices and braids:Interesting carbon nanostructures" Mat. Res. Bull. 38 (2003) 261-267

[244]: Lakeman, C.D.E.; Pan, G.; Muto, N.; Miyayama, M.; Yanagida, H.; Payne, D.A.: "Coiled carbon-fibers from PAN precursors" Mat. Lett. 13 (1992) 330-335

[245]: Pan, L.J.; Hayashida, T; Zhang, M.; Nakayama, Y.: "Field emission properties of carbon tubule nanocoils" Jpn. J. Appl. Phys. 40 (2001) 235-237

[246]: Motojima, S.; Hoshiya, S.; Hishikawa, Y.: "Magnetoresistance in carbon microcoils/PMMA composite beads in W-bands" Carbon 41 (2003) 2658-2660

[247]: Fujii, M.; Matsui, M.; Motojima, S.; Hishikawa, Y.: "Magnetoresistance in carbon micro-coils annealed at various temperatures" J. Cryst. Growth 237 (2002) 1937-1941

[248]: Chiu, H.S.; Lin, P.I.; Wu, H.C.; Hsieh, W.H.; Chen, C.D.; Chen, Y.T.: "Electron hopping conduction in highly disordered carbon coils" Carbon 47 (2009) 1761-1769

[249]: Volodin, A.; Ahlskog, M.; Seynaeve, E.; Van Haesendonck, C.; Fonseca, A.; B.Nagy, J.: "Imaging the Elastic Properties of Coiled Carbon Nanotubes with Atomic Force Microscopy" Phys. Rev. Lett. 84 (2000) 3342-3345

[250]: Volodin, A.; Van Heasendonck, C.; Tarkiainen, R.; Ahlskog, M.; Fonseca, A.; B.Nagy, J.: "AFM detection of the mechanical resonances of coiled carbon nanotubes" Appl. Phys. A 72 (2001) S75-S78

[251]: Volodin, A.; Buntinx, D.; Ahlskog, M.; Fonseca, A.; B.Nagy, J.; Van Haesendonck, C.: "Coiled carbon nanotubes as self-sensing mechanical resonators" Nano Lett. 4 (2004) 1775-1779

[252]: Barreir, A.; Rurali, R.; Hernández, E.R.; Moser, J.; Pichler, T.; Forró, L.; Bachtold, A.: "Subnanometer motion of cargoes driven by thermal gradients along carbon nanotubes" Science 320 (2008) 775-778

[253]: Regan, B.C.; Aloni, S.; Ritchie, R.O.; Dahmen, U.; Zettl, A.: "Carbon nanotubes as nanoscale mass conveyors" Nature 428 (2004) 924-927

[254]: Lau, K.T.; Lu, M.; Liao, K.: "Improved mechanical properties of coiled carbon nanotubes reinforced epoxy nanocomposites" Composites Part A: Appl. Sci. Manufact. 37 (2006) 1837-1840

[255]: Williams, D.B.; Carter, C.B.: "Transmission electron microscopy: A textbook for materials science" 2nd Edition Springer (2009) pp. 760

[256]: Csanady, A.; Kalman, E.; Konczos, G.: "Bevezetés a nanoszerkezetű anyagok világába" MTA Kemiai Kutatoközpont, ELTE Eötvös Kiado Kft., Budapest (2009) pp. 313

[257]: Burger K.: "Az analitikai kémia alapjai: Kémiai és műszeres elemzés" Alliter Kiadó és oktatásfejlesztő alapítvány, Budapest (2002) pp. 642

[258]: Bister, G.: "Etude de la synthése par CCVD et du méchanisme de formation des nanotubes de carbone monoparois" PhD thesis, Facultés Universitaires Notre-Dame de la Paix; Faculté des Sciences (2005) pp. 267

[259]: Reznik, D.; Olk, C.H.; Neumann, D.A.; Copley, J. R.D.: "X-ray powder diffraction from carbon nanotubes and nanoparticles" Phys. Rev. B 52 (1995) 116-124

[260]: Zhang, M.; Xu, C.L.; Cao, L.M.; Wu, D.H.; Wang, W.K.: "Deformation of catalytically grown carbon nanotubes induced by annealing under high pressure" J. Mat. Res. 15 (2000) 253-261

[261]: Bíró, L.P.; Márk, G.I.: "STM investigation of carbon nanotubes" Carbon filaments and Nanotubes: Common Origins, Differing Applications? Editors: Bíró, L.P.; Bernardo, C.A.; Tibbets, G.G.; Lambin, Ph.; Dordrecht, Kluwer Academic Publishers (2001) 219-231

[262]: Bíró, L.P.: "Atomic force microscopy investigation of carbon nanotubes" Carbon filaments and Nanotubes: Common Origins, Differing Applications? Editors: Bíró, L.P.; Bernardo, C.A.; Tibbets, G.G.; Lambin, Ph.; Dordrecht, Kluwer Academic Publishers (2001) 219-231

[263]: Rao, A.M.; Richter, E.; Bandow, S.; Chase, B.; Eklund, P.C.; Williams, K.A.; Fang, S.; Subbaswamy, K.R.; Menon, M.; Thess, A.; Smalley, R.E.; Dresselhaus, G.; Dresselhaus, M.S.: "Diameter-Selective Raman Scattering from Vibrational Modes in Carbon Nanotubes" Science 275 (1997) 187-191

[264]: Yu, Z.H.; Brus, L.: "Rayleigh and Raman scattering from individual carbon nanotube bundles" J. Phys. Chem. B 105 (2001) 1123-1134

III. Experimental

III.1. Applied Materials:

Catalyst Preparation:

$Co(CH_3COO)_2*4H_2O$ (Aldrich)

$Fe(NO_3)_2*9H_2O$ (Aldrich)

$Pr(NO_3)_3*6H_20$ (Aldrich)

SiO_2 gel (Aldrich, Merck)

Al_2O_3 (Aldrich)

Sepiolite (Fluka)

NH_4OH 30%(Aldrich)

CNT Synthesis:

C_2H_2 (Air Liquide)

C_2H_4 (Air Liquide)

N_2 (Air Liquide)

Sample Preparation for Microscopy:

Ethanol (Sigma-Aldrich)

Patosolv(Molar Chemicals)

Thermal Analysis:

Air (Air Liquide);

Oxygen (Air Liquide);

III.2. Catalyst Preparation

III.2.1. Alumina-supported catalysts:

The alumina-supported catalysts were prepared with the impregnation method. The metal salts were dissolved in distilled water, the support material was added to the solution while stirring. The pH was adjusted adding ammonia solution. The mixture was filtered and washed

with distilled water. The filtered cake was dried at 120°C overnight and was grinded using ball-milling.

III.2.2. Silica-supported catalysts:

The silicagel supported catalyst were prepared by the ion-adsorption precipitation method, since this preparation method using silicagel support was prooved to be more efficient for the synthesis of carbon nanotubes especially for the coiled carbon nanotubes ***[1]***.

The Co^{2+} ions can be precipitated in Co $(OH)_2$ form with the addition of ammonia-solution, in case of high ammonia concentration Co^{2+} amino complexes are also formed that influence the quality of the catalyst and the product after the synthesis ***[2, 3]***. The ion concentration of the solution is determined by the following reactions:

$$Co^{2+}+2OH^- = Co(OH)_2$$

$$CH_3COO^-+HOH=CH_3COOH+OH^-$$

$$NH_3^+ + HOH = NH_4^+ + OH^-$$

$$CO(NH_3)^{2+}_n + NH_3 = Co(NH_3)^{2+}_{n+1}$$

The precipitated metal salts are colloidal and generally have asymmetric form. These particles get easily adsorbed on the surface of the silicagel particles. Changing the pH of the Co-solution Co-particles of different sizes are formed. In case of higher pH bigger $Co(OH)_2$ aggregates are formed, hence the possibility of the asymmetric aggregations is higher. This explains the fact that with higher pH more helicoidal nanotubes are formed.

The metal salts were dissolved in 30-50 ml of distilled water and sonicated for 15 minutes. Afterwards, the silicagel was added. The desired pH was obtained by the addition of 30% NH_3 solution. The so-obtained suspension was stirred for 24 hours. The pH of the mixture was controlled and reset to the desired value, after it was filtered and washed with distilled water. The catalyst was dried overnight in the oven at 120°C.

III.2.3. Sepiolite-supported catalysts:

Sepiolite is a hydrated magnesium silicate which consists of fibrous talc-like layers stacked in long ribbons with micro channels and grooves parallel to the fiber axis, and its ideal chemical formula can be given as $Si_{12}Mg_8O_{32}.nH_2O$ ***[4]***. It attracts significant industrial interest mostly due to its properties. Its specific structure, high surface area outstanding physicochemical activity and high thermal resistance permits numerous applications in various fields. Sepiolite is used in filtering, molecular sieving, adsorption and catalysis. Due to its high thermal resistivity, high surface area and extraordinary sorption properties it is a suitable support material for the CVD synthesis of carbon nanotubes ***[5, 6]***.

The appropriate amount of sepiolite (Fluka) was suspended in distilled water and the so obtained suspension was stirred mechanically at 80 ^oC for 1h. The dissolved Co and Fe salts (Co acetate: Co $(CH_3COO)_2x4\ H_2O$ Aldrich, and Fe nitrate: $Fe(NO_3)_2x9H_2O$ Aldrich) were added to the sepiolite suspension. The total metal content of the catalyst was 5wt%. After the addition of the metal salts the suspension was stirred for other 3h maintaining the temperature at 80 ^oC. Then it was either freezed and lyophilized, or filtered and dried overnight in the oven at 80°C and then grinded.

III.3. Carbon Nanotube Synthesis:

The carbon nanotubes were synthesized in a fixed bed flow reactor (Figure III.1.). Two furnaces were used in the course of this work. The two used systems differed concerning the dimensions of the furnaces and the reactors. The same plot can be used for their description. The catalyst was placed in a quartz boat inside a quartz reactor (d: 3cm; l: 50 cm in case of the smaller reactor and d: 4cm; l: 120cm for the big reactor). To reach the high temperatures of the synthesis the reactor was introduced into a furnace (CENTION EUROTHERM 3216 and CARBOLITE GHA 12/1050).

The temperature profile of the furnace was determined. The gas flows were calibrated using a soap-film flow meter.

In the case of the big reactor at the University of Calabria the gases were led from the gas-cylinders to the reactor using Swagelok tubes and valves; the gas flows were controlled by Brooks flow controllers. The system was projected and installed by our research group.

During the reactions ethylene or acetylene was used as carbon source, and N_2 was applied for the evacuation and as carrier gas. After placing the quartz boat in the reactor the air was evacuated flowing N_2 for 10 or 20 minutes depending on the gas flow rate. For the reaction itself the reactor was placed into the furnace and the carbon source flow was launched. After the reaction the reactor was drawn out of the furnace and cooled down in nitrogen flow. The product was weighed and stored in a plastic flask for further analysis.

The carbon deposit and the carbon yield are two parameters that characterize the productivity of the CNT synthesis and can be calculated according to the following equations:

Carbon deposit (wt %) =($(m_{product} - m_{catalyst})/m_{catalyst}$)*100

Carbon yield (wt %) = $(m_{product}/m_{introduced\ carbon})$*100

The blank reactions were carried out using the exact same parameters as for the CNT synthesis reactions in absence of the carbon source. These reactions were used to determine the weight loss of the catalyst.

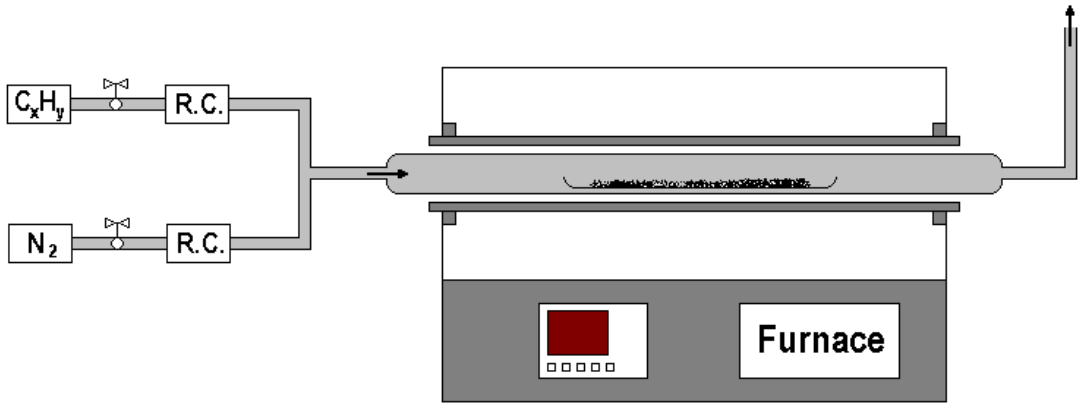

Figure III.1.: Scheme of the experimental setup for CNT synthesis

III.4. Sample Characterization:

III.4.1. Thermal Analysis:

The thermal behaviour of the catalysts and the synthesized carbon nanotube samples were analyzed either with a SHIMADZU DTG-60 simultaneous TG/DTA analyzer. 10-40 mg of the sample were placed in a platina sample holder and heated to 850°C with a 5-10°C/min ramp in 20 ml/min air flow; or with a SETARAM LABSYS S60 simultaneous TG/DTA analyzer in 20 ml/min oxygen-flow applying the previously described conditions. The

obtained TGA and DTA diagrams provide qualitative and quantitative information of the samples. The carbon deposit was also calculated form the TGA diagrams and compared to the values obtained by weighing the sample after the synthesis reaction.

III.4.2. X-Ray Diffraction:

The X-ray diffractograms were obtained using a Rigaku Miniflex II Desktop X-Ray Diffractometer applying a Ni-filtered Cu-Kα radiation The diffractograms were taken at a continuous scanning method applying a scanning speed between 1.5-4°/min in the 2θ range of 5-80°.

III.4.3. Transmission Electron Microscopy:

The quality and morphology of the synthesized carbon nanotube samples were analysed using this technique. Some mg-s of the sample was suspended by sonication in 2-3ml of ethanol or patosolv and consequently drop-dried on holey carbon film coated 200 mesh copper grids. The TEM micrographs were taken with a Philips CM 10 microscope operating at 100 kV. The micrographs were taken with digital cameras. For the evaluation and the determination of the diameter distribution of the samples Soft Imaging Viewer and ImageJ softwares were used. The diameter distribution graphs were prepared using STATISTICA or ORIGIN software, exploiting data of at least 200 measured nanotubes.
Electron diffraction patterns were taken with a FEI TECNAI G^2 transmission electron microscope operating at 200 kV. Samples were prepared in the above described way.

III.4.4. Scanning Electron Microscopy:

The surface of the synthesized samples was examined with an ESEM –FEG QUANTA 200 electron microscope. The samples were covered with a thin gold layer obtained with the metalisation method.

References:

[1]: Szabo A., Fonseca A., Biro L.P., Konya Z., Kiricsi I., Volodin A., Van Hasendonck C., B.Nagy J.: „Synthesis, Characterization and Use of Coiled Carbon Nanotubes" Nanopages 1 (2006)3, 263-293

[2]: Piedigrosso, P;, Kónya Z.; Colomer, J.-F.; Fonseca, A.; Van Temdeloo, G.; B.Nagy, J.: "Production of differently shaped multi-wall carbon nanotubes using various cobalt supported catalysts" Phys. Chem. Chem. Phys. 2(2000)163-170

[3]: Hernádi, K.; Thien-Nga, L.; Forró, L: "Growth and Microstructure of Catalytically Produced Coiled Carbon Nanotubes". J. Phys. Chem. B 105 (2001) 12464-12468

[4]: Goktas, A.A.; Misirli, Z.; Baykara, T.: „Sintering behaviour of sepiolite". Ceram. Int. 23 (1997) 305-311

[5]: Okte, A. E.; Saymsoz, E.: "Characterization and photocatalytic activity of TiO_2 supported sepiolite catalysts". Sep. Purif. Techn. 62 (2008) 535-543

[6]: Destrée, A.: "Syntheses de nanotubes de carbone sur catalyseur á base de l'argile. Perspectives d'utilisation dans des nanocomposites á matrices souples" PhD thesis, University of Namur, Belgium (2007) 166 pp

IV. Results and Discussion

IV.1. Calibration of the oven and gas flows

The first part of the experimental work of the thesis was the installation of the experimental setup (described in the previous chapter) and the calibration of the furnace.

IV.1.1. Calibration of the oven

As the temperature is a critical parameter for the CCVD synthesis of the carbon nanotubes, it is necessary to define the temperature profiles of the furnace. It is to be emphasized that the oven remains open at both ends.

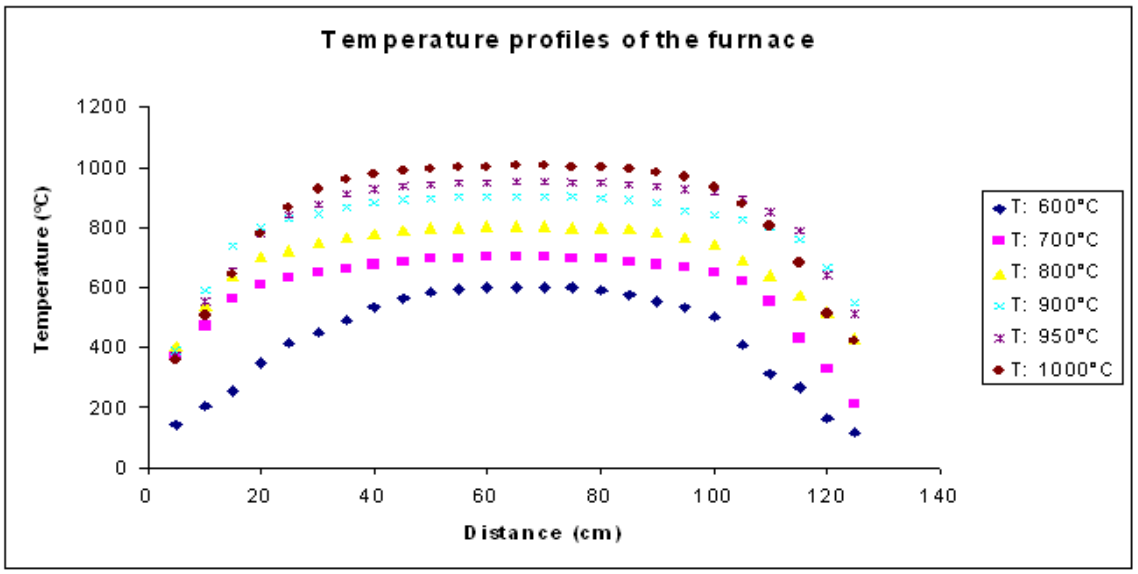

Figure IV.1.: Temperature profiles of the Carbolite furnace

We can observe on the temperature profiles (Figure IV.1.), that the furnace has a constant temperature zone of about 40-45 cm, where the measured temperature inside the furnace is equal to the one set; hence the quartz boat with the catalyst has to be placed in this zone.

IV.1.2. Gas flow calibration

To determine the effective gas flow that enters the reactor a simple bubble flow-meter was applied. The gas flow rates in ml/min were determined in function of the aperture of the valve (%). The effective flows of nitrogen, ethylene, acetylene, methane, hydrogen, helium and oxygen were monitored. Figures IV.2. and IV.3. show the calibration curves of the gases applied in the present work.

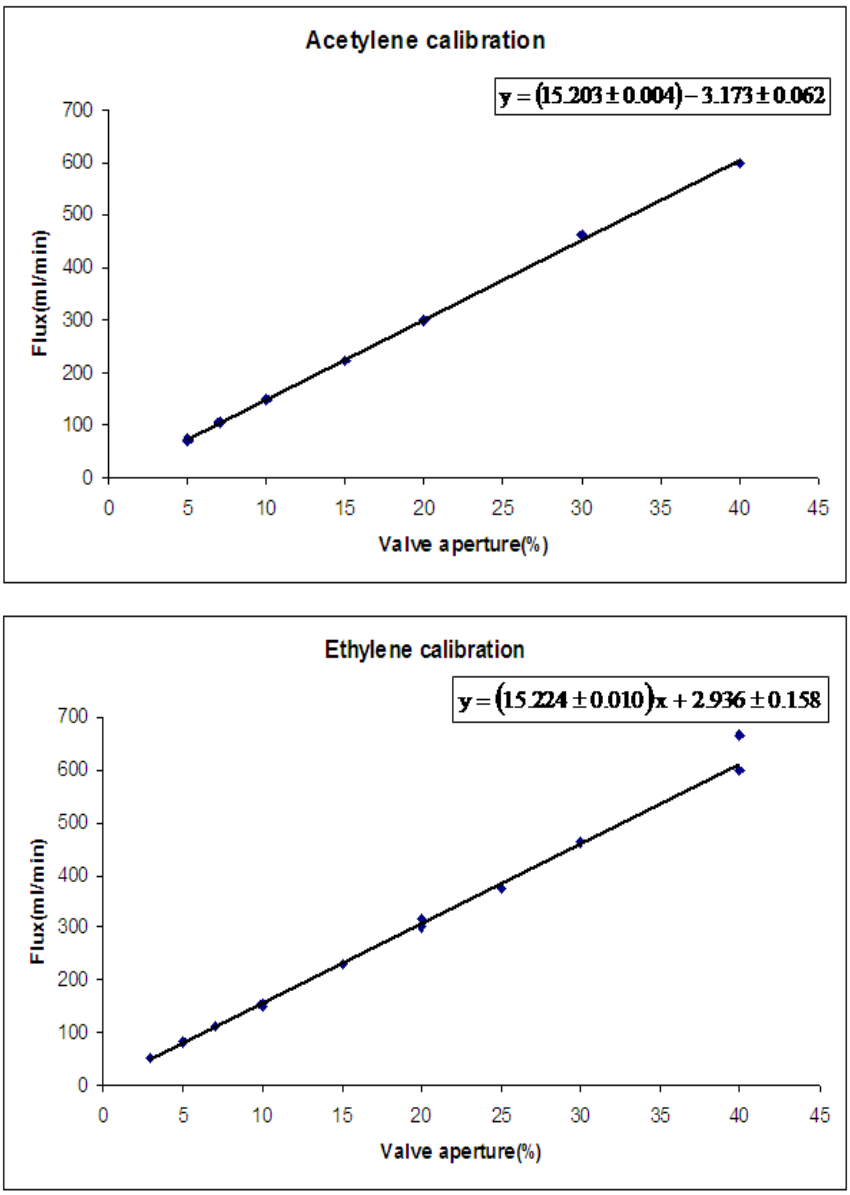

Figure IV.2.: Calbiration curves of applied carbon source gases

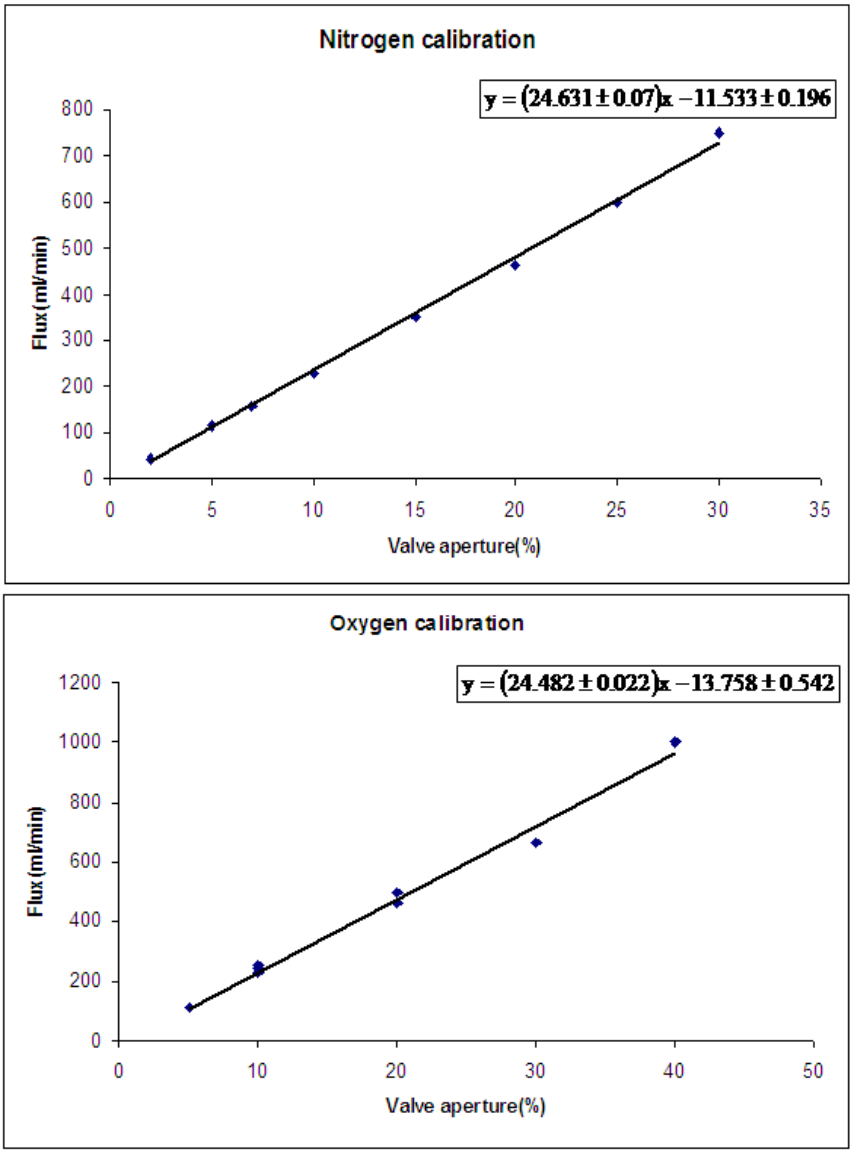

Figure IV.3.: Calbiration curves of nitrogen and oxygen

IV.2. Alumina Supported Catalysts

Alumina supported transition metal catalysts are widely used for the production of carbon nanotubes also at industrial scale (NANOCYL produces multiwalled carbon nanotubes, using this support). The main advantages of this support material are the high carbon deposit and the relatively low amount of amorphous carbon in the obtained product ***[1].*** This was the reason why we chose this support material. Szabo et al. previously reported the successful

synthesis of coiled carbon nanotubes on Co-Fe/Al_2O_3 catalyst using 30 ml/min acetylene flow at 700°C. However, the quantity of the coiled CNTs compared to straight ones was low ***[2].*** Changing the carbon source, the reaction temperature and the gas flow we aimed to investigate whether the ratio of the helicoidal CNTs in the product can be significantly augmented. Ethylene and acetylene were both tested as carbon source at different gas flows at temperatures varying from 600 to 700°C on 3.5%Co-1.5%Fe/Al_2O_3 catalyst that resulted in producing helically coiled CNTs in the highest ratio of alumina supported catalysts according to previous studies ***[2, 3].*** The applied catalyst mass was 1 g and the reaction time was 30 min in all the cases.

IV.2.1. Effect of gas flow rates and carbon sources

Carbon source	Gas flow (ml/min)	Carbon Deposit (%)	Carbon Yield (%)	TEM observations
Ethylene	300	182.1	19.9	Long wavy bundles, straight well-graphitized nanotubes, small amount of amorphous carbon
Ethylene	1000	203.2	6.6	Long wavy bundles, straight well-graphitized nanotubes, small amount of amorphous carbon
Acetylene	70	162.1	75.6	Long nanotubes in wavy bundles, some helicoidal CNTs and Y-junctions observed
Acetylene	43	115.8	88	Long nanotubes in wavy bundles, some wavy but not regularly coiled CNTs

Table IV.1.: Products synthesized on 3.5%Co-1.5%Fe/Al_2O_3 catalyst using ethylene or acetylene as carbon source at 700°C

Table IV.1. shows the carbon deposit and carbon yield values obtained on the tested catalyst (3.5%Co-1.5%Fe/Al_2O_3) applying different gas flow rates of ethylene or acetylene. Using ethylene as carbon source straight, long well-graphitized tubes were formed. Helically coiled CNTs were not observed in the synthesis products even at higher gas flow rates. In the case of acetylene the increase of the gas flow from 43 ml/min to 70 ml/min leads to approximately 35% increase in the carbon deposit. Regularly coiled nanotubes were occasionally observed at the samples prepared with 70 ml/min acetylene flow. However, TEM investigations revealed

no significant increase in the quantity of the observed helices by increasing the applied gas flow. Concerning the carbon sources, in the case of acetylene some coiled nanotubes were observed by microscopic analyses. Ethylene was not active in the formation of helicoidal nanotubes in our reaction conditions.

Thermal analyses of the synthesis products confirm the high obtained carbon deposit. The presence of a low amount of amorphous carbon is suggested by a small peak on the TG curves between 300-330°C for all the samples. Typical TG, DrTG (Derivative TG) and DTA curves of the samples synthesized on alumina supported 3.5%Co-1.5%Fe catalyst can be seen in Figure IV.4. Figure IV.4.(a) shows the TG, DrTG and DTA curves of a sample synthesized at 600°C using 70 ml/min acetylene as carbon source. On the DTA curve two peaks can be observed. A small peak can be found at around 300°C which corresponds to the amorphous carbon in the sample, and a tall, relatively thin peak at 516°C corresponding to the multiwalled CNTs. The total weight loss between 400 and 700°C is 64%, this is the weight loss related to the second peak on the DTA curve, hence the carbon nanotubes. In Figure IV.4.(b) we can see the thermal analysis diagram of a CNT product synthesized at 700°C using 300 ml/min ethylene as carbon source. Here the peak corresponding to the disorganized carbon is small on the DTA curve of this sample as well, however it can be found at a slightly higher temperature: 336°C. While the peak germane to the multiwalled CNTs, found at 540°C is larger, that can suggest a not so uniform or poorer graphitized product compared to the previous case. The large peak can also be caused by the different morphology, maybe density of the long CNTs bundles, the different organization of the tubes inside the bundles. While in Figure IV.4.(c) a larger peak can be observed that starts at around 400°C and goes till 600°C. This seems to be composed of two peaks that are close: a first one at 466°C and a second one at around 520°C. Probably both of the peaks correspond to graphitised carbon, considering the further transmission electron microscopy observations, to multiwalled carbon nanotubes. Also in this case the DTA curve suggests a not so uniform product or poorer graphitized product, or a diverse morphology or density of the bundles.

a)

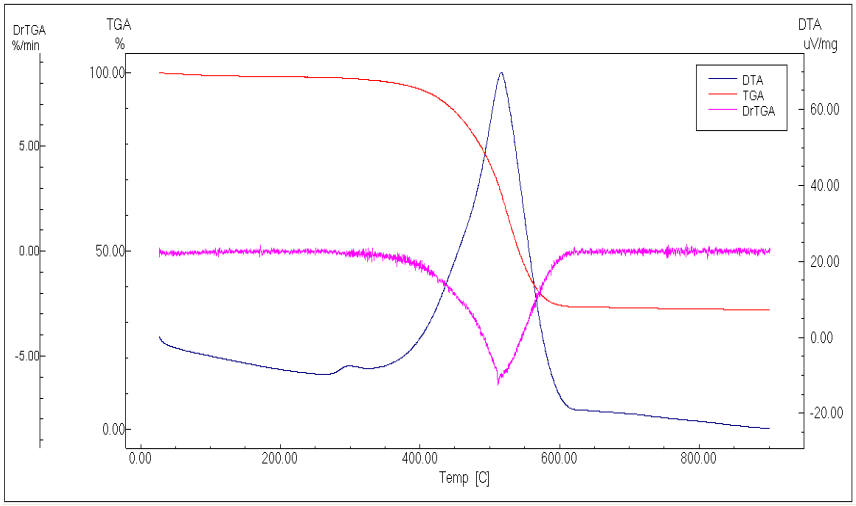

b)

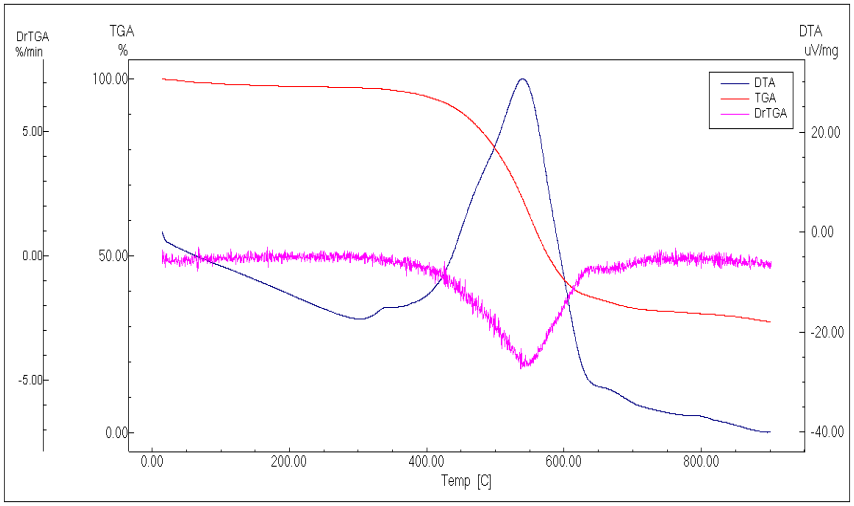

c)

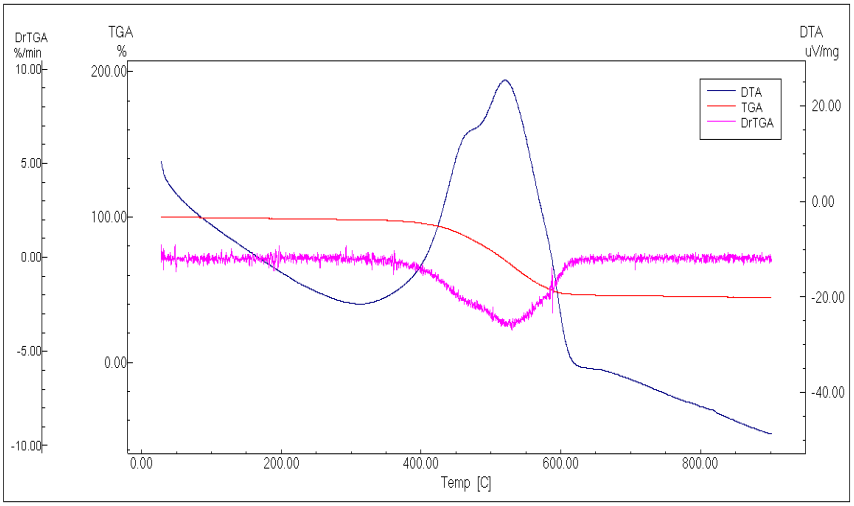

Figure IV.4.: TG, DrTG and DTA curves of synthesis products prepared on 3.5%Co-1.5%Fe/Al_2O_3 catalysts: a) carbon source: acetylene (70 ml/min) T:600°C; b) carbon source: ethylene (300 ml/min) T:700°C; c) carbon source: ethylene (1000 ml/min) T:700°C

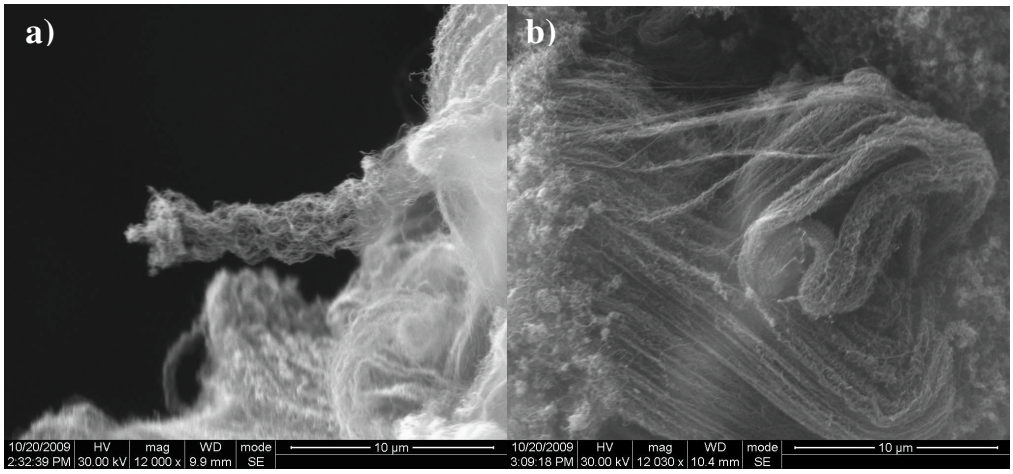

Figure IV.5.: SEM images of samples synthesized on alumina supported Co-Fe catalysts using ethylene as carbon source (gas flows: a) 300 ml/min; b) 1000 ml/min). The long, wavy bundles are characteristic of this support.

On SEM micrographs (Figure IV.5.) of samples synthesized using either ethylene or acetylene as carbon source we can observe the characteristic long wavy bundles**.** Numerous 10-50 µm long bundles can be seen. The thickness of the bundles varies between 1-20 nm; they are often twisted or bent. The catalyst surface is totally covered by the synthesized tubes.

Looking inside the long, wavy bundles with transmission electron microscopy (Figure IV.6.) long, wavy nanotubes can be observed which are not regularly coiled in most of the cases, but they are often bent possibly for the sake of their length. The tubes are hollow inside, and have mainly closed tips. Catalyst particles can be occasionally observed inside the tubes. The walls of the tubes present many defects, which are characteristic for the CNTs produced by catalytic way. Figure IV.7. shows the diameter distribution of two MWCNT samples synthesized at 700°C. The mean diameter values range from 5.2 to 5.8 nm for all the synthesized samples. The outer diameters of the multiwalled CNTs in the samples are between 2-12 nm, but around 50% of the analyzed tubes have diameters between 4-6 nm.

In the samples synthesized using acetylene as carbon source some regularly coiled CNTs can be observed. These helicoidal CNTs have diameters between 4-8 nm. According to our observations, their coil pitches vary from 15 to 270 nm and their coil diameters are between 13-96 nm. The observed coils are generally S-shaped. Tight or spring-like coils were not found in the sample. Calculating the coil curvature values they vary between 5-90.

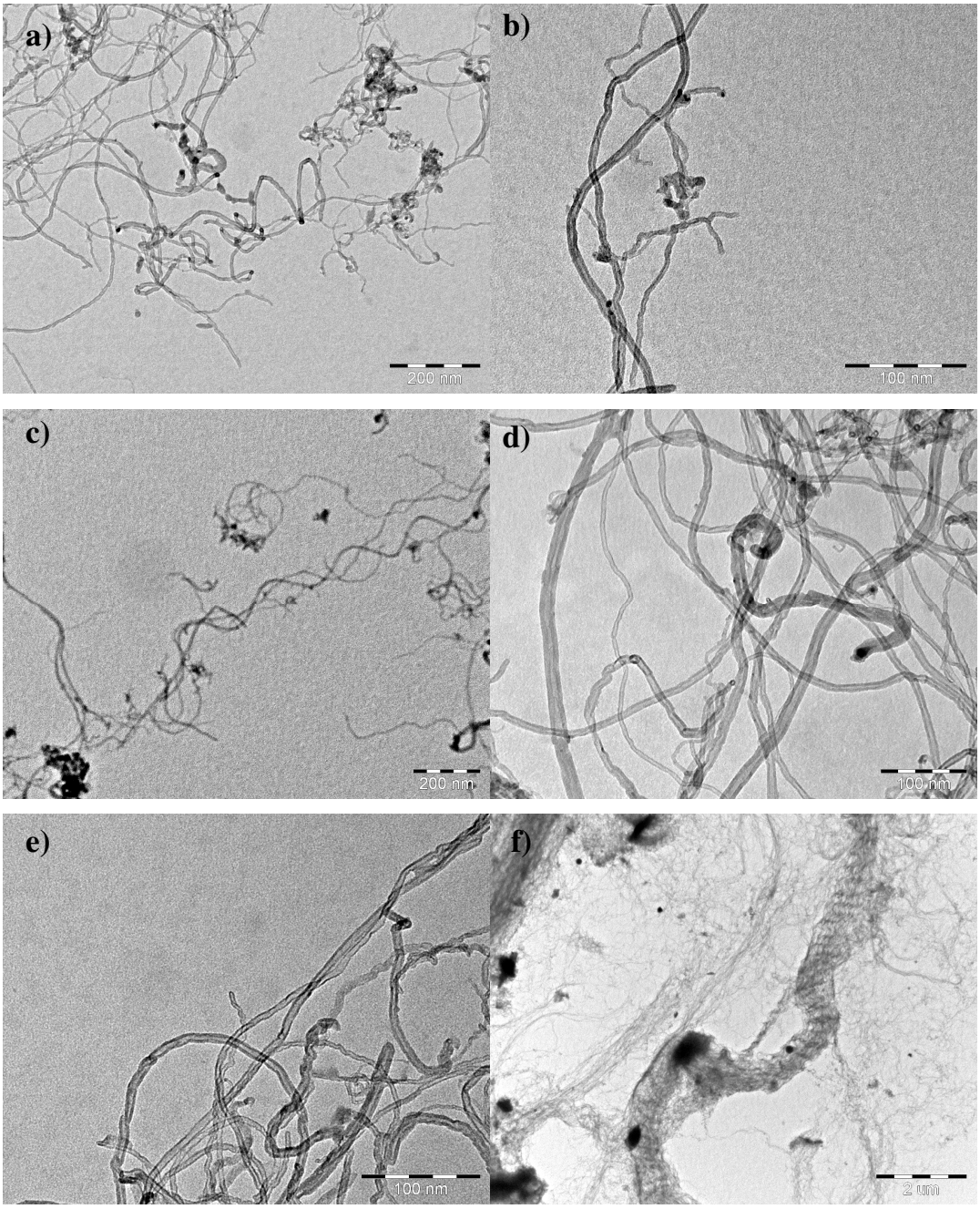

Figure IV.6.: TEM micrographs of samples synthesized on 3.5%Co-1.5%Fe/alumina catalysts: a) and c) short wavy coiled tubes; b) Y-junction; d-e) curved tubes but no regular coils; f) wavy bundles of long multiwalled CNTs

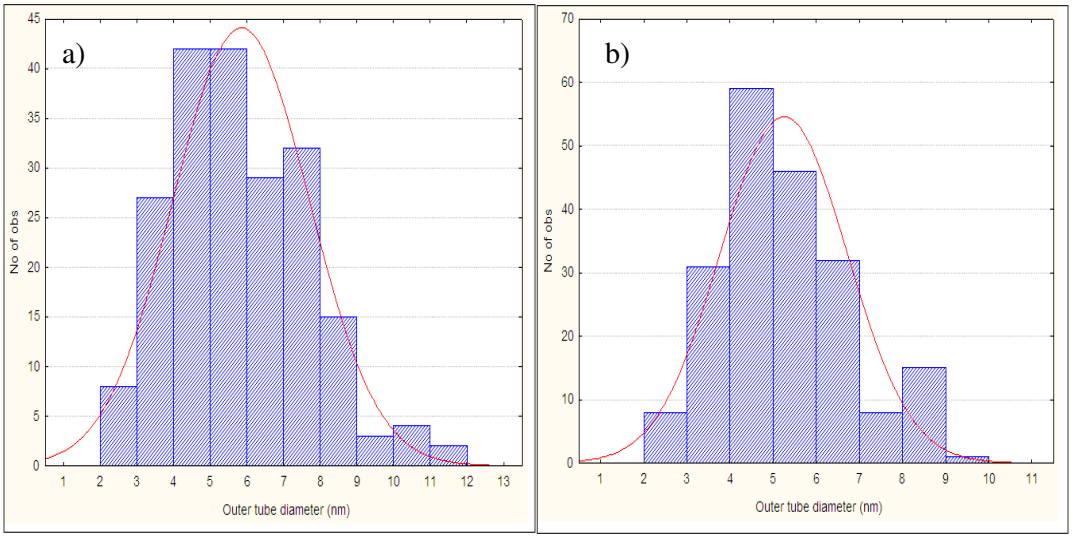

Figure IV.7.: Diameter distribution of multiwalled CNTs synthesized on 3.5%Co-1.5%Fe/Al_2O_3 catalyst: a) carbon source: acetylene (43 ml/min); b) carbon source: ethylene (300ml/min) at 700°C

IV.2.2. Effect of the reaction temperature

Synthesis temperature (°C)	Carbon Deposit (%)	Carbon Yield (%)	TEM observations
600	112.6	85.6	Long nanotubes in wavy bundles, some wavy but not regularly coiled CNTs
650	114.7	87.1	Long nanotubes in wavy bundles, some wavy but irregularly bent, curved CNTs and some regularly coiled CNTs
700	115.8	88	Long nanotubes in wavy bundles, some wavy but irregularly bent, curved CNTs and some regularly coiled CNTs

Table IV.2.: Product synthesized on 3.5%Co-2.5%Fe/Al_2O_3 catalyst using acetylene as carbon source (43 ml/min) at different temperatures.

Observing the data presented in the Table IV.2. we can see that changing the synthesis reaction temperature from 600 to 700°C applying 43 ml/min C_2H_2 flow does not imply significant changes in the carbon deposit and the carbon yield in the reactions. This can also

be due to the high value of carbon yield obtained already at 600°C. Already at this temperature 85% of the entering carbon source is transformed into some kind of carbonaceous synthesis product. However, considering the results obtained applying a higher flow of acetylene: 70 ml/min, the carbon deposit values are higher (around 155-160%) and the carbon yield values are lower (73-75%), but the changes induced by the change of the reaction temperature between 600-700°C remain practically negligible.

As for the morphology of the analysed samples, from TEM micrographs we can establish that in the synthesis product synthesized at 600°C with 43 ml/min and 70 ml/min acetylene flow no regularly coiled CNTs were found. However, in the samples synthesized at 650°C and 700°C we can observe occasionally some regularly coiled CNTs, and some nanotubes where a part of the nanotube is coiled and than it becomes straight.

In conclusion, we can say that the characteristic long, twisted, wavy bundles of multiwalled CNTs can be easily observed also at lower resolution SEM micrographs. Looking inside the bundles with TEM we can observe that the tubes are generally wavy, but not regularly coiled. Some exceptions can be rarely observed. Synthesis of Y-junctions was also occasionally observed in the obtained products. We can conclude that changing the reaction conditions to this extent did not lead to significant increase in the proportion of helically coiled CNTs in the synthesis product: they remain occasional and can be considered as by-products in the samples. Their quantity compared to the straight multiwalled CNTs in the sample remains inferior to 1%.

IV.3. Sepiolite Supported Catalysts

During a previous study carried out in our laboratory ***[4]*** multiwalled carbon nanotubes were synthesized on sepiolite supported Co-Fe catalysts with high yield. In some synthesized CNT samples besides thin straight multiwalled carbon nanotubes, regularly coiled CNTs were also observed in a low percentage. Hence further experiments were carried out with this support investigating the possibility of increasing the ratio of coiled multiwalled CNTs in the synthesis product. Acetylene and ethylene were both used as carbon source. The standard applied gas flows were 1400 ml/min C_2H_4; 140ml/min N_2 for ethylene and 30 ml/min C_2H_2 and 300 ml/min N_2 for acetylene. Co-Fe mixed catalysts and Pr-containing catalyst were tested in the synthesis reactions. The total metal concentration of the catalysts was 5 wt% for all the tested catalysts in this work.

IV.3.1. Co-Fe mixed catalysts

Regularly coiled multiwalled carbon nanotubes were observed in CNT samples synthesized at 700°C on 2.5%Co-2.5%Fe/SEP catalysts. 1400 ml/min C_2H_4 flow was used as carbon source and 140 ml/min N_2 as carrier gas. These reaction conditions lead to a high carbon deposit value, however the carbon yield remains low also due to the high gas flows applied. Thermal analysis results (Figure IV.8.a)) show a weight loss of around 80%: this represents the ratio of the carbonaceous material in the synthesis product. The DTA curve shows one relatively thin peak around 565-570°C, this corresponds to the multiwalled nanotubes in the synthesis product. On the DTA curve we can equally observe a really small peak at around 330°C that corresponds to the amorphous carbon. The fact that this peak is small and we cannot observe either a corresponding peak on the DrTGA curve or a significant weight loss on the TG curve around this temperature means that the relative amount of this disorganized carbon in the synthesis product is low. Around 820°C another small peak can be observed on the DTA curve corresponding to the conversion of the sepiolite into its anhydrous form ***[5, 6].***

For the samples synthesized on the 4% Co-1%Fe catalyst the DTA and DrTGA peaks are thicker (Figure IV.8.b)). The peaks indicating the presence of the amorphous carbon and the recrystallization into clino-enstatite are higher and more visible.

Mutliwalled carbon nanotubes are obtained in better quality and higher quantity on the 2.5%Fe-2.5%Co catalyst. This can be due to the better distribution or stabilization of the catalyst particles on the sepiolite support applying Fe and Co in this proportion.

Figure IV.9. shows some TEM micrographs taken on the samples synthesized on Co-Fe /SEP catalysts with different metal proportions.

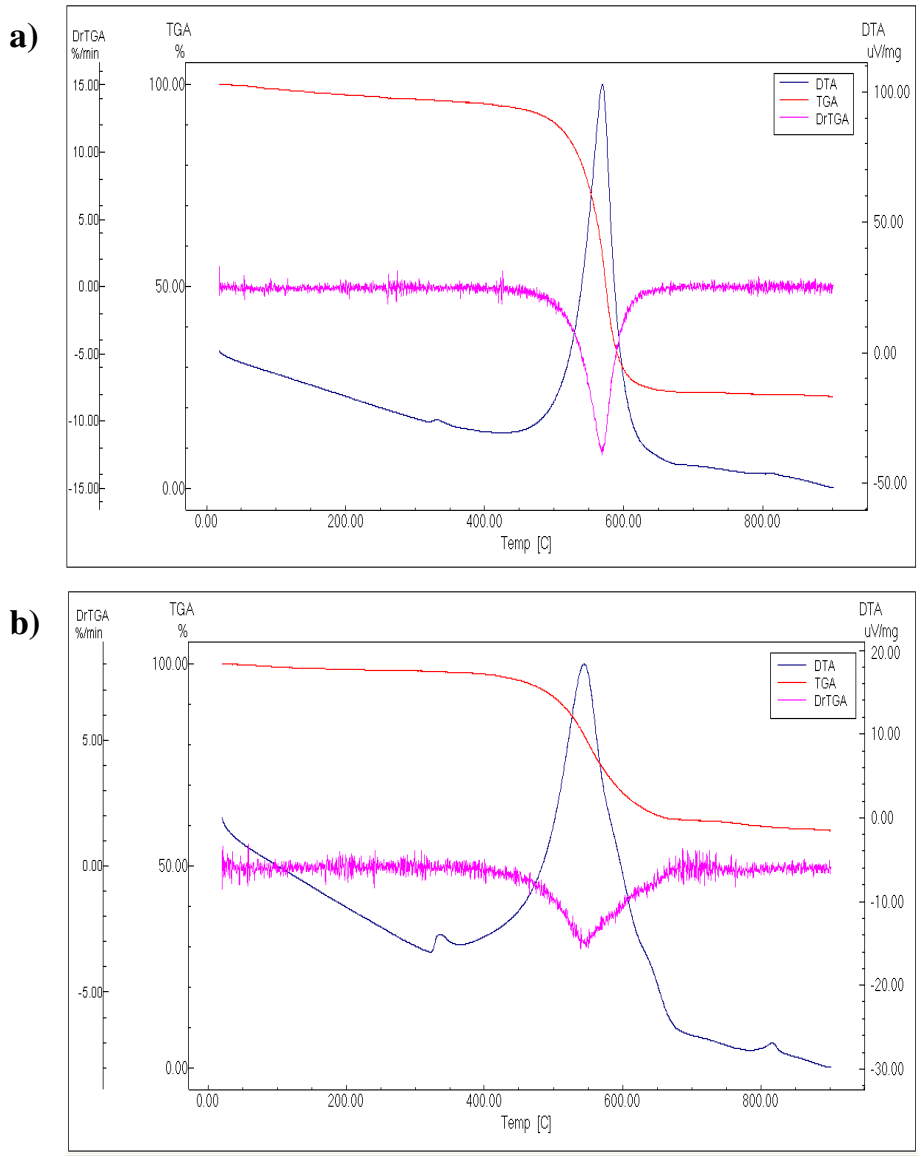

Figure IV.8: TG, DTG and DTA curves of CNT samples synthesized on a) 2.5%Co-2.5% Fe sepiolite-supported catalysts (lyophilised); b) 4%Co-1%Fe sepiolite-supported catalysts (dried in the oven)

Coiled CNTs were regularly found in each sample. Synthesis products prepared on 2.5%Co-2.5%Fe/SEP catalyst contain regularly coiled CNTs. However, their quantity is really low compared to the number of straight tubes: inferior to 1% in the whole product. Mainly S-formed spirals were observed. Their coil pitches varied from 20 to 130 nm, and their coil diameters between 28-40 nm. The spirals are generally some hundreds of nm to 1µm long. Short spirals and ones with changing coil diameter and pitch can also be observed. The

diameter of the spirals found in the sample synthesized on the 4%Co-1%Fe catalyst is between 10-14 nm. The coil pitches (P) of the spirals vary less: they are between 50-70 nm while the coil diameters range from 30 to 40 nm. The spirals are 1-2% of the total number of tubes. Also in this case S-formed helices were observed, tight coils are not present in the sample. The coiled CNTs are generally shorter in these samples: many of them are 200-400 nm long, longer coils of around 1 μm were rarely found. The slight increase of the relative quantity of helically coiled CNTs by changing the ratio of the metals in the catalyst can also be due to the occasionally bigger or less stable catalyst nanoparticles.

The coil curvature (ρ) of a helix can be calculated according to the following equation:

$$\rho = \frac{R^2 + (P/2\pi)^2}{R} \quad \text{where } R = \frac{D-d}{2}$$

R is the coil radius, D is the coil diameter, d the outer tube diameter of the helix while P is the coil pitch. Calculating the coil curvature (ρ) values of all the helices observed on sepiolite catalysts in most cases they remain between 11-23. There are some exceptions: very rarely coiled CNTs with coil curvatures of around 40 are found in the synthesis products. Calculating the corresponding P/R values for more than 50% of the found helices in this case are between 5 and 6.

Y-junctions were also found occasionally in the sample synthesized on 4%Co-1%Fe catalyst.

Table IV.3. summarises the characteristics of produced coiled carbon nanotubes.

Catalyst	**Carbon deposit (wt%)**	**Characteristics of Coiled CNTs in the sample**			
		Quantity (%)	**Outer tube diameter (nm)**	**Coil pitch (nm)**	**Coil diameter (nm)**
2.5%Co-2.5%Fe	150%	<1%	7-12	20-130	28-40
4%Co-1%Fe	67%	1-2%	10-14	50-70	30-40
1%Co-4%Fe	46%	1-2%	10-13	40-70	30-40

Table IV.3.: Characteristics of CNT samples and coiled CNTs synthesized on Co-Fe/SEP mixed catalysts (T:700°C, 1400 ml/min C_2H_4; 140ml/min N_2, reaction time: 20 minutes)

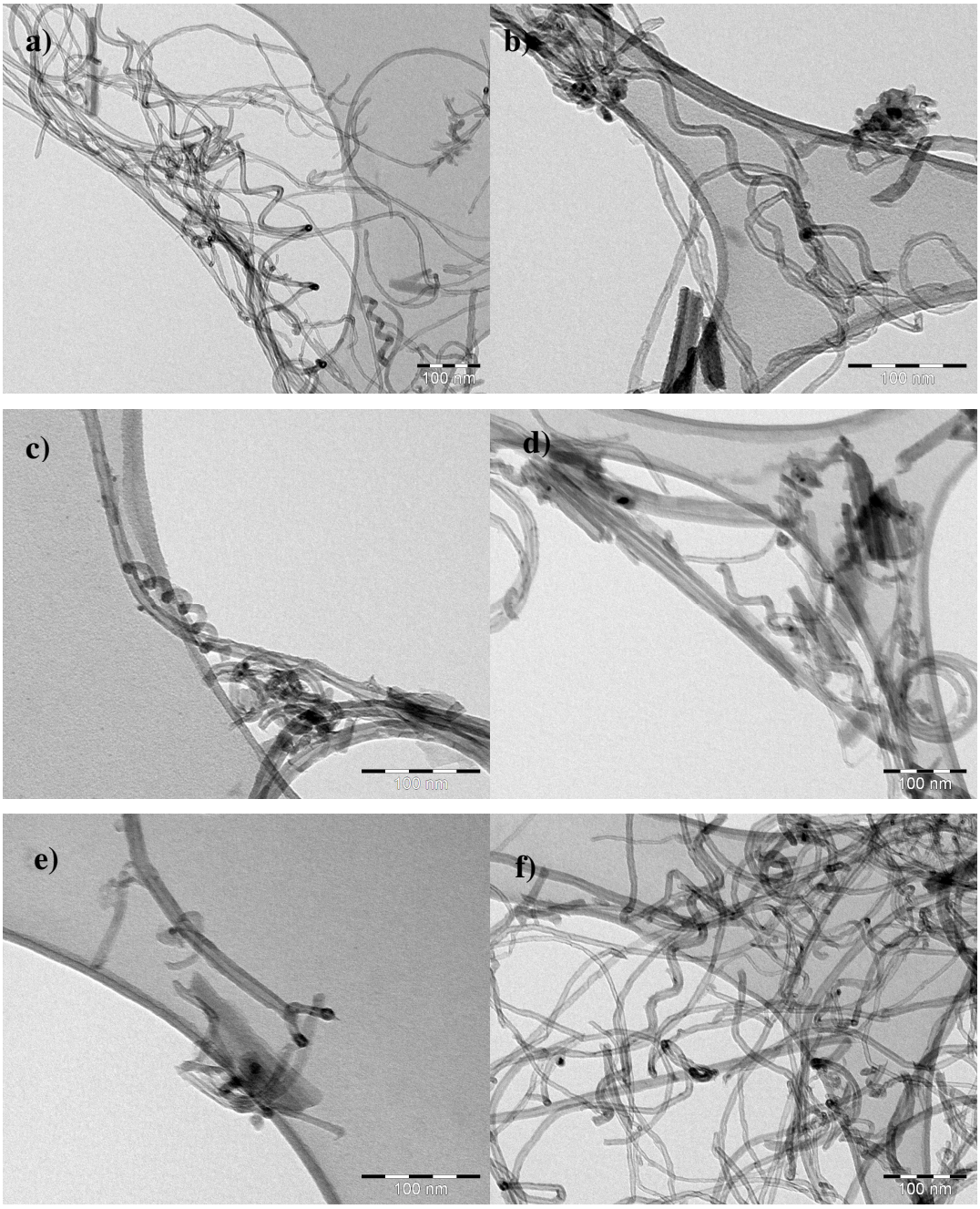

Figure IV.9.: TEM pictures synthesized on sepiolite-supported catalysts: a) and f) 2.5%Fe-2.5%Co/SEP; b)-d) 4%Co-1%Fe/SEP; e) Y-junction in a sample synthesized on 4%Co-1%Fe/SEP catalyst

According to our observations relatively thin, well graphitized multiwalled carbon nanotubes are produced on the 2.5%Co-2.5%Fe catalyst. The XRD diffraction pattern of purified sample synthesized on 2.5%Co-2.5%Fe lyophilised catalyst can be seen in figure IV.11. The

diameters of the synthesized tubes are between 3-14 nm. The average diameter is of 7.5 nm. Figure IV.10. shows the diameter distribution of the multiwalled carbon nanotubes synthesized on this catalyst. The diameter distribution histogram is prepared from details obtained by measuring the outer diameters of 200 tubes. We can notice that the outer diameters of more than 50% of the analyzed tubes are between 5-8 nm. Samples synthesized on the 4%Co-1%Fe and the 1%Co-4%Fe catalyst have outer diameters between 3 and 17 nm. The average diameter is of 8.35nm for the 4%Co-1%Fe catalyst and of 8.12nm for the 1%Co-4%Fe catalyst. For these catalysts relatively thicker tubes are more frequently present in the sample. This may be due to the presence of bigger catalyst particles, as according to previous studies the inner diameters of multiwalled CNTs follow the diameters of the catalyst particles on which they were grown ***[7, 8].*** Table IV.4. summarises the diameter characteristics of analyzed nanotubes.

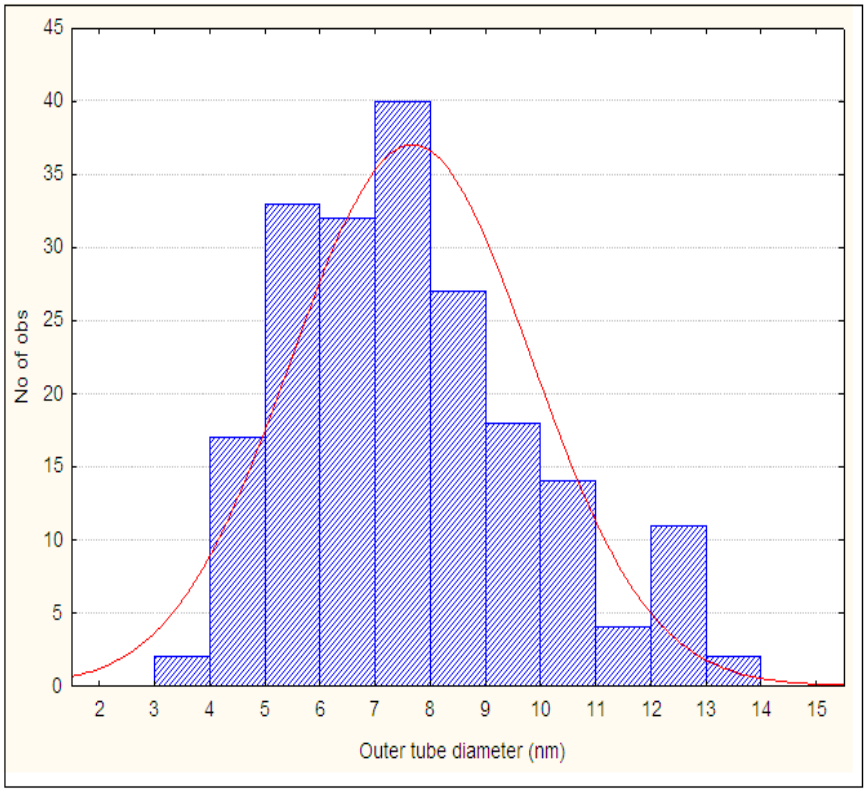

Figure IV.10.: Diameter distribution of multiwalled CNTs synthesized on 2.5%Co-2.5%Fe/SEP lyophilized catalyst

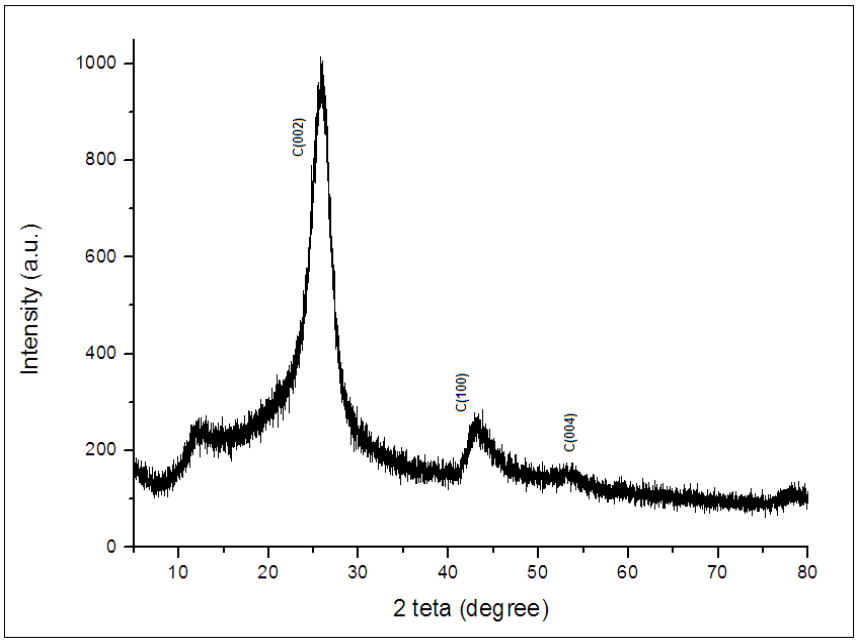

Figure IV.11: XRD diffraction of purified CNTs synthesized on 2.5%Co-2.5%Fe/SEP lyophilized catalyst

Catalyst	CNT diameter (nm)	Mean diameter (nm)	Standard deviation
2.5%Co-2.5%Fe	3-14	7.51	2.15
4%Co-1%Fe	3-17	8.35	2.73
1%Co-4%Fe	3-17	8.12	2.72

Table IV.4.: Characteristics of multiwalled CNTs synthesized on Co-Fe/SEP mixed catalysts (T:700°C, 1400 ml/min C_2H_4; 140ml/min N_2, reaction time: 20 minutes)

IV.3:2. Praseodymium as co-catalyst using sepiolite as catalyst support

Praseodymium was applied as co-catalyst for the synthesis of coiled CNTs in previous studies ***[2].*** Praseodymium containing sepiolite supported catalysts were also prepared and tested in synthesis reactions. Ethylene and acetylene were both used as carbon source. During the catalyst preparation, the drying step was carried out either by drying the catalyst simply in the oven, or by lyophilisation. This drying step resulted in causing important changes in the catalyst activity and the quality and quantity of the obtained product in a previous study

carried out in our laboratory. Lyophilised catalysts lead to higher carbon deposit and lower amorphous carbon production during the synthesis reactions ***[4]***. The characteristics of the obtained products can be seen in Table IV.5. and Figure IV.12.

Catalyst	Drying method	Carbon deposit	TEM observations
2.5%Co-2.5%Pr	oven	22.9	Some straight multivalled carbon nanotubes occasionally present, bamboo-like tubes also observed, and amorphous carbon
2.5%Co-2.5%Pr	liophilization	31.3	Some straight multivalled carbon nanotubes occasionally present with amorphous carbon
2.5%Fe-2.5%Pr	oven	21.2	No carbon nanotubes observed, amorphous carbon in low amount
2.5%Fe-2.5%Pr	liophilization	20.9	No carbon nanotubes observed, amorphous carbon in low amount

Table IV.5.: Praseodymium containing sepiolite supported catalysts

TEM investigations show no production of CNTs on the Fe-Pr/SEP catalyst, the presence of amorphous carbon and sepiolite can be seen in the TEM micrographs (Figure IV.12.a)). The Co-Pr catalyst led to the formation of some straight nanotubes, bamboo-like tubes and amorphous carbon (Figure IV.12.b)-c)). The diameters of the rarely observed multiwalled CNTs vary from 8 to 20 nm according to our measurements using ImageJ software. Regularly coiled CNTs were not observed on these catalysts.

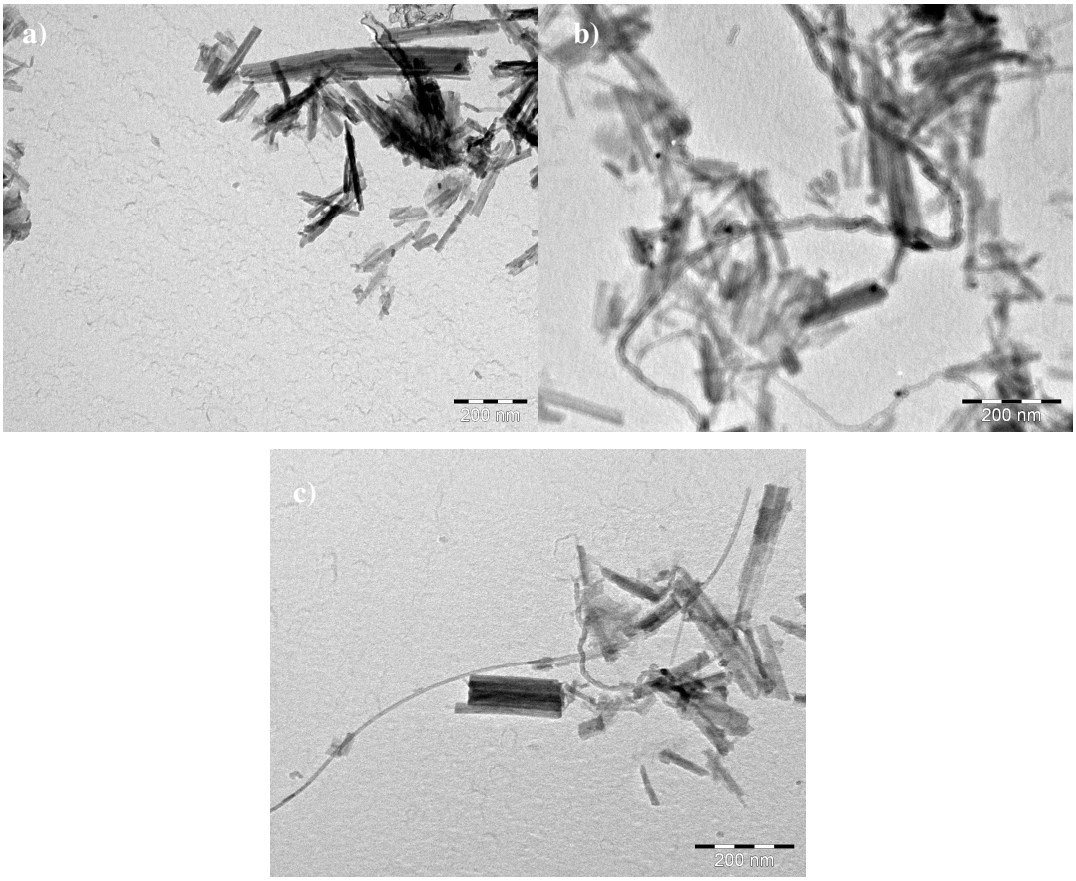

Figure IV.12.: TEM images of praseodymium containing sepiolite supported catalyst: a) 2.5%Fe-2.5%Pr/SEP (dried in the oven); b)-c) 2.5%Co-2.5%Pr/SEP (lyophilised)

IV.4. Silica Supported Catalysts

So far the application of silica as support material led to the formation of helicoidal CNTs in the highest ratio, thus we conducted a more detailed study applying this support material. For the catalyst preparation method both the ion-adsorption precipitation (IAP) and the sol-gel process was described to bring good results. We chose to further study the activity of silica supported catalysts prepared by the IAP method in the formation of helically coiled carbon nanotubes.

IV.4.1. Preliminary study: Effect of the pH on the synthesis product

As it was emphasized in a previous chapter when using catalysts prepared with the ion-adsorption precipitation (IAP) method, the pH applied during the preparation of the catalyst has a crucial role as far as the quality and quality and the CNT products is concerned. Previous studies already pointed out the importance of the pH ***[2]***, thus a preliminary study was carried out aiming to determine the optimal pH value of the catalyst in our experimental setup.

Test reactions were carried out with both ethylene (30 ml/min) and acetylene (30 ml/min) as carbon source. 5%Co and 5%Fe catalysts were prepared at different pH values. The carbon source:carrier gas ratio was 1:10. The applied reaction time was 20 min. The reaction temperature was set to 700°C and the 0.25 g catalyst was placed in the quartz boat (Thesis of Tommaso Veneziano).

Here we give a short summary on the results obtained using the 5%Co/silica catalyst which were prepared by ion-adsorption method adjusting the pH to 8; 8.5; 9; 10; 11; or without pH modification (pH: 7-7.5).

IV.4.1.1. Acetylene as carbon source

No carbon nanotubes could be observed in the sample with transmission electron microscopy when acetylene was applied as carbon source and the catalysts were prepared either without pH modification (pH: 7-7.5) or at pH values of 8 and 10. Despite these observations, a positive carbon deposit values were measured varying from 8 % to approximately 22 %, but this is due to the formation of disorganized carbon, presumably formed from the homogeneous decomposition of acetylene at the reaction temperature.

When the pH of the applied catalyst was set to 8.5 the obtained synthesis products contained tangled MWCNTs and some helically coiled CNTs (Figure IV.14.a)-b)). The outer diameters of the MWCNTs in this sample vary from 6 to 20 nm. They are many times curved and have numerous defects in the walls. The regular helices found in this sample have diameters between 10 and 20 nm, while the values of their coil pitches cover a broad range from 27 to 255 nm. The coil diameters of the observed helices are between 24 and 135 nm. The inhomogeneity of the few formed helices can be seen in Figure IV.14.a). We notice a large

wavy coil with a coil pitch value of a 188 nm and a tube diameter of 16 nm while just next to it another short coil can be seen with a coil pitch of 27 nm and a tube diameter of 10 nm.

Adjusting the pH of the catalyst to 9 in the applied reaction conditions led to the formation of significant amount of amorphous carbon and few tangled MWCNTs in the synthesis reactions (Figure IV.14.c)). The diameters of the MWCNTs observed on TEM micrographs vary from 9 to 25 nm.

The catalyst prepared at pH=11 led to the formation of helically coiled and straight MWCNTs (Figure IV.14.d)-e)). In this case, with respect to the previously described samples the formation of disorganized carbon was lower. The MWCNTs are abundantly present in the samples, and the ratio of regularly coiled MWCNTs is around 4-5%. In Figure IV.13. the diameter distribution of the obtained nanotubes is presented. The outer tube diameters range from 6 to 30 nm, however we can notice that around 70% of the tubes have diameters between 10 and 18 nm. This permits us to hypothesize that the size of the catalyst particles is not uniform ***[9]***. This can be caused by the catalyst-support interaction or by the formation of bigger, asymmetric catalyst particle aggregates induced by setting the pH with ammonia solution ***[3]***.

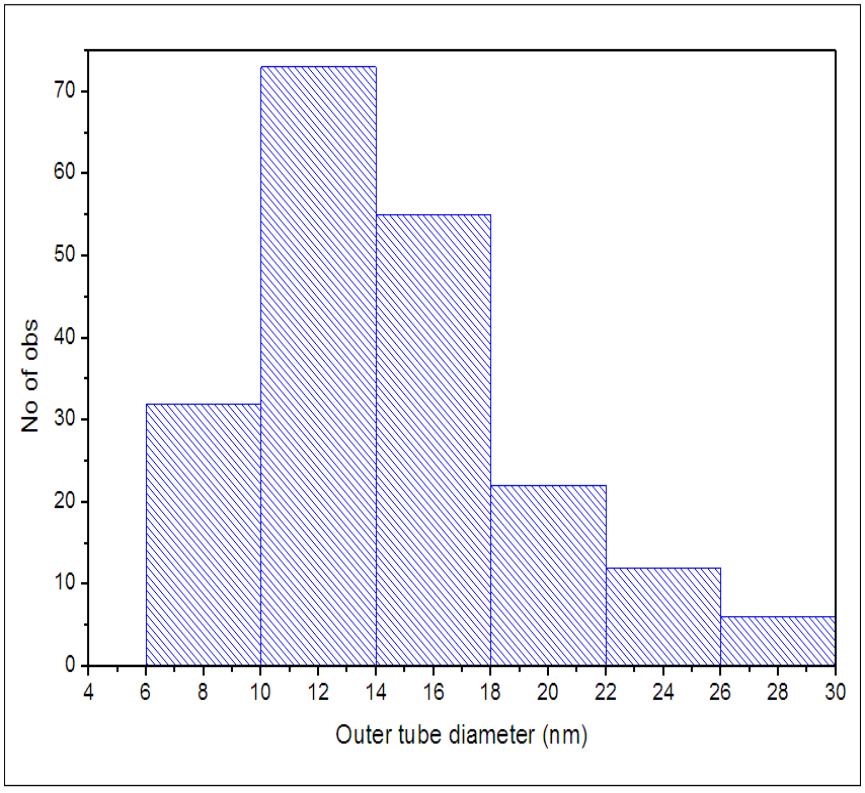

Figure IV.13.: Diameter distribution of MWCNTs synthesized by the decomposition of acetylene on 5% Co catalyst prepared at pH=11

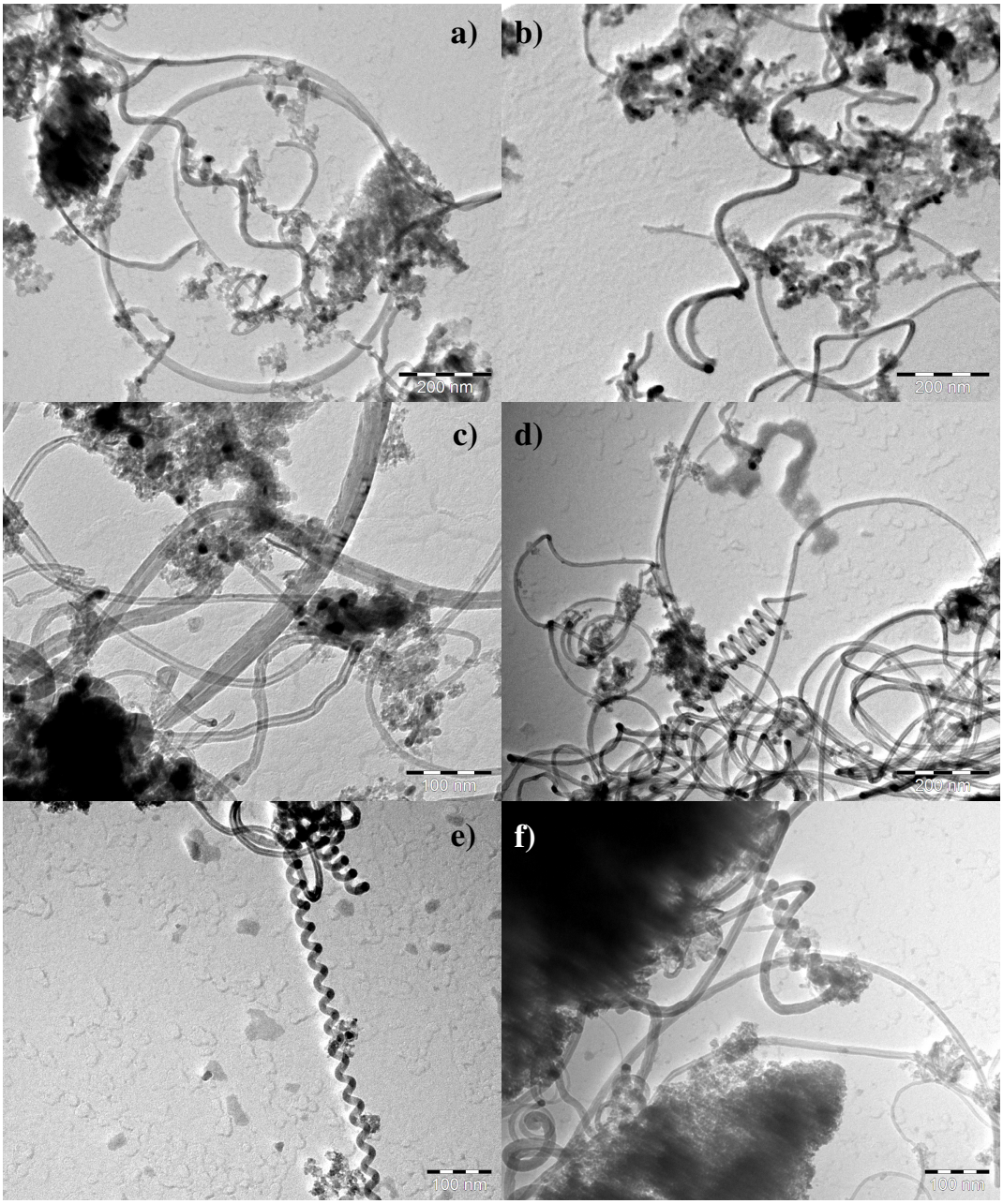

Figure IV.14.: TEM pictures of CNT products synthesized by the decomposition of acetylene over 5%Co/SiO_2 catalyst prepared at: a)-b) pH=8.5; c) pH=9; d)-f) pH=11

Thermal analysis results of samples synthesized on catalysts prepared at different pH values can be seen in Figure IV.15.

The TGA curve of the sample prepared at pH=8.5 (Figure IV.15.a)) shows a total weight loss of about 35 %. It is in good accordance with the calculated value of 40 %, derived from the

weight of the catalyst before and after the synthesis reaction. On the DTA curve only a small peak can be observed at around 350°C that can be attributed to amorphous carbon. Instead a relatively thin and tall peak is present at around 520°C. This latter peak is attributed to the MWNCTs present in the sample.

The TGA and DTA curves presented in Figure IV.15.b) belong to the sample synthesized by the decomposition of acetylene on the catalyst prepared at pH=9. In this case the DTA curve shows a bigger peak in the temperature range of 280-370°C that indicates the presence of higher amount of amorphous carbon in the sample, in accordance with our transmission electron microscopy observations. The peak attributed to the MWCNTs on the DTA curve at 550°C is however quite thin.

When a pH value of 10 was applied at the catalyst preparation no CNTs were observed in TEM micrographs, only disorganized carbon was present in the samples. However the DTA curve (Figure IV.15.c)) shows a peak at around 500°C this can be due to different carbonaceous products that are to some extent graphitized, for example metal catalyst particles recovered by layers of graphitized carbon.

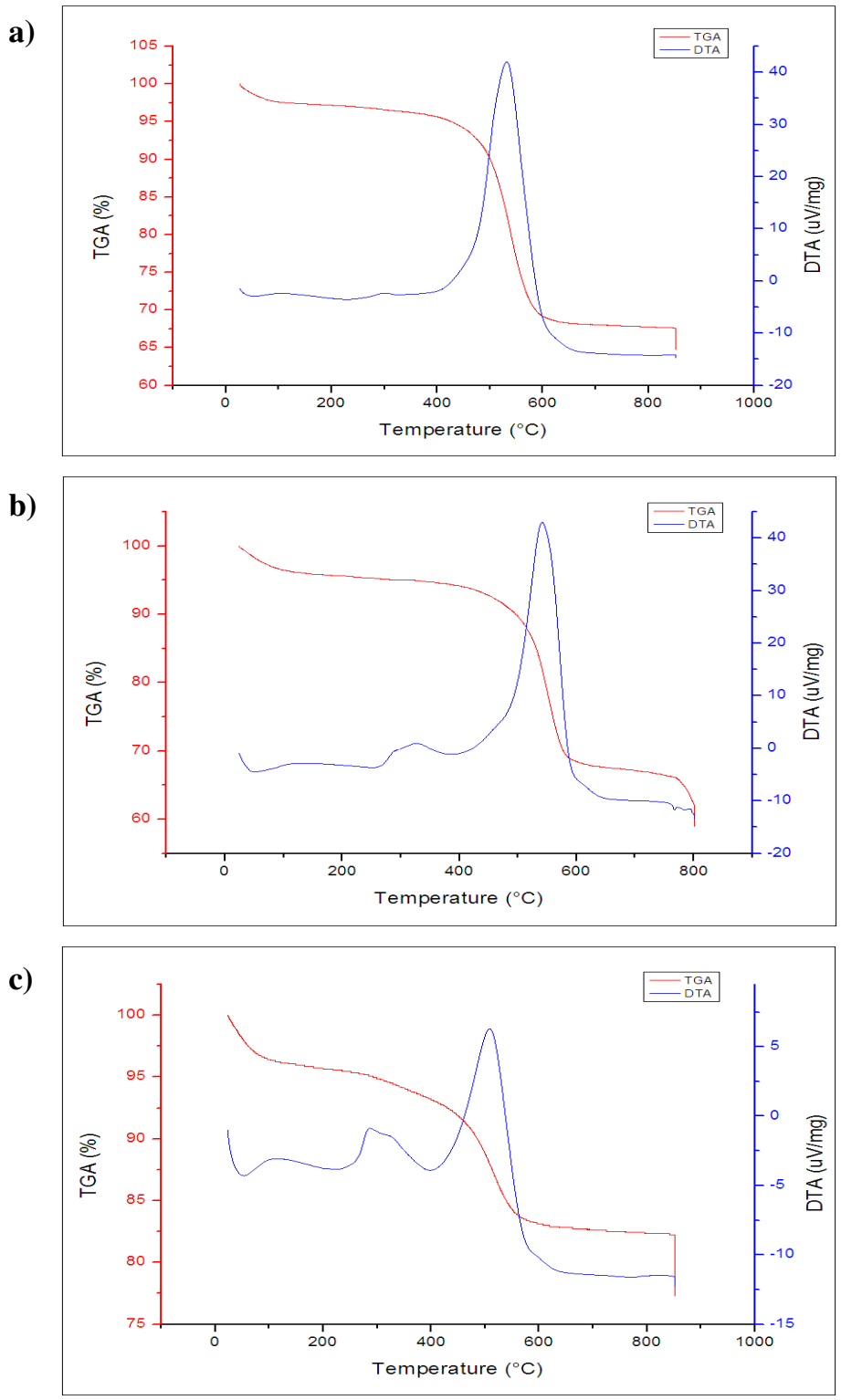

Figure IV.15.: Thermal analysis of CNT samples synthesized by the decomposition of acetylene at 700°C on 5%Co/SiO_2 catalysts prepared at different pH: a) pH=8.5; b) pH=9; c) pH=10

IV.4.1.2. Ethylene as carbon source

When ethylene was used as carbon source, catalyst prepared at pH=10 and 11 and the one without adjusting the pH led to the formation of CNTs. The other catalyst prepared by adjusting the pH to 8; 8.5 or 9 led to the formation of disorganized carbon.

Figure IV.16.a) and b) shows TEM micrographs of CNT product synthesized by the decomposition of ethylene on 5%Co catalyst without adjusting the pH. In this case, TEM observations show abundant presence of CNTs in the sample, and low amount of amorphous carbon. The outer diameters of the synthesized nanotubes vary from 2 to 30 nm, although around 80 % of the tubes have diameters from 6 to 18 nm (Figure IV.17.). Regularly and irregularly coiled helices were also found in this synthesis product. Their ratio compared to all the nanotubes is around 3-4 %. The outer tube diameters of the helices vary from 6 to 20 nm, while their coil pitches are in the range of 20-82 nm. The coil diameters of the helices are between 38-82 nm.

Figure IV.16.c) and d) show TEM micrographs of carbon nanotubes samples synthesized by the decomposition of ethylene on 5%Co/SiO_2 catalyst, adjusting the pH of the catalyst to 10. Straight MWCNTs of outer diameters between 4-30 nm, and regularly coiled CNTs are found in the sample. In some cases, the coils which turn into straight tubes or which continue in irregular form were also observed in the sample. The outer tube diameters of the HCNTs are in the range of 10-20 nm, their coil pitches vary from 30 to 60 nm while the coil diameters of the helices have values between 28 and 78 nm. However, the tubes and catalyst particles are often covered by disorganized carbon.

Adjusting the catalyst pH to 11 caused the formation of tangled thin nanotubes. TEM image of the obtained product is shown in Figure IV.16.e). These CNTs have diameters between 4-7 nm and are covered by amorphous carbon.

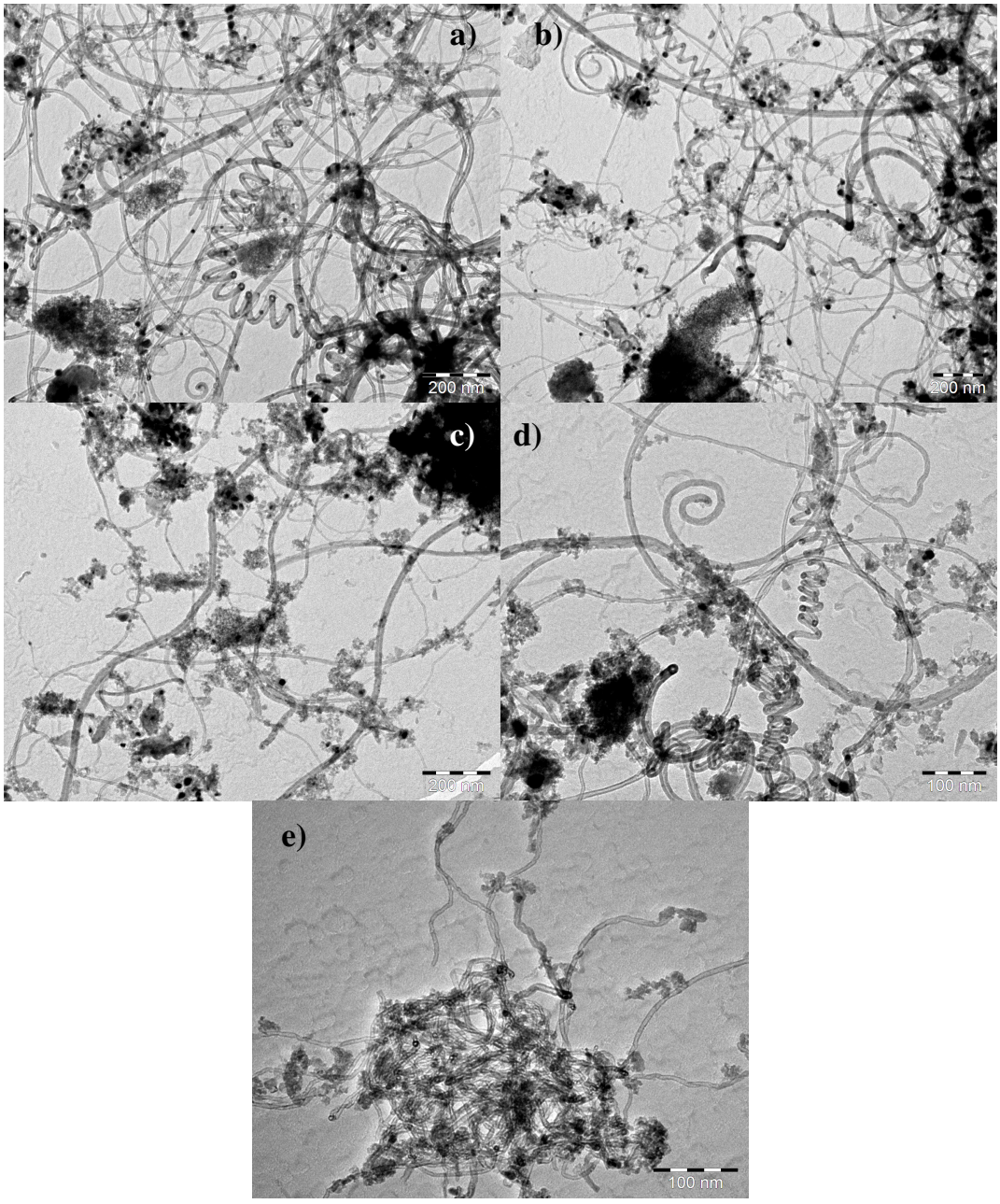

Figure IV.16.: TEM pictures of CNT products synthesized by the decomposition of ethylene over 5%Co/SiO_2 catalyst prepared: a)-b) without pH modification; c)-d) at pH=10; e) at pH=11

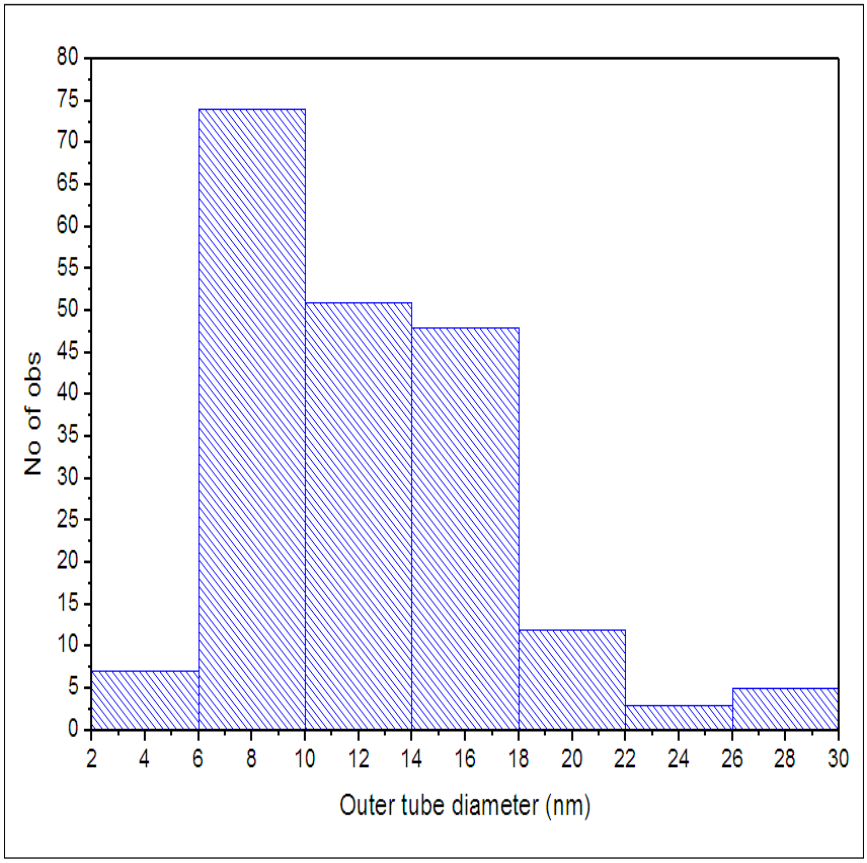

Figure IV.17.: Diameter distribution of CNTs synthesized by the decomposition of ethylene on 5% Co catalyst prepared without pH modification

IV.4.1.3. Conclusions

Tables IV.6.-8. summarize the results obtained during the preliminary study considering the variation of pH values of the basic catalyst suspension. We can conclude that the pH at the catalyst preparation has significant effect on the synthesis product in our synthesis reactions.
As far as acetylene is concerned as carbon source adjusting the pH of the 5%Co catalyst to 8.5 and 11 led to the formation of the best product. In the synthesis products straight MWCNTs as well as regularly coiled CNTs are present. The obtained carbon deposit values for the catalysts prepared at pH=8.5 and 11 are 40 % and 45 %, respectively, that is a medium value for this type of catalysts compared to the literature ***[3]***. Thermal analysis and TEM observations show higher amount of amorphous carbon formed using the catalyst prepared at pH=11. The ratio of the HCNTs compared to the straight CNTs is also slightly higher in this case. Previously Hernádi et al. ***[10]*** studied how the pH of the Co-acetate solution used for the

preparation of Co/SiO_2 catalyst influences the CNT product obtained by the decomposition of acetylene. They concluded that setting the pH to 8-9 enhances the CNT formation with respect to lower pH values. This is in accordance with the results obtained in our system considering that the unmodified pH of the catalyst led to no CNT formation by the decomposition of acetylene.

HCNTs with various morphology, coil pitch, coil diameter and tube diameter values were found in the samples prepared both in the case of the samples of pH 8.5 and 11.

Catalysts prepared without pH modification and at pH=8, 9, and 10 were not active in the formation of HCNTs by the decomposition of acetylene in the applied reaction conditions. Table IV.6. summarizes the quantitative and qualitative characteristics of the obtained products synthesized at above-mentioned reaction conditions.

Catalyst pH	**Carbon deposit (%)**	**Carbon yield (%)**	**Carbon nanotubes**	**Coiled carbon nanotubes**
Unmodified	8.3	3.4	Amorphous carbon formation, no CNTs observed	-
8	21.7	8.6	Amorphous carbon formation, no CNTs observed	-
8.5	40.0	17.2	Tangled MWCNTs few helically coiled CNTs	1-2%
9	39.1	15.5	Some straight MWCNTs , significant amount of amorphous carbon	-
10	14.3	5.2	Amorphous carbon formation, no CNTs observed	-
11	45.0	15.5	Many straight CNTs, helically coiled CNTs are also present in the sample. Low amount of amorphous carbon	4-5%

Table IV.6.: Results obtained applying acetylene as carbon source (30 ml/min) using $5\%Co/SiO_2$ catalysts prepared at different pH values. (T: 700°C, t: 20 min)

Using ethylene as carbon source the $5\%Co/SiO_2$ catalysts prepared without pH modification led to the formation of most helices in our reaction conditions. In this case the measured

carbon deposit value is low, although TEM measurements show numerous well-graphitised multiwalled carbon nanotubes, regular helices and lower amorphous carbon content.

The catalyst prepared at pH=10 was also active in the formation of CNTs and HCNTs as well. In this case the carbon deposit value is higher, however the HCNT/MWCNT ratio is lower compared to the sample without pH modification.

Table IV.7. summarizes the characteristics of the carbon deposit produced on 5%Co/SiO_2 catalysts with ethylene as carbon source.

Catalyst pH	**Carbon deposit (%)**	**Carbon yield (%)**	**Carbon nanotubes**	**Coiled carbon nanotubes**
Unmodified	4.6	1.7	Low amount of amorphous carbon, many CNTs also helices are regularly observed	3-4%
8	66.7	24.1	Amorphous carbon formation, no CNTs observed in the sample	-
8.5	40.9	15.5	Amorphous carbon formation, no CNTs observed in the sample	-
9	4.4	1.7	Amorphous carbon formation, no CNTs observed in the sample	-
10	17.4	6.8	MWCNTs present in the sample with significant amount of amorphous carbon; HCNTs are rare	1-2%
11	45.0	15.5	Tangled thin nanotubes, high amount of amorphous carbon	-

Table IV.7.: Results obtained applying ethylene as carbon source (30 ml/min) using 5%Co/SiO_2 catalysts prepared at different pH values (T: 700°C; t: 20 min)

The characteristics of the synthesized HCNTs are summarized in Table IV.8. Helices with wavy and telephone-cord-like morphology were observed in the sample.

In the case of acetylene as hydrocarbon, the catalysts with pH values of 8.5 and 11 were active in the formation of helically coiled carbon nanotubes. Regularly coiled, loose spring-like nanotubes were observed by TEM in higher ratio in the carbon deposit produced by catalyst with pH=11. Catalyst with pH=8.5 produced more S-shaped coils with larger coil diameter than in the previous case.

Catalysts with unmodified pH and pH adjusted to 10 were active in the decomposition of ethylene under our reaction conditions. The catalyst without pH modification was more active in the coil formation than the ones of pH=10. Helices with regular pitch and irregularly coiled carbon nanotubes were observed in the sample. The morphology of the observed helices is more irregular compared to the ones produced by the decomposition acetylene, but their dimensions, like coil pitch and coil diameter vary in a narrower range. This phenomenon can be explained by the more uniform decomposition of ethylene in our reaction conditions.

Carbon source	Catalyst pH	Coiled CNT	Outer tube diameter (nm)	Coil pitch (nm)	Coil diameter (nm)
acetylene	8.5	1-2%	10-20	27-256	24-132
acetylene	11	4-5%	9-22	26-152	26-77
ethylene	Native	3-4%	6-20	30-82	12-80
ethylene	10	1-2%	10-20	30-60	26-78

Table IV.8.: Characteristics of regularly coiled CNTs synthesized by the decomposition of ethylene or acetylene at different pH values

IV.4.2. Preliminary study with the small reactor

A preliminary study was carried out testing different silica supported catalyst in the decomposition of acetylene with a small reactor (d=3 cm; l=50 cm), at the University of Szeged. 0.1 g catalyst was placed in the quartz boat. For the further work acetylene was chosen as carbon source because this hydrocarbon was the most successful in the synthesis of HCNTs in previous studies. The reactions were carried out at 700°C applying 15 ml/min acetylene and 150 ml/min N_2. The gas flows were recalibrated each time for the better precision. The reaction time was 30 minutes. Co-; Fe-; Co-Fe; and Co-Pr catalyst were prepared with the ion-adsorption precipitation method adjusting the pH to ca. 8.5-8.75 by the addition of ammonia solution. The aim of the preliminary study was to choose the catalysts that provide the highest ratio of helicoidal CNTs for further optimisation. The main analysis method used during this period was transmission electron microscopy as we were interested in the morphology of the synthesized CNTs.

IV.4.2.1. Co-containing catalysts

Figure IV.18. shows TEM micrographs of carbonaceous products synthesized by the decomposition of acetylene at 700 °C using 10%Co/SiO_2 and 5%Co/SiO_2. In both samples MWCNTs and HCNTs are present. The ratio of the regularly coiled tubes compared to straight CNTs is around 5% in both samples. The CNT product obtained by the decomposition of acetylene on 10%Co/SiO_2 catalyst contained less carbon nanotubes and higher amount of amorphous carbon according to electron microscopy observations. In this case the CNTs are covered by amorphous carbon (Figure IV.18.a)). The sample synthesized on the 5%Co catalyst (Figure IV.18.b)) contains more nanotubes. However, the ratio of the coiled CNTs compared to all the tubes is similar to the previous one.

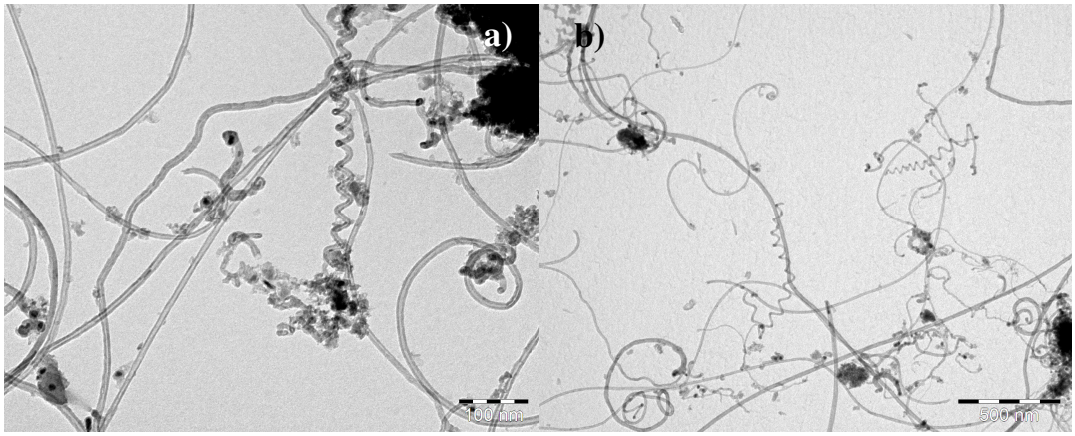

Figure IV.18.: TEM pictures of CNTs synthesized on SiO_2 supported Co catalysts: a) 10%Co; b) 5%Co (T: 700°C; 15 ml/min C_2H_2 flow; 150 ml/min N_2 flow; t: 30 min)

IV.4.2.2. Fe-containing catalysts

5%Fe/silica catalyst was also prepared and tested in the decomposition of acetylene at 700°C in the small reactor. The reaction conditions remain the same as in the case of the Co supported silica catalysts.

TEM observations show the presence of muliwalled CNTs with outer tube diameters varying from 5 to 20 nm. The tubes are often tangled and bent or partially coiled (Figure IV.19.a)), no helix with a regular coil pitch was found. Presence of low amount of amorphous carbon can be observed by electron microscopy.

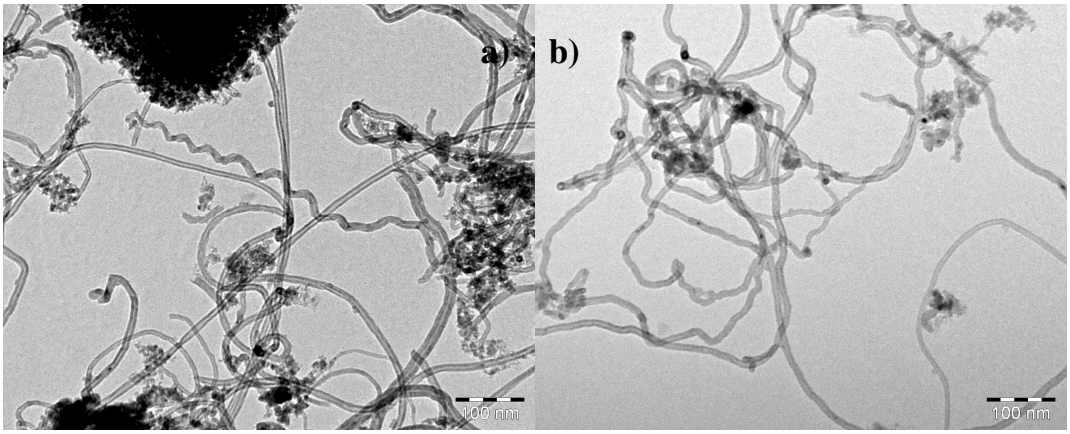

Figure IV.19.: TEM pictures of samples synthesized on 5%Fe/SiO_2 catalysts (T: 700°C 15 ml/min C_2H_2 flow; 150 ml/min N_2 flow; t: 30 min)

IV.4.2.3. Co-Fe Bimetallic Catalysts

Co-Fe catalyst with a cumulative metal content of 5% were prepared and tested in CNT synthesis in the small reactor. Silica supported catalysts with the following metal loadings were prepared: 2.5%Co-2.5%Fe, 4%Co-1%Fe, 1%Co-4%Fe.

In the samples prepared with the 2.5%Co-2.5%Fe/silica catalyst well graphitized MWCNTs with outer diameters between 5-25 nm can be observed. Helicoidal CNTs are present in the sample. They give 1-2 % of all the counted nanotubes. Their diameters vary from 7 to 20 nm with mainly large coil pitches (wavy tube). Irregularly coiled CNTs were more often observed in the synthesis products: mostly long wavy tubes with not regular large pitch (Figure IV.20.c)-d)).

On the 4%Co-1%Fe catalyst few regular helices are observed. HCNTs are present in 1-2 % compared to all the CNTs in the sample. The outer tube diameters of the synthesized multiwalled CNTs range between 5-25 nm, while that of the HCNTs vary from 8 to 20 nm. Irregularly coiled spring-like CNTs are observed in the sample, as well as straight carbon nanotubes that end in some coiled form (Figure IV.20.a)-b)).

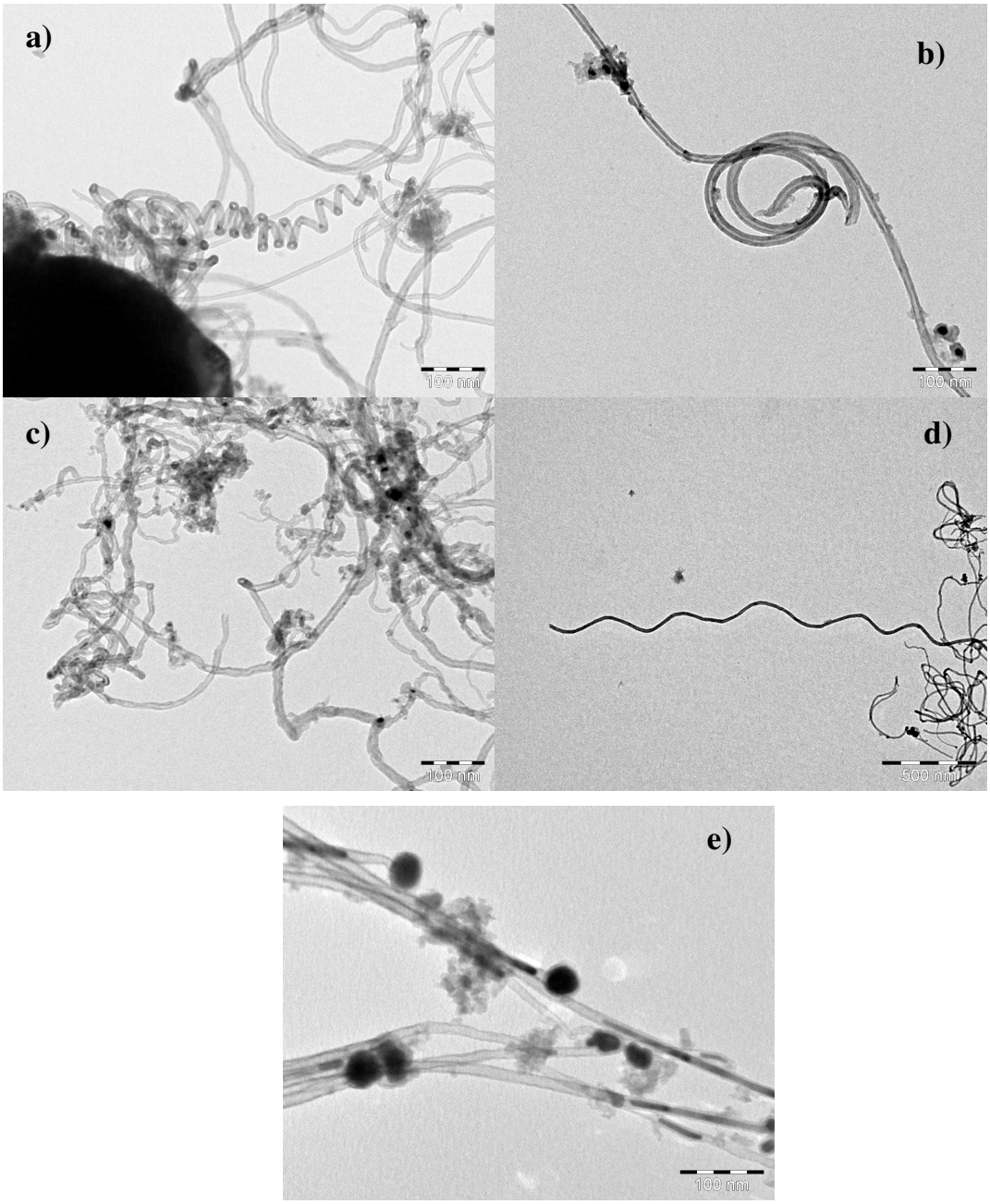

Figure IV.20.: Different forms of multiwalled CNTs synthesized on Co-Fe/SiO_2 catalysts: a)-b) 4%Co-1%Fe catalyst; c)-d) 2.5%Co-2.5%Fe catalyst; e) 4%Fe-1%Co catalyst (T: 700°C; 15 ml/min C_2H_2 flow; 150 ml/min N_2 flow; t: 30 min)

On the 4%Fe-1%Co catalyst the formation of strange, partly filled tubular structures was observed (Figure IV.20.e)). These structures have diameters between 10-15 nm and end in a filled cap. Hernádi et al. ***[11]*** observed already similar carbonaceous products formed by the

catalytic decomposition of acetylene over SnO_2 although, they were significantly thicker and longer. The further investigation of the crystalline structure and the composition of these carbonaceous products could be interesting.

Table IV.9. summarizes the characteristics of synthesis products obtained on 5%Co, 5%Fe and 5%Co-Fe catalysts. We can say that applying 5% Co-Fe bimetallic catalysts did not lead to the formation of HCNTs in high ratio in the applied reaction conditions. Multiwalled carbon nanotubes were formed on most catalysts, and applying bimetallic catalysts we could observe less amorphous carbon in the samples by electron microscopy.

Catalyst	**Carbon deposit (%)**	**Carbon yield (%)**	**Carbon nanotubes**	**Coiled carbon nanotubes**
5%Co	58	18.4	Straight and helically coiled CNTs	5%
5%Fe	41	13	Straight and tangled MWCNTs	No regular helices
2.5%Fe-2.5%Co	42	13.9	Well-graphitized nanotubes and relatively low amount of amorphous carbon	1-2%
1%Fe-4%Co	41	13	Well-graphitized nanotubes and some amorphous carbon	1-2%
4%Fe-1%Co	42	13.9	Strange tubular structures (Figure IV.19.e))	No regular helices

Table IV.9.: Carbon yield and carbon deposit values, and product characteristics of samples synthesized on Co-Fe catalysts (T: 700°C; 15 ml/min C_2H_2 flow; 150 ml/min N_2 flow; t: 30 min)

IV.4.2.4. Preliminary study applying Pr as co-catalyst

Pr as co-catalyst to Co/silica catalysts was proved to enhance the ratio of regularly coiled CNTs in synthesis products obtained by the decomposition of acetylene at 700°C. The carbon source:carrier gas ratio was 1:10. The reaction time was 30 min. Szabó et al. tested Co-Pr catalysts with varying Pr content ***[2, 3]***. We tested some of the Co-Pr catalyst that led to the

formation of the highest amount of helices in previous studies and tried catalysts with different metal ratios as well.

The 2.5%Co-2.5%Pr catalyst was active in the formation of helicoidal CNTs. The carbon nanotubes are abundantly present in the synthesis product. Their outer diameters range from 4 to 25 nm, while the outer diameters of regularly coiled CNTs vary from 6 to16 nm. Concerning the morphology of the formed helices we found mainly wavy HCNTs, spring-like structures. Tight coils were just occasionally observed (Figure IV.21.d)-e)).

The 1%Co-4%Pr catalyst led to the formation of fewer MWCNTs with a slightly higher ratio of coiled CNTs according to our TEM observations (Figure IV.21.g)-h)). The CNTs produced on this catalyst have outer diameters between 4 and 22 nm as it is shown in Figure IV.22. while the diameters of the helices vary between 6-16 nm. The coil pitches of the helices range from 20 to 70 nm while the coil diameters are between 55 and 70 nm. The obtained coils have various morphology, wavy coils are still prevalent, however other forms such as autoassociated chains of HCNTs (Figure IV.21.h)) and loosely formed springs are also observed.

Carbonaceous products obtained by the decomposition of acetylene on 4%Co-1%Pr catalyst contain more MWCNTs compared to the product obtained with the 1%Co-4%Pr catalyst, however the ratio of HCNTs:all MWCNTs is lower (Figure IV.21.f)). The outer tube diameters synthesized on this catalyst vary from 5 to12 nm. The coil pitch and coil diameter values are between 30-45 nm and 20-70 nm, respectively (Table IV.11.).

The 5%Co-5%Pr catalyst led to the formation of 10% HCNTs in the product. The synthesis product contains also significant amount of amorphous carbon that often covers the helices and straight CNTs (Figure IV.21.a)). The helices have coil diameters between 25-120 nm and the values of the coil pitches range from 30 to 150 nm.

Helically coiled CNTs of outer tube diameters between 7-28 nm, with coil pitches varying from 28-150 nm and coil diameters in the range of 47-120 nm were synthesized on the 7.5%Co-2.5%Pr catalyst (Figure IV.21.b)). The helices also in this case are mostly wavy. The synthesized product contains 10% coils compared to all the MWCNTs. The amorphous carbon content in the product does not seem extremely high according to TEM observations.

Using the 2.5%Co-7.5%Pr; the 10%Co-2.5%Pr (Figure IV.21.i)); or the 12%Co-2.5%Pr (Figure IV.21.j)) catalyst for the decomposition of acetylene at 700°C in our reaction conditions caused the formation of few CNTs and high amount of amorphous carbon. Nevertheless, the ratio of the HCNTs compared to all the CNTs is still around 15%, the quantity of the CNTs present in the sample compared to the amorphous carbon is really low.

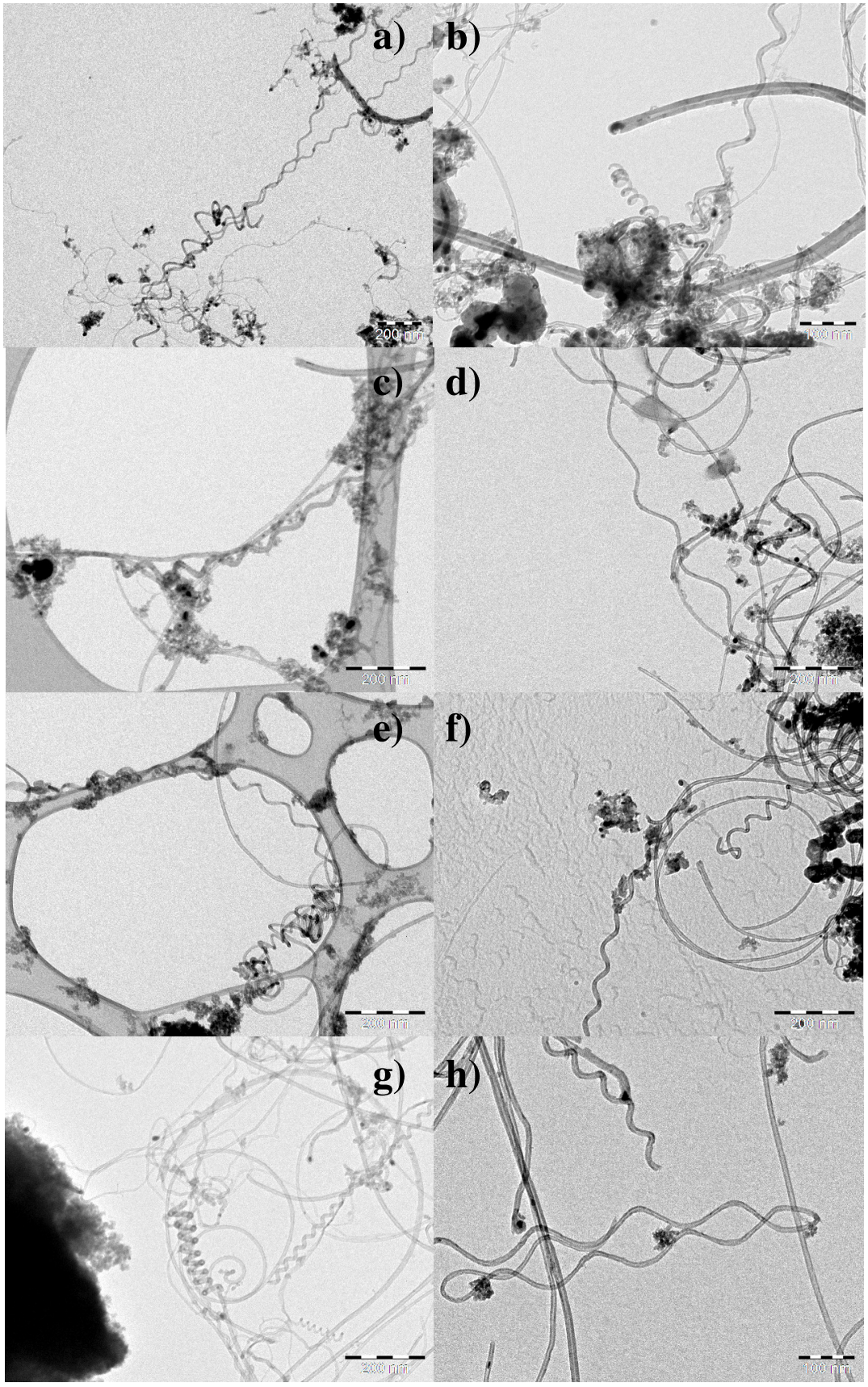
a)
200 nm
b)
100 nm
c)
200 nm
d)
200 nm
e)
200 nm
f)
200 nm
g)
200 nm
h)
100 nm

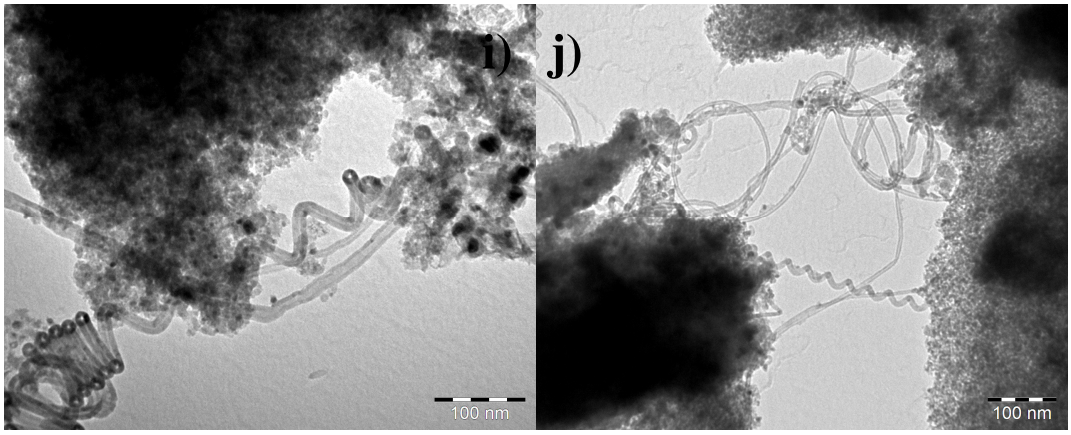

Figure IV.21.: TEM pictures of CNTs synthesized on SiO_2 supported Co-Pr catalysts: a) 5%Co-5%Pr; b) 7.5%Co-2.5%Pr;c)-e) 2.5%Co-2.5%Pr; f) 4%Co-1%Pr; g)-h) 1%Co-4%Pr; i) 10%Co-2.5%Pr; j) 12.5%Co-2.5%Pr

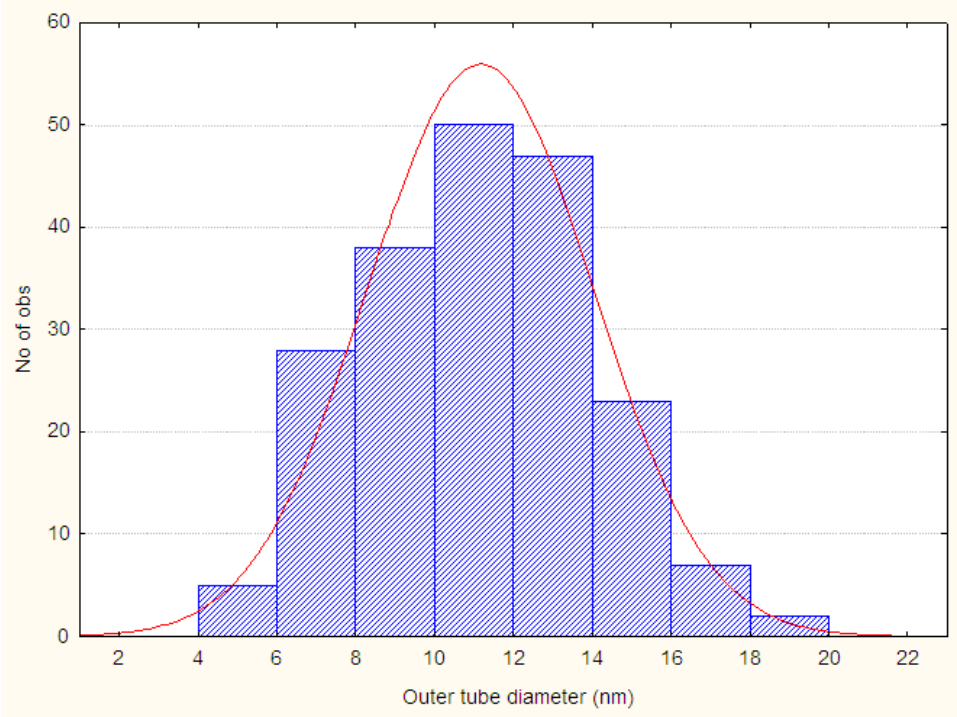

Figure IV.22.: Diameter distribution of the MWCNTs synthesized on 1%Co-4%Pr catalyst

Praseodymium was tested also as single-metal catalyst, but it was not active in the formation of CNTs. A low amount of amorphous carbon was observed via TEM.

Table IV.10. summarises the qualitative and quantitative characteristics of carbon deposits obtained on Co-Pr/silica catalysts with different Co-Pr ratios. Considering the carbon deposit

values, they vary between 5-63 % while for carbon yield values, they are in the range of 3-20%. The 2.5%Co-2.5%Pr and the 7.5%Co-2.5%Pr catalysts led to the highest carbon deposit, however the 1%Co-4%Pr and the 4%Co-1%Pr catalyst resulted in slightly lower carbon deposit. The amount of helically coiled nanotubes is relatively high in most of the cases of the applied catalyst.

Catalyst	**Carbon deposit (%)**	**Carbon yield (%)**	**Carbon nanotubes**	**Coiled carbon nanotubes**
5%Co	58.3	18.4	Straight and helically coiled CNTs, some amorphous carbon	5%
10%Co	38.3	11.9	Straight and helically coiled CNTs, some amorphous carbon	5%
2.5%Co-2.5%Pr	63.2	20	Straight and helically coiled CNTs, some amorphous carbon	15%
1%Co-4%Pr	53	16.9	Straight and helically coiled CNTs, relatively high amount of amorphous carbon	15-17%
4%Co-1%Pr	56.8	17.8	Straight and helically coiled CNTs	10%
5%Co-5%Pr	50.4	15.8	Straight and helically coiled CNTs, amorphous carbon	10%
7.5%Co-2.5%Pr	62.7	19.1	Straight and helically coiled CNTs	<5%
2.5%Co-7.5%Pr	10.5	3.2	Straight and helically coiled CNTs, high amount of amorphous carbon	<5%
10%Co-2.5%Pr	36.7	11	High amount of amorphous carbon, few nanotubes covered by amorphous carbon, helices	15%
12.5%Co-2.5%Pr	40.1	12	High amount of amorphous carbon, few nanotubes covered by amorphous carbon, helices	15%
5%Pr	5.7	1.8	No CNTs were observed in the samples	-

Table IV.10.: Carbon yield and carbon deposit values and product characteristics of samples synthesized applying Pr as co-catalyst

Catalyst	Outer tube diameter CNTs (nm)	Outer tube diameter HCNTs	Coil pitch (nm)	Coil diameter (nm)
2.5%Co-2.5%Pr	4-25	6-16	20-170	27-70
1%Co-4%Pr	4-20	6-16	20-70	55-90
4%Co-1%Pr	4-28	5-12	30-45	20-70
5%Co-5%Pr	5-30	7-28	30-150	25-120
7.5%Co-2.5%Pr	5-32	7-28	28-150	47-120
2.5%Co-7.5%Pr	5-25	5-20	30-70	50-130
10%Co-2.5%Pr	5-22	5-15	30-70	45-110
12.5%Co-2.5%Pr	4-14	5-12	30-60	50-120

Table IV.11.: Characteristics of CNTs synthesized applying Pr as co-catalyst

Table IV.11. summarises the characteristics of carbon nanotubes and coils produced by decomposition of acetylene on Co-Pr/silica catalysts with various metal loading.
In conclusion, we can say that concerning the quality of the product and the ratio of helically coiled CNTs compared to straight ones, the catalysts that seem to be the most promising are the ones with 5% total metal content. In the conditions applied in the small reactor the 1%Co-4%Pr catalyst produced HCNTs in the highest ratio. The 2.5%Co-2.5%Pr catalyst and the 4%Co-1%Pr catalyst is also promising. The 10%Co-2.5%Pr and the 12.5%Co-2.5%Pr catalysts permitted to obtain carbonaceous products with a high ratio of HCNTs compared to all the CNTs. However, this high ratio is partly caused by the presence of few nanotubes in the sample.

IV.4.3. Optimization of the reaction conditions on Co-Pr catalysts

Consequently to results of the preliminary study carried out in the small reactor the 2.5%Co-2.5%Pr/SiO_2, the 4%Co-1%Pr/SiO_2 and the 1%Co-4%Pr/SiO_2 catalyst were chosen for the optimization of the reaction conditions in the big reactor installed by our group in the Laboratory of Industrial Chemistry at University of Calabria. The effect of the reaction temperature, the carbon source and carrier gas flow was investigated. 1 g catalyst was placed in a quartz boat. The reaction time was set to 30 minutes as it was previously optimized concerning the carbon deposition and carbon yield obtained in the small reactor.

IV.4.3.1. Effect of the reaction temperature on the synthesis product

The temperature is a crucial parameter when it comes to the synthesis of carbon nanotubes. The quality and the quantity of the obtained carbonaceous product changes significantly with the reaction temperature. We carried out CNT synthesis reactions at 600, 650 and 700°C. The reaction time was maintained at 30 min. The acetylene flow was set to 30 ml/min while the carrier gas flow was 300 ml/min.

a) 2.5%Co-2.5%Pr catalyst

For the 2.5%Co-2.5%Pr catalyst only some thin straight MWCNTs and amorphous carbon were formed in the catalytic reactions at 600°C. Figure IV.23.a) and b) show the morphology of the obtained material. The outer diameters of the tubes varied from 4 to7 nm. Thermal analysis carried out in oxygen atmosphere (Figure IV.24.a)) shows a double peak on the DTA curve: one around 400°C and another one around 450°C. The peak at lower temperature can be caused by the decomposition of thin tubes due to their thickness, and the other peak by destruction of graphitized carbon which cannot be observed at TEM analysis because of the large amount of the support material in the samples.

Augmenting the reaction temperature to 650°C leads to the formation of more and thicker nanotubes, and also regular helices (Figure IV.23.c)-d)). The outer diameters of the synthesized tubes are between 4-15 nm. Regularly and irregularly coiled CNTs were found in the sample. The irregular helices are mainly composed of a straight and a coiled part. Regular helices were observed with coil diameters in the range of 35-90 nm and coil pitches between 46-215 nm. Their outer diameter ranged from 9 to 15 nm. The helices are mainly short. The HCNTs are approximately 10% of the synthesized CNTs. Amorphous carbon is present in the sample but its quantity remains relatively low compared to other synthesis products obtained using this catalyst. On the DTA curve (Figure IV.24.b)) we can observe two sharp peaks at about 320°C and 350°C, and a double peak at 400°C and 450°C similar to that of the synthesis product obtained at 600°C. The first two peaks are the contributes of amorphous carbon materials. These latter peaks can be related to the different types of CNTs. The tubes having thinner diameter can be burned out at lower temperature at about 400°C, as we described before, while the variously coiled carbon tubes and thicker straight tubes can be more resistible and decompose at 450°C. The reactions carried out at 700°C produced a

carbonaceous sample with a 15% HCNTs content compared to all the nanotubes (Figure IV.23.d)-e)). This product contains helices with outer tube diameters between 6-16 nm, their coil pitches vary from 15 to 170 nm, while the coil diameters are in the range of 20-55 nm. These coils demonstrate a thinner distribution range as for coil pitch like coil diameter compared with those produced at 650^{o}C. It can be explained by the more homogeneous distribution of hydrocarbon molecules at higher reaction temperature. Metal particles were not observed in the HCNTs obtained with this catalyst, either on their caps or inside the central canal. Occasionally small metal particles were found at the tips of straight MWCNTs. Comparing the DTA curve of this product (Figure IV.24.c)) with the ones obtained at 600 and 650°C we can see one sharp peak at about 350^{o}C and second single broader peak at about 450°C. The first smaller peak corresponds to the amorphous carbon, while the second one corresponds to carbon nanotubes. This change in the DTA curve may suggest a change in the quality or morphology of the synthesis product.

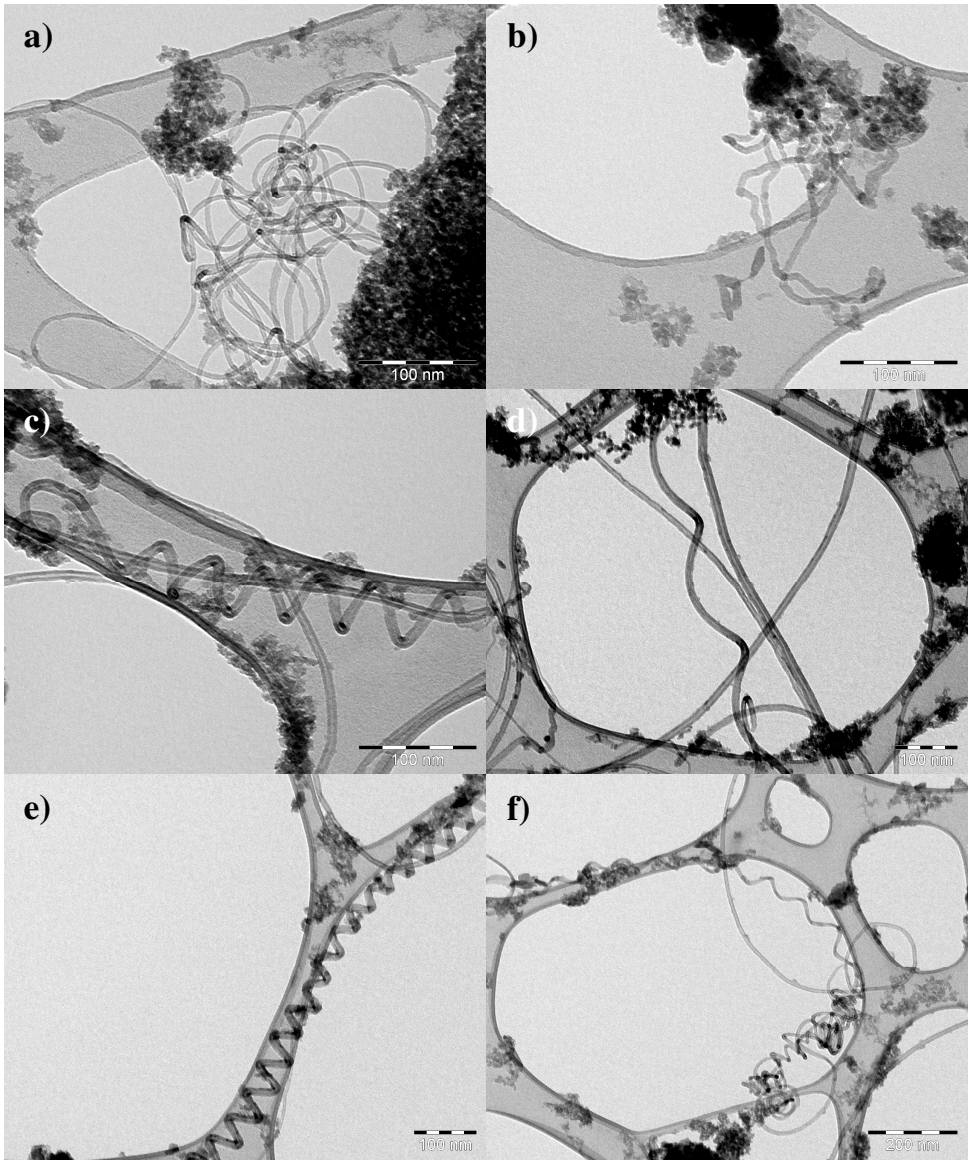

Figure IV.23.: TEM micrographs of synthesis products prepared on 2.5%Co-2.5%Pr/SiO_2 catalyst at different reaction temperatures: a)-b) T: 600°C; c-d) T: 650°C; e)-f) T: 700°C (t=30 min; 30 ml/min C_2H_2/300 ml/min N_2)

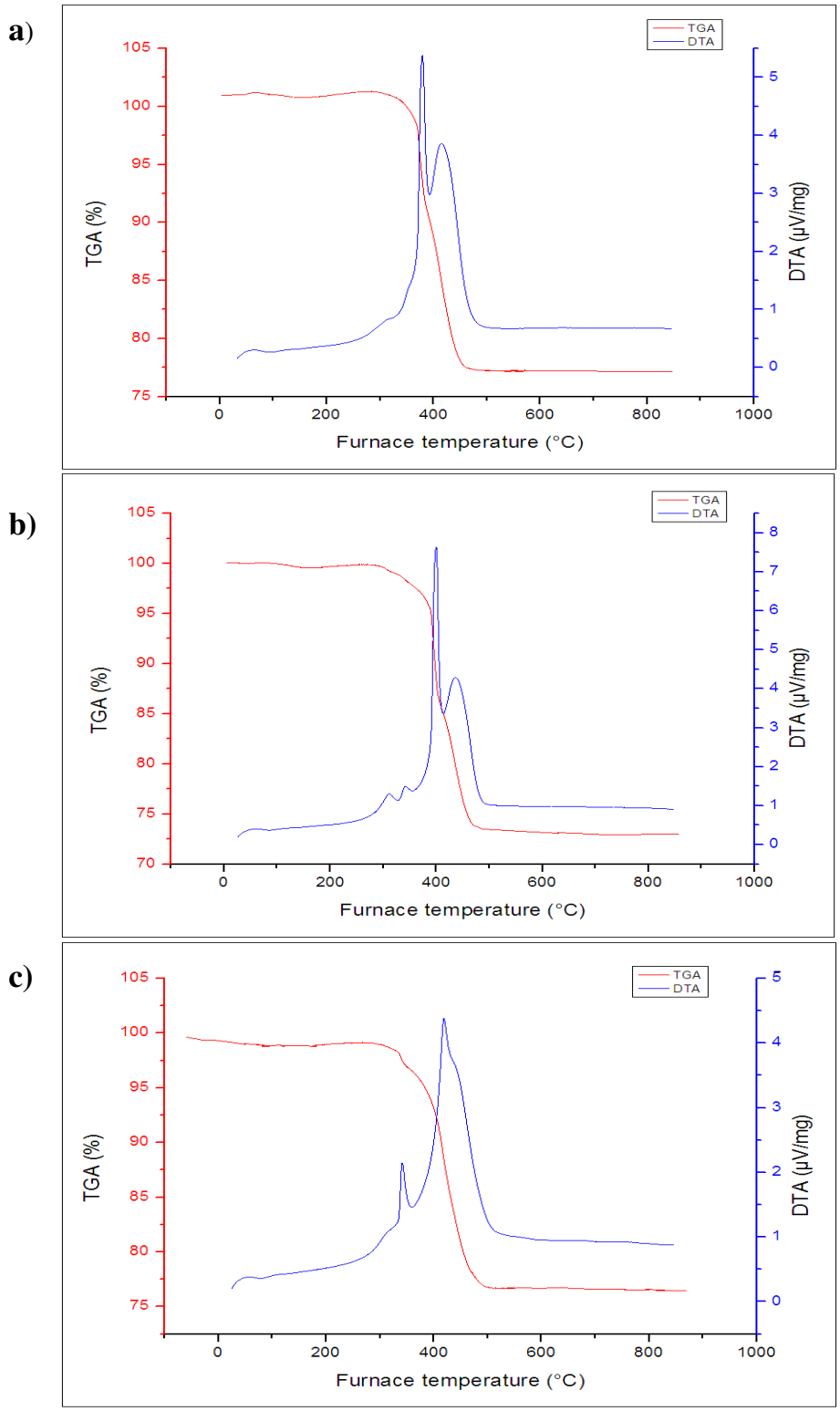

Figure IV.24.: TGA and DTA curves of CNT samples synthesized on 2.5%Co-2.5%Pr/SiO_2 catalyst at different reaction temperatures: a) T: 600°C; b) T: 650°C; c) T: 700°C (analysis carried out in 20 ml/min oxygen flow)

b) 4%Co-1%Pr/SiO_2 catalyst

The 4%Co-1%Pr catalyst was active in the formation of MWCNTs at 600°C (Figure IV.25.a)-b)). The obtained CNTs are tangled and mostly thin, their outer tube diameters are between 6-12 nm. Occasionally short helices were found in the sample, but their quantity remains inferior to 1%. The outer tube diameters of the regular helices observed varied from 8 to 12 nm, their coil pitches were between 70-130 nm, while the coil diameters ranged from 75 to 90 nm. The CNT synthesis reactions carried out at 650°C with the same catalyst led to the formation of thicker CNTs and the presence of HCNTs in the sample (Figure IV.25.c)-d)). The diameter distribution of the synthesized CNTs can be seen in Figure IV.26. The outer diameters of MWCNTs are between 4 and 24 nm, however approximately 50% of the NTs have outer diameters between 10-14 nm, which indicate the formation of rather uniform nanotubes. The ratio of regular helices compared to all the CNTs was 14-15 %. The helices have coil diameters between 30-100 nm, their coil pitches range from 38 to 145 nm, while their outer diameters are between 8-20 nm. Many irregularly bent or irregularly coiled CNTs with changing pitch were observed during TEM analysis.

When the synthesis reaction was carried out at 700°C regular helices were 10 % of all the counted nanotubes. Figure IV.25.e) shows the synthesis product and Figure IV.25.f) is the image of regularly coiled nanotubes. The coil diameters varied from 25 to 100 nm. The values of the coil pitches changed from 40 to 170 nm, and the outer diameters of the tubes were between 7-20 nm.

Carbon deposit values do not vary significantly in this temperature range applying the 4%Co-1%Pr catalyst. They remain in the range of 32-35 %. The reaction temperature which led to the formation of most helices applying this catalyst was 650°C. At this temperature 14-15 % of all the synthesized tubes are regularly coiled CNTs. Their morphology is not uniform, wavy coils as well as loose-springs are present in the samples, however the latter morphology is rare. The sample synthesized at 700°C also led to the formation of helically coiled tubes: 10 % of all the nanotubes. Wavy coils with high coil pitch values are prevalent in this sample.

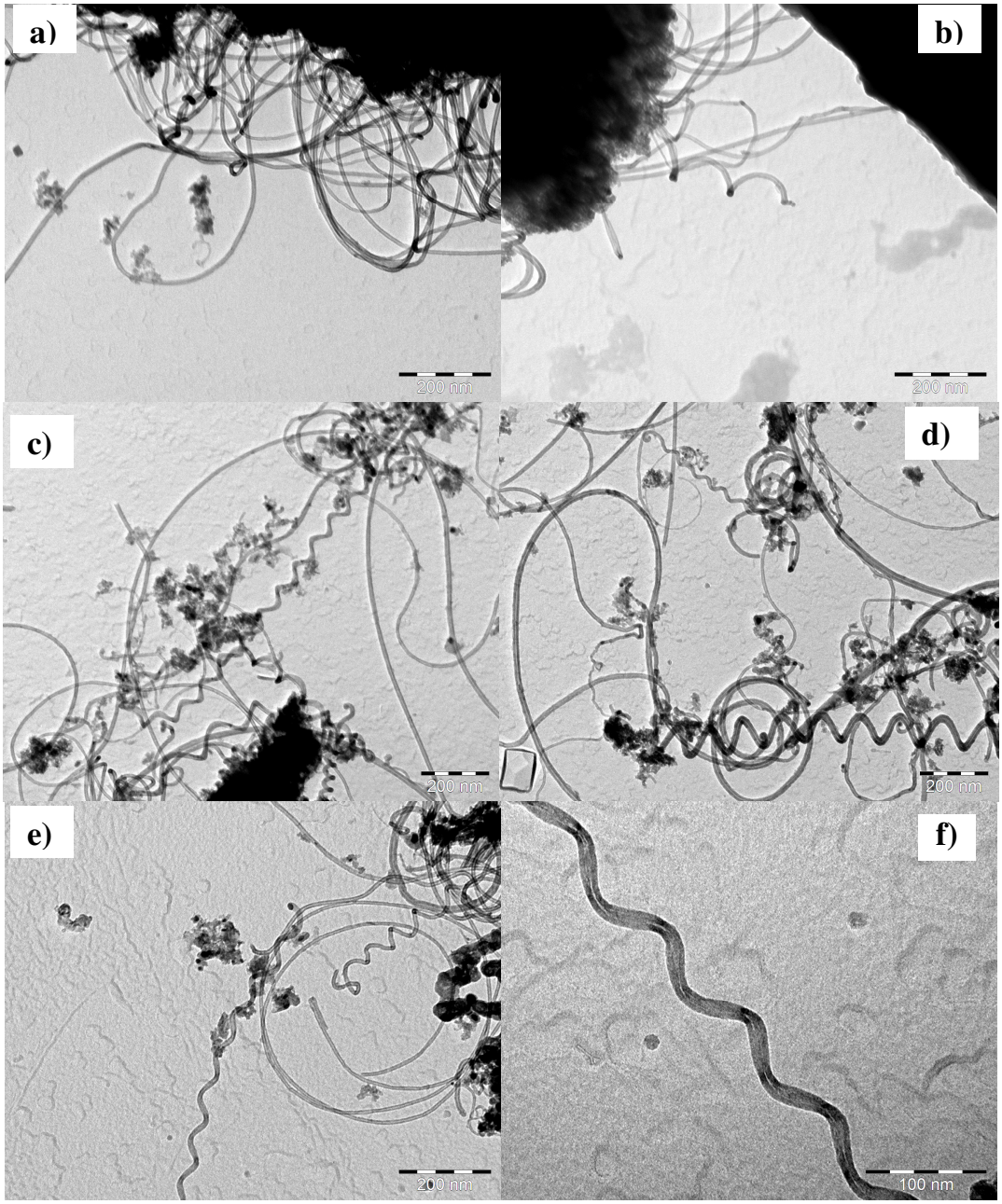

Figure IV.25.: TEM micrographs of synthesis products prepared on 4%Co-1%Pr/SiO_2 catalyst at different reaction temperatures: a) and b) T: 600°C; c) and d) T: 650°C; e) and f) T: 700°C (t=30 min; 30 ml/min C_2H_2/300 ml/min N_2)

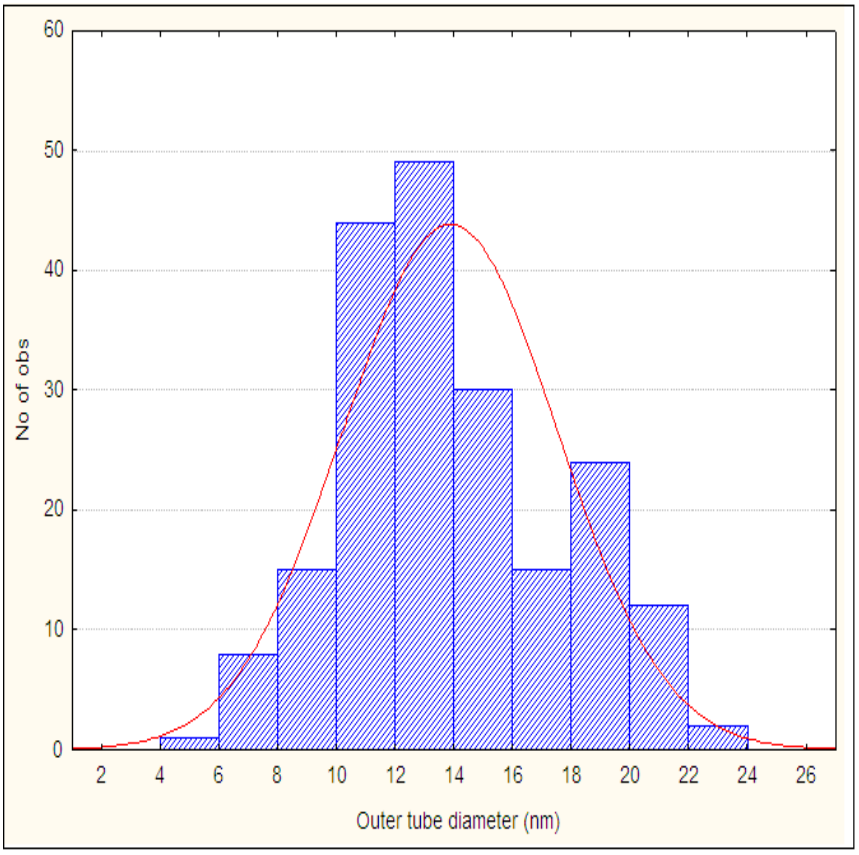

Figure IV.26.: Diameter distribution of CNTs synthesized on 4%Co-1%Pr/SiO_2 catalyst at 650°C (t=30 min; 30 ml/min C_2H_2/300 ml/min N_2)

c) 1%Co-4%Pr catalyst

In our test reactions with the small reactor the 1%Co-4% Pr catalyst was the most active in the formation of helices: 15-17% of the synthesized CNTs were regularly coiled. Thus also this catalyst was selected for further optimization in the big reactor.

At 600°C the 1%Co-4%Pr catalyst was not active in the formation of carbon nanotubes. The obtained carbon deposit composed of amorphous carbon or to some extent graphitized carbon. When the synthesis temperature was raised to 650°C both straight and helically coiled CNTs are present in the sample (Figure IV.27.a)-b)). The ratio of regular helices to straight nanotubes is around 7-8 %. Tight coils are also observed in the sample shown in Figure IV.27.a). In the case of tight coils measuring the coil pitch value can be difficult on TEM micrographs. This is caused by the fact that TEM pictures give a cross-sectional image, and in this case neither of the dimensions of the carbonaceous structure is negligible. However, the

measured coil pitch values excluding really tight coils range from 35 to 180 nm, while their coil diameters vary from 50 to 85 nm, and the outer tube diameters of the helices are between 14-20 nm. The average length of the helices is between 5-600 nm. Asymmetric metal particles were observed inside the tubes.

When the reaction temperature was raised to 700°C the ratio of the HCNTs in the sample increased significantly: 15-17% of all the synthesized CNTs were regular helices. The most common morphology of the helices found in this samples can be seen in Figures IV.27.c) and d). Tight coils that were characteristic for the sample synthesized at 650°C, cannot be observed in the synthesis product of 700°C. The observed helices have outer tube diameters between 12-22 nm. Their coil pitches vary from 35 to 180 nm, while their coil diameters range from 30 to 100 nm.

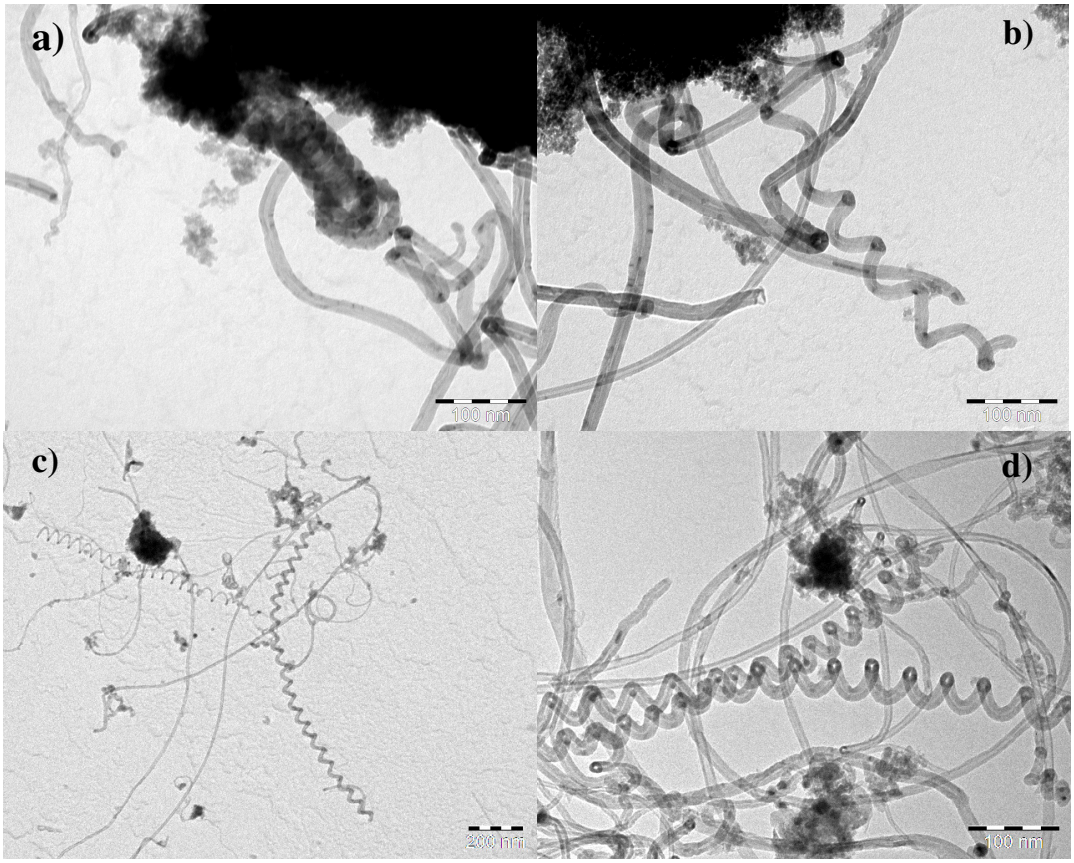

Figure IV.27.: TEM micrographs of synthesis products prepared on 1%Co-4%Pr/SiO_2 catalyst at different reaction temperatures: a) and b) T: 650°C; c) and d) T: 700°C (t=30 min; 30 ml/min C_2H_2/300 ml/min N_2)

For this catalyst the carbon deposit changes significantly with the reaction temperature: at 600°C where no carbon nanotube formation occurs, the carbon deposit is 22 %, while rising the temperature to 650°C or 700°C 31 % and 34 % of carbon deposit can be measured, respectively.

The reactions carried out at 650°C and 700°C led to the formation of HCNTs in 7-8 % and 15-17%, respectively. The sample synthesized at 650°C contains really tight coils that were not observed in the product synthesized at 700°C. However, the helices formed at this reaction temperature present more regular and homogeneous coiled structures.

d) Summary

Tables IV.12. and IV.13. summarize the results obtained on the Co-Pr/silica catalysts with different metal loading ratio at the tested reaction temperatures: 600°C; 650°C and 700°C. We can conclude that the value of the reaction temperature is a crucial parameter in the formation of the helices. The behaviour of the three tested catalysts is not uniform considering the reaction temperature. For the 2.5%Co-2.5%Pr and the 1%Co-4%Pr catalysts the reaction temperature that led to the best synthesis product considering the ratio of the helices was 700°C. However, HCNTs were also formed in significantly high ratio on the 4%Co-1%Pr catalyst at 650°C.

Carbon deposit varying with the reaction temperature in the range of 30-55 %. Higher amount of produced materials was obtained utilizing 2.5%Co-2.5%Pr catalyst at all of the tested temperatures. Carbon deposit values do not exceed the 35 % in other two cases. It can be explained by more homogeneous dispersion of metal particles on the catalyst surface.

As Table IV.12 shows the coil pitches of the produced helices are more or less uniform, while the coil diameter values show some differences. In the product synthesized on the 2.5%Co-2.5%Pr catalyst at 700°C helices with slimmer coil diameters are present in the sample. Concerning the diameters the 1%Co-4%Pr catalyst produces slightly thicker tubes compared to the other two catalysts.

Catalyst	Reaction temperature (°C)	Carbon deposit (%)	Carbon nanotubes	Coiled CNTs
2.5%Co-2.5%Pr	600	48	Straight MWCNTs with small diameters	-
	650	53	Straight CNTs, helices, some amorphous carbon	10%
	700	55	Straight CNTs, helices, some amorphous carbon	15%
4%Co-1%Pr	600	32	Mainly straight CNTs few helices	<1%
	650	33	Straight CNTs, regularly coiled CNTs, some amorphous carbon	14-15%
	700	35	Straight CNTs, helices, some amorphous carbon	10%
1%Co-4%Pr	600	22	No nanotube formation	-
	650	31	Straight CNTs, and helices, some amorphous carbon	7-8%
	700	34	Straight CNTs, and helices, some amorphous carbon	15-17%

Table IV.12.: Summary of synthesized carbonaceous products at different reaction temperatures (t=30 min; 30 ml/min C_2H_2/300 ml/min N_2)

Catalyst	Reaction temperature (°C)	Outer tube diameter (nm)	Coil pitch (nm)	Coil diameter (nm)
2.5%Co-2.5%Pr	650	9-15	45-215	35-90
	700	6-16	35-170	23-55
4%Co-1%Pr	600	8-12	70-130	75-90
	650	8-20	38-145	30-100
	700	7-20	40-170	25-100
1%Co-4%Pr	650	14-20	35-180	50-85
	700	12-22	35-180	30-100

Table IV.13.: Summary of the characteristics of helices synthesized at different reaction temperatures (t=30 min; 30 ml/min C_2H_2/300 ml/min N_2)

Raising the reaction temperature over 700°C significantly increases the production of amorphous carbon according to some previous test reactions carried out with the small reactor, thus we did not continue the study applying higher reaction temperatures.

IV.4.3.2.Effect of the carbon source flow on the synthesis product

The carbon source flow is also a crucial parameter for the CNT synthesis. In a previous work Szabo ***[3]*** suggested that augmenting the carbon source flow in the synthesis reactions of CNTs can lead to the formation of helices in higher ratio. Thus we tested acetylene flows of 50 and 70 ml/min, maintaining the carbon source: carrier gas ratio at 1:10. We chose a reaction temperature of 700°C for this experiment. The reaction time was 30 minutes.

a) 2.5%Co-2.5%Pr catalyst

For the 2.5%Co-2.5%Fe catalyst the augmenting the carbon source flow to 50 ml/min led to significant increase in the carbon deposit. However, the ratio of helices decreased in the sample. Considering the morphology of the helices no significant difference can be observed compared to the sample synthesized with 30 ml/min acetylene flow. The coil pitches of the synthesized tubes vary from 50 to 140 nm. Their coil diameters are between 30-100 nm. The outer tube diameters of the helices are between 10-14 nm.
When the acetylene flow was set to 70 ml/min the ratio of helices compared to all the synthesized MWCNTs was around 10 % in the sample. In this case the presence of significant amount of amorphous carbon could be observed by transmission electron microscopy. The outer diameters of the synthesized helices varied between 12-15 nm, their coil diameters ranged from 35 to 140 nm and their coil pitches varied from 30 to 170 nm.

b) 4%Co-1%Pr catalyst

The effect of the carbon source flow on the synthesis product was also investigated in the case of the 4%Co-1%Pr catalyst. In this case we also chose 700°C as reaction temperature.
Figure IV.28.a) shows the DTA, TGA and DrTGA curves of the sample synthesized applying 50 ml/min acetylene flow. We can observe a big, relatively thin peak on the DTA curve at around 570°C corresponding to the MWCNTs in the sample. A smaller peak at 321°C

indicates the presence of disorganized carbon in the synthesis product. The carbon deposit in this reaction conditions is higher (40.6%) compared to the one obtained with 30 ml/min carbon source flow (32.3%).

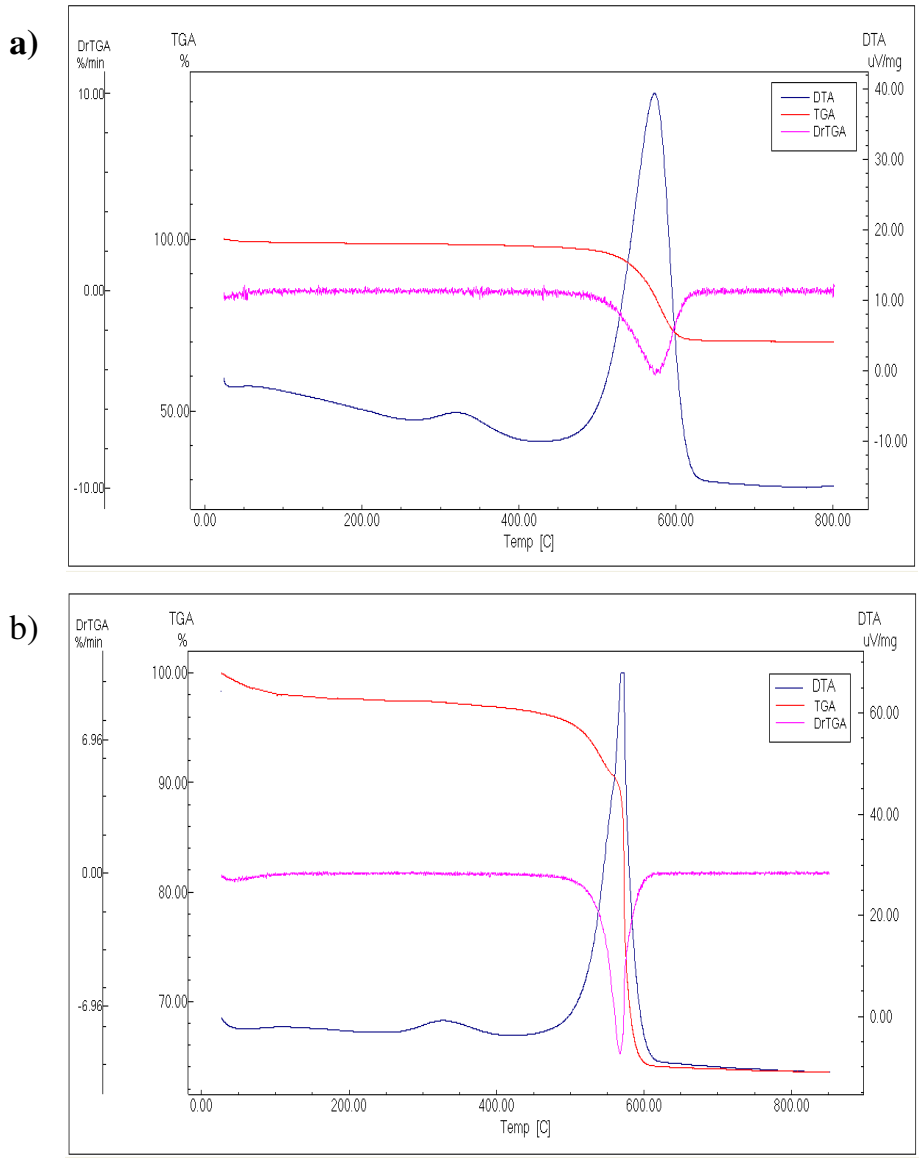

Figure IV.28.: Thermal analysis results of CNT samples synthesized on 4%Co-1%Pr catalyst varying the acetylene flow: a) 50 ml/min; b) 70 ml/min (T: 700°C; t=30 min). Thermal analysis carried out in 20 ml/min air flow.

In TEM micrographs (Figure IV.29.a)-b)) we can observe significant amount of amorphous carbon. The catalyst particles in the sample are often covered by a thick layer of amorphous

carbon. The ratio of the produced helices is around 10 %. However, this is also due to the few CNTs produced in these reaction conditions. The formed helices are often loose springs, wavy coils were rarely observed in the sample.

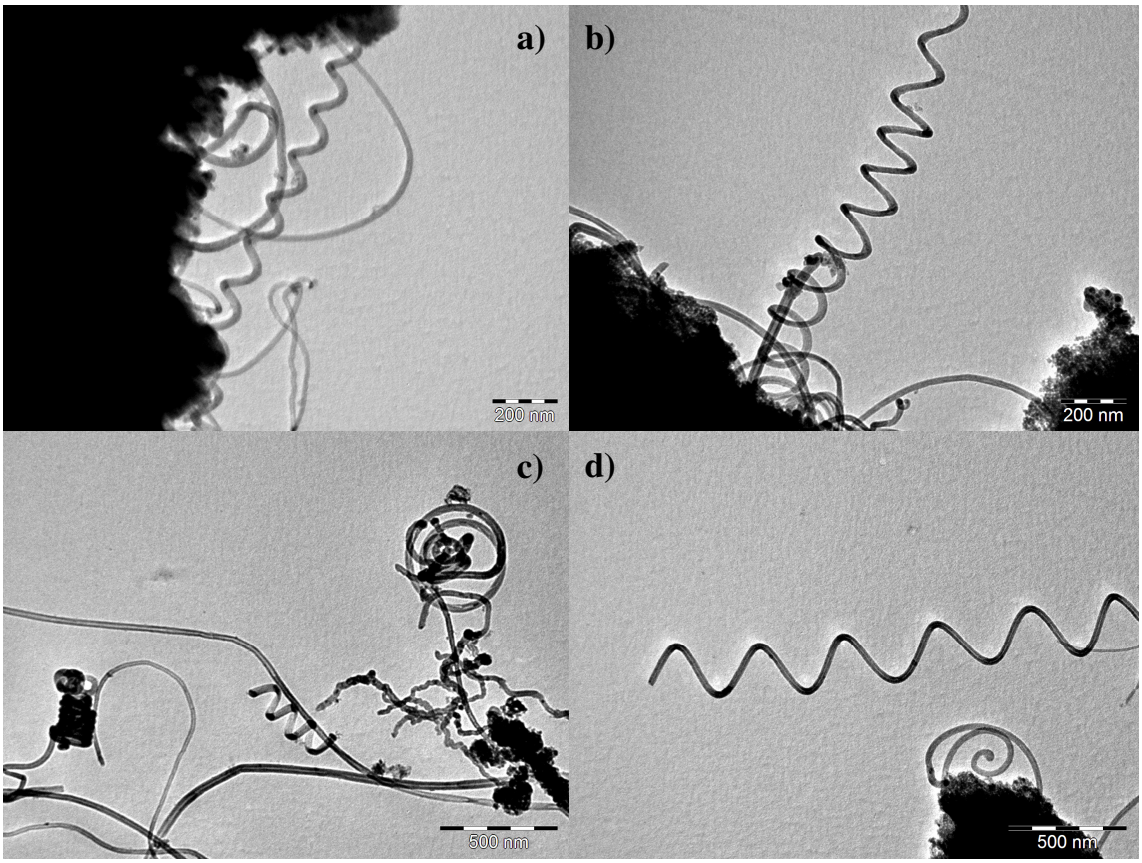

Figure IV.29.:TEM pictures of CNT samples synthesized on 4%Co-1%Pr catalysts applying different C_2H_2 flow: a)-b) 50 ml/min; c)-d) 70 ml/min (T: 700°C; t=30 min)

Figure IV.28.b) shows thermal analysis results of the sample synthesized applying 70 ml/min carbon source flow. On the DTA curve two peaks can be observed: one at around 570°C corresponding to the produced CNTs, and a smaller hill-like peak at around 330°C represents amorphous carbon.

According to TEM observations the ratio of helices is 10 % in the sample. Tight coils are also regularly observed (Figure IV.29.c)), but the majority of the HCNTs are wavy or loose-spring like (Figure IV.29.d)). The coil diameters of the synthesized coils vary between 70-170 nm their coil pitches are between 130-500 nm and the outer diameters of the coiled tubes are in the range of 27-35 nm.

Increasing the carbon source flow during the synthesis reactions led to the increase of the carbon deposit. However, the ratio of HCNTs in the synthesis product remains unchanged.
The morphology of the HCNTs changes significantly by the change of the carbon source flow. At 70 ml/min C_2H_2 flow tight coils are regularly observed.

c) 1%Co-4%Pr catalyst

Figures IV.30.a) and b) show the comparison of TGA and DTA curves of the synthesis products produced on 1%Co-4%Pr catalysts at different acetylene flow rates. We can observe on the TGA curves that the amount of carbon deposit does not change significantly increasing the gas flow rate. The values remain always at about 35-46 %. DTA curves show strange almost doubled peaks at around 530-550^{o}C for the samples 50 ml/min and 70 ml/min acetylene flow, while the DTA peak of the sample synthesized at 30 ml/min gas flow is uniform. In the first two cases, the escalation of the peaks can be caused by the large scale of different carbonaceous materials (CNTs with various diameters, with more defects in their walls, variously bent, and the formation of high amount of amorphous carbon) present in the analysed samples, while for the 30 ml/min acetylene flow the reaction product can contain structures with more homogeneous characteristics and smaller amount of amorphous carbon formed.
According to TEM observations few regular and some irregular helices are formed when applying 50 ml/min acetylene flow (Figure IV.31.a)). The ratio of regular helices is inferior to 1% of the observed nanotubes. Increasing the carbon source flow to 70 ml/min leads to the formation of no helices and some tangled MCNTs (Figure IV.31.b)).
We can conclude that in the case of the 1%Co-4%Pr catalyst in contempt of our expectations the production of HCNTs decreased increasing the carbon source flow. At 70 ml/min carbon source flow no helices were formed, while in the sample produced with 50 ml/min gas flow regular helices are observed only occasionally.

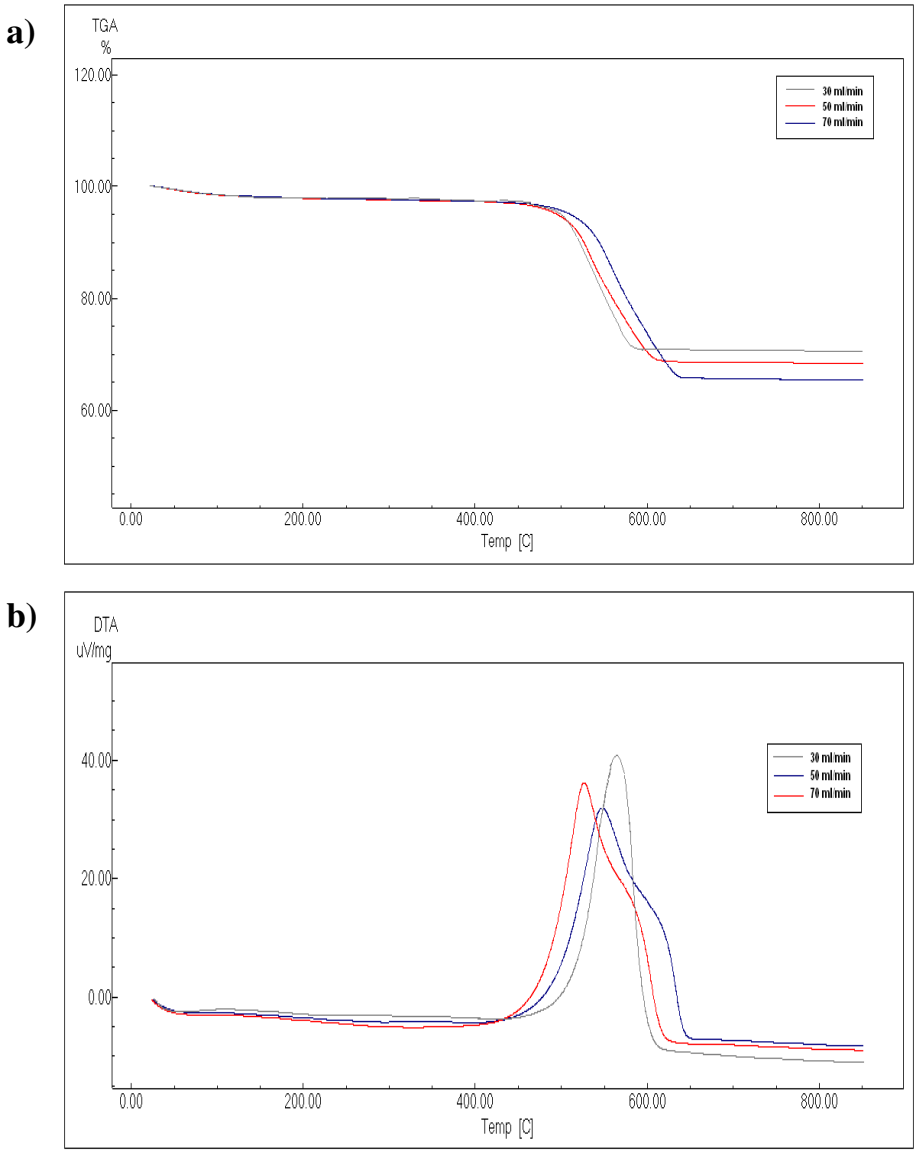

Figure IV.30.: Comparison of TGA (a) and DTA (b) curves of CNT samples synthesized on 1%Co-4% Pr catalysts varying the carbon source flow. (T: 700°C, t=30 min) Thermal analysis carried out in 20 ml/min air flow.

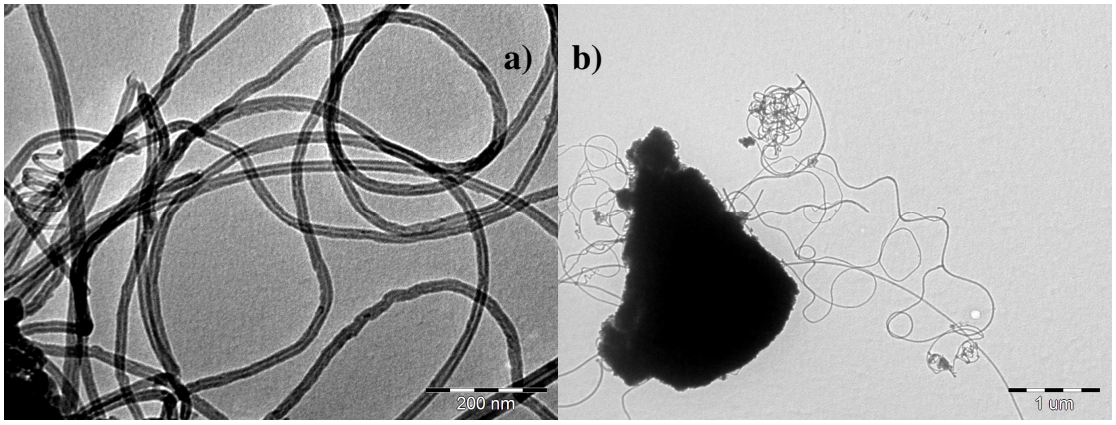

Figure IV.31.: TEM pictures of CNT samples synthesized on 1%Co-4%Pr catalysts applying different C_2H_2 flows: a) 50 ml/min; b) 70 ml/min (T: 700°C; t=30 min)

d) Summary

2.5%Co-2.5%Pr; 1%Co-4%Pr and 4%Co-1%Pr catalysts were applied in CNT synthesis reactions. Augmenting the carbon source flow did not enhance the formation of the HCNTs. However, in the case of the 4%Co-1%Pr catalyst it influenced the morphology of the synthesized coils. When applying 70 ml/min acetylene flow tight coils were regularly observed in the sample. Concerning the 1%Co-4%Pr catalyst increasing the carbon source flow led to lower activity in the CNT as well as in the HCNT production. At 70 ml/min acetylene flow only tangled MWCNTs were observed and some irregularly bent coils. Also the samples prepared with 50 ml/min acetylene flow contained few helices. The characteristics of the synthesized products and the regular helices present in the samples are summarized by Tables IV.14 and IV.15, respectively.

Catalyst	2.5%Co-2.5Pr			1%Co-4%Pr			4%Co-1%Pr		
C_2H_2 flow (ml/min)	30	50	70	30	50	70	30	50	70
Carbon deposit (%)	55.6	68.1	69.2	34.7	38.7	46.2	32.3	40.6	49.5
Carbon yield (%)	51.6	42.8	31.03	36.6	24.8	21.2	35.6	25.5	22.2
% Coiled	15	10	10	15-17	<1	-	10	10	10

Table IV.14.: CNT products synthesized on 5% Co-Pr catalysts applying different carbon source flows (T: 700°C, t=30 min)

Catalyst	C_2H_2 flow (ml/min)	Outer tube diameter (nm)	Coil pitch (nm)	Coil diameter (nm)
2.5%Co-2.5%Pr	30	6-16	35-170	23-55
	50	10-14	50-140	30-100
	70	12-15	35-140	30-170
4%Co-1%Pr	30	7-20	40-170	25-100
	50	21-23	120-140	80-170
	70	27-35	130-500	70-170
1%Co-4%Pr	30	12-22	35- 180	30-100
	70	18-20	130-300	120-170

Table IV.15.: Characteristics of synthesized helices at different C_2H_2 flow rates.
(T:700°C ;t=30 min)

IV.4.3.3. Effect of the carrier gas flow on the synthesis product

The effect of the carrier gas flow rate was also investigated. These reactions were carried out at 700°C maintaining the C_2H_2 flow at 30 ml/min. The reaction time was 30 minutes and 1 g catalyst was placed in the quartz boat. The nitrogen gas flow was investigated at values of 150 ml/min; 300 ml/min; 450 ml/min and 600 ml/min.

a) 2.5%Co-2.5%Pr catalyst

In the case of the 2.5%Co-2.5% Pr catalyst modifying the nitrogen flow to 150 ml/min lead to a decrease in the quality of the synthesis product. In the samples, few tangled CNTs were present together with amorphous carbon. Regular helices were not found. The carbon deposit in this case did not differ significantly from the value obtained at 300 ml/min gas flow.
Augmenting the N_2 flow to 450 ml/min leads to the presence of HCNTs in the sample. Their ratio is around 6-7 %. While applying a 600 ml/min gas flow HCNTs are present in the samples in approximately the same ratio, however fewer nanotubes are synthesized and higher amount of amorphous carbon formed at this carrier gas flow.

b) 4%Co-1%Pr catalyst

The sample synthesized with 150 ml/min nitrogen flow did not lead to the formation of helices. Tangled CNTs are present covered with amorphous carbon (Figure IV.32.a)-b)) Some irregularly bent nanotubes and tubes composed of a small coiled and a longer straight part were found in the synthesis product. In the tangled tubes asymmetric egg-shaped metal particles were often observed. On the DTA curve of this sample (Figure IV.33.b) red line) we can observe two peaks: a small hill-like peak corresponding to disorganized carbon at around 320-340°C, and a thin high peak at around 520°C indicates the presence of MWCNTs in the sample confirmed also by TEM analysis.

When 450 ml/min N_2 flow was applied the ratio of HCNTs in the sample is around 10%. It does not change significantly compared to the one obtained in our basis reaction with 300 ml/min carrier gas flow. HCNTs with various morphology, coil pitch and coil diameter values were observed (Figure IV.32.c)-d)). Outer tube diameters of the helices vary from 7 to 40 nm, their coil pitches are in the range of 57-190 nm, while their coil diameters are between 30-130 nm. On the DTA curve of this product (Figure IV.33.b) blue line)we can observe the small thin peak indicating the presence of amorphous carbon at around 290°C, and a large peak corresponding to graphitized carbon at 550°C. Taking in consideration our TEM investigations this peak corresponds to the MWCNTs in the sample.

Applying 600 ml/min nitrogen flow, in our conditions led to the formation of high amount of amorphous carbon and few MWCNTs. According to TEM observations, high percentage of the produced nanotubes are coiled. For this reason, the ratio of coiled CNTs compared to all the CNTs increased to 14-15%. The outer tube diameters of the helices vary between 12-40 nm, their coil pitches are in the range of 23-290 nm and their coil diameters range from 40 to 200 nm. Tight coils as well as wavy CNTs with large pitch values are also observed in the sample (Figure IV.32.e)-f)). On the DTA curve of this sample (Figure IV.33.b) green line) we can observe a hill-like low peak from 260 to 380°C and a tall peak at 580°C corresponding to graphitised carbon, in our case the MWCNTs in the sample.

In Figure IV.33. we can observe the TGA and DTA curves of the synthesis products obtained at different nitrogen flow rates. In the TGA curves we can see slight differences in the weight loss between 450 and 600°C (this is the temperature where MWCNTs burnt). The carbon deposit changes slightly varying the carrier gas flow rates from 150 to 600 ml/min. The DTA curves of the samples show two peaks one small, in most cases hill-like peak from 300 to 400°C corresponding to amorphous carbon. For the sample prepared with 450 ml/min N_2

flow, however transmission electron microscopy observations did not show higher amorphous carbon content compared to the sample synthesized applying different gas flow rates.

However, the change of the nitrogen flow significantly influenced the morphology of the synthesized product. At 150 ml/min N_2 flow no HCNTs were observed in the sample. At 300-450 ml/min nitrogen flow HCNTs are 10% of all the nanotubes synthesized. The ratio of the coils compared to all the MWCNTs increased to 14-15 % when applying 600 ml/min nitrogen flow.

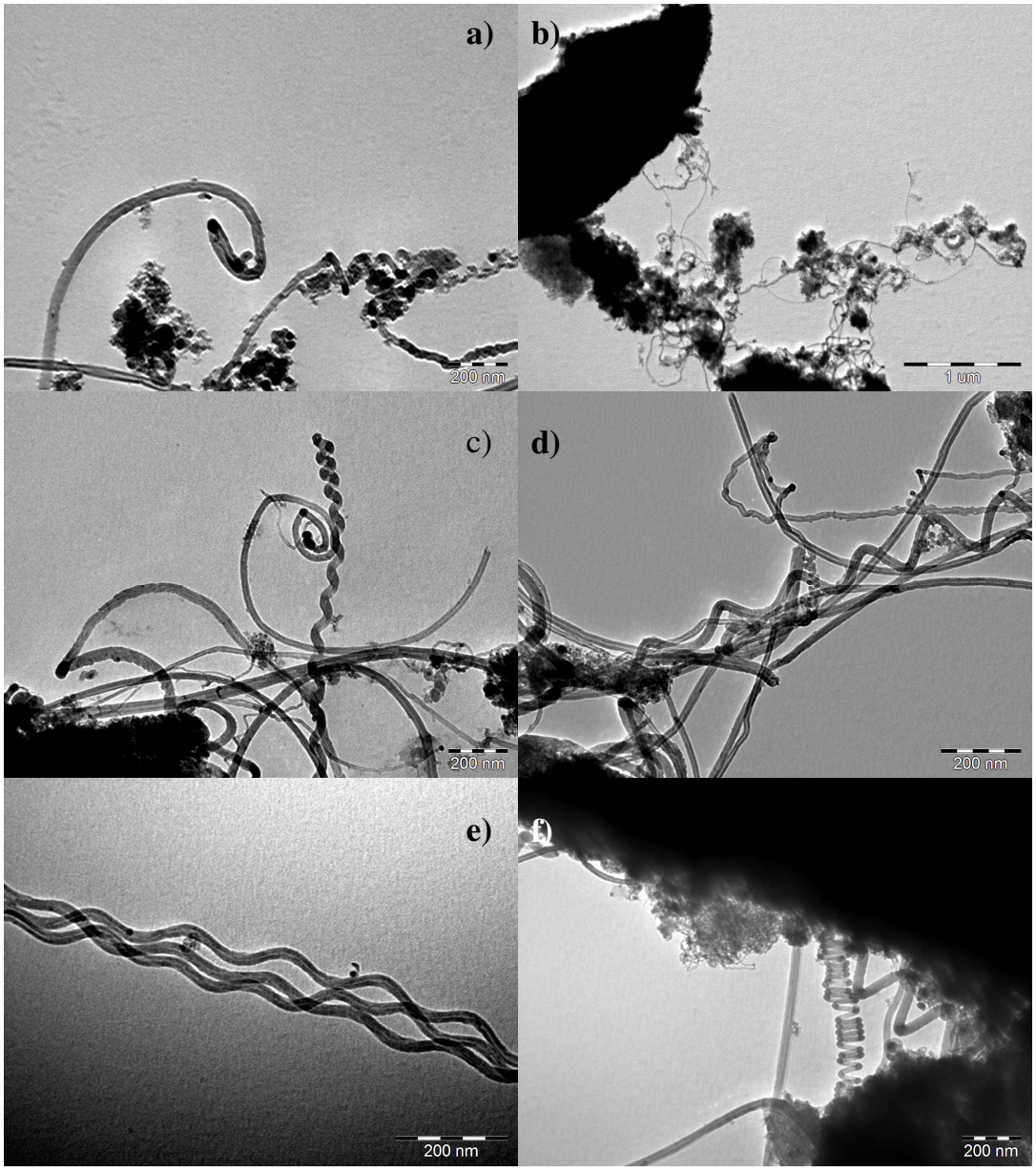

Figure IV. 32.:TEM pictures of CNT samples synthesized on 4%Co-1%Pr catalysts applying different N_2 flows: a)-b) 150 ml/min; c)-d) 450 ml/min; e)-f) 600 ml/min (T: 700°C; C_2H_2 30 ml/min; t=30 min)

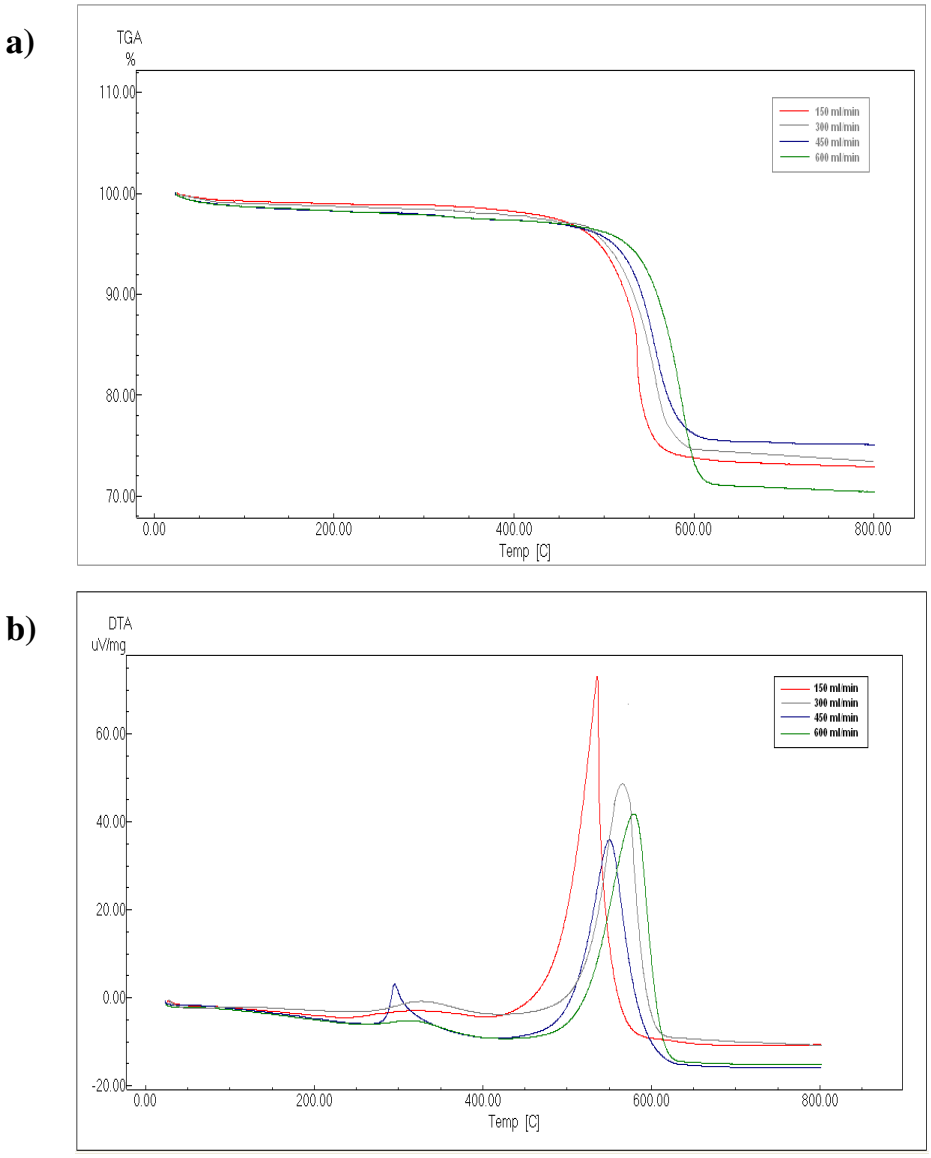

Figure IV.33.: Comparison of the TGA (a) and DTA (b) curves of synthesis products synthesized with different N_2 flows on 4%Co-1%Pr catalyst

c) 1%Co-4%Pr catalyst

Applying the 1%Co-4%Pr catalyst the synthesis product obtained with 150 ml/min N_2 flow did not contain CNTs.

When the nitrogen flow was set to 450 ml/min the CNTs in the samples are often covered by amorphous carbon. Helices with different pitches and coil diameters are present in the samples. The coil pitches of the HCNTs range from 45 to 80 nm, their coil diameters are in

the range of 50-90 nm. The DTA curve (Figure IV.35.a)) of the synthesis product shows one peak at 530°C that corresponds to the MWCNTs present in the sample. Figures IV.34.a)-b) are TEM images of the analysed sample. The ratio of the coiled CNTs is 9-10 %. The helices are often loose springs. In the samples we found some coils that starts as a loose spring and consequently becomes a straight coil. Relatively few CNTs are produced in this sample compared to the synthesis product prepared with 300 ml/min N_2 flow.

At 600 ml/min N_2 flow rate a high amount of amorphous carbon can be observed that covers the CNTs. 14-15% of all the counted tubes are helices. Short, loose-spring like and long wavy coils are prevalent among the helices (Figure IV.34.c)-d)), however tight coils occasionally are also observed. The DTA curve (Figure IV.35.b)) of the sample shows one peak at 520°C, this probably corresponds to the MWCNTs in the sample.

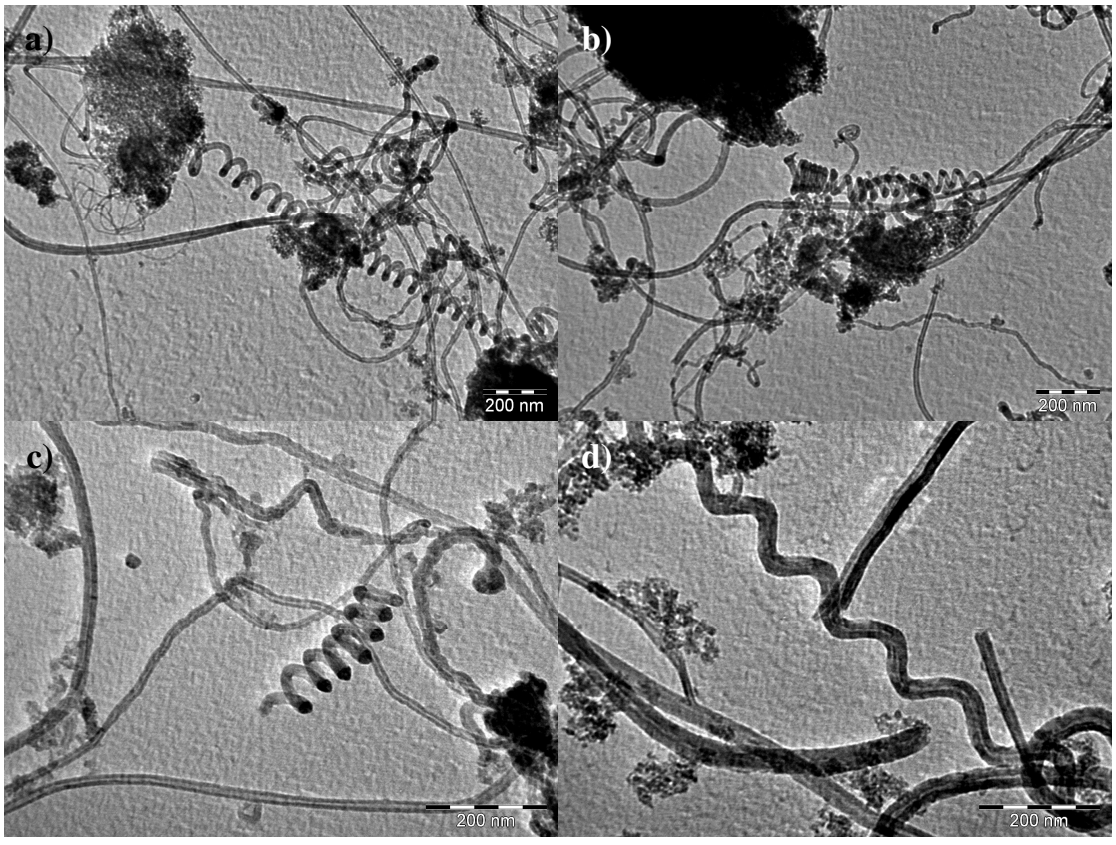

Figure IV.34.: TEM micrographs of CNT products synthesized with different N_2 flows on 1%Co-4%Pr catalyst. a)-b): 450 ml/min; c)-d): 600 ml/min N_2 flow (T: 700°C; C_2H_2 flow: 30 ml/min)

a)

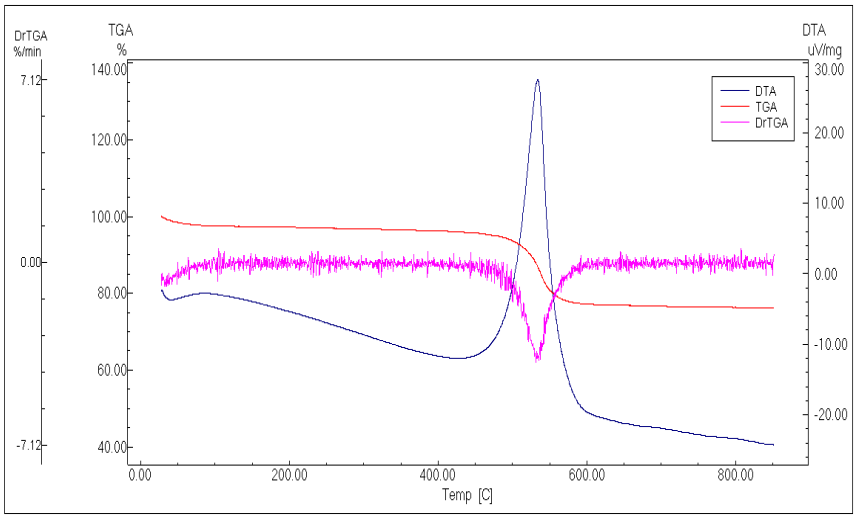

b)

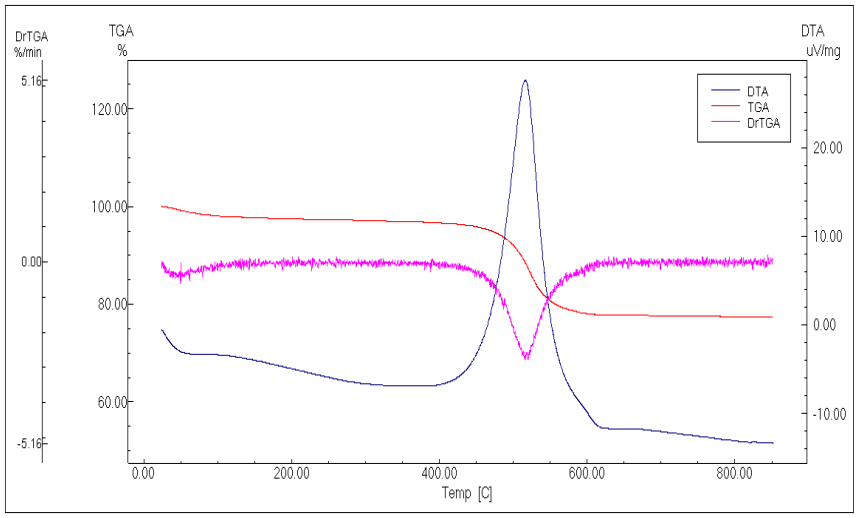

Figure IV.35.: TG; DTA and DrTG curves of CNT products synthesized with different N_2 flows on 1%Co-4%Pr catalyst: a) 450 ml/min; b) 600 ml/min N_2 flow (T: 700°C; C_2H_2 flow 30 ml/min; Thermal analysis carried out in 20 ml/min air flow.)

d) Summary

Tables IV.16 and IV.17 summarize the characteristics of the products synthesized with different N_2 flow rates. We can conclude that no HCNT production was observed on the catalysts used with 150 ml/min gas flow rate.

Increasing the nitrogen flow to 600 ml/min using 4%Co-1%Pr catalyst led to higher HCNT/CNT ratio under our reaction conditions. 14-15 % of the synthesized tubes were helically coiled. For the 1%Co-4%Pr catalyst the advantageous nitrogen flow rate remains

300 ml/min. Also at 600 ml/min nitrogen flow regularly coiled CNTs are 15 % of all the nanotubes, however in this case fewer CNTs were observed in the product. For the 2.5%Co-2.5%Pr catalyst increasing the N_2 flow led to a decrease in the HCNT ratio.

Catalyst	N_2 flow (ml/min)	Carbon deposit (%)	Product characteristics	Coiled (%)
2.5%Co-2.5%Pr	150	57	Few tangled CNTs high amount of amorphous or graphitised carbon	-
	300	55	Straight CNTs, HCNTs and some amorphous carbon	15
	450	62	Straight CNTs, HCNTs and low amount of amorphous carbon	6-7%
	600	67	Straight CNTs, regular coils and CNTs with, amorphous carbon	6-7%
4%Co-1%Pr	150	29	Few tangled CNTs and large amount of amorphous carbon	-
	300	32	CNTs, HCNTs and low amount of amorphous carbon	10
	450	37	Straight CNTs, regular coils and CNTs with changing pitch	10
	600	36	Few CNTs, catalyst particles covered with amorphous carbon, regular helices	14-15
1%Co-4%Pr	150	16	No CNTs only amorphous carbon	-
	300	34	CNTs, HCNTs and amorphous carbon	15-17
	450	26	High amount of amorphous carbon CNTs, HCNTs	10
	600	29	HCNTs covered by amorphous carbon, few CNTs	14-15

Table IV.16.: Summary of synthesis products obtained on 2.5%Co-2.5%Pr; 4%Co-1%Pr; 1%Co-4%Pr catalysts at different nitrogen flow rates (T: 700°C; C_2H_2 30 ml/min)

Catalyst	N_2 flow (ml/min)	Outer tube diameter (nm)	Coil pitch (nm)	Coil diameter (nm)
4%Co-1%Pr	300	7-20	40-170	25-100
	450	7-40	57-190	30-130
	600	12-40	23-190	40-200
1%Co-4%Pr	300	12-22	35-180	30-100
	450	13-18	45-80	50-90
	600	13-33	40-170	60-90

Table IV.17. Characteristics of coiled CNTs obtained on 4%Co-1%Pr; 1%Co-4%Pr catalysts at different nitrogen flow rates (T: 700°C; C_2H_2 30 ml/min)

We can note that the coil diameters of helices prepared on 4%Co-1%Pr catalyst increase applying higher nitrogen flow rate, while the values for the coils on 1%Co-4%Pr catalyst remain in the same range. Concerning coil pitches, we can note that coiled CNTs produced on helices formed on 1%Co-4%Pr with 450 ml/min flow of nitrogen have unusually uniform coil pitch values.

IV.4.4. Morphology of the synthesized coiled CNTs

Figure IV.36. shows the characteristic coils present in the samples synthesized on Co-Pr catalysts. In most cases wavy coils and S-shape telephone-cord like CNTs were prevalent in the samples. However, tight coils (Figure IV.36.e)) could be found regularly varying the nitrogen flow rate when the 1%Co-4%Pr and the 4%Co-1%Pr catalysts were used. By transmission electron microscopy we observed strange forms of helices as well. Auto-associated coils, HCNTs with changing coil pitch and coil diameter were observed in the samples. The ratio of the coil pitch and coil diameter determine the coil curvature and the morphology of the formed helices. We examined 300 helices syntehsized on 5%Co-Pr/SiO_2 catalysts, and analyzed their coil pitch, coil diameter and outer tube diameter values. Figure IV.37. shows the coil pitch of the helices as a function of the coil diameter. We can say helices having a certain pitch value can have different coil diameters.

Figure IV.38 a) and b) represents the number of helices with defined coil pitches and coil diameters and belonging to different diameter distribution categories. Observing figure IV.38.a) we can say that the most frequent coil diameter values are between 20-50 nm. Helices having these coil diameter values have mostly small outer tube diameters: inferior to

20 nm. Coil diameter values higher than 100 nm are rare. Around 90% of the examined helices synthesized on 5%Co-Pr/SiO_2 catalysts have coil diameters inferior to 100 nm. Comparing with the results of Szabó who examined 300 helices prepared in different laboratories, using different catalysts ***[3]*** the tendency is similar. However, in this previous work higher coil diameter values until 300 nm were also observed and coil diameter values superior to 100 nm are slightly more frequent.

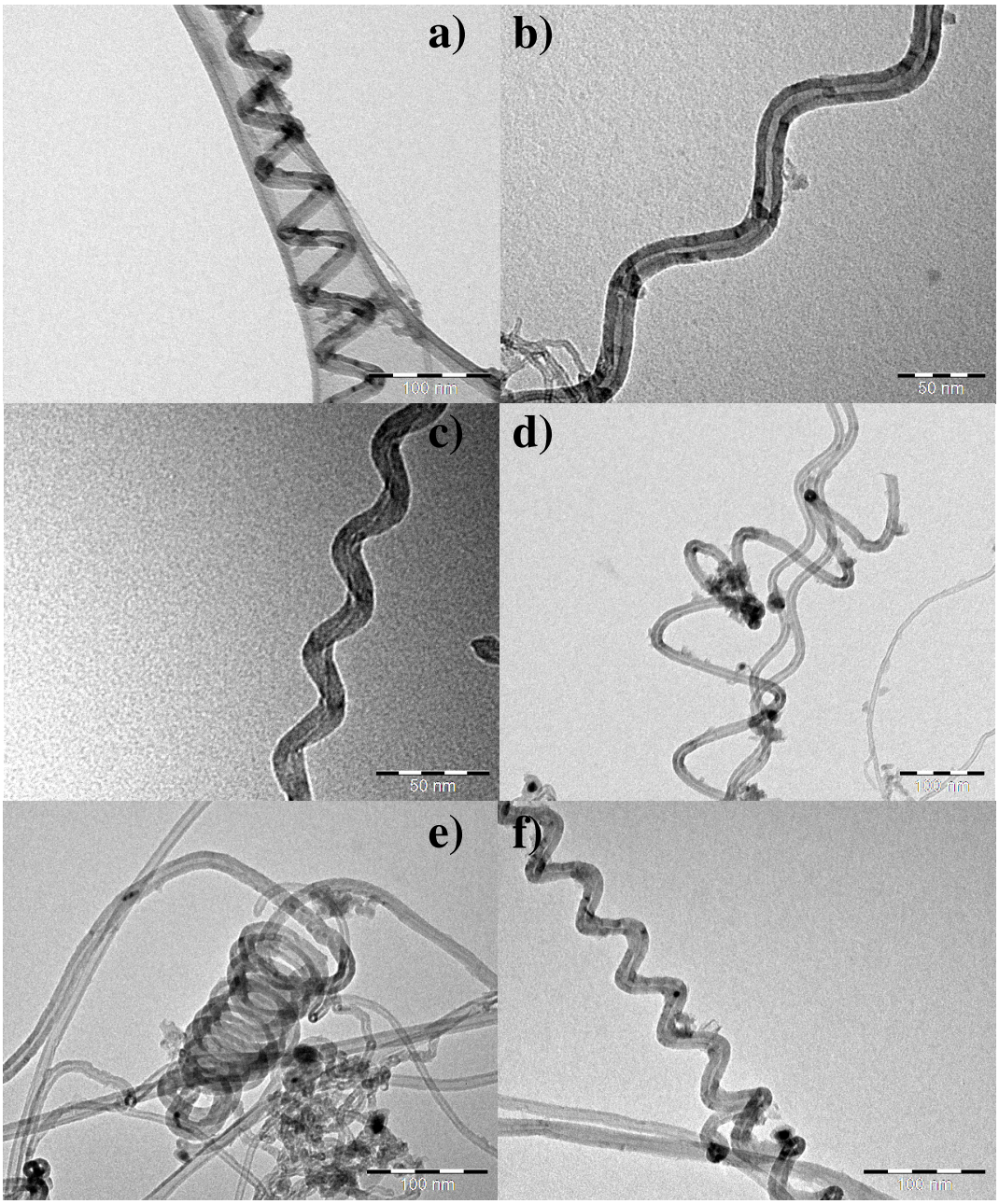

Figure IV.36.: Different forms of helical CNTs with varying coil diameter and coil pitch synthesized on Co-Pr/SiO_2 catalysts with different metal loadings. a) 2.5%Co-5%Pr, b-c) 7.5%Co-2.5%Pr, d) 5%Co-5%Pr, e)-f) 1%Co-4% Pr

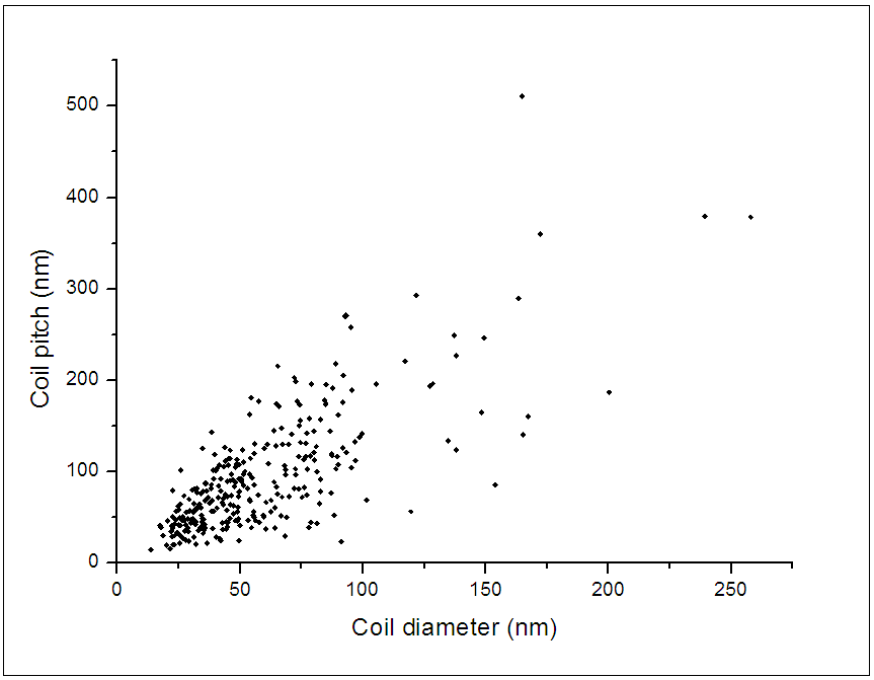

Figure IV.37: Variation of the coil pitch in function of the coil diameter for HCNTs synthesized on 5% Co-Pr catalysts

We can observe that the most frequent coil pitch value is between 40-50 nm (an overriding peak is present at this pitch fraction). Concerning the coil pitch values (IV.38. b)) we can say that their distribution is nearly lognormal (Figure IV.39.). This distribution was frequently observed in the nature for example in the case of diameter distributions of grinded particles. We carried out a Chi-square test to control if the distribution of the pitches is really lognormal. The significance level of the calculated $\chi 2$ values of our results is 0.22 thus the hypothesis that distribution is lognormal can be accepted (Figure IV.39.).

a)

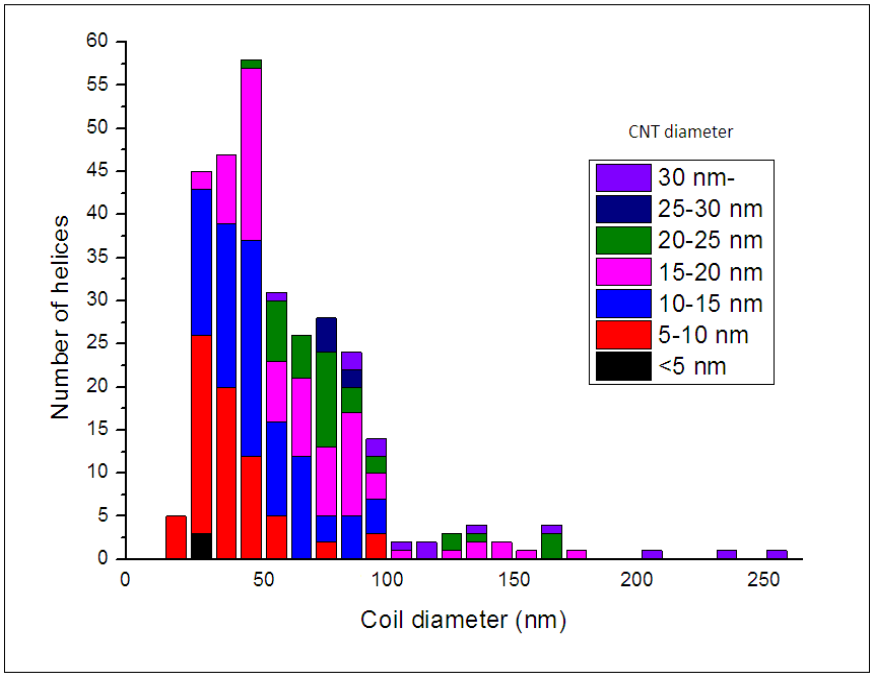

b)

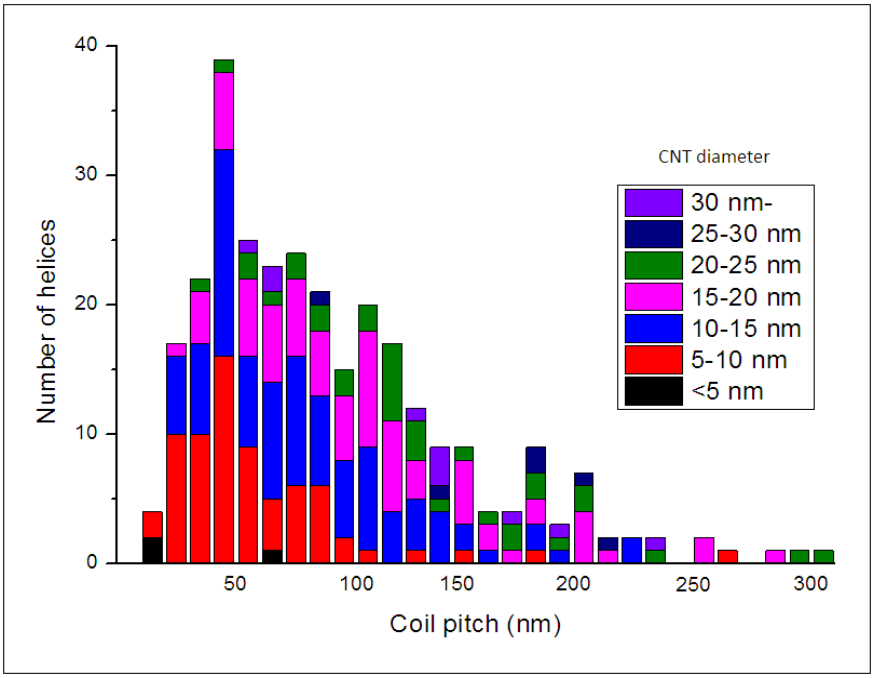

Figure IV.38: a) Number of HCNTs synthesized on 5%Co-Pr catalysts and their coil diameters featuring the diameter distribution categories; b) Number of HCNTs synthesized on 5%Co-Pr catalysts and their coil pitches featuring the diameter distribution categories

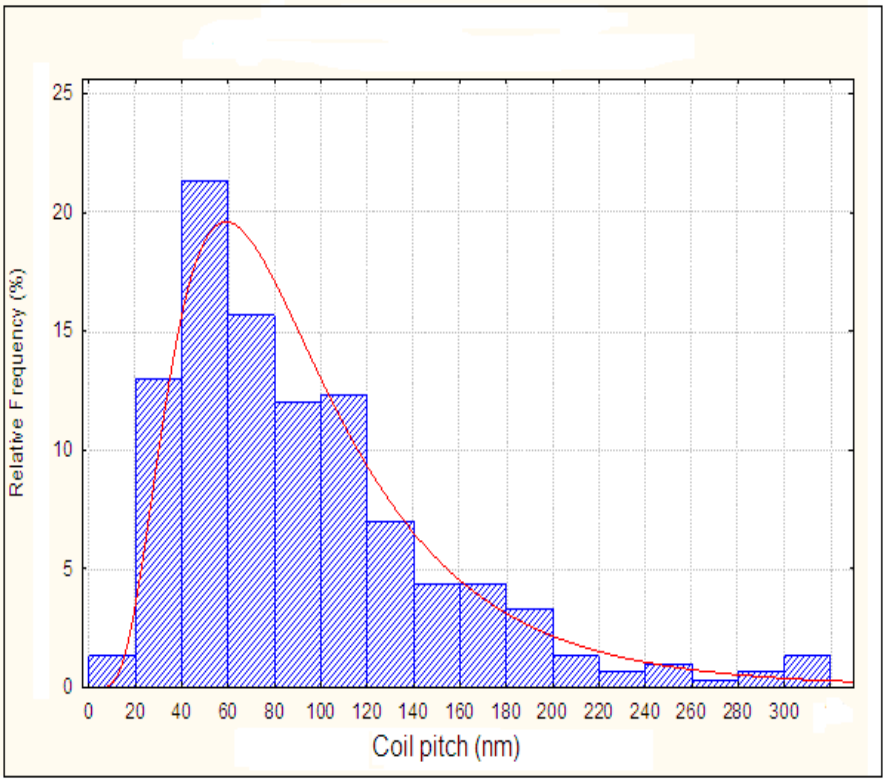

Figure IV.39.: Distribution of the coil pitch values

Analyzing the coil pitch and coil diameter values (Figure IV.40.) we can make some comparison with previous results obtained by Szabó ***[2, 3].*** We noted some areas where significantly more helices can be found than in others. Three of these regions were identified. The first one includes helices with coil diameter of 30 nm and pitch range from 30 nm to 60 nm. More than 10% of the examined helices have these pitch and coil diameter values. Inside this region the most HCNTs can be found with coil diameter and pitch values of 30-40 nm and 30-50 nm, respectively. While the first type of coils belong to type 2.3, the latest ones to the type 1.1 of stability islands mentioned in previous studies ***[2, 3]***. Coils with 40 nm diameter having a pitch in the range of 40-90 nm are presented in the second region. The third group is formed by helices having a coil diameter of 50 nm and pitch in the range of 30-120 nm. Here, comparing with the studies of Szabo et al. ***[2, 3]*** helices with 50-50 nm coil diameter-pitch values belong to type 2.4, and helices having 50-70 nm coil diameter-coil pitch values pertain to type 1.3 stability islands. Also numerous coils can be found with coil diameter and coil pitch values of 50-80 nm and 50-110 nm. The high coil diameter values can be explained by the shape of the produced helices: in most of the cases S-shaped coils are prevalent in our samples.

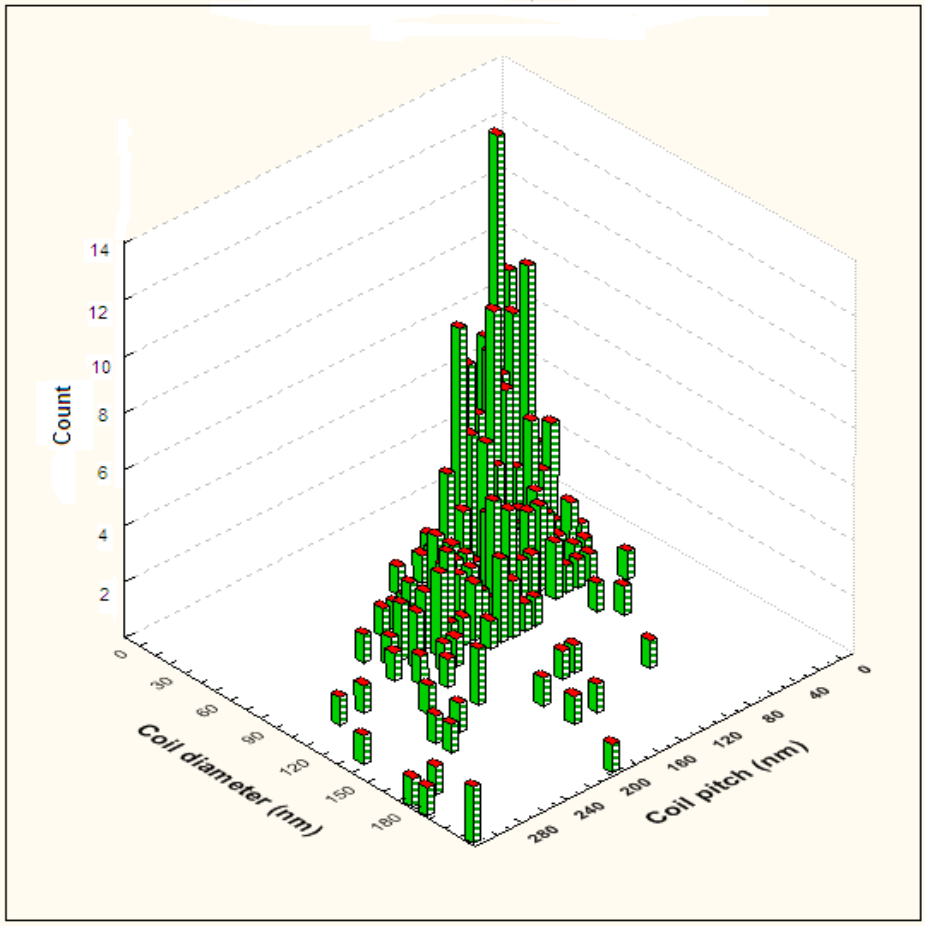

Figure IV.40.: 3D diagram of the number of observed helices as a function of coil pitch and coil diameter

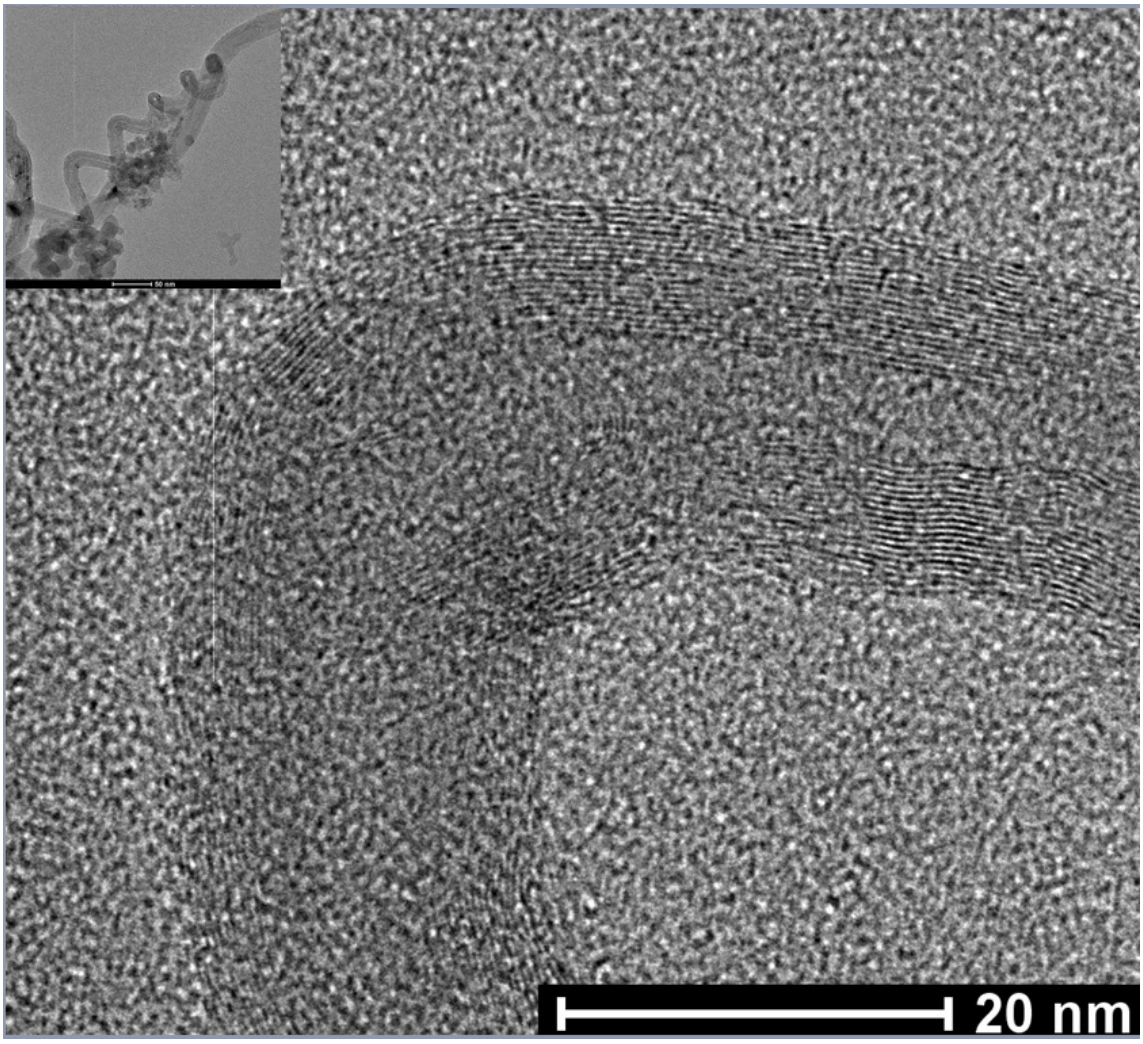

Figure IV.41.: HRTEM images of an irregular coil

HRTEM pictures of Coiled CNTs synthesized on 5%Co-Pr/SiO_2 catalysts with different morphologies were taken. Figure IV.41. shows an irregular coil with changing coil pitch and coil diameter. Looking at the graphene layers at the HRTEM picture, at the curvature the nanotube seems to be composed of straight segments. Where these segments meet the graphene layers seem to take different directions.

Looking at the curvature of an elongated S-shaped HCNT (Figure IV.42.) with coil pitch and coil diameter values over of 450 and 280 nm, respectively we can observe braid-like formation of the graphene layers. While getting further from the curvature, the tube is composed of straight segments of parallel graphene layers.

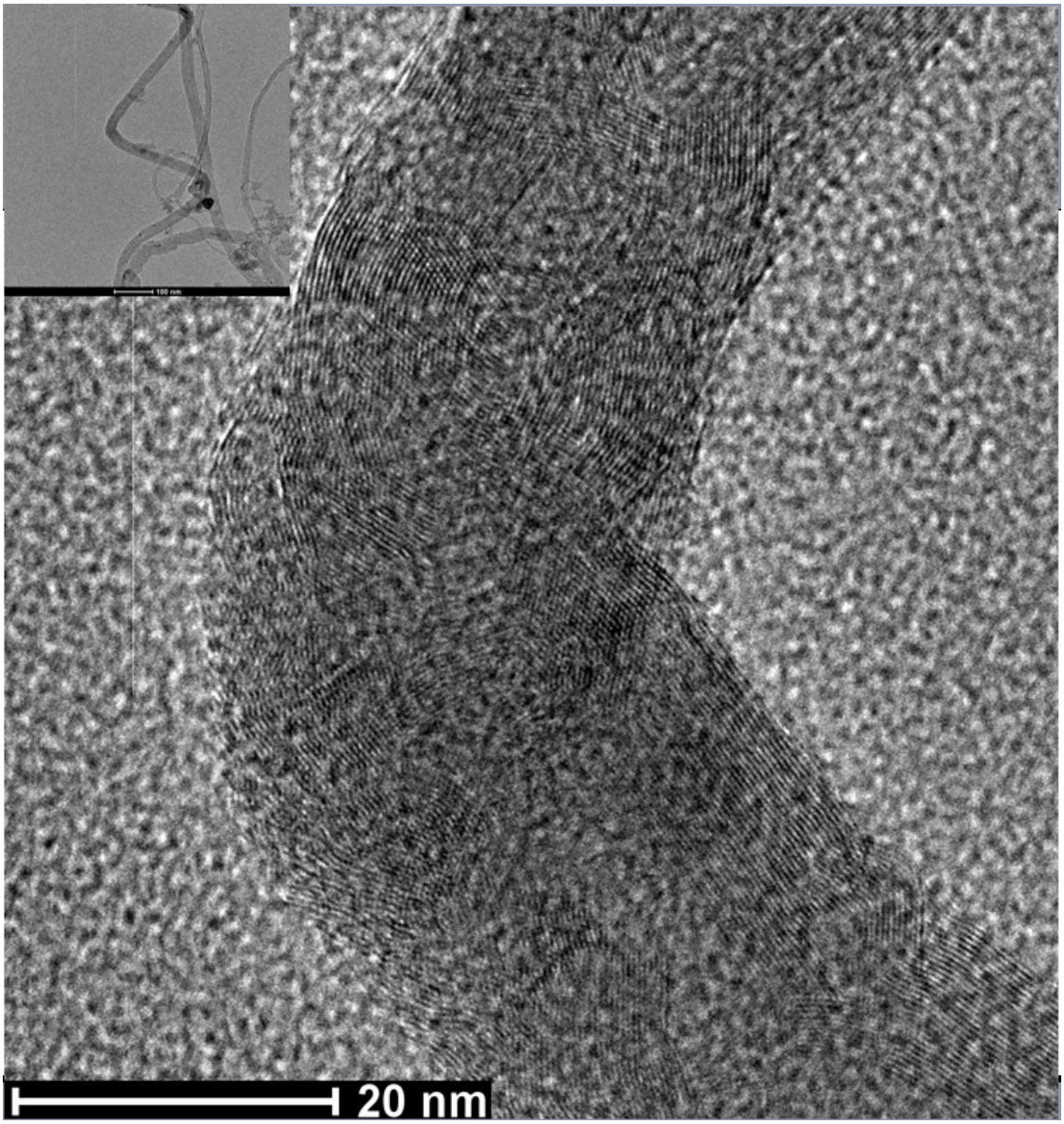

Figure IV.42.: HRTEM image of S-shaped carbon nanotube

Figure IV. 43. shows HRTEM image of a regular coil with coil diameter of 75 nm and coil pitch of 100 nm.Here we can se a continous curvature, however the layers are overlapped as the tube twists.

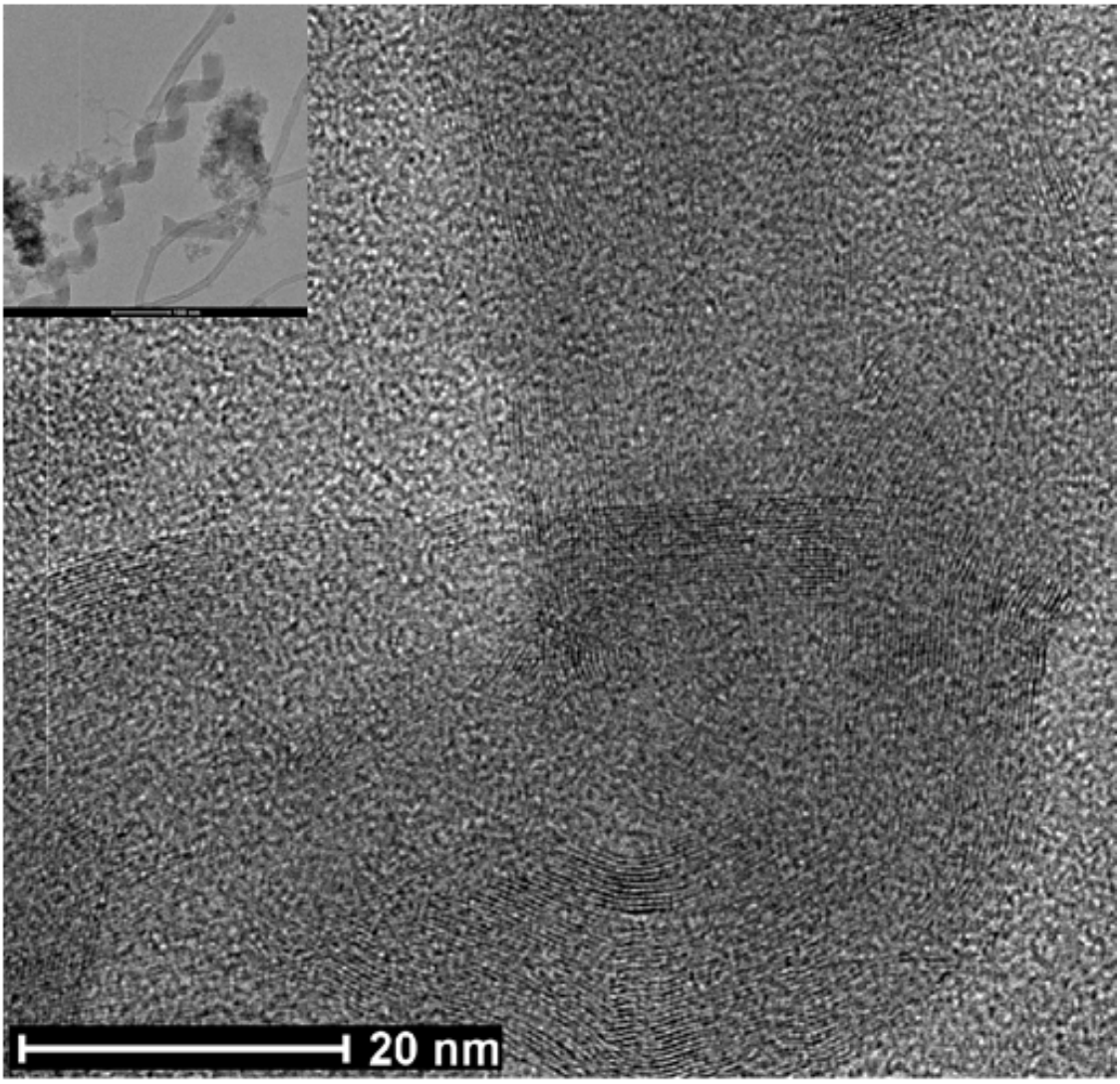

Figure IV.43.: HRTEM photo of regular helix

IV.4.5. Selected area electron diffraction (SAED) of coiled CNTs synthesized on Co-Pr/SiO_2 catalysts

Selected area electron diffraction patterns of helices of different morphology were taken (Figure IV.44). We can observe the spotty arcs of d002 graphite reflection in the ED patterns of all the analysed coils. The light blurry circles are due to the carbon film coating on the grid. Figure IV.45. shows the SAED pattern of a straight nanotube. There we can observe 2 spots, instead of the dotty line. The difference comes from the morphology of the coiled CNTs.

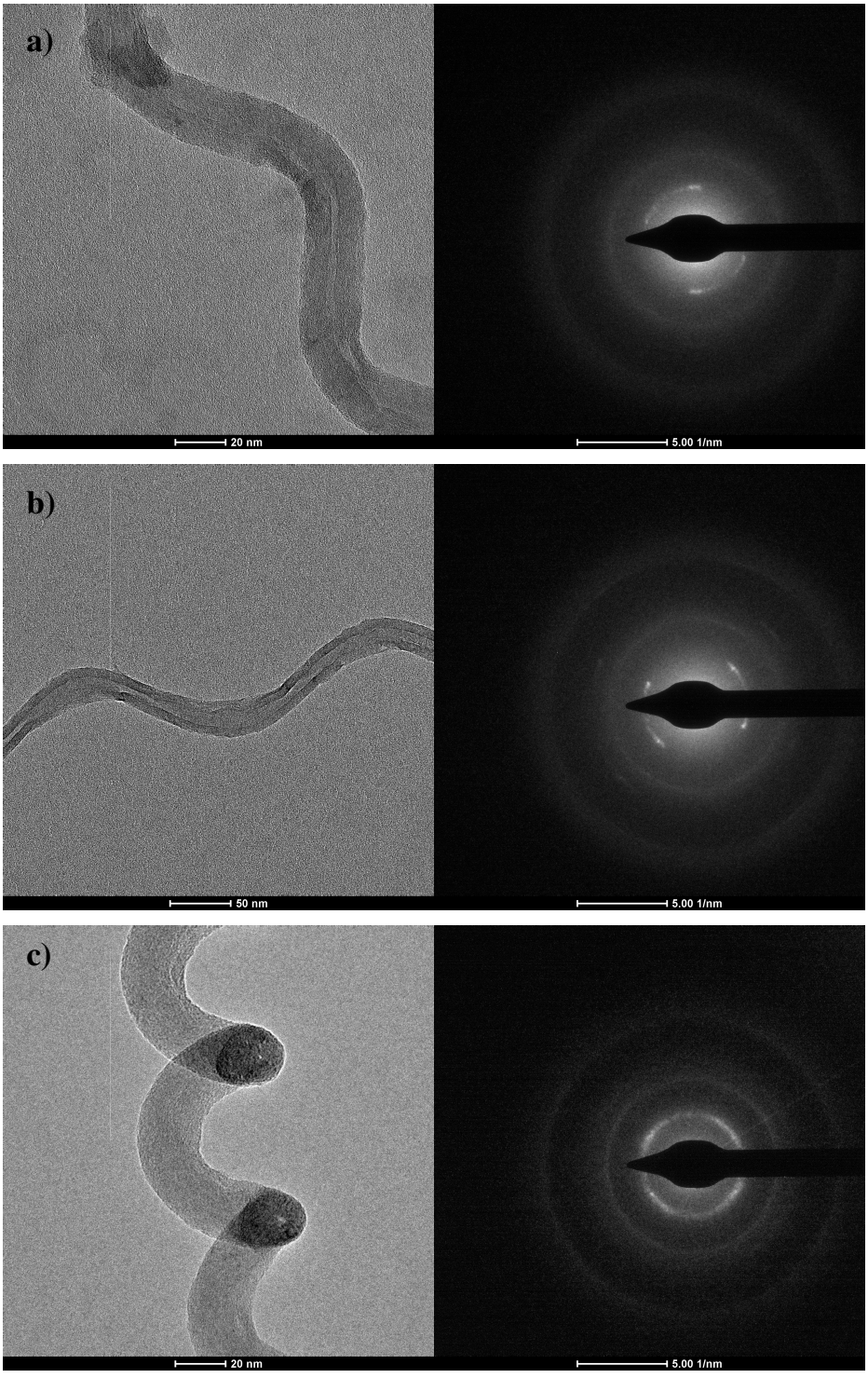
a)
20 nm
5.00 1/nm
b)
50 nm
5.00 1/nm
c)
20 nm
5.00 1/nm

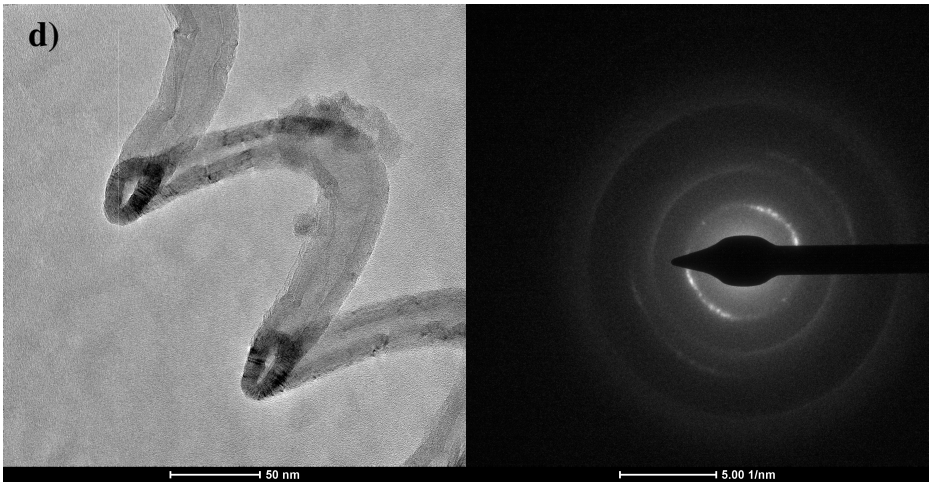

Figure IV.44.: TEM micrographs and SAED patterns of HCNTs with different coil pitch and coil diameter

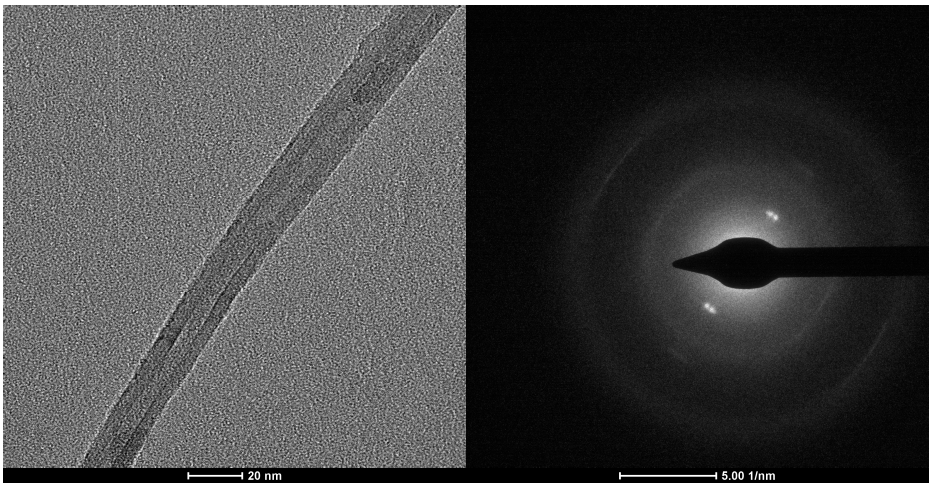

Figure IV.45.: TEM micrograph and SAED pattern of a straight CNT

References:

[1]: Kumar, M.; Ando, Y.: "Chemical vapour deposition of carbon nanotubes: a review on gowth mechanism and mass production" J. Nanosci. Nanotech. 10 (2010) 3739-3759

[2]: Szabo, A.; Fonseca, A.; Biro, L.P.; Konya, Z.; Kiricsi, I.; Volodin, A.; Van Hasendonck, C.; B.Nagy, J.: "Synthesis, characterization and use of coiled carbon nanotubes" Nanopages 1 (2006) 263-293

[3]: Szabó, A.: "Spirális szén nanocsövek katalitikus előállítása és jellemzése" PhD thesis, Szegedi Tudományegyetem Alkalmazott és Környezeti Kémiai Tanszék (2005) pp. 87

[4]: Giraldi, N.: "Ottimizzazione della sintesi di nanotubi di carbonio con il metodo CCVD tramite catalizzatore supportato da sepiolite" Masters Thesis Universitá della Calabria (2009) pp. 135

[5]: Frost, R.L.; Ding, Z.: "Controlled rate thermal analysis and differential scanning calorimetry of sepiolites and palygorskites" Thermochimica Acta 397 (2003) 119-128

[6]: Goktas, A.A.; Misirli, Z.; Baykara, T.: "Sintering behaviour of sepiolite" Cer. Int. 23 (1997) 305-311

[7]: Fonseca, A.; Hernadi, K.; B.Nagy, J.; Lambin, Ph.; Lucas, A A.:"A model structure of perfectly graphitizable coiled carbon nanotubes " Carbon 33 (1995) 1759-1775

[8]: Lu, M., Liu, W.-M.; Guo, X.-Y.; Li, H.-L.: "Coiled carbon nanotubes growth via reduced-pressure catalytic chemical vapor deposition" Carbon 42 (2004) 805-811

[9]: Kónya, Z.; Biró, L.P.; Hernádi, K.; B.Nagy, J.; Kiricsi, I.: "Szén nanocsövek előállítása, tulajdonságai és alkalmazási lehetőségei" A kémia legújabb eredményei 2001, Akadémiai Kiadó Budapest (2002) 121-300

[10]: Hernádi, K.; Fonseca, A.; Piedigrosso, P.; Delvaux, M.; B.Nagy, J.; Bernaerts, D.; Riga, J.: "Carbon nanotube production over Co/silica catalysts" Cat. Lett. 48 (1997) 229-238

[11]: Hernádi, K; Fonseca, A.; B.Nagy, J.; Fudala, Á.; Bernaerts, D.; Kiricsi I.: „Catalytic production of carbon nanofibers over iron carbide doped with Sn^{2+}" Appl. Cat. A 228 (2002) 103-113

V. Conclusions and Perspectives

The aim of the here presented work was the synthesis and characterization of helically coiled CNTs. Although carbon microcoils and nanocoils that have similar coiled structure, as well as multiwalled carbon nanotubes can already be synthesized on large scale, the production of helically coiled CNTs and their formation mechanism is still a challenge.

In this work we aimed to enhance the production of coiled CNTs by testing different metal catalysts and support materials. We attempted to augment the proportion of HCNTs in the synthesized nanotube samples, starting from previous studies.

We tested three different support materials: sepiolite, alumina and silica. The latter one was chosen because so far it was proved to be the support that favors most the formation of the helices.

Sepiolite is a natural clay used for various industrial applications. Its high surface area and peculiar structure makes it ideal not only as filler for composite materials but as catalyst supports as well. Its outstanding ion-exchange properties and thermal stability is not negligible. Co-Fe, Co-Pr and Fe-Pr bimetallic catalysts were prepared. For the Co-Fe catalysts regular helices were found in the synthesized samples, however their quantity is maximum 1-2 %. Applying 4%Co-1%Fe catalyst Y-junctions were found in the sample. Applying Pr as co-catalyst did not lead to the formation of HCNTs, CNTs are also rarely observed in the synthesis products.

Starting from a study carried out by Szabo et al. 3.5%Co-1.5%Fe/Al_2O_3 catalyst was tested in the synthesis reactions. Ethylene and acetylene were both used as carbon source, the reaction temperatures were changed from 600 to 700°C. MWCNTs in high yield were obtained as the result of the synthesis reactions. Examining the samples with SEM we could see the long, wavy bent bundles that are characteristic of this support. However, looking into the bundles with transmission electron microscopy helically coiled CNTs were just occasionally observed in some samples. Y-junctions were also present in the synthesis product obtained from the decomposition of acetylene at 700°C.

A more detailed study was carried out applying silica as support material. In a first phase of the study the effect of the pH at the preparation of the catalyst was investigated. When using acetylene as carbon source setting the pH of the Co-acetate solution to 8.5 and 11 resulted the formation of helically coiled CNTs in the synthesis product. However, their ratio remained maximum 4-5 % at pH=11, and high amount of amorphous carbon formation was also

observed. When ethylene was applied as carbon source the catalyst prepared at unmodified pH (7-7.5) and the one where the pH was adjusted to 10 was active in the formation of HCNTs. The characteristics of the coils in the samples are shown in table V.1.

Carbon source	**Catalyst pH**	**Coiled CNT**	**Outer tube diameter (nm)**	**Coil pitch (nm)**	**Coil diameter (nm)**
acetylene	8.5	1-2%	10-20	27-256	24-132
acetylene	11	4-5%	9-22	26-152	26-77
ethylene	Native	3-4%	6-20	30-82	12-80
ethylene	10	1-2%	10-20	30-60	26-78

Table V.1.: Characteristics of HCNTs produced with silica supported catalysts of different pH

We chose to set the pH of our catalyst to 8.5-8.75 for the further studies and chose acetylene as carbon source.

A next part of our study was a preliminary study with a smaller reactor to observe the behavior of different silica supported catalyst. Co-; Fe-; Co-Fe and Co-Pr catalysts were prepared with different metal loadings by the IAP method. Special attention was dedicated to the Co-Pr catalysts.

Table V.2 summarizes the results obtained with the different catalysts.

Fe and Co-Fe catalysts produced few regular helices. In samples synthesized on 2.5%Fe-2.5%Co and 1%Fe-4%Co catalyst 1-2 % of all the nanotubes are helically coiled. The 4%Fe-1%Co catalyst did not lead to the formation of regular helices, however strange tubular carbonaceous structures with filled caps can be observed.

5%Co- and 10%Co/silica catalysts were more active in the HCNT production, however also in this case coils were 5 % of all the produced CNTs.

The tested Co-Pr catalysts were all active in the coiled CNT production. The one that produced HCNTs in the highest ratio was the 1%Co-4%Pr catalyst. In this case the regularly coiled CNTs were 15-17% of all the nanotubes. The helices had coil diameters between 55-70 nm, their coil pitches changed from 20 to 70 nm while the diameters of the helices were in the range of 6-16 nm. The 2.5%Co-2.5% Pr catalyst was also very active in the formation of the helices, the HCNT/CNT ratio was 15 % in this sample.

Catalyst	Carbon deposit(%)	Carbon yield (%)	Coiled carbon nanotubes
5%Fe	41	13	-
2.5%Fe-2.5%Co	42	13.9	1-2%
1%Fe-4%Co	41	13	1-2%
4%Fe-1%Co	42	13.9	-
5%Co	58.3	18.4	5%
10%Co	38.3	11.9	5%
2.5%Co-2.5%Pr	63.2	20	15%
1%Co-4%Pr	53	16.9	15-17%
4%Co-1%Pr	56.8	17.8	10%
5%Co-5%Pr	50.4	15.8	10%
7.5%Co-2.5%Pr	62.7	19.1	<5%
2.5%Co-7.5%Pr	10.5	3.2	<5%
10%Co-2.5%Pr	36.7	11	15%
12.5%Co-2.5%Pr	40.1	12	15%
5%Pr	5.7	1.8	-

Table V.2.: Carbon deposit, carbon yield and HCNT/CNT ratio of CNT samples produced on different silica supported catalysts

The 4%Co-1%Pr is also promising. 10 % of the synthesized tubes were HCNTs. The outer diameters of the coiled CNTs ranged from 5 to 12 nm. The coil pitches and coil diameters of the observed CNTs were between 30-45 nm and 20-70 nm, respectively.

Samples synthesized on the 10%Co-2.5%Pr and the 12.5%Co-2.5%P catalyst contained also HCNTs in a high ratio compared to all the CNTs, albeit in these cases few nanotubes are formed and the CNTs in the sample are covered with amorphous carbon.

The 5%Co-5%Pr catalyst led to the formation of 10 % HCNTs in the product. The synthesis product contains significant amount of amorphous carbon that often covers the helices and straight MWCNTs. The other Co-Pr catalyst with various metal loadings led to a product that contains HCNT at maximum 5 % of the product, while praseodymium as monometallic catalyst was not active in the synthesis of CNTs.

Consequently to this preliminary study we chose the 1%Co-4%Pr, 2.5%Co-2.5%Pr and the 4%Co-1%Pr catalyst for further optimization. We aimed to enhance the ratio of HCNTs in the samples. The effect of the reaction temperature, the carbon source and carrier gas flow was investigated.

The temperature was varied between 600-700°C. The activity of the three catalysts in the formation of HCNTs changed differently with the change of the reaction temperature. Decreasing the synthesis temperature to 650°C led to an increase in the HCNT/CNT ratio for the 4%Co-1%Pr catalyst. In the case of the 2.5%Co-2.5%Pr and 1%Co-4%Pr catalyst the helices were formed in the highest ratio at 700°C. Table V.3 summarizes the characteristics of the synthesized samples.

Catalyst	**Reaction temperature (°C)**	**%HCNT**	**Outer tube HCNT diameter (nm)**	**Coil pitch (nm)**	**Coil diameter (nm)**
2.5%Co-2.5%Pr	650	10	9-15	45-215	35-90
	700	15	6-16	35-170	23-55
4%Co-1%Pr	600	<1	8-12	70-130	75-90
	650	14-15	8-20	38-145	30-100
	700	10	7-20	40-170	25-100
1%Co-4%Pr	650	7-8	14-20	35-180	50-85
	700	15-17	12-22	35-180	30-100

Table V.3.: Quantity and characteristics of HCNTs synthesized on 2.5%Co-2.5%Pr; 4%Co-1%Pr; 1%Co-4%Pr catalysts at different reaction temperatures

Augmenting the carbon source flow did not increase the ratio of HCNTs in the samples, moreover it caused the formation of less helices compared to the CNTs. Table V.4. summarizes the characteristics and ratio the of the synthesized HCNTs.

The effect of the N_2 flow variation was also studied. Applying 150ml/min N_2 flow did not lead to the formation of any helices in our reaction conditions. For the 2.5%Co-2.5%Pr catalyst the ratio of the HCNTs in the samples decreased at higher N_2 flow rates. For the 1%Co-4%Pr and the 4%Co-1%Pr catalysts 14-15% of the synthesized CNTs were helically coiled when applying 600 ml/min nitrogen flow.

Catalyst	C_2H_2 flow (ml/min)	%HCNT	HCNT outer tube diameter (nm)	Coil pitch (nm)	Coil diameter (nm)
2.5%Co-2.5%Pr	30	15	6-16	35-170	23-55
	50	10	10-14	50-140	30-100
	70	10	12-15	35-140	30-170
4%Co-1%Pr	30	10	7-20	40-170	25-100
	50	10	21-23	120-140	80-170
	70	10	27-35	130-500	70-170
1%Co-4%Pr	30	15-17	12-22	35- 180	30-100
	70	<1	18-20	130-300	120-170

Table V.4.: Quantity and characteristics of HCNTs synthesized on 2.5%Co-2.5%Pr; 4%Co-1%Pr; 1%Co-4%Pr catalysts applying different acetylene flows

In conclusion, we can say that around 15% HCNT content in the sample compared to all the CNTs could be reached with all the three catalysts. In Table V.5. the most favorable reaction conditions are listed. The helices are present in the samples with different morphologies, wavy, telephone cord-like coils, loose spring and tight coils are observed in TEM micrographs.

Catalyst	Reaction temperature (°C)	C_2H_2 flow (ml/min)	N_2 flow	%HCNTs
2.5%Co-2.5%Pr	700	30	300	15
4%Co-1%Pr	650	30	300	14-15
4%Co-1%Pr	700	30	600	14-15
1%Co-4%Pr	700	30	300	15-17
1%Co-4%Pr	700	30	600	14-15

Table V.5.: Most favorable reaction conditions for HCNT formation over 5%Co-Pr catalysts with different metal ratios

Applying the reaction conditions presented in Table V.5. the synthesis products contain approximately 15% helically coiled MWCNTs. So far maximum this ratio could be obtained

of thin tubular structured carbonaceous helices. This gives the possibility to use these synthesized HCNTs in nanocomposite materials, and exploit the peculiar properties of these structures. However, the purification process of the samples should be optimized.

Considering the morphology of the synthesized helices on 5%Co-Pr/SiO_2 catalysts 90% of the HCNTs have coil diameters inferior to 100 nm. However, compared to previous studies higher ratio of HCNTs with coil pitch values superior to 100 were found. This can be explained by the fact that S-shaped, elongated helices are prevalent in our samples. 10% of the synthesized helices have 30 nm coil pitches and coil diameter values between 30-60 nm.